A Field Cycling NMR Relaxometry Study on Molecular Liquids and Plastically Crystalline Phases

Von der Universität Bayreuth zur Erlangung des
Grades eines Doktors der Naturwissenschaften
(Dr. rer. nat.) genehmigte Abhandlung

von Max Flämig aus Berlin

1. Gutachter: Prof. Dr. E. A. Rössler

2. Gutachter: Prof. Dr. W. Köhler

Tag der Einreichung: 20.05.2020

Tag des Kolloquiums: 23.10.2020

Contents

Abstract

We apply field-cycling (FC) nuclear magnetic resonance (NMR) relaxometry to measure the spin-lattice relaxation rate R_1 in condensed matter as a function of Larmor frequency ω and temperature T. We present the results by means of five publications, three of which deal with the molecular liquid glycerol, while the latter two address the dynamics of the plastically crystalline phase of cyanoadamantane. In the case of protons (^{1}H), the focus of the present work, R_1 reflects the fluctuations of the magnetic dipole-dipole interactions transmitted through intra- and intermolecular pathways. As a consequence, we gain insight to translational as well as rotational dynamics of the molecules.

We describe a relaxation model for molecular liquids which includes three distinct relaxation phenomena. Following the results of dielectric and light-scattering experiments, the rotational susceptibility is described by a main relaxation process and a high frequency excess wing. At low frequencies $\omega\tau < 1$ we consider a translational relaxation contribution which is given by the force-free hard sphere model describing diffusion in spin systems. In general, translation and rotation in molecular liquids are coupled and take place approximately on the same time scale τ. In glycerol however, they are separated well enough to result in a distinct bimodal relaxation behavior. It turns out that applying our model to master curves extending over 15 decades in frequency, which are constructed by assuming frequency-temperature superposition (FTS), facilitates the analysis. We include in the analysis the $R_1(T)$ data of Noack, for which reproduction of our data is demonstrated.

In a next step, we analyze ^{1}H relaxation data of mixtures of glycerol with either dimethyl sulfoxide (DMSO) or pyridine, with the help of our relaxation model. This allows us to investigate the translational and rotational dynamics in a component selective way. The change

of the separation of the dynamics is addressed as a function of concentration and temperature. In case of DMSO/glycerol, no decoupling of the rotational dynamics of the components is observed. Moreover, the separation of time scales of translation and rotation is described as constant. This is in contrast to the mixture with pyridine, where a systematic change of the separation is observed with concentration. In all cases, we describe the extent of separation as temperature independent.

Regarding the analysis of the dynamics in plastically crystalline phases we first focus on cyanoadamantane. Applying FTS once more, we characterize the non-Lorentzian character of the spectral density reflecting the 90-degree jumps of the molecule. At low temperatures, the NMR relaxation is determined by the rotation of the molecule around its three-fold axis, the dynamics of which is described by a broad distribution of activation energies. As FTS does not apply in this case, we suggest a scaling procedure which again provides master curves in the case of dynamics controlled by thermally activated processes. Following these ideas, we investigate the NMR relaxation of other plastically crystalline phases like cyano cyclohexane, diaza [2,2,2] bicyclooctane and m-carborane.

Kurzdarstellung

Wir wenden Feldzyklus (FC) Kernspinresonanz-(NMR)-relaxometrie an um die Spin-Gitter-Relaxationsrate R_1 in kondensierter Materie als Funktion der Larmorfrequenz ω und Temperatur T zu messen. Wir stellen die Ergebnisse anhand von fünf Veröffentlichungen dar. Dabei handeln drei von der molekularen Flüssigkeit Glyzerin, und zwei behandeln die Dynamik in der plastisch kristallinen Phase von Cyanoadamantan. Für Protonen (^{1}H), dem Fokus dieser Arbeit, gibt R_1 die Fluktuation der magnetischen Dipol-Dipol Wechselwirkung wider, die durch intra- und intermolekulare Pfade vermittelt werden. Folglich erhalten wir Einblick in die translatorische und rotatorische Dynamik der Moleküle.

Wir beschreiben ein Relaxationsmodell für molekulare Flüssigkeiten, welches drei ausgeprägte Relaxationsphänomene einschließt. Den Ergebnissen der Dielektrik und Lichtstreuung folgend, wird die rotatorische Suszeptibilität von einem Hauptrelaxationsprozess und einer hochfrequenten Überschussflanke beschrieben. Bei kleinen Frequenzen $\omega\tau < 1$ betrachten wir einen translatorischen Relaxationsbeitrag, der durch das Model kraftfreier harter Kugeln gegeben ist und die Diffusion in Spinsystemen beschreibt. Im Allgemeinen sind Translation und Rotation in molekularen Flüssigkeiten gekoppelt und finden ungefähr auf gleicher Zeitskala τ statt. In Glyzerin sind die Zeitskalen jedoch stark genug getrennt um ein ausgeprägtes bimodales Relaxationsverhalten zu verursachen. Es stellt sich heraus, dass die Anwendung des Modells auf Hauptkurven, die sich über 15 Frequenzdekaden erstrecken, die unter der Annahme von Frequenz-Temperatursuperposition (FTS) erstellt werden, die Analyse vereinfacht. Wir beziehen die Daten $R_1(T)$ von Noack in unsere Analyse ein und demonstrieren Übereinstimmung mit unseren Daten.

In einem weiteren Schritt analysieren wir ^{1}H-Relaxationsdaten von Mischungen von Glyzerin

entweder mit Dimethylsulfoxid (DMSO) oder mit Pyridin, mit Hilfe unseres Relaxationsmodells. Dies erlaubt uns Translations- und Rotationsdynamik komponentenselektiv zu untersuchen. Die Veränderung der Trennung dieser Dynamik wird als Funktion der Konzentration und der Temperatur betrachtet. Im Fall der Mischung DMSO/Glyzerin ist keine Entkopplung der Rotationsdynamik der beiden Komponenten zu beobachten. Weiterhin wird die Trennung der Zeitskalen von Rotation und Translation als konstant beschrieben. Im Gegensatz dazu ändert sich die Zeitskalentrennung von Rotation und Translation in der Mischung mit Pyridin systematisch mit der Konzentration. In allen Fällen beschreiben wir das Ausmaß der Trennung als temperaturunabhängig.

Bezüglich der Analyse der Dynamik in plastisch kristallinen Phasen beschränken wir uns zunächst auf Cyanodamantan. Wieder unter der Anwendung von FTS beschreiben wir den nicht lorentzartigen Charakter der Spektraldichte, die die 90-Grad Sprünge der Moleküle widerspiegelt. Bei tiefen Temperaturen wird die NMR-Relaxation durch die Rotation des Moleküls um dessen dreizählige Achse beschrieben. Diese Dynamik wird durch eine breite Verteilung der Aktivierungsenergie beschrieben. Da in diesem Fall FTS nicht gilt, schlagen wir ein Skalierungsverfahren vor, welches Hauptkurven auch im Fall einer thermisch aktivierten Dynamik liefert. Diesen Ideen folgend, untersuchen wir die NMR-Relaxation anderer plastisch kristalliner Phasen, beispielsweise von Cyanocyclohexan, Diaza[2,2,2]bicyclooctan und m-Carboran.

Extended Abstract

1. Methods for Analyzing $R_1(\omega, \tau)$ in Liquids and Glassy Crystals

Shortly after the Nobel prize-wining discovery of nuclear magnetic resonance (NMR) in condensed matter by the groups of F. Bloch (Stanford) and E.M. Purcell (Harvard) in 1946, a paper appeared entitled "Relaxation Effects in Magnetic Resonance Absorption" by N. Bloembergen, E.M. Purcell, and R.V. Pound (BPP, 1948),[1] which has become one of the most cited works in NMR. The authors discussed the ^{1}H spin-lattice and spin-spin relaxation time T_1 and T_2 describing the thermal equilibration of the nuclear magnetization. Applying time-dependent second order perturbation theory, BPP derived the now well-known BPP equations. They relate the relaxation rate $R_1 = 1/T_1$ and $R_2 = 1/T_2$ with a spectral density $J(\omega)$ taken at multiples of the Larmor frequency $\omega = \gamma B$ given by the applied external magnetic field B and the gyromagnetic ratio γ. For ^{1}H they read in their final form [2,3]

$$R_1(\omega) = K \left[J(\omega) + 4J(2\omega) \right]$$

$$R_2(\omega) = K/2 \left[3J(0) + 5J(\omega) + 4J(2\omega) \right] \tag{1}$$

Here, K denotes some coupling constant (specified later). The equations can be exactly derived in the frame of the Bloch, Wangsness and Redfield theory for the case of a liquid. [4,5] Moreover, the spectral density $J(\omega)$, which is the Fourier transform of its corresponding correlation function, is connected to the susceptibility $\chi''(\omega) = \omega J(\omega)$. Hence, we can write [6,7]

$$\omega R_1(\omega) = K \cdot \left(\chi''(\omega) + 2 \cdot \chi''(2\omega) \right) \cong 3 \cdot K \chi''_{FC}(\omega) \equiv \chi''_{NMR}(\omega). \tag{2}$$

In the susceptibility representation $\chi''_{NMR}(\omega)$ relaxation processes appear as peaks, as observed in other methods such as dielectric spectroscopy (DS).

We discuss the constraints of the applicability of equation (1) in subchapter 1.1.. As the accessible frequency range of the commercial FC relaxometer is still narrow, our analysis takes recourse to the construction of master curves, i.e. we apply frequency-temperature superposition (FTS). We explain the procedure in subchapter 1.2. and will apply it to liquids, mixtures and plastic crystals.[6,8,9] In subchapter 1.3. we deduce a relaxation model for $\chi''_{NMR}(\omega)$ that applies to liquids and takes molecular rotation and translation into account. In subchapter 1.4., a thermally activated process is considered with a temperature independent distribution of activation energies $g(E)$. Such cases are found for example in glassy crystals as cyanoadamantane. Here, we provide a scheme to calculate the temperature independent distribution $g(E)$ from ^{1}H spin-lattice relaxation data, and hence, to construct master curves.

1.1. Constraints of the Applicability of BPP close to T_g: $\tau > 1/\omega$ (Pub. 1)

In order to study the glass transition of liquids by means of R_1, we want to ascertain applicability of the BPP equations (1), in particular for R_1. The Bloch, Wangsness, Redfield (BWR) equations are the fundamental equations describing the spin relaxation in condensed matter. [3-5,10] They constitute differential equations describing relaxation in terms of kinetic coefficients, which can be expressed by linear combinations of spectral densities.

The BWR equations are approximations, as it is well known, from the Mori-Zwanzig formalism for example,[5,11] that profound equations should have integro-differential character. Such integro-differential equations can be approximated by appropriate differential equations in situations for which the kernels are fast decaying in comparison to the unknown function. The limit for which BWR equations correctly describe NMR relaxation is called the short correlation time approximation or the Redfield limit which reads: [3-5,10]

$$T_1(\omega), T_2(\omega) \gg \tau \tag{3}$$

The correlation time τ characterizes the time scale of the relevant correlation function. In simple terms: molecular motions in the system should be much faster than its relaxation times.

This condition is correct if we attempt to describe both spin-spin and spin-lattice relaxation simultaneously. Usually, this is done by considering the master equation obtained from time-dependent second order perturbation, which is the starting point for the derivation of the Bloch equation and finally yields the expression for the relaxation rates R_1 and R_2, equations (1). However, when considering spin-lattice relaxation only, the Redfield limit is less strict (at least for the initial rate of the spin-lattice relaxation):

$$T_1(\omega) > \min(\omega^{-1}, \tau), \tag{4}$$

i.e., $T_1(\omega)$ should be longer than either ω^{-1} or τ. This is deduced in the appendix of Pub. 1 by explicitly calculating expectation values of the magnetization and, subsequently, the rates R_1 and R_2.

Let's have a closer look at the implications for ^{1}H spin-lattice relaxation measurements at T_g, where by definition $\tau(T_g) \equiv 100$ s holds. First, we consider the Stelar Spinmaster2000 used in this work, covering $10\,\text{kHz} < \omega/2\pi < 30\,\text{MHz}$.[12] The prevailing formulation of the Redfield-limit, Equation (3), reads in this case $T_1, T_2 \gg 100$ s. Usually, we avoid measurements of $T_1 > 5$ s, because the mechanical stress on the instrument increases for longer polarization times, which leaves us in conflict with Equation (3). However, the formulation of the Redfield-limit for T_1 presented here, Equation (4), reads $T_1 > \min(1/2\pi \cdot 10\,\text{kHz}, 100\,\text{s}) = 16\,\mu\text{s}$ (at 10 kHz) and $T_1 > 5.3$ ns (at 30 MHz). For the case of the Stelar Spinmaster2000 with its switching time $t_{swt} \cong 3$ ms, the Redfield limit is always fulfilled, as the accessible ^{1}H spin-lattice relaxation times are much larger than 100 μs (hence $T_1 > 16\,\mu\text{s}$ always holds).[12]

For the homebuilt relaxometer in Darmstadt, frequencies down to $\omega/2\pi = 100$ Hz can be routinely measured.[13-15] Accordingly, at correlation times $\tau > 1.6$ ms, equation (4) becomes

important even more. In order to reach such low fields, additional resistive Helmholtz coils are needed. The control loop of the instrument is currently optimized to switching times of about $t_{swt} \cong 10\ ms$.[13-15] Consequently, accessible spin-lattice relaxation times fulfill $T_1 \gg 1\ ms$. Even in the case of state-of-the-art equipment, a violation of the Redfield limit cannot occur during ^{1}H spin-lattice relaxation measurements.

With these sophisticated details from theory and experiment in mind, we understand why a violation of the Redfield limit hasn't been observed in the manifold systems studied over the past 30 years: a violation wasn't technically feasible. With the information provided here, one might find a situation (experimentally or theoretically), where the Redfield limit is indeed violated and the spin-lattice relaxation can be studied beyond the scope of typical NMR relaxation literature.

1.2. Frequency-Temperature Superposition and Low-Frequency Dispersion: Two Concepts of a Model Independent Analysis of Relaxation (Pub. 1 and Pub. 3)

Frequency-temperature superposition: The master curve construction is a concept originally developed to overcome the small frequency range of rheological instruments used to study polymers,[16] which feature segmental dynamics and chain dynamics slower by order of magnitudes.[17,18] It was adopted afterwards for other methods such as broadband dielectric spectroscopy (DS), or depolarized light scattering (LS) where it can be used to compare relaxation spectra independent of a model.[19] The fundamental assumption is that the shape of relaxation spectra does not change with temperature, e.g. frequency-temperature superposition (FTS) holds. This usually works well for relaxation processes governed by collective dynamics, as found in liquids, polymers or even plastic crystals. It usually does not apply to complex systems (such as proteins, tissue and porous material) or in the case of relaxation governed by NMR specific interactions, i.e. where the coupling constant depends on ω. Also, FTS doesn't

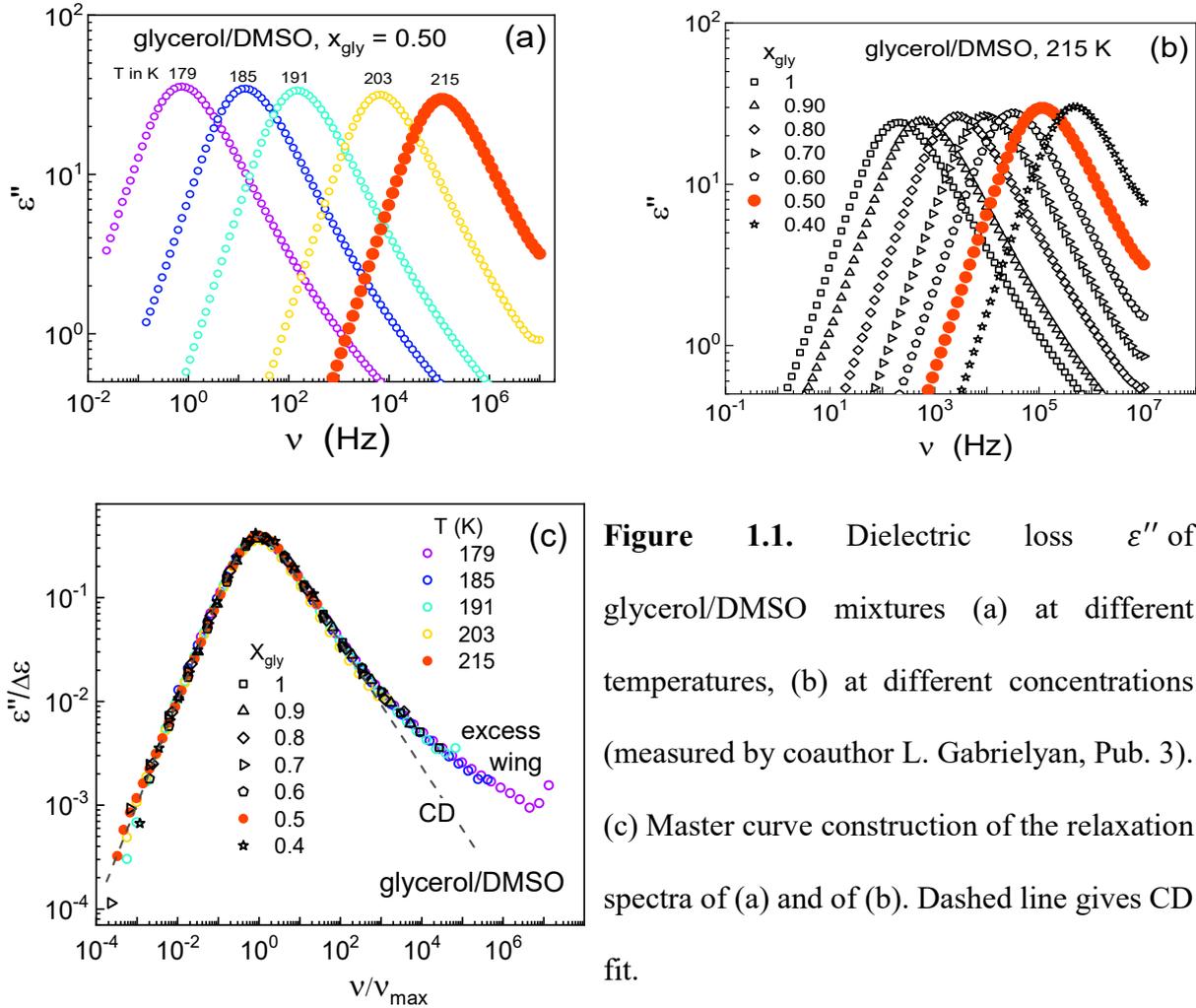apply for the dynamics observed in the glassy crystal cyanoadamantane (cf. 4.2.).

Figure 1.1. Dielectric loss ε'' of glycerol/DMSO mixtures (a) at different temperatures, (b) at different concentrations (measured by coauthor L. Gabrielyan, Pub. 3). (c) Master curve construction of the relaxation spectra of (a) and of (b). Dashed line gives CD fit.

In Figure 1.1. we see the spectra of the dielectric loss $\varepsilon''(\nu)$ of glycerol/DMSO mixtures which allow to demonstrate FTS. In (a) the relaxation peak shifts to lower frequencies upon cooling, i.e., the rotational dynamics probed by DS become slower, and the phenomenon of the glass transition is observed. Upon cooling, we also observe a slight increase of the amplitude of the relaxation process, following Curie's law. In (b) the relaxation peak of glycerol ($x_{gly} = 1$, open squares) shifts to higher frequencies upon dilution with DMSO, corresponding to faster rotational dynamics.

To obtain a master curve as shown in (c), we divide the frequency axis by the frequency of the maximum of the individual relaxation spectra $\nu_{max}(T, x)$. We scale out the relaxation strength

$\Delta\varepsilon = \varepsilon_s - \varepsilon_\infty$ as obtained from the real part of the spectra ε', where ε_s and ε_∞ are the low and high frequency dielectric constants. We observe no change in the spectral shape of the relaxation spectrum, i.e. FTS holds and we obtain a master curve. In this particular case, we find a master curve not only for different temperatures, but also for different concentrations (black symbols), a peculiarity of the present binary system which will be described in chapter 3.1.. By constructing a master curve, we overcome the frequency limit of the dielectric instrument, as different parts of the relaxation spectra measured at different T are combined to one master curve.

Analogously, NMR spin-lattice relaxation data $\chi''_{NMR}(\nu)$ can be used to construct master curves.[20] We use shift factors only along the frequency axis. In principle, the frequency axis can be divided by the position of the maxima ν_{max} of the individual data. As FC NMR relaxation spectra feature maxima only for a few temperatures, the relaxation spectra χ''_{NMR} can be shifted until best overlap is achieved, alternatively. If the master curve features a maximum, it may be used afterwards for scaling, for example to yield $\omega\tau_{rot}$ by applying a Cole-Davidson (CD) fit. We do not scale the amplitude χ''_{NMR}, as the temperature dependence of the NMR coupling constant K can usually be neglected ($< 5\%$, merely visible on a logarithmic scale), in contrast to $\Delta\epsilon$ in the case of DS. We emphasize, that the construction of master curves is particularly important in FC NMR in order to compete with more broadband techniques such as DS.

Low frequency dispersion: For long times, the dipolar correlation function follows the power law $\propto t^{-3/2}$, characteristic for free diffusion and independent of a specific model. Hence, to access the dispersion of ^{1}H spin-lattice relaxation, we can take recourse to the "square root law" holding for small frequencies:[21-24]

$$R_1(\omega) = R_1(0) - B \cdot D_{trans}^{-3/2} \cdot \sqrt{\omega} \tag{5}$$

Here, $R_1(0)$ is the rate at zero frequency, D_{trans} is the translational diffusion coefficient and

$B = \frac{\pi}{30}\left(1 + 4\sqrt{2}\right)\left(\frac{\mu_0}{4\pi}\hbar\gamma^2\right)^2 N$ depends only on physical constants and the spin density N, i.e.

the number of spins per unit volume. In other words, this gives translational diffusion

coefficients without assuming a specific relaxation model. This method was applied to many

systems and agreement of the extracted diffusion coefficient with FG NMR is reported.[25-29]

1.3. A Model for NMR Relaxation in Liquids (Publication 1)

After exploiting the model independent relaxation analysis, we turn our attention to a specific

relaxation model in order to quantitatively describe the spin-lattice relaxation in liquids. The

proton spin-lattice relaxation rate, $R_1(\omega)$, is a sum of inter- and intramolecular

contributions:[3,6,29]

$$R_1(\omega) = R_{1,\text{intra}}^{\text{rot}}(\omega) \ + \ R_{1,\text{inter}}^{\text{rot}}(\omega) + \ R_{1,\text{inter}}^{\text{trans}}(\omega) \tag{6}$$

The intramolecular relaxation rate $R_{1,\text{intra}}(\omega) = R_{1,\text{intra}}^{\text{rot}}(\omega)$ reflects interactions between protons

belonging to the same molecule. Thus, it probes molecular rotation.[a] The intermolecular rate,

$R_{1,\text{inter}}(\omega)$, originates from interactions between protons of different molecules. It is caused by

translational as well as rotational dynamics.[30, 31] Within the framework of our additive ansatz,

the individual relaxation contributions are determined by corresponding spectral densities, as

given by Equation (1). We now assume that the spectral density of rotational motions is the

same for inter- and intramolecular nuclei,

$$R_1(\omega) \cong R_1^{\text{rot}}(\omega) + \ R_1^{\text{trans}}(\omega) \tag{7}$$

In order to proceed, we specify the spectral densities $J(\omega)$ entering via Equation (1). Let's start

with the spectral density for rotation. The rotational contribution to relaxation in a liquid is

---

[a] We do not consider internal dynamics, i.e. molecules behave as rigid entities would.

described by a non-exponential correlation function, and, accordingly, a Cole-Davidson (CD) function is often used.[32] At highest frequencies, deviations from a CD function are observed in DS (cf. Figure 1.1. (c)) and photon correlation spectroscopy (PCS), the so-called excess wing, appears.[33-36] In analogy to DS and PCS, we describe R_1^{rot} with a sum of two CD spectral densities. They introduce stretching parameters β_{CD} and γ_{CD} describing the high-frequency flank, and a shared time constant τ_{CD} determining the frequency of the maximum of χ''_{NMR} (cf. Equation (11) below). The corresponding coupling constant entering equation (1) for the rotational relaxation contribution in the case of ^{1}H reads

$$K_{rot} \cong K_{intra} = \frac{3}{10}\left(\frac{\mu_0}{4\pi}\gamma^2\hbar\right)^2 \Sigma\frac{1}{r_{ij}^6} \tag{8}$$

with r_{ij} being the interspin distance.

Next, we consider the spectral density for translation, taking recourse to the force-free hard sphere (FFHS) model, which depicts molecules as non-interpenetrating spheres.[23,37] It uses the translational correlation time $\tau_{trans} = d^2/2D_{trans}$ as the only model parameter, where d is the diameter of the spheres (or distance of closest approach). Moreover, we define a spectral separation parameter $r = \tau_{trans}/\tau_{rot} = \tau_{trans}/\tau_{CD}\beta_{CD}$, which connects the time constants of translational and rotational spectral density. The corresponding coupling constant K_{trans} is given by

$$K_{trans} \cong K_{inter} = \left(\frac{\mu_0}{4\pi}\hbar\gamma^2\right)^2 \frac{8\pi}{15}\frac{n}{d^3}I(I+1) \tag{9}$$

where n denotes the spin density which is calculated from the mass density and the number of protons in the molecule. As mentioned, contributions due to the eccentricity effect in the equations for the ^{1}H coupling constants are neglected. [30, 31]

Later on, we will also apply the model for ^{2}H relaxation. Therefore, we define the quadrupolar coupling constant K_Q[3]

$$K_Q = \frac{3}{10}\pi^2 C_Q^2, \quad \text{with } C_Q = e^2 qQ/h \tag{10}$$

where eq denotes the field gradient and eQ the quadrupolar moment. The ^{2}H relaxation in molecular organic liquids is given by reorientation, i.e. $K_{trans} \equiv 0$. Moreover, the quadrupolar coupling constant is easily determined, e.g. from a solid state ^{2}H NMR spectrum at low temperatures.

Altogether, we obtain the following model equation for the ^{1}H NMR susceptibility

$$
\begin{aligned}
\chi''_{NMR} = \; & A_{rot}^{CD} \cdot \left\{ \frac{\sin(\beta_{CD} \cdot arctan(\omega\tau_{CD}))}{(1 + (\omega\tau_{CD})^2)^{\frac{\beta_{CD}}{2}}} + 4\frac{\sin(\beta_{CD} \cdot arctan(2 \cdot \omega\tau_{CD}))}{2 \cdot (1 + (2 \cdot \omega\tau_{CD})^2)^{\frac{\beta_{CD}}{2}}} \right\} + \\[2mm]
& A_{ex}^{CD} \cdot \left\{ \frac{\sin(\gamma_{CD} \cdot arctan(\omega\tau_{CD}))}{(1 + (\omega\tau_{CD})^2)^{\frac{\gamma_{CD}}{2}}} + 4\frac{\sin(\gamma_{CD} \cdot arctan(2 \cdot \omega\tau_{CD}))}{2 \cdot (1 + (2 \cdot \omega\tau_{CD})^2)^{\frac{\gamma_{CD}}{2}}} \right\} + \\[2mm]
& K_{trans}\omega \frac{54}{\pi} \left\{ \int_0^\infty \frac{u^2}{81 + 9u^2 - 2u^4 + u^6} \frac{u^2\tau_{trans}}{u^4 + (\omega\tau_{trans})^2} du \right. \\[2mm]
& \left. + 4 \cdot \int_0^\infty \frac{u^2}{81 + 9u^2 - 2u^4 + u^6} \frac{u^2\tau_{trans}}{u^4 + (2 \cdot \omega\tau_{trans})^2} du \right\}
\end{aligned}
\tag{11}
$$

A_{rot}^{CD} and A_{ex}^{CD} specify the weight of the CD relaxation contributions; they add up to the rotational relaxation constant $A_{rot}^{CD} + A_{ex}^{CD} = K_{rot}$. The model takes seven fit parameters, explicitly A_{rot}^{CD}, A_{ex}^{CD}, K_{trans}, β_{CD}, γ_{CD}, τ_{CD}, and τ_{trans}. We stress here, that the experimentally accessible coupling constants K_{inter} and K_{intra} are not part of the model. However, ^{1}H coupling constants are usually not at hand in any case, because they need to be determined from the second moment of spectra measured in continuous wave (CW) experiments $K \propto M_2$, which are no longer possible with most modern NMR equipment.

In molecular liquids, rotation and translation take place on similar time scales.[3,38,39] Hence, the favorable situation of two well separated relaxation peaks is usually not observed. Instead, a single peak is accompanied by a shoulder. Consequently, the determination of coupling

constants and time constants of the second peak may become ambiguous to some extent. The separation of rotational and translational dynamics may increase when looking to other systems such as plastic crystals (cf. Chapter 4.).

1.4. Thermally Activated Processes with Distribution of Activation Energies (Pub. 5)

In the preceding sections, we gave a description useful in cases of collective motion as found in liquids. Next, we want to develop a scheme for the construction of master curves for the relaxation process prevailing in the glassy crystalline phase of cyanoadamantane (CNADA). The relaxation in the solid is modulated by uniaxial rotation around the C_3 symmetry axis of the molecule (for a ball and stick model see Figure 4.1.). The scheme generally applies for dynamic processes governed by a temperature independent distribution of activation energies $g(E)$. FTS fails in these cases.[40] The corresponding (normalized) distribution of correlation times $G(\ln \tau)$ strongly broadens upon lowering the temperature along

$$G(\ln \tau) = RT \, g\left(RT \ln\left(\frac{\tau}{\tau_0}\right)\right) \tag{12}$$

Here, we assume an Arrhenius temperature dependence for each lattice site, specifically $\ln(\tau/\tau_0)=E/RT$, where τ_0 denotes an exponential pre-factor or attempt time which is taken to be temperature independent. Such distributions $G(\ln \tau)$ become extremely broad at low temperatures and are used to describe dynamic heterogeneities.

Considering ^{1}H, for which spin diffusion is efficient, spin-lattice relaxation is exponential even in the case of dynamic heterogeneities, and the relaxation rate averaged over the heterogeneous dynamics is given by the convolution of the BPP Equation (1) with $G(\ln \tau)$. We write

$$R_1(\omega) = K \int_{-\infty}^{\infty} G(\ln \tau) \left(\frac{\tau}{1+(\omega\tau)^2} + 4\frac{\tau}{1+(2\omega\tau)^2}\right) d\ln \tau \tag{13}$$

As introduced in Equation (2), the relaxation data described by Equation (13) transformed to the susceptibility representation $\chi''_{NMR} = \omega \cdot R_1$ yields a relaxation peak due to terms like

$\frac{\omega\tau}{1+(\omega\tau)^2}$. In the case of a single correlation time $G(\ln\tau) = \delta(\ln\tau)$, we recover the BPP Equation (1) with a Lorentzian spectral density.

In the case of a broad distribution $g(E)$ and thus a broad distribution $G(\ln\tau)$, the susceptibility $\chi''_{NMR}(\omega)$ directly reflects the distribution of correlation times $G(\ln\tau)$. In particular, the broadening of $G(\ln\tau)$ is reflected in $\chi''_{NMR}(\omega)$. By compensating the broadening of $\chi''_{NMR}(\omega)$, we can calculate the underlying temperature independent distribution $g(E)$. By doing so, we take recourse to a master curve construction applied before to dielectric or light scattering data.[41-44] The only difference is that the NMR relaxation is described by two susceptibility functions (*cf.* Equation (2)). Hence, under the condition of a broad $G(ln\tau)$, the sum of the two Lorentzians within the integrand of Equation (13) can be approximated by a delta function at the position of the maximum of this function, which is given by $\tau_{max} \approx 0.616/\omega \equiv 1/(\alpha\omega)$. Thus, we write

$$\frac{\omega\tau}{1+(\omega\tau)^2} + 4\frac{\omega\tau}{1+(2\omega\tau)^2} \cong \frac{3\pi}{2}\delta(\ln\tau - \ln(1/(\alpha\omega))) \qquad (14)$$

Note that the factor $\pi/2$ results from the integral over the Lorentzian, and the factor 3 follows from the definition of the NMR susceptibility (cf. Equation (2)). Introducing this into Equation (13), we can calculate the mean relaxation rate.

$$\omega \cdot R_1(\omega) = \frac{3}{2}\pi K \int_{-\infty}^{\infty} G(\ln\tau)\ \delta(\ln\tau - \ln(1/\alpha\omega)) = \frac{3}{2}\pi K G(\ln(1/\alpha\omega)) \qquad (15)$$

Finally, introducing $g(E)$ we receive

$$K \cdot g(E) = K \cdot g\left(RT\left(\ln\frac{\nu_0}{\nu} - 0.48\right)\right) \cong \frac{2}{3\pi RT}\omega R_1(\omega) \qquad (16)$$

with $\nu = \omega/(2\pi)$ and $\nu_0 = 1/(2\pi\tau_0)$. In words, plotting the right hand side of Equation (16) versus $RT(\ln(\nu_0/\nu)-0.48)$ yields a master curve which reveals the distribution $g(E)$. Here, the attempt frequency ν_0 is assumed to be constant for all E. Generally, we obtain ν_0 by bringing

measurements at different T and v to best overlap, as is the case in the master curve construction explained above. In cases when only one data set is at hand, we fix v_0 via the integration of Equation (16), making use of the normalization of $g(E)$. For this, K has to be taken from an independent experiment.

2. Glycerol

In this chapter we discuss ^{1}H and ^{2}H FC NMR data of glycerol. In the first section, we reanalyze ^{1}H FC NMR relaxation data from Gainaru et al.[19] to obtain a quantitative description. (Pub. 1) In the second section, we discuss the advantages and limitations of ^{2}H FC NMR regarding the paradigmatic liquid glycerol. (Pub. 2) Finally, we obtain a quantitative description of ^{2}H NMR relaxation data of glycerol by using the results of ^{1}H NMR solving a long-standing problem of NMR relaxation.

2.1. ^{1}H FC NMR - glycerol-h₈ (Pub. 1)

In this section we attempt a quantitative description of the ^{1}H spin-lattice relaxation of glycerol in a broad temperature range down to T_g. Glycerol is a common chemical compound. It was already discussed in the first papers on NMR relaxation by BPP.[1] Later, Noack used glycerol to demonstrate the capabilities of his multi-channel NMR covering 10 kHz - 120 MHz, which constitutes the best data of $R_1(\omega)$ so far.[45] His attempts to quantitatively describe the relaxation considering either inter- or intramolecular relaxation pathway failed.[45, 46] Zeidler performed an isotope dilution experiment to isolate the intramolecular R_1 of glycerol and was able to describe it with a CD spectral density.[47] In the late 90's, when a commercial FC NMR relaxometer became available, the Spinmaster FFC 2000 (STELAR, Italy), the relaxometry community had shifted its focus to different topics. Yet, testing the new relaxometer, Gainaru et al. reinvestigated glycerol.[19] Instead of discussing $T_1(T)$, as Noack had before, the attention was shifted toward the dispersion $T_1(\nu)$. Moreover, the susceptibility representation χ''_{NMR} was used to build a master curve of the NMR relaxation spectrum by applying FTS, revealing its bimodal structure that was not yet understood.[19] Later, the bimodality of $\chi''_{NMR}(\omega\tau)$ was explained with

the help of isotope dilution experiments, demonstrating the dominance of translational relaxation at low and rotational relaxation at high frequencies.[28]

We analyze the ^{1}H FC NMR data of Gainaru et al. by reconstructing the master curve $\chi''_{NMR}(\omega\tau)$ including temperatures down to T_g (cf. Figure 2.1. (a)).[19] The time constants used for the master curve construction nicely match with literature data for the rotational correlation time $\tau_{rot}(T)$ (c. f. Figure 2.1. (b)), yielding $\tau_{rot} \cong 10s$ at lowest temperatures.[33,35,48] The super-Arrhenius dependence of $\tau_{rot}(T)$ is reproduced by the phenomenological Vogel-Fulcher-Tammann equation (solid line). We show in the theoretical introduction that our subsequent analysis of χ''_{NMR} is not hampered by long correlation times, as observed here close to T_g (c.f. Chapter 1.1.).
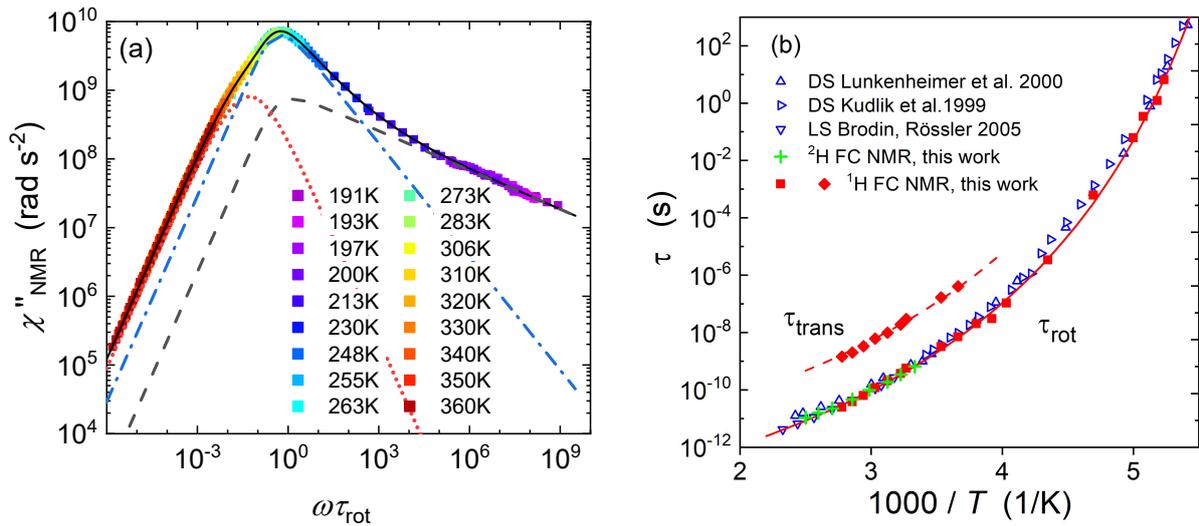

Figure 2.1. (a) Susceptibility master curve of glycerol-h8, temperatures indicated by color. The model Equation (11) was fitted to describe the data (solid line); individual relaxation contributions are given by dotted (translation), dashed (excess wing) and dash-dotted (rotation) lines. (b) Time constants of the overall reorientation of glycerol as given by our analysis of ^{1}H and ^{2}H FC NMR data (full symbols) as well as literature data from DS[33, 35] and LS[48]. Solid line gives interpolation with a Vogel-Fulcher-Tammann equation. Translational time constants are added.

As observed by Gainaru, the master curve yields a peak featuring a low frequency shoulder and two distinct high frequency regimes.[19] We describe the master curve in terms of the relaxation model Equation (11). The model relies on the assumption that the rotational parts of inter- and intra-molecular relaxation contributions differ neither in spectral shape, nor in their time constant, specifically $J_{rot}^{intra}(\omega, \tau_{rot}) + J_{rot}^{inter}(\omega, \tau_{rot}) \cong J_{rot}(\omega, \tau_{rot})$.

The rotational contribution dominates the peak and high frequencies of $\chi_{NMR}''(\omega\tau)$. The rotational dynamics in supercooled liquids are typically described with a CD spectral density.[32, 33] Our model introduces a second CD function for describing the excess wing, as done in LS.[49] Thus, the rotational behavior is modelled by a sum of two CD spectral densities; one for the main relaxation (dash-dotted line), one for the excess wing (dashed line). We note, that introducing a second CD changes the stretching exponent β_{CD} of the first CD function (cf. dash-dotted line). This is only possible when lowest temperatures are included in order to correctly take the excess wing into account. In contrast to earlier findings, using a second CD for the excess wing yields a temperature independent β_{CD}.[50]

The shoulder at low frequencies reflects translational dynamics described by the FFHS spectral density (dotted line). It has a lower amplitude than the rotational contribution. More importantly, the two processes are separated and $\tau_{trans}(T)$ is included in Figure 2.1. (b). We will come back to the separation later. The dominance of intermolecular relaxation contributions is reflected in an analysis independent of master curves or relaxation models by applying Equation (5); at low frequencies, the dispersion of $R_1(\nu)$ in liquids is governed by an universal square root law due to Fickian diffusion.[21-24] We extract the diffusion coefficient $D_{trans}(T)$ and find agreement with FG NMR data (c.f. Diamonds in Figure 3.2. (b)).[38]

In order to compare the present FC NMR results with literature data, we display $T_1(T)$ for different frequencies ν in Figure 2.2, the typical representation of conventional NMR data. Excellent agreement of Noack's data[46] and the present data was found for seven frequencies

(traces 4-11 in Figure 2.2. (a)). By the interpolation of $\tau_{rot}(T)$ (solid line in Figure 2.1. (b)), a model calculation along Equation (11) of $T_1(T)$ becomes possible and reproduces the present data (cf. solid lines in Figure 2.2.). Moreover, a prediction of Noack's dataset, which includes higher frequencies (up to $120\ MHz$), demonstrates the agreement of the data sets and the applicability of our approach.
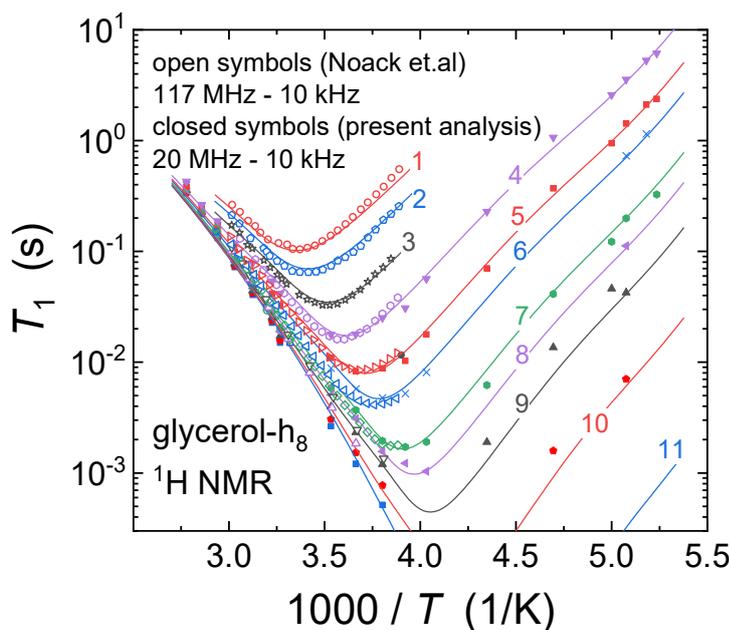

Figure 2.2. ^{1}H spin-lattice relaxation time at different frequencies as a function of temperature; present data (full symbols); data from Noack and coworkers (open symbols).[46] Solid lines: model predictions according to the master curve. Numbers 1-11 correspond to following Larmor frequencies in MHz: 117, 80, 40, 20, 10, 5, 2, 1.2, 0.5, 0.1, 0.01

One parameter makes the associated liquid glycerol (and its homologues[51]) special. The extent of separation of molecular rotation and translation given by the separation parameter $r = \tau_{rot}/\tau_{trans} \cong 56$. This isn't conform to the Stokes-Einstein-Debye (SED) relation, which predicts $r_{SED} = 9.$[3] The large r-value is connected with an anomalously small hydrodynamic radius R_H, which can be derived independently of the relaxation model by calculating D_{trans}/D_{rot}. Here, D_{trans} is given by the low frequency behavior of $R_1(v)$ and $D_{rot} = 1/6\tau_{rot}$

is given by the shift factors of the master curve construction. We find $R_H = 0.9$ Å compared to the van-der-Waals radius of the molecule $R_{vdW} = 2.7$ Å.[52] This is in agreement with findings by Chang and Sillescu, who used DS or shear viscosity together with field-gradient NMR to test the SED relation.[38] Here, ^{1}H FC NMR provides the unique possibility to access rotational as well as translational dynamics within one experiment.

In non-associated liquids like o-terphenyl or m-tricresylphosphate, for example, the bimodal structure of the susceptibility is hardly visible due to smaller r-values.[39,53] In those cases, it is challenging to determine the r-value and the coupling constant K_{trans} from the relaxation spectra. This may hamper interpretation of ^{1}H NMR spin-lattice relaxation data without further information provided from isotope dilution experiments. However, an isotope dilution experiment was carried out for OTP and results suggest the applicability of the suggested model also to non-associated liquids.[39]

As mentioned above, Chang and Sillescu tested the SED relation, $D_{trans}\eta/T$ and $D_{trans}\tau_{DS}$. In particular, they investigated it as a function of temperature for different molecular liquids.[38] They observed an increase in translational diffusion with respect to rotational diffusion and shear viscosity with decreasing temperature, close to T_g, which is a breakdown of the SED relation. Regarding glycerol, the situation Chang and Sillescu described was less clear. Yet, an increase at lowest temperatures close to T_g was identified, challenging FTS.[38] A further insight from FC NMR cannot be expected, as the desired D_{trans} cannot be evaluated for temperatures close to T_g along the square root law (5), because the low frequency limit is not covered experimentally.

Two remarks are noteworthy. First, Noack and BPP tried to work with a single relaxation pathway, either inter- or intramolecular relaxation. Second, the attempts using those models to describe the relaxation data only fail because of glycerol's large r-value ($r = \tau_{trans}/\tau_{rot}$), which motivated an isotope dilution experiment in the first place. At the same time, the

separation of dynamics helped to analyze and interpret the isotope dilution experiments.

Altogether, the proposed relaxation model captures all experimental relaxation features and was successfully applied to describe the master curve $\chi''_{NMR}(\omega\tau_{rot})$ over 15 decades of frequency (cf. solid line, Figure 2. 1. (a)). The parameters of the master curve description will be used in the next section to describe the ^{2}H NMR relaxation $T_1(\tau)$ in order to demonstrate the potential of our analysis.

While the master curve construction isn't necessary to apply the proposed relaxation model, it may help to come up with a fitting strategy by avoiding over-parameterization. More importantly, a brief overview of the relaxation behavior of a given system can be provided even in cases where no relaxation model is established, which fosters comparisons between different systems. The benefits of constructing master curves were demonstrated in pub. 4 for several cases: liquids, polymers and plastic crystals.

2.2. ^{2}H FC NMR - Glycerol-d$_5$ (Pub. 2)

The application of ^{2}H FC NMR to molecular liquids is interesting in itself, yet it is rarely done as there are many obstacles to overcome. To investigate the potential of this technique in soft matter, we measured several paradigmatic systems like glycerol, toluene, poly-ethylene-propylene and polybutadiene. The quadrupolar moment of ^{2}H interacts with an electric field-gradient (EFG), as it is induced by the charge distribution of the C-D bond, and the ^{2}H relaxation probes the bond reorientation.[3] Hence, organic molecular liquids can be studied without the interference of intermolecular relaxation contributions discussed above in the case of ^{1}H relaxation. Accordingly, ^{2}H NMR reduces the complexity of the analysis, reducing the number of necessary parameters.
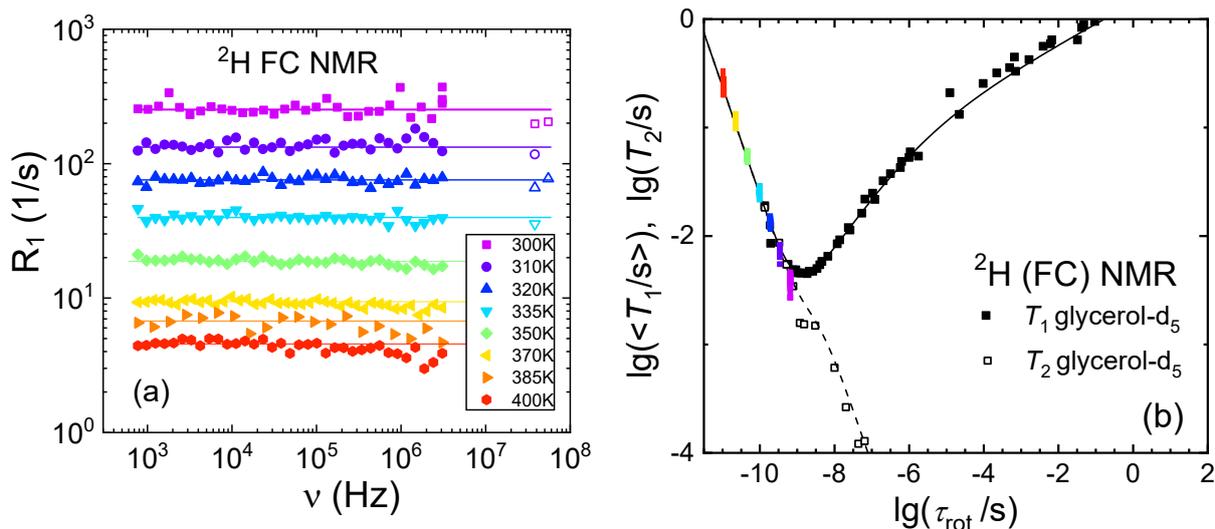
Figure 2.3. (a) ^{2}H spin-lattice relaxation rates of glycerol-d$_5$ from FC NMR (full symbols). For comparison high frequency NMR data are added (open Symbols, 55 MHz[54] and 38 MHz[55]). Horizontal lines guide the eye. (b) Mean deuteron spin-lattice relaxation time $<T_1>$ (colored symbols, this work; black full symbols, ref. 54) and spin-spin relaxation time T_2 (open symbols, ref. 54) of glycerol-d$_5$ as function of τ_{rot} (taken from ref. 33); solid lines: predictions for $<T_1>$ (solid line) and T_2 (dashed line) deduced from ^{1}H FC NMR master curve results (see text).

The ^{2}H FC NMR relaxation of glycerol-d$_5$, measured with the same relaxometer as the data above, is displayed in Figure 2.3. and reveals no dispersion. The signal-to-noise ratio is a major concern when working with detection fields of about 0.5 T (^{2}H detection frequency about 3 MHz). After expanding the upper limit of the frequency window to 55 MHz with the help of conventional high-field NMR from literature[54, 55] (open symbols) this doesn't change, yet we find good agreement with the present data. From the average rate, time constants are extracted using the quadrupolar coupling constant given by solid-state ^{2}H NMR[54]. The results for τ_{rot} agree with other techniques (cf. green pluses in Figure 2.1 (b)). We use the extracted time constants τ_{rot} to build a ^{2}H master curve (cf. Figure 7, Pub. 2). The shoulder observed in the ^{1}H FC NMR study for all the glycerol-h$_{3/5/8}$ is absent in ^{2}H NMR.[39] This demonstrates once

more, that the shoulder is related to intermolecular interactions, which is in line with the previous analysis. Moreover, the obtained master curve is compared to DS relaxation spectra, revealing a more or less universal $\chi''(\omega\tau_{rot})$ in the case of glycerol.[36]

Weak dispersion effects at high temperatures may be explained by technical difficulties (e.g. temperature drift during measurement time $t_{mes} \cong 14h$ at 400 K) or by physical reasons, e.g. hydrogen exchange as observed in water.[56]

Altogether, the results of ^{1}H and ^{2}H NMR suggest that FTS works well at least in the case of glycerol. Successful FTS implies ω and τ_{rot} are interchangeable variables. This is exploited in Figure 2.3. (b) where we plot ^{2}H spin-lattice relaxation data measured at 55 MHz (black symbols),[54] together with ^{2}H FC NMR data (colored symbols) versus τ_{rot} from an independent source (taken from DS) on a log-log scale.[33] The result resembles a reciprocal susceptibility $1/\chi''$, demonstrating that ω and τ_{rot} are indeed interchangeable.

The parameters used in the description of the rotational part of the ^{1}H master curve for glycerol-h$_8$ (cf. Figure 2.1. (a)) are reused to predict the ^{2}H (FC) NMR relaxation data (c.f. solid line in Figure 2.2. (b)). K_Q is calculated from the quadrupolar coupling constant $C_Q = 165$ kHz to replace the ^{1}H coupling constant.[57] The relative relaxation strength A_{ex}^{CD}/A_{rot}^{CD} of excess wing and main relaxation and the stretching parameters are taken from the analysis of the ^{1}H master curve. In conclusion, the prediction gives a quantitative interpolation of the ^{2}H data.

While the low signal-to-noise ratio remains a problem of ^{2}H FC NMR, it doesn't principally prevent measurements. In fact, it can be overcome by using a sample shuttling technique, where the NMR sample relaxes in the stray field of a cryo-magnet and is mechanically shuttled to a high detection field.[58] The sample shuttling technique would furthermore allow access to frequency-resolved $R_1(\nu)$, i.e. resolving the chemically different sites of a molecule. Electronic ^{2}H FC NMR allows access to site resolution, too. This was demonstrated in the case of liquid toluene-d$_8$, along its bi-exponential magnetization decay reflecting methyl and ring dynamics,

respectively. From this, the anisotropic reorientation can be discussed using ^{2}H FC NMR (cf. Appendix of Pub. 2).

On a different note, typical values for K_Q result in high spin-lattice relaxation rates, conflicting somewhat with the switching time of electronic FC ($t_{swt} \cong 3\ ms$), and even worse in sample shuttling experiments ($t_{swt} > 100\ ms$). In order to expect some dispersion, we should measure the minimum of $T_1(\tau)$. However, in the vicinity of the minimum, T_2 becomes very short, and causes an additional signal loss due to a short FID. Echo pulse techniques would help to overcome this limitation, yet, the successful implementation of an echo for such use cases remains a challenge because of phase instabilities in electronic FC relaxometers. It may be considered one of the most pressing limitations for the application of ^{2}H FC NMR to simple molecular systems (e.g. glycerol or toluene), whereas the slow rotational dynamics of polymers display dispersion (cf. Pub. 2 Figure 9).

Another problem inherent to ^{2}H NMR relaxometry concerns non-exponential magnetization decays close to T_g, or more generally in the solid-state, which makes analyses ambiguous.[57, 59] In contrast, ^{1}H relaxation remains exponential due to effective spin diffusion and thus can be analyzed as shown in section 1.1. and applied in section 2.1.. However, we demonstrate that ^{2}H relaxation can be interpreted consistently by the result of ^{1}H relaxometry up to $\tau_{rot} \leq 0.1\ s$ (cf. Figure 2.3. (b)).

3. Binary Mixtures of Liquids and the Ratio D_{trans}/D_{rot}

We already discussed the case of glycerol as an illustrative example with an extensive NMR history. In this subchapter we want to go one step further and apply the methodology established above (applying FTS to construct master curves which are described by the additive ansatz Equation (11)), to mixtures with glycerol. Instead of comparing isotherms, the construction of master curves allows to compare iso-frictional data, compensating for the well-known plasticizer effect, which speeds up the high T_g component upon mixing. Here, NMR offers the possibility of component selective investigation of the dynamics.
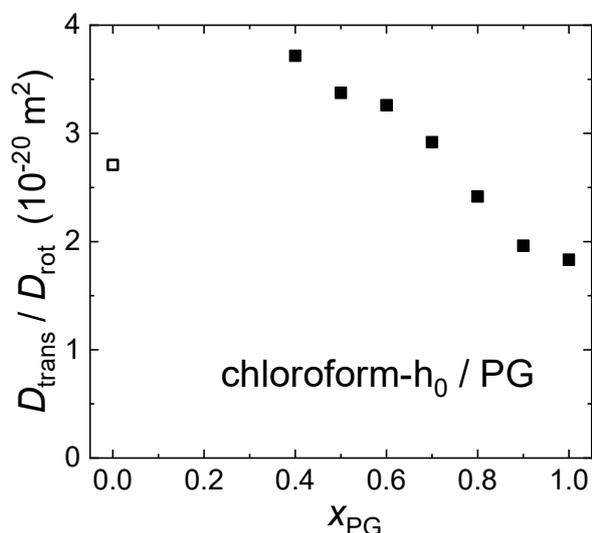
Figure 3.1. The ratio of diffusion constants D_{trans}/D_{rot} as a function of molar solvent concentration x for deuterated chloroform in PG. Data from FC NMR,[53] except $x_{PG} = 0$ (D_{rot} from DS[60] and D_{trans} from FG NMR[61]).

In a previous study it was shown that in an isotope dilution experiment (glycerol-h₅ in glycerol-h₀) the r-value of the neat system is conserved,[b] as expected.[28, 53] However, a systematic change of the r-value with molar concentration x was documented using propylene-glycol (PG) in the deuterated aprotic solvent chloroform-h₀. A decrease from $r = 35$ to 14 was observed with decreasing concentration $1 \geq x_{PG} \geq 0.6$, until no clear cut bimodal $\chi''_{NMR}(\omega\tau)$ was observed at $x_{PG} = 0.4$.[53] Additionally, the ratio $D_{trans}/D_{rot}(x_{PG})$ can be accessed independent of the model. We expect it to be proportional to r^{-1}. Indeed, the decline of $r(x_{PG})$ is accompanied by a continuous increase of $D_{trans}/D_{rot}(x_{PG})$ upon dilution (c.f. Figure 3.1.), which is linked to

---

[b] At the same time the plasticizer effect was small, yet non-negligible.

an increase of the hydrodynamic radius R_H becoming more physically reasonable in the diluted system. In the mixture, the dynamics of PG is sped up by several orders of magnitude, due to the plasticizer effect of chloroform. In contrast, the change in the spectral separation of translation and rotation, r, as well as in D_{trans}/D_{rot} is only around 2.

As demonstrated, glycerol displays a rather large $r = \tau_{trans}/\tau_{rot}$, which is connected to a pronounced bimodal structure of ^{1}H $\chi''_{NMR}(\omega)$. Hence, mixtures with glycerol promise the largest effect studying the dependence of the r-value on molar concentration x. To isolate the dynamics of glycerol in an isotope dilution experiment, the solvent should be available deuterated. Additionally, to avoid proton exchange, the solvent should be aprotic. Here, preliminary results of an unpublished study of glycerol-h5 in pyridine-h0 are presented alongside a study of glycerol in dimethyl-sulfoxide (Pub. 3).

3.1. DMSO in Glycerol: (Pub. 3)

In the following study we investigate the binary mixture of dimethyl sulfoxide (DMSO) and glycerol by means of DS and ^{1}H FC NMR. The dielectric relaxation strength is comparable for DMSO and glycerol $\Delta\epsilon_{gly} \approx \Delta\epsilon_{DMSO}$. Accordingly, the DS relaxation depends on the dynamics of both components. The spectra $\chi''_{DS}(\omega)$ do not change their shape with temperature or molar concentration x_{gly} and display a master curve (cf. Figure 1.1. (c)).[c] Accordingly, we apply FTS to construct master curves $\chi''_{NMR}(\omega\tau_{ro})$ in the case of ^{1}H FC NMR also (Figures 8 and 9 in Pub. 3). As expected, the extracted time constants change with molar concentration (cf. Figure 3.2. (a)). Upon dilution of glycerol, the plasticizer effect occurs, i.e. the rotational dynamics of (viscous) glycerol become faster when adding DMSO (cf. inset of Figure 3.1. (a)) because of the lower T_g of DMSO. A linear extrapolation of $\ln\tau_{rot}(x_{gly})$ to zero concentration provides

---

[c] Note in Pub. 3 we referred to x_{DMSO}. This was changed to x_{gly} for this work, in order to be in line with earlier work.

an estimate of the time constant of DMSO. Likewise, a linear extrapolation of $T_g(x_{gly})$ reveals T_g of DMSO and thereby the T_g contrast of the neat components $\Delta T_g \cong 39$ K.
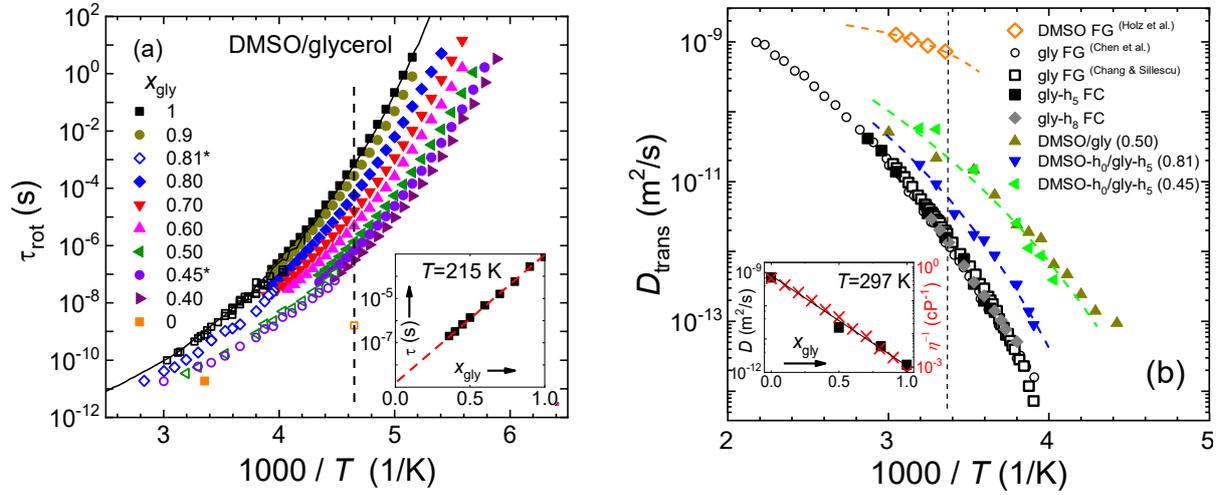

Figure 3.2. (a) Temperature dependence of the correlation time τ_{rot} for DMSO/glycerol mixtures as obtained by DS (full symbols) and by ^{1}H FC NMR relaxometry (open symbols) complemented by literature data for pure glycerol[62] and pure DMSO.[63] Inset: Dependence of DS correlation time with molar concentration at $T = 215$ K (dashed line: guide for the eye). (b) Diffusion coefficient $D_{trans,gly}$ for $x_{gly} = 0.81$ and 0.45 and $\widetilde{D}_{trans}$ for $x_{gly} = 0.50$ as measured by ^{1}H FC NMR; we added $D_{trans}(T)$ of pure glycerol (-h8 and –h5) obtained by FC NMR (full symbols)[50] as well as by FG NMR (open symbols)[38,64] and of pure DMSO obtained from FG NMR (open diamonds)[65]. Inset: Diffusion coefficient and reciprocal viscosity (taken from ref. 66) as a function of x_{gly} at room temperature (solid line: guide for the eye).

In an isotope dilution experiment of DMSO-h0 and glycerol-h5, ^{1}H FC NMR specifically accesses the dynamics of glycerol. Performing such experiments for concentrations $x_{gly} = 0.81, 0.45$ allows to extract the reorientational time constants of glycerol $\tau_{rot,gly}(T, x_{gly})$ in the mixture. No systematic discrepancy of $\tau_{rot,gly}$ and dielectric $\tau_{rot,DS}$ is found (cf. Figure 3.2. (a)), even though in the case of DS both components are detected. Therefore, we suggest that

glycerol and DMSO reorient on the same time scale. This is in contrast to other binary systems, such as quinaldine with toluene for example, where the relaxation decouples and two relaxation peaks are found in the dielectric relaxation spectrum (cf. Figure 4 (b) in Pub. 3).

Moreover, translational diffusion coefficients were extracted from ^{1}H FC NMR spin-lattice relaxation data analyzing the low-frequency square root law (cf. Equation (5)). The result is shown in Figure 3.2. (b), together with FG NMR literature data.[38,64,65] When both components are protonated ($x_{gly} = 0.50$), an effective diffusion coefficient $\widetilde{D}_{trans}$ is measured. The inset connects the translational diffusion coefficient with the shear viscosity, demonstrating $D_{trans} \propto 1/\eta$, as suggested by the SED equation.[66]

We further demonstrate in Pub. 3, that the quantitative description of all the master curves $\chi''_{NMR}(\omega\tau)$ is possible with a constant r-value ($r = 54$), i.e. no effects of decreasing separation of the dynamics are observed. Before, we connected the large r-value of glycerol to its three-dimensional hydrogen bond network. We find, that the r-value persists in the binary mixture DMSO/glycerol. Accordingly, we suggest that DMSO is incorporated into the hydrogen bond network of glycerol within the concentration range studied.

3.2. Pyridine-h$_0$ in Glycerol-h$_5$: (unpublished results)

Investigating glycerol-h$_5$/pyridine-h$_0$ mixtures with help of isotope dilution ^{1}H FC NMR experiments is an attempt to reaffirm the phenomenon concerning $D_{trans}/D_{rot}(x)$ found in a mixture of chloroform-h$_0$/PG (cf. Figure 3.1.).[53] In the following, we present the preliminary results of our study, which makes use of the large r-value of glycerol, hoping to increase the contrast of the ratios $\frac{D_{trans}}{D_{rot}}\left(x_{gly} = 0\right) / \frac{D_{trans}}{D_{rot}}\left(x_{gly} = 1\right)$ to demonstrate the effect more clearly.

The ^{1}H spin-lattice relaxation of glycerol-h$_5$ in pyridine-h$_0$ was measured for $198\,K < T <$

$333\,K$ and $0.2 \leq x_{gly} \leq 1$. From the dispersion of $R_1(\sqrt{\omega})$ at low frequencies, we obtain the translational diffusion coefficient $D(T, x_{gly})$ along Equation (5) (cf. Figure 3.3. (a)).[6] In Figure 3.3. (b) we demonstrate the linear dependence of $\lg D(x_{gly})$.
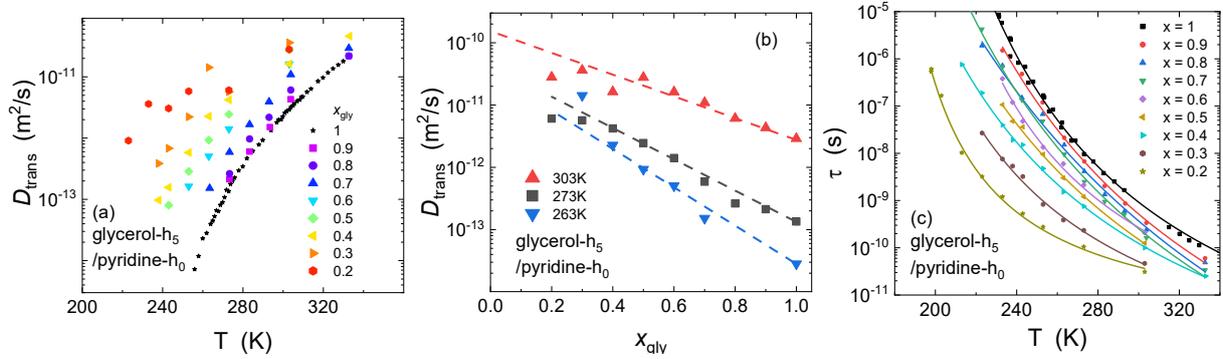

Figure 3.3. (a) Diffusion coefficient $D_{trans}(T)$ of glycerol in pyridine/glycerol mixtures (as determined from the low-frequency square root law of R_1) for different molar concentrations. For $x_{gly} = 1$ data from FG NMR[38] was added. (b) Diffusion coefficient of (a) versus molar concentration. (Dashed lines: guide for the eye.) (c) The temperature dependence of the rotational time constants τ_{rot} in the mixtures. Solid lines give interpolations with Vogel-Fulcher-Tammann equation.

Assuming FTS provides a master curve for each concentration (cf. Figure 3.4. (a)). The amplitude of the main relaxation decreases continuously with decreasing x_{gly} as the intermolecular relaxation contribution decreases along the spin density. The amplitude of the shoulder at low frequencies decreases even stronger, yet, from $0.5 > x_{gly} > 0.2$ the decrease is less pronounced. The apparent slope at high-frequencies (e.g. the broadening of the main relaxation) is independent of concentration (except for $x_{gly} = 0.3$, which was discarded from the quantitative analysis).

The time constants $\tau_{rot}(T, x_{gly})$ used to obtain the master curve, are shown in Figure 3.3. (c). The plasticizer effect is well recognized: the time constants become short upon adding pyridine.

We recognize a linear behavior of $\lg \tau(x)$ (cf. dashed line in the lower panel of Figure 3.4. (b)). Exemplarily extrapolating the time constants for $T = 303$ K to $x_{gly} \rightarrow 0$, we obtain an estimate for the correlation time at infinite dilution $\tau_{rot}(x_{gly} = 0) = 1.3 \cdot 10^{-11}$ s. The value is in fair agreement to results obtained by ^{2}H NMR for neat pyridine,[67] suggesting that a glycerol molecule in the mixture reorients together with the surrounding pyridine molecules. This behavior resembles the one of DMSO/glycerol mixtures, where we find no decoupling of the components' rotational dynamics. We note here, that the displayed time constants τ_{rot} are slightly changed with respect to time constants determined by peak picking, due to the model calculations used (see below).
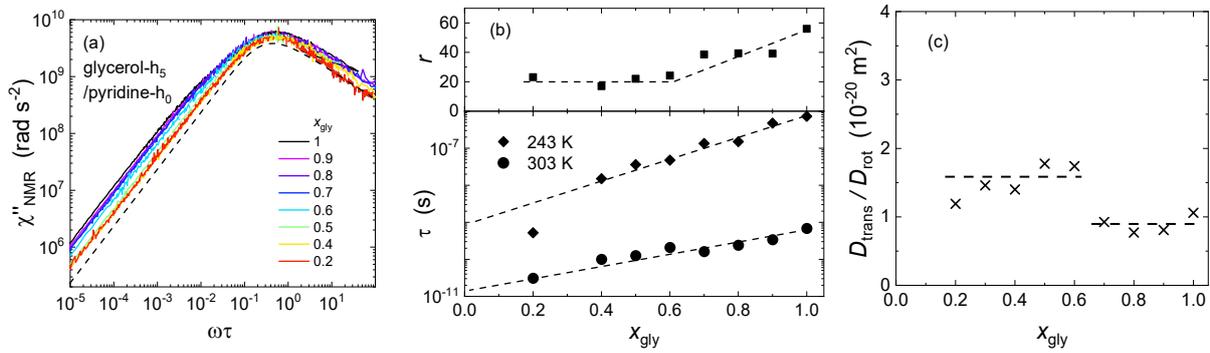

Figure 3.4. (a) Master curves $\chi''_{NMR}(\omega\tau)$ for glycerol-h5/pyridine-h0 (molar concentration x_{gly} indicated by color). Dashed line: CD function representing the rotational relaxation. (b) Lower and upper panel give r-values as extracted from fits to $\chi''_{NMR}(\omega\tau)$ and time constants extracted from the master curve construction as functions of x_{gl}. (Dashed lines: guide for the eye.) (c) The model independent ratio D_{trans}/D_{rot} as a function of x_{gly}. (Dashed lines: guide for the eye).

The time constants together with the translational diffusion coefficient allows to calculate the ratio $D_{trans}/D_{rot}(T, x_{gly})$ from a single experiment. The ratio turns out to be independent of temperature. The corresponding concentration dependence displays a step below $x_{gly} = 0.6$

from $D_{trans}/D_{rot} \cong 1 \cdot 10^{-20} m^2$ to $1.5 \cdot 10^{-20} m^2$ (cf. Figure 3.4. (c)). As for PG/chloroform and in contrast to DMSO glycerol, we find a systematic change of $D_{trans}/D_{rot}(x)$ here.[53]

The conclusions above were drawn without taking recourse to a specific relaxation model. Next, we specify a model to describe $\chi''_{NMR}(\omega\tau, x_{gly})$ quantitatively, despite the scatter of the data. We neglect heteronuclear $^1H - {}^2H$ relaxation and reuse the additive ansatz Equation (11) and adopt the model for an isotope dilution experiment. Explicitly we write

$$R_1 = K_{rot}(x_{gly})[J_{CD}(\omega) + 4J_{CD}(2\omega)] + K_{trans}(x_{gly}, d)\,[J_{FFHS}(\omega) + 4J_{FFHS}(2\omega)] \qquad (17)$$

with a single Cole-Davidson spectral density[32] for rotation and the FFHS spectral density[37] for translation. The coupling constants K_{rot} and K_{trans} are changing with concentration, as the density of protons (i.e. the spin density) changes. For infinite dilution, the translational coupling constant is zero by definition. Assuming that the distance of closest approach d doesn't change with x_{gly}, $K_{trans}(x_{gly}, d)$ is calculated along

$$K_{trans}(x_{gly}, d) = x_{gly} \cdot K_{trans,h5} \qquad (18)$$

where $K_{trans,h5} = 8.3 \cdot 10^8 Hz^2$ is extracted from the data of glycerol-h5 as published by Meier et al..[53] K_{rot} can be calculated along

$$K_{rot}(x_{gly}) = K_{intra,h5} + x_{gly}(K_{rot,h5} - K_{intra,h5}) \qquad (19)$$

The rotational coupling constant $K_{rot,h5} = 5.7 \cdot 10^9 Hz^2$ is extracted from the results from Meier et al., who performed an isotope dilution experiment, which also allows to access $K_{intra,h5} = 3.2 \cdot 10^9 Hz^2$.[53] All coupling constants were extracted by reanalyzing the data of Meier et al.[53] by applying model Equation (17), in order to provide consistent results within the present analysis.

The stretching parameter β_{CD}, describing the high frequency flank of the peak of $\chi''_{NMR}(\omega\tau)$, can be taken from the power law describing $\chi''_{NMR}(\omega)$ at low temperatures. The stretching

parameter $\beta_{CD} = 0.48 \pm 0.02$ is found to be concentration independent. The remaining parameters, the time constants $\tau_{rot}(x_{gly}, T)$[d] and the separation parameter $r(x_{gly})$ are determined by a least-square method. The model calculations (not shown) reproduce the individual master curves and the resulting parameters $\tau_{rot}(x_{gly})$ and $r(x_{gly})$ are displayed in Figure 3.4. (b).

The separation parameter $r = \tau_{trans}/\tau_{rot}$ decreases from 56 at $x = 1$ to 24 at $x = 0.6$, where it stays constant. This is in contrast to the previous study of DMSO/glycerol, where the data was described with a concentration independent r-value. Whereas the high value of r of glycerol was associated with its 3d hydrogen bond network, a separation $r \cong 25$ was reported in mono-alcohols.[68] Moreover, the overall trend of the r-value is consistent with the expectation put forth by $D_{trans}/D_{rot} \propto r^{-1}$.

In the community of associated liquids, the cluster size of hydrogen bonded molecules is an important result of simulations. The mapping of cluster size to experimental observables is desirable. The r-value certainly cannot provide a 1:1 mapping. Still, it seems to be a useful quantity to compare systems as above. A last concern regards the extraction of the r-value: it is not unambiguously possible to extract r from ^{1}H FC NMR data as long as the relaxation contributions do not show as two discernible maxima in χ''_{NMR}. Instead, r is correlated with the coupling constants, in particular K_{trans}.

---

[d] The model calculation introduces minor corrections ($< 10\%$) with respect to time constants given by the construction of master curves. Reported in Figure 3.3. (c) are time constants as given by the relaxation model.

4. Plastic Crystals

We understand plastic crystals (PCs)[e] as model systems for studying the glass transition phenomenon.[69-71] In contrast to structural glasses, they show positional order but orientational disorder. Provided that the transition to an orientationally ordered crystalline phase is avoided below the transition temperature T_t, i.e. super-cooling the PC phase, a progressive slow-down of the overall molecular reorientation is achieved. Finally, the orientational disorder can be arrested by cooling below the glass transition temperature T_g, yielding a so-called glassy crystal.[72,73] Many such systems were studied in the past using a variety of different techniques,[74-79] yet FC NMR studies are still rare.[75,80,81] The presence of some extent of cooperativity for the overall reorientation in PCs is the reason for regarding them as model systems for the glass formation. We draw a distinction between PC phases and rotor-phases. The latter is observed e.g. in solid benzene, where a 60° jump process is induced by the molecular symmetry. Such rotor phases lack a cooperative process and consequently do not serve as model systems for glasses.

In the PC phase, in addition to a cooperative process, we often observe single particle dynamics, which may dominate relaxation in the glassy crystal ($T < T_g$). This results in pre-averaged NMR spectra at higher temperatures.[82-84] The rotational potential varies spatially due to the orientational disorder of the molecules. Hence, the rotation is characterized by a distribution of activation energies $g(E)$. The resulting distribution of correlation times $G(\ln \tau)$ leads to pronounced dynamic heterogeneities which are reflected by two-phase spectra and non-exponential ^{2}H spin-lattice relaxation.[84] As will be demonstrated, FTS is violated in such cases.

---

[e] In the following we use the abbreviation PC for the term "plastic crystal" and "plastically crystalline" interchangeably.

Given the mechanism of reorientation by ^{2}H NMR, our ^{1}H FC NMR provides insight into the spectral density $J(\omega)$ of the dynamics. As in the case of liquids, we attempt a quantitative description.

Among other techniques, translational dynamics in PCs were addressed by FG NMR and radiotracer experiments;[85] first FC studies were published by Stapf and Kimmich[75] and by Kimmerle et al.[80] One of the PCs studied was cyclohexane.[75] Measuring the dispersion of the proton spin-lattice relaxation time in dilution with deuterated cyclohexane, the low-frequency dispersion was identified to be dominated by intermolecular relaxation, whereas the high-frequency part was interpreted as predominantly of intramolecular origin. From the low-frequency part the diffusion coefficient was extracted along the square root dispersion for three dimensional diffusion (cf. Equation (5)).[22] The values agreed well with those measured by FG NMR.
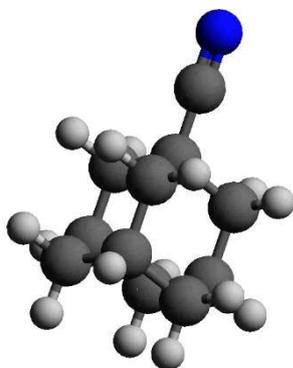

Figure 4.1. Ball and stick model of CNADA. (blue: N, black: C, grey: H)

The molecular structure of cyanoadamantane (CNADA) ($C_{11}H_{15}N$) is based on a globular adamantane cage to which a $C\equiv N$ group was added (c.f. Figure 4.1.). At room temperature it forms a PC phase and comes as powder with a melting point of $T_m = 462$ K.[81] Below the transition temperature $T_t = 280$ K we can circumvent crystallization, i.e. we supercool the PC phase.[81] Below $T_g = 170$ K we obtain a glassy crystal.[78]

Following previous work,[84,86] we dissect the rotational dynamics of CNADA in the PC phase into two distinct processes: a uniaxial jump rotation of 120° about the CN-axis and a slower isotropic 90° jump reorientation of the CN-axis, i.e. an overall reorientation of the molecule. While the uniaxial rotation reflects the symmetry of the molecule and can be performed independently of the other molecules' rotation, the 90° jump reorientation reflects the symmetry of the face centered cubic (fcc) lattice[87] and is

of cooperative nature[86].

4.1. Cyanoadamantane – High Temperature Regime (Pub. 4)

The ^{1}H spin-lattice relaxation data of CNADA, was measured from temperatures close to T_m down to temperatures below T_g, $153\,\mathrm{K} < T < 433\,\mathrm{K}$ in a frequency range $10\,\mathrm{kHz} < \nu < 30\,\mathrm{MHz}$. Limiting factors for the measurements are sublimation close to T_m as well as the high and low temperature limit of the relaxometer.

In a first step to analyze the spin-lattice relaxation data, we assume FTS and construct a master curve $\chi''_{NMR}(\omega\tau)$ regarding the main relaxation, including temperatures between $233\,\mathrm{K} < T < 433\,\mathrm{K}$ (cf. Figure 4.2. (a)). We attribute the relaxation peak to the (isotropic) overall reorientation. We observe deviations from a master curve at low frequencies as a consequence of vacancy diffusion as discussed by Amoureux et al.[83] At highest frequencies deviations appear due to the uniaxial rotation which will be discussed below. We compare the extracted time constants with corresponding correlation times in literature[78,86,88-90] in Figure 4.2. (b) (large symbols). We find essential agreement, an indication that FTS holds. We obtain an activation energy of $E_{iso} = 52\ kJ/mol$, in fair agreement with the value reported by Amoureux et al..[83]

We describe the relaxation peak $\chi''_{NMR}(\omega\tau)$ with a CD spectral density ($\beta_{CD} = 0.83$, cf. dashed line in Figure 4.2. (a)) to account for the weak non-Lorentzian behavior, typical for collective overall reorientation of a molecule. This is in agreement with a DS[78] and a ^{2}H NMR study[86] reporting a stretched exponential correlation function. The underlying non-exponential correlation function sets our analysis apart from the work of Amoureux et al., who assumes exponentiality.[83] We compare the coupling constant $K = 1.78 \cdot 10^9 s^{-2}$, obtained by describing the master curve, to the second moment $\Delta M_{2,iso}$ deduced from CW NMR measurements of Amoureux et al. via $\Delta M_{2,iso} = 1.5 \cdot K\gamma^{-2}$.[83] We observe a deviation of 20%.
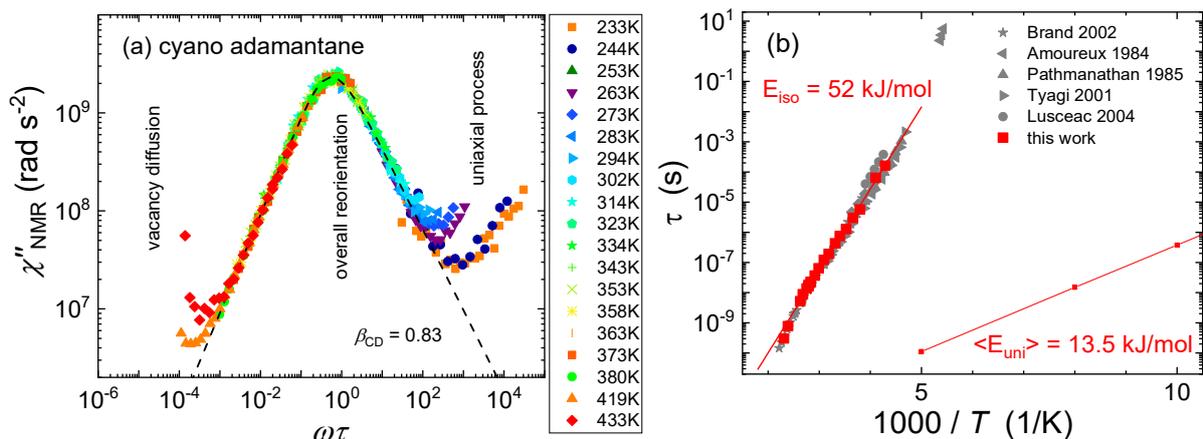
Figure 4.2. (a) Susceptibility master curve $\chi''_{NMR}(\omega\tau)$ of CNADA. Different colors indicate temperatures; a Cole-Davidson (CD) function (dashed line) describes the peak; relaxation processes are indicated. (b) Time constants of the overall reorientation are shown; the Arrhenius law with an activation energy $E_{iso} = 52$ kJ/mol is displayed; for comparison, literature data from several sources are included.[78,86,88-90] Additionally, the most probable time constant of the uniaxial reorientation is displayed together with its Arrhenius behavior (see text).

4.2. Cyanoadamantane – Low Temperature Regime (Pub. 5)

Next, we turn our attention to the analysis of the low-temperature ^{1}H spin-lattice relaxation rate, in the region $4 \gtrsim 1000$ K $/ T$ (cf. Figure 4.3. (b)). Here we include FC NMR as well as conventional high-field NMR data[91,83] and observe a second minimum. It is solely determined by the uniaxial 120° jump rotation of the CNADA molecule about the CN axis. The uniaxial rotation is reflected in deviations from the master curve at high frequencies (cf. Figure 4.2. (a)). We know from a ^{2}H NMR study that the reorientation in the glassy crystal, i.e., below $T_g = 170$ K, is described by a broad distribution of correlation times $G(\ln \tau_{uni})$ reflecting heterogeneous dynamics.[84] The reorientation is determined by a single activation energy at a given site in the glassy crystal. Due to the disordered spatial distribution of the orientation of

cyano groups, the local potentials vary, and we assume a distribution of activation energies $g(E)$ independent of temperature. However, the resulting distribution $G(\ln \tau_{uni})$ is not temperature independent, it broadens with $1/T$ along Equation (12).
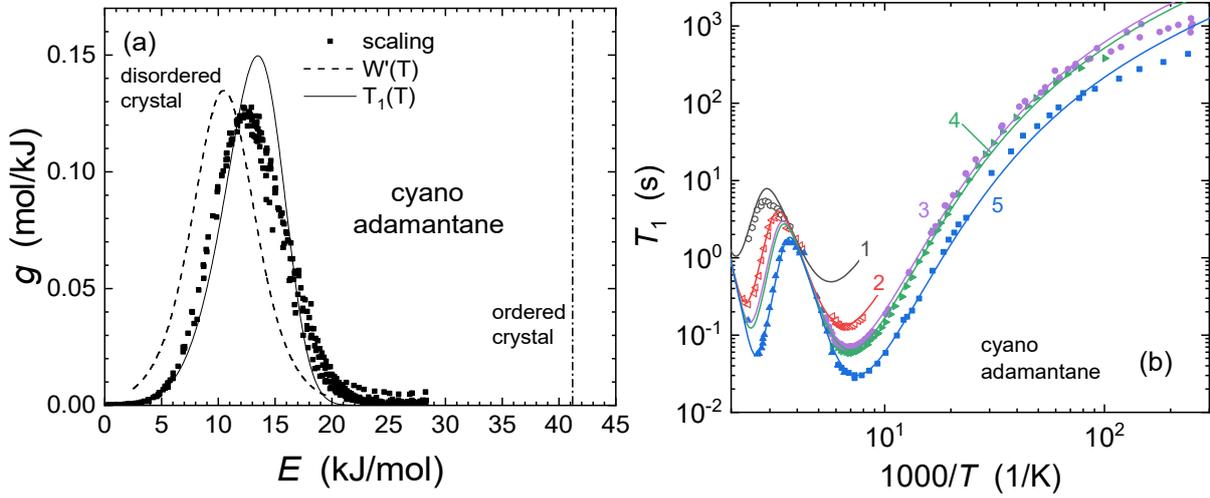

Figure 4.3. (a) Distribution of activation energy $g(E)$ of the uni-axial reorientation of CNADA. For comparison, we added the delta distribution of the ordered crystal (dash-dotted line).[84] (b) Proton relaxation time of CNADA as a function of reciprocal temperature in a double-log plot; solid lines: calculation including overall reorientation and uni-axial rotation (see text). Numbers 1-5 correspond to frequencies in MHz: 400,[83] 100[83], 54.15,[91] 46.06,[91] and 20.5[91].

Consequently, FTS does not apply. However, a master curve can be constructed by appropriately compensating the broadening with $1/T$, an approach well established in DS.[40] The sum of two spectral densities appearing in the BPP Equation (1) leads to a shift of $-0.48RT$ in Equation (16). Explicitly, we plot $\frac{2}{3\pi RT}\omega\langle 1/T_1(\omega)\rangle$ versus $RT(\ln(v_0/v)-0.48)$. We choose the attempt frequency $v_0 = \frac{1}{2\pi\tau_0}$ such that the second moment obtained by integrating $g(E)$ conserves the ratio of the second moments $\Delta M_{2,iso}/\Delta M_{2,uni}$ calculated by Amoureux et al. within a Frenkel model.[83] Here, $\Delta M_{2,iso} = 3.75 \cdot 10^{-8}$ T^2 is taken from the high temperature

T_1 analysis. The resulting value reads $\tau_0 = 3.3 \cdot 10^{-14}$ s. We show in Figure 4.3. (a) the such obtained master curve, which provides a first estimate of the distribution $g(E)$ (black points).

A more advanced analysis of $T_1(T)$ follows Equation (13) and attempts to find a distribution of activation energies $g(E)$, which simultaneously describes the low temperature relaxation data for all frequencies in Figure 4.3. (b). As discussed above, the choice of τ_0 influences the extracted value of the associated second moment $\Delta M_{2,uni}$. Correspondingly, it influences the height of the minimum of $T_1(T)$. In addition, the low-energy flank $\lim_{E \to 0} g(E)$ sensitively determines $T_1(T)$ at lowest temperatures (see Figure 1 of Pub. 5). At high temperatures $T > 170$ K, relaxation by the overall reorientations interferes. In order to proceed, we take the second moment $\Delta M_{2,uni} = 14.8 \cdot 10^{-8}$ T^2 and $\tau_0 = 3.3 \cdot 10^{-14}$ s as for the scaling analyses above. A slightly left skewed Gaussian distribution allows to reproduce the T_1 data down to about $10 - 30$ K in Figure 4.3. (b), where we include the overall reorientation as additive contribution (cf. solid lines). The derived distribution $g(E)$ is included in Figure 4.3. (a) (solid line) essentially demonstrating agreement with the data from the scaling procedure (full squares). Moreover, the analysis of two-phase spectra is included in Figure 4.3. (a) (dashed line), which provides $g(E)$ independent of spin-lattice relaxation, also demonstrating agreement (see also Pub. 5).

Subtle enhancement of $g(E)$ on the low-energy flank (about 1 ‰ of the amplitude) would provide even better agreement with $T_1(T)$ at low temperatures. Yet, such tiny changes would not be discernible in Figure 4.3. (a). Also, we cannot exclude that paramagnetic impurities control the relaxation at lowest temperatures, although the samples were carefully degassed. The activation energy in the PC phase is significantly lower than in the orientationally ordered phase (cf. dash-dotted line in Figure 4.3. (a)), where a single activation energy describes the uniaxial rotation. On a different note, the evolution of $G(\ln \tau_{uni})$ becomes extremely broad at low temperatures (cf. Figure 6, Pub. 5), as expected for the thermally activated process in a PC.

The corresponding most probable time constant τ_{uni} is plotted in Figure 4.2. (b), providing its activation energy $\langle E_{uni} \rangle = 13.5$ kJ/mol. We also establish a second example where a conflict of previous formulations of the Redfield-limit exist, as $T_1 > \tau$ doesn't hold for all τ of $G(\ln \tau)$, yet, no indication of a violation of the Redfield-limit is observed as expected within our reformulation of the Redfield-limit Equation (4).

4.3. Three Other Plastic Crystals (unpublished results)

In this section we document preliminary results obtained from ^{1}H FC NMR relaxometry data of cyano cyclohexane (CNCH), 1,4-Diazabicyclo[2.2.2]octane (DABCO) and m-carborane for later use in publications.
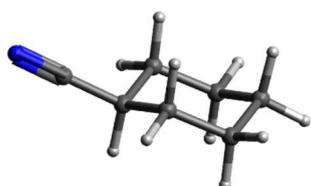
Figure 4.4. Ball and stick model of CNCH (blue: N, black: C, grey: H)

CNCH: The molecular structure of CNCH ($C_6H_{11}CN$) is based on a cyclohexane ring, to which a CN group was added (cf. Figure 4.4.). In contrast to other systems studied in this chapter, CNCH is considered a non-rigid molecule which shows rich polymorphism.[92,93] Axial and equatorial conformations of CNCH are equally populated in the liquid (as well as in the PC phase), and the energy barrier for the interconversion is $\Delta E = 34$ kJ/mol.[93] It forms a PC with a fcc lattice below $T_m = 285$ K.[94] In the PC phase, the quadrupolar coupling is averaged to zero and it was concluded, that the molecules perform an overall reorientation in the PC, with small and large angular jumps – resembling a liquid.[79] The reorientation slows down upon cooling and a glass transition occurs at $T_g = 135$ K which can only be observed by avoiding a transition to the orientationally ordered phase which may occur below $T_t = 217$ K. [94,95]

We collect ^{1}H spin-lattice relaxation data and transfer it to the susceptibility representation $\chi''_{NMR}(\nu)$ (cf. full squares in Figure 4.5. (a)). As an example, we compare the susceptibilities of

^{1}H FC NMR $\chi''_{NMR}(\nu)$ and DS $\chi''_{DS}(\nu)$ of CNCH measured at essentially the same temperature in Figure 4.5. (a). As both techniques display a maximum at virtually the same frequency, we conclude the relaxation is modulated by the same dynamical process, namely the overall reorientation of the molecule.[79,93] CD functions interpolate the relaxation in both cases (cf. solid lines in Figure 4.5. (a)). On a different note, the stretching parameter β_{CD} differs by a factor of 2, a fact which was also observed in liquids (cf. Pub. 3) and is not yet fully understood.

We assume FTS and construct a master curve including temperatures $172 \text{ K} < T < 273 \text{ K}$. We depict the result in Figure 4.5. (b), where the maximum for the overall reorientation can be observed. Moreover, deviations from a master curve are observed at high and low frequencies, which is evocative of $\chi''_{NMR}(\omega\tau)$ of CNADA (cf. Figure 4.2. (a)). We compare the shift factors used for the master curve construction with the corresponding correlation times τ from ^{2}H NMR[79] and DS[96] in Figure 4.5. (c). The agreement of the techniques is an indication for the applicability of FTS. Also, we take this as a second confirmation that the main relaxation indeed is governed by the overall reorientation of the molecules, as it follows from the ^{2}H NMR study.[79] Time constants from DS of a secondary process are included for completeness.[78,] Overall, a super-Arrhenius behavior is observed which can be described by a phenomenological Vogel-Fulcher-Tammann equation (solid line in Figure 4.5. (c)). At high temperatures, an apparent activation energy of the time constants can be given $E_a = 40 \text{ kJ/mol}$ (dotted line). We note, that it is somewhat higher than the energy barrier of the interconversion of axial and equatorial conformation $\Delta E = 34 \text{ kJ/mol}$.[93] Finally, in the melt $1000\text{K}/T < 3.51$, the correlation times as measured by LS (open triangles) become significantly shorter as expected.[97]
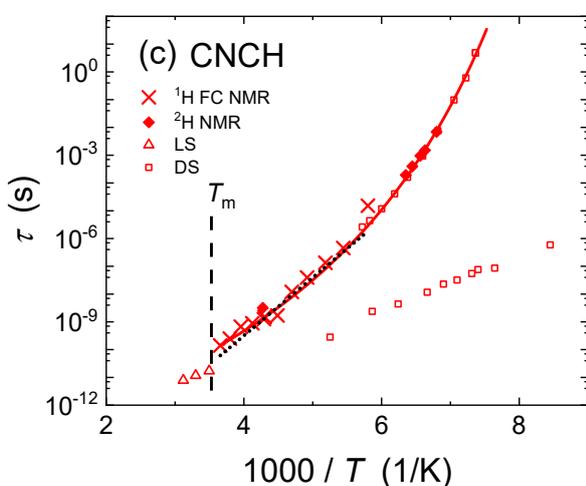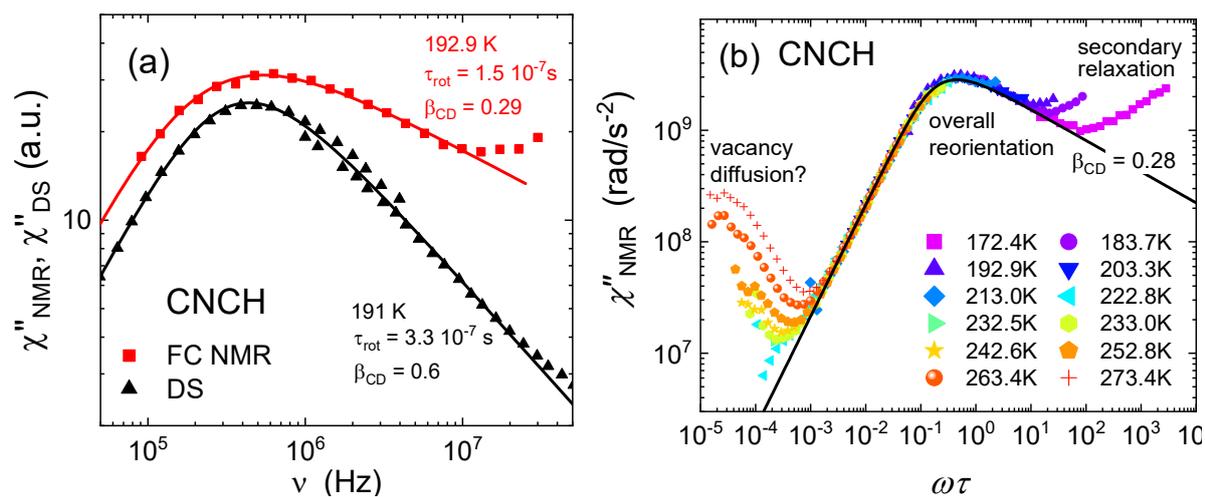
Figure 4.5. (a) A comparison of $\chi''(\nu)$ for CNCH as measured by ^{1}H FC NMR and DS[96] (temperatures indicated). (b) Susceptibility master curve of CNCH, covering 172 K < T < 273 K. A CD function (solid line) describes the peak. (c) Time constants from the master curve construction are shown; the Arrhenius law with an activation energy $E_a = 40$ kJ/mol is displayed (dotted line); literature data from DS[96] (open squares), LS[97] (open triangles) and ^{2}H NMR[79] (full diamonds) are included together with a Vogel-Fulcher-Tammann function graph obtained by a global fit (solid line).

The master curve is described by a CD spectral density using a stretching parameter $\beta_{CD} = 0.28 \pm 0.06$ and coupling constant $K = (2.3 \pm 0.3) \cdot 10^9$ s^{-2} (cf. solid line in Figure 4.5. (b)). In particular we find $\beta_{CD} < 1$, as expected for a cooperative process and stronger than in CNADA ($\beta_{CD,CNADA} = 0.83$). We interpret deviations from the CD spectral density at high frequencies as a consequence of a secondary relaxation process, which is also observed by DS[96] and ^{2}H NMR[79]. It appears to have a larger relaxation strength compared to the overall reorientation in ^{1}H NMR. The opposite is true for DS, where it accounts to roughly 2 % of the

relaxation.[96] We conclude, that the relative amplitudes of main and secondary relaxation are different in DS and ^{1}H NMR. Finally, we interpret the deviations at low frequencies as a third process. In analogy to CNADA, we suspect the relaxation to be modulated by vacancy diffusion, assuming the relaxation is determined by dynamics. The maximum appears to grow with increasing temperature. We are not aware of a relaxation model specifically suited to this case.
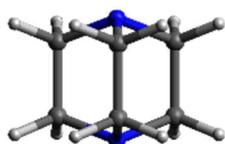

Figure 4.6. Ball and stick model of DABCO (blue: N, black: C, grey: H)

DABCO: In Figure 4.6., we see the globular cage structure of DABCO with the chemical formula $C_6H_{12}N_2$ (also known as triethyl-diamine, TEDA). It melts above $T_m = 433$ K,[98] below it crystalizes into a fcc lattice with four molecules per unit cell, forming a PC, in which the molecules perform an overall reorientation.[98,99] In contrast to the previous systems, we didn't supercool the PC phase. Instead, we investigated the orientational ordered hexagonal closed packed (hcp) crystalline phase occurring below $T_t = 351$ K. There, the molecules are known to perform a single particle uniaxial 120° jump rotation[f] about their N-N axis, which superimposes a slower wobbling of the N-N axis.[100] What is known about the dynamics of DABCO is largely due to the thorough analysis of comprehensive ^{1}H linewidth data from Smith.[100]

This motivates us to investigate the ^{1}H linewidth as measured with our commercial FC NMR relaxometer as an instructive example. Of course, electronic FC instruments weren't designed with linewidth experiments in mind. However, recording the entire FID comes at no additional cost and may provide qualitative insights. We measure the FID after a single 90° radio-frequency pulse ($t_p = 7$ μs), and Fourier transform its real part after phase correction to obtain a spectrum. In Figure 4.7. (a) we display the full width at half maximum $FWHM(T)$ (full squares), and compare it to ^{1}H linewidth measurements by Smith.[100] The linewidth shows a

---

[f] Because of the molecules high symmetry, also 60 ° jumps are debated in literature.

plateau at low temperatures. It drops to a smaller shoulder which disappears for higher temperatures, where a second plateau is established. Above T_t the linewidth is abruptly narrowed, until all dipolar coupling is averaged out at highest temperatures. We capture those temperature trends in their detail. However, we fail to reproduce the absolute scale by a factor $\cong 1.5$. Consequently, a quantitative analysis of the measurement is of no use at the current stage. Nonetheless, monitoring the FID in FC NMR helps monitoring a strong drop of the line shape due to the motion in the new fcc phase. Moreover, it uncovers a small shoulder, which reflects the slowdown of the wobbling motion ($T \cong 250$ K). At about $FWHM \geq 30$ kHz ($T \leq 213$ K), the FID is lost during dead time $t_{dead} \cong 3 - 15$ µs. As echo pulse techniques aren't available to refocus the FID, the applicability of FC NMR is limited to rather narrow spectra. Moreover, quantitative analysis of the data is not possible. We note, that also a homebuilt FC NMR relaxometer fails to quantitatively reproduce conventional ^{1}H linewidth measurements.[101] Finally, Smith observed a small wing in the CW spectra for 250 K $< T < 300$ K, which he assigned to a second linewidth.[100] Such spectral details weren't resolved in our measurements.
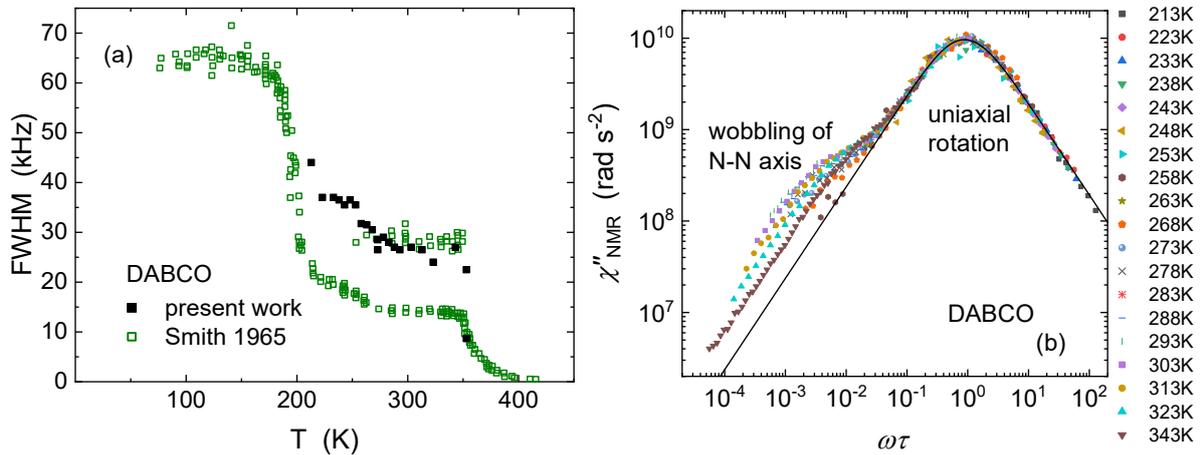

Figure 4.7. (a) FWHM of DABCO from ^{1}H FC NMR (full squares) are plotted versus temperature. For comparison, linewidth data of Smith[100] were added. (b) The susceptibility master curve of DABCO in the hcp phase is displayed, including $213K < T < 343K$. A Debye spectral density (solid line) was added to describe the relaxation peak ($\beta_{CD} \equiv 1$).

Next, we discuss the ^{1}H spin-lattice relaxation of DABCO in the hcp phase. We again transfer the data to the susceptibility representation and attempt to construct a master curve $\chi''_{NMR}(\omega\tau)$ by assuming FTS (243 K $< T <$ 343 K). We assign the peak of $\chi''_{NMR}(\omega\tau)$ displayed in Figure 4.7. (b) to the uniaxial 120° jump rotation. We describe the main relaxation with a CD function with $K_{uni} = 6.8 \cdot 10^9$ s^{-2} and $\beta_{CD} = 1$, i.e. the corresponding correlation function is an exponential function, as expected for a process induced by molecular symmetry. In contrast to the data of CNADA, the present data show no indication for dynamic heterogeneity (cf. chapter 4.2.). We observe no deviations of the master curve at high frequencies in contrast to CNADA and CNCH, while at low frequencies a shoulder appears (see below). We interpret the shift factors of the master curve construction as time constants, displayed in Figure 4.9. (b) (green x). They display an Arrhenius temperature dependence (straight line) with an activation energy of $E_a = 35$ kJ/mol in good agreement with reports by Smith, $E_a = (30 \pm 5)$ kJ/mol (deduced from ^{1}H linewidth data).[100]

As mentioned before, in the hcp phase we observe an additional low frequency shoulder in $\chi''_{NMR}(\omega\tau)$, i.e. a relaxation process slower with respect to the uniaxial rotation (cf. Figure 4.7. (b)). We assign it to the next slower dynamical process, i.e. the wobbling of the N-N axis described by Smith.[100] In order to obtain a better understanding of the relaxation process, we go back to the susceptibility $\chi''_{NMR}(\omega)$ (cf. Figure 4.8. (a)). We isolate the shoulder by subtracting the contribution of the uniaxial rotation $\chi''_{NMR,uni}(\omega)$, which is given by the CD function (dashed line). Explicitly we write $\chi''_{NMR,wobble}(\omega) = \chi''_{NMR}(\omega) - \chi''_{NMR,uni}(\omega)$. $\chi''_{NMR,wobble}(\omega)$, which is isolated in this process, is depicted in Figure 4.8. (b), where we observe that the amplitude of the peak grows with increasing temperature, until it stabilizes at high temperatures $T > 290$ K. Besides, the peak appears to shift in frequency. This peculiar behavior of the relaxation strength is not fully understood. Moreover, we find no indication of a stretched high frequency flank.

Next, we attempt a quantitative description of the total relaxation $\chi''_{NMR}(\omega)$ with two additive contributions. The first contribution is due to the uniaxial rotation where we fix all parameters by the master curve description. The second relaxation contribution is approximated by a second CD with $\beta_{CD} = 1$. We fix the apparent coupling constant at high temperatures, $T > 290$ K at $K_{wobble} = 2.5 \cdot 10^8$ s^{-2} (cf. Figure 4.8. (d)). As a consequence, the spectral separation $r_{wobble} = \tau_{wobble}/\tau_{uni} \cong 170$ decreases at $T > 290$ K (cf. Figure 4.8. (c)). In total, we obtain a model calculation interpolating $\chi''_{NMR}(\omega)$ (solid lines in Figure 4.8. (a)). The resulting time constants τ_{wobble} are included in Figure 4.9. (b) (blue x). The temperature dependence $\tau_{wobble}(T)$ is more or less parallel to $\tau_{uni}(T)$.
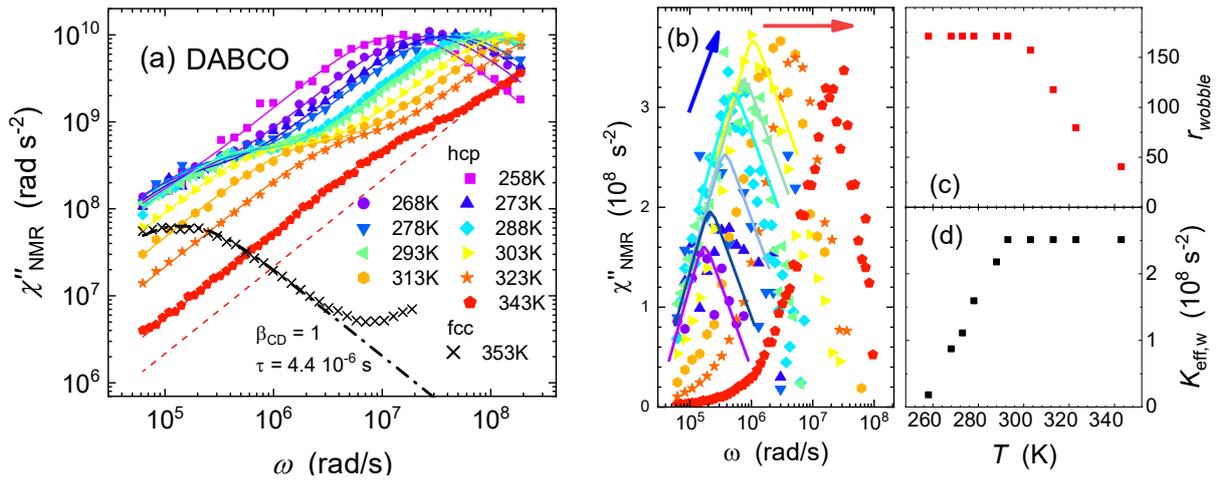

Figure 4.8. (a) ^{1}H NMR susceptibility of DABCO versus Larmor frequency ω in the ordered crystal (hcp) phase and PC (fcc) phase (258 K $\leq T \leq 353$ K). The dashed line is the prediction of the master curve at $343K$. Solid lines: description with a relaxation model. (b) Isolated relaxation contribution $\chi''_{NMR,wobble}(\omega)$ (see text). Arrows and solid lines are guides for the eye. (c) and (d) show the temperature dependence of the model parameters $r_{wobble}(T)$ and $K_{eff,w}$.

Additionally, we check the relative relaxation strength of the two processes. We calculate the ratio of the coupling constants $K_{wobble}/K_{uni} \cong 3\,\%$ and compare it with the ratio $\Delta M_{2,wobble}/\Delta M_{2,uni} \cong 10\%$ using the corresponding plateau values according to Smith.[100] In

other words, in both cases the strength of the wobbling motion is weak compared to the uniaxial rotation. We take into account the rather large uncertainty with which $\Delta M_{2,wobble}$ is extracted and conclude that the ratios are in fair agreement.

Finally, at the highest temperature measured, $T = 353$ K, we enter the fcc PC phase, accompanied by a jump of $T_1(T)$ as well as of $FWHM(T)$. We find a maximum of $\chi''_{NMR}(\omega)$ (cf. Figure 4.8. (a)), again. It occurs at lowest frequencies, and is ascribed accordingly to the next slower dynamical process, i.e. the (isotropic) overall reorientation of the molecule.[100] The maximum can be described by a CD spectral density with $K_{iso} = 4.5 \cdot 10^7 s^{-2}$ and $\beta_{CD} = 1$. The extracted time constant $\tau_{iso} = 4.4 \cdot 10^{-6}$ s is included in Figure 4.9. (b) (red x). It agrees with results from ^{1}H linewidth measurements, supporting our assignment of the relaxation to the overall reorientation.[100]
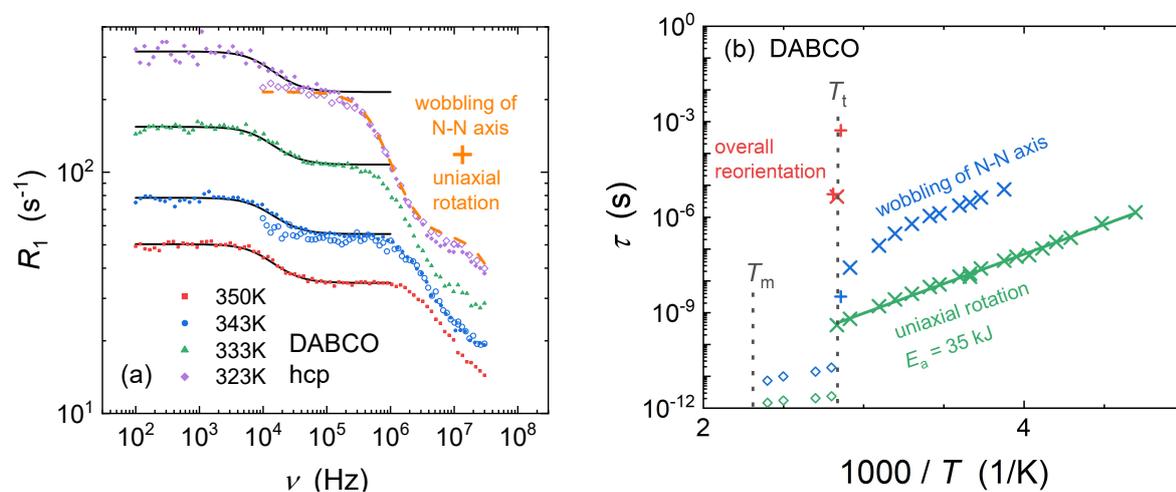

Figure 4. 9. (a) ^{1}H spin-lattice relaxation of DABCO in its hcp phase as measured by FC NMR in Darmstadt (full symbols) and Bayreuth (open symbols). Solid lines show calculation for the additional relaxation (see text). (b) Time constants for overall reorientation (red), the wobbling of the N-N axis (blue) and the uniaxial reorientation (green) as extracted from ^{1}H FC NMR data (x), together with literature data from QENS[98] (open diamonds) and from ^{1}H linewidth[100] (+). A solid line yields the activation energy $E_a = 35$ kJ/mol for uniaxial reorientation.

Smith speculates, that the overall reorientation of the molecule also takes place in the hcp phase, yet slowed down (cf. Figure 4.9. (b)).[100] He argues, that the slowdown takes place because of decreased free volume in the hcp phase. He estimated the correlation frequency to be a few hundred Hz. We then would expect another shoulder in Figure 4.8. (a). Hence, we looked for traces of an additional relaxation process in the hcp phase measuring $R_1(\omega/2\pi)$ in a broad frequency range 100 Hz $\leq \omega/2\pi \leq$ 30 MHz, using a home built relaxometer in Darmstadt (cf. full symbols, Figure 4.9. (a)).[13-15] No deviations with respect to the measurements with the commercial relaxometer in Bayreuth are found (cf. open symbols, Figure 4.9. (a)). The model calculation reflecting the uniaxial rotation and the wobbling about the N-N axis is shown for $T = 323$ K (dashed line). Below some kHz, an additional step in the relaxation dispersion appears, which seems not to shift with temperature. Its stretching parameter is concealed by the relaxation plateau of the wobbling motion. Hence, we set $\beta_{CD} = 1$ and describe the process with a temperature independent correlation time $\tau = 6.8 \cdot 10^{-6}$s, (cf. Figure 4.9. (b)). As a consequence, the process's amplitude decreases from $K_{eff} = 3.0 \cdot 10^6$ s^{-2} at 323 K to $0.46 \cdot 10^6$ s^{-2} at 350 K. At first glance it is tempting to assign the additional relaxation to yet another dynamical process. However, the behavior of $\tau(T)$ as well as K_{eff} is rather atypical for a relaxation governed by dynamics. Moreover, in the solid hcp phase the interpretation of R_1 may be hampered when the local field is of the same order of magnitude as the external field.[58] A more thorough analysis of the data is of interest but beyond the scope of the present work. We only note here, that it may help to test the adiabicity of the field cycle by varying the slew rate, i.e. the velocity with which the external magnetic field is switched (in our case 10 MHz/ms).[58] It is possible that zero-field coherences may be observed.
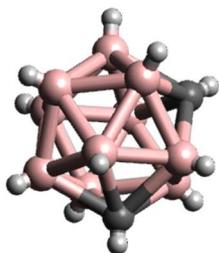
Figure 4. 10. Ball and stick model of m-carborane. (pink: B, black: C, grey: H)

m-carborane: The icosahedral molecular structure of m-carborane ($B_{10}C_2H_{12}$) is shown in Figure 4.10. Below its melting point $T_m = 546K$ it crystallizes into a plastically crystalline fcc phase.[102] The ^2H NMR spectra show a narrow Lorentzian line, indicating a fast[g] overall reorientation of the molecule.[103] Below the solid-solid phase transition of m-carborane, around $T_t \cong 285\,K$, an orthorhombic unit cell forms.[103] It was shown that an anisotropic rotation in the orthorhombic phase occurs, which is neither C2 nor C5 uniaxial rotation. Instead, a tilt and jump model was proposed for describing the extensive ^2H NMR data.[104] In the present study, we investigate m-carborane above $T = 165\,K$, below which another phase transition occurs.[102]
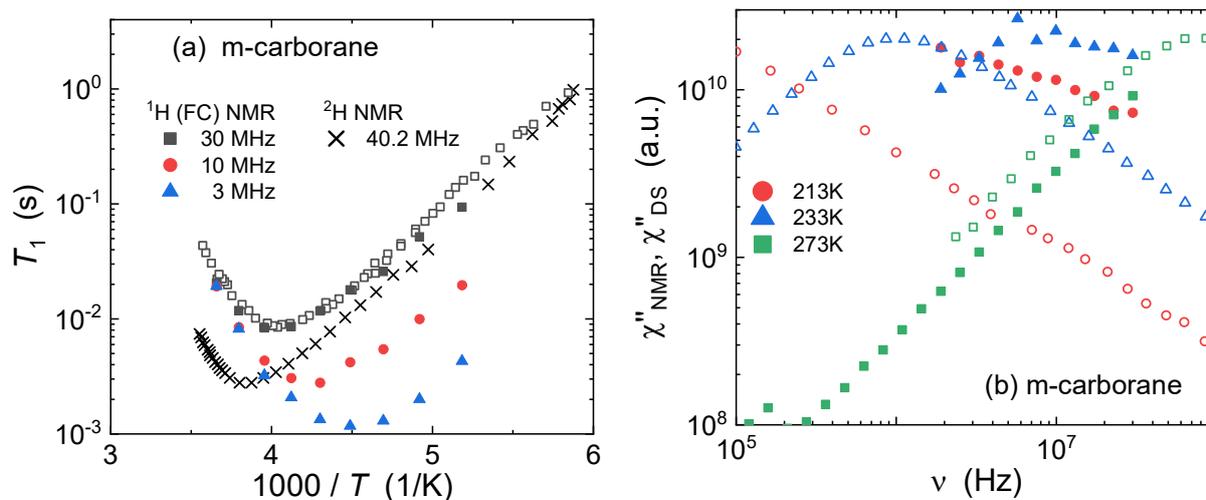

Figure 4.11. (a) A comparison of ^2H (ref 103) and ^1H (ref. 105 as open and present work as full symbols) spin-lattice relaxation time $T_1(T)$ of m-carborane (see legend). (b) The NMR susceptibility χ''_{NMR} of m-carborane is plotted versus frequency $\nu = \omega/2\pi$ for selected temperatures (full symbols, see legend). For comparison dielectric data χ''_{DS} at similar temperature[78] is included (open symbols).

---

[g] The reorientation is fast with respect to the NMR time scale.

First, we demonstrate agreement of the present ^{1}H spin-lattice relaxation time $T_1(T)$ at $\nu = 30$ MHz (full squares) with literature data[105] (open squares) in the orthorhombic phase of m-carborane (cf. Figure 4.11. (a)). At lower Larmor frequencies ν the minimum of $T_1(T)$ shifts to lower temperatures, as expected (e.g. triangles). In accordance, the minimum of the ^{2}H spin-lattice relaxation time $T_1(T)$ measured at a higher ν is shifted to a higher temperature (x).[103] The amplitude of the minimum of the ^{1}H $T_1(T)$ increases with increasing ν, as expected. In contrast for the ^{2}H $T_1(T)$ measured at the highest ν, the amplitude of the minimum is lower due to a larger coupling constant.

Next, we show the ^{1}H FC NMR data in the susceptibility representation $\chi''_{NMR}(\nu)$ (full symbols in Figure 4.11. (b)). A maximum is covered only for a single temperature $T = 233K$. More importantly, we compare χ''_{NMR} to χ''_{DS} from literature at comparable temperatures ($\Delta T < 3$ K).[78] To establish comparable amplitudes, we scale the data $\varepsilon''/\Delta\varepsilon$ with a temperature independent factor (cf. open symbols in Figure 4.11. (b)). Clearly, the position of the maximum of χ''_{NMR} is shifted to lower frequencies $\nu_{max,NMR} \cong 8 \cdot \nu_{max,DS}$. The slope of the dielectric data agrees with the slope of the NMR data at low frequencies, as expected, whereas the slopes differ at high frequencies. Moreover, the shift of χ''_{NMR} with respect to χ''_{DS} appears to increase with decreasing temperature. The unexpected deviations are commented on below. Before, we note that the shape of the dielectric loss is reported to depend on temperature ($0.5 < \beta_{CD} < 0.7$).[78]

Nonetheless, we attempt a master curve construction of the data χ''_{NMR} measured in the orthorhombic phase in Figure 4.12. (a). Given the scatter and the limited frequency window of the FC NMR data, we observe no systematic deviation of FTS and describe the master curve $\chi''_{NMR}(\omega\tau)$ by a CD spectral density with $\beta_{CD} = 0.5$, $K = 11 \cdot 10^9 s^{-2}$. At low frequencies, we observe deviations from the experimental data with respect to the CD function. The shift factors used for the construction of the master curve are displayed in Figure 4.12. (b) as full squares. Moreover, the ^{1}H spin-lattice relaxation, $T_1(T)$ is evaluated using K and β_{CD} from the master

curve description to obtain τ (open squares).[106] Analogously, ^{2}H spin-lattice relaxation is evaluated using $K_Q = (130 \text{ kHz})^2$ from literature.[103, 106] The evaluation via the master curve and $T_1(T)$ provides essentially the same $\tau(T)$. Adding literature data $\tau(T)$ from DS (x), we recognize a difference between the time constants obtained from the three techniques. An Arrhenius law reported for DS with an activation energy $E_a = 52 \text{ kJ/mol}$ (solid line) can be shifted by a factor of about 10 to essentially describe $\tau(T)$ extracted from ^{1}H (dashed line). In other words, the different techniques monitor a common activation energy and see faster or slower components of the rotation. This can be qualitatively explained for an anisotropic reorientation, as it is suggested for the orthorhombic phase of m-carborane in the literature.[104]
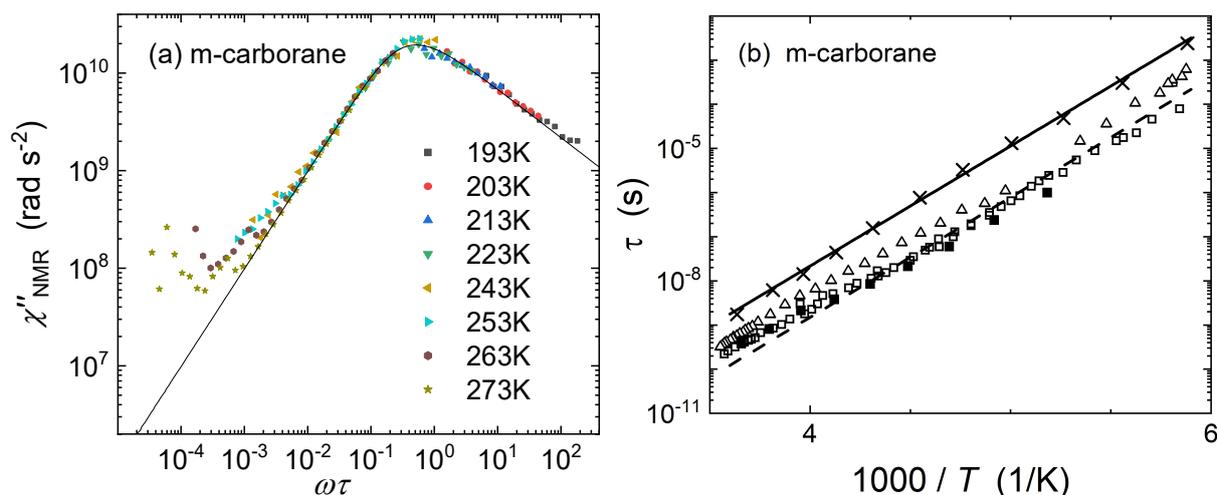

Figure 4.12. (a) Susceptibility master curve $\chi''_{NMR}(\omega\tau)$ of m-carborane covering temperatures $193\,K < T < 283\,K$ (see legend). A CD function ($\beta_{CD} = 0.5$) was added to describe the data (solid line). (b) The time constants $\tau(T)$ used for the master curve construction (full squares), are compared to data from conventional ^{1}H NMR[105] (open squares), ^{2}H NMR[103] (triangles) and DS[78] (x). The Arrhenius law (solid line) gives an interpolation of τ_{DS}. The dashed line is shifted about a decade with respect to the solid line.

Publications

List of publications as referred to in this thesis

Pub. 1   NMR Relaxometry: The Canonical Case Glycerol

Flämig, M.; Hofmann, M.; Fatkullin, N.; Rössler, E. A.

J. Phys. Chem. B, **2020**, *124*, 1557.

Pub. 2   Perspectives of Deuteron Field-Cycling NMR Relaxometry for Probing Molecular Dynamics in Soft Matter

Flämig, M.; Becher, M.; Hofmann, M.; Körber, T.; Kresse, B.; Privalov, A. F.; Willner, L.; Kruk, D.; Fujara, F.; Rössler, E. A.

J. Phys. Chem. B, **2016**, *120*, 7754.

Pub. 3   Dielectric Relaxation and Proton Field-Cycling NMR Relaxometry Study of Dimethyl Sulfoxide/Glycerol Mixtures Down to Glass-Forming Temperatures

Flämig, M.; Gabrielyan, L.; Minikejew, R.; Markarian, S.; Rössler, E. A.

Phys. Chem. Chem. Phys., **2020**, Advance Article.

Pub. 4   Field-Cycling NMR relaxometry: the benefit of constructing master curves

Flämig, M.; Hofmann, M.; Fatkullin, N.; Rössler, E. A.

Mol. Phys., **2019**, *117*, 887.

Pub. 5   The Dynamics of the Plastically Crystalline Phase of Cyanoadamantane Revisited by NMR Line Shape Analysis and Field-Cycling Relaxometry

Flämig, M.; Fatkullin, N.; Rössler, E. A.

J. Chem. Phys., **2019**, *151*, 224507.

Individual contributions to joint publications

Pub. 1   Measurements originally published by Gainaru et al. (ref). I performed all (re-) analysis during my Ph. D. studies.

Pub. 2   I conducted the FC NMR experiments on glycerol-d_5 and performed the analysis of the glycerol as well as the toluene data. Measurements and analysis were all done during my Ph. D. studies.

Pub. 3   I conducted all NMR experiments, except the measurement of glycerol-h_8/DMSO-h_6 (carried out by Liana Gabrielyan under my supervision). I performed the analysis of the NMR data. Measurements and analysis were all done during my Ph. D. studies.

Pub. 4   I conducted the experiments on cyanoadamantane and performed the corresponding preliminary analysis. Measurements and analysis were all done during my Ph. D. studies.

Pub. 5   I conducted the FC NMR experiments. I performed all the analysis except for the simulation of the ^{1}H line shape (carried out to the best of my knowledge by N. Römer). I performed all analysis during my Ph. D. studies.

Further publications

[1]   B. Schmidtke, N. Petzold, M. Flämig, and E.A. Rössler:
        *From boiling point down to the glass transition – Dynamics of molecular liquids
        described by a generalized Angell plot,* Hindustan Book (**2014**).

[2]   F. Mohamed, M. Flämig, M. Hofmann, L. Willner, N. Fatkullin, N. Aksel, E.A.
        Rössler:
        Scaling analysis of the viscoelastic response of linear polymers, J. Chem. Phys. 149,
        044902 (**2018**).

[3]   M. Hofmann, M. Flämig, E.A. Rössler: *Dynamics of Polymer Systems Studied by NMR
        Field-cycling Relaxometry,* NMR Methods for Characterization of Synthetic and
        Natural Polymers, 20, 101 (**2019**).

[4]   M. Flämig, M. Hofmann, A. Lichtinger, E.A. Rössler:
        *Application of Proton Field-Cycling NMR Relaxometry for Studying Translational
        Diffusion in Simple Liquids and Polymer Melts*, Magn. Reson Chem. (**2019**).

Publication 1

NMR Relaxometry: The Canonical Case Glycerol

Flämig, M.; Hofmann, M.; Fatkullin, N.; Rössler, E. A.
J. Phys. Chem. B, **2020**, *124*, 1557

NMR Relaxometry: The Canonical Case Glycerol

M. Flämig, M. Hofmann, N. Fatkullin, and E. A. Rössler*

Cite This: *J. Phys. Chem. B* 2020, 124, 1557−1570

Read Online

ACCESS | Metrics & More | Article Recommendations | Supporting Information

ABSTRACT: We present a quantitative description of the proton spin−lattice relaxation rate $R_1(T,\omega)$ of glycerol including temperatures from 191 to 360 K and a frequency range 10 kHz $< \omega/2\pi <$ 20 MHz covered by the field-cycling technique. The analysis encompasses the data compiled by Noack and co-workers in 1971, so far, the most complete data set (10 kHz $> \omega/2\pi <$ 117 MHz). Applying frequency−temperature superposition, master curves are constructed extending over 15 decades in frequency/time. They are described by contributions reflecting translational and rotational dynamics mediated by inter- and intramolecular relaxation pathways. The rotational part of the spectral density/susceptibility shows high similarity with those reported by dielectric spectroscopy or photon correlation spectroscopy (PCS). In addition to a Cole-Davidson-like peak, a high-frequency "excess wing" has to be accounted for. Quantitative agreement with the PCS susceptibility is found which probes the same order of the rotational correlation function. The translational contribution is reproduced by applying the force-free hard sphere model, describing diffusion of dipolarly coupled spin systems. Rotational and translational time constants are compared to those from other techniques. Our approach is paradigmatic for the analysis of spin relaxation in glass-forming liquids. It also solves long-standing deficiencies regarding the analyses of deuteron relaxation. Moreover, the case of glycerol is special as its large separation of translation and rotation dynamics, probably because of its hydrogen bond network, is not found in nonassociated liquids.
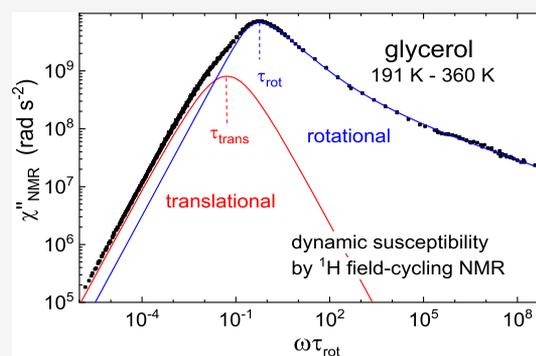
INTRODUCTION

Shortly after the Nobel prize-winning discovery of nuclear magnetic resonance (NMR) in condensed matter by the groups of Bloch (Stanford) and Purcell (Harvard) in 1946, a paper entitled "Relaxation Effects in Magnetic Resonance Absorption" by Bloembergen, Purcell, and Pound ("BPP", 1948) was published,[1] a paper which has become one of the most cited works in NMR. The authors discussed the proton spin−lattice and spin−spin relaxation time T_1 and T_2, describing the thermal equilibrium of the nuclear magnetization because of spin−lattice interactions. In the case of protons, the magnetic dipole−dipole interaction plays the major role, and the relaxation is determined by its fluctuations caused by molecular rotation and translation, for example, in a liquid—and BPP considered glycerol in particular.

Applying the time-dependent second-order perturbation theory, BPP derived the now well-known "BPP equations" relating the relaxation rates $R_1 = 1/T_1$ and $R_2 = 1/T_2$ with spectral density $J(\omega)$ taken at multiples of the Larmor frequency $\omega = \gamma B$ given by the applied external magnetic field B and the gyromagnetic ratio γ. In their final and general form, they read[2,3]

$$R_1(\omega) = K[J(\omega) + 4J(2\omega)]$$

$$R_2(\omega) = K/2[3J(0) + 5J(\omega) + 4J(2\omega)] \quad (1)$$

Here, K denotes some coupling constant (specified later). The equations can be exactly derived in the frame of the Bloch, Wangsness, and Redfield theory for the case of a liquid (see the Supporting Information).[4,5] After considering the situation for water, for which the extreme narrowing condition applies ($\omega\tau \ll 1$) and no dispersion effects were observed, BPP discussed the case of glycerol, a viscous liquid at ambient temperatures. Here, molecular motion is sufficiently slow to provide the condition for which strong dispersion effects in T_1 have to be expected, that is, the corresponding correlation time τ is on the order of the reciprocal Larmor frequency ($\omega\tau \cong 1$).

Measuring the relaxation rate at two Larmor frequencies, the salient features of eq 1 were reproduced: the $T_1(T)$ trace displayed a minimum with an amplitude being larger for the higher frequency. In contrast, spin−lattice relaxation time T_2 declined steadily with decreasing temperature until the limit of essentially rigid molecules in the highly viscous liquid close to T_g is reached. Attempting a quantitative description, BPP assumed an exponential correlation function, leading to Lorentzian spectral density which, however, failed to reproduce

quantitatively the T_1 data, in particular, at low temperatures and for the absolute amplitudes of T_1 at the relaxation maxima.

From the very beginning, it was thus desirable to collect relaxation data covering a broad range of Larmor frequencies to unravel details of the spectral density. Here, an important step forward was presented in 1969/1971 by the works of Noack and co-workers.[6,7] The authors measured the temperatures dependence of T_1 (and T_2) of glycerol in a frequency range from 10 kHz to 117 MHz. In their first study, they assumed that translational diffusion can be neglected because of the high viscosity of glycerol, and they discussed eq 1 in terms of various spectral densities for rotational dynamics first introduced to explain dielectric relaxation data. However, none of those was successful, in essential agreement with earlier findings by Luszczynski et al. interpreting $T_1(T)$ and $T_2(T)$.[8] Introducing "diffusion distribution", a satisfying interpolation of dispersion was possible. However, the extracted activation energy differed from that reported by dielectric spectroscopy (DS) studies. Moreover, the physical meaning of the "diffusion distribution" originally introduced for describing translational dynamics was unclear. In their second paper,[7] Noack and Co. changed gears and assumed the dominance of translational dynamics. This approach was inspired among others by the then-established fact that the dispersion of liquids in the low-frequency limit displays a $\omega^{1/2}$ dispersion characteristic of translational diffusion mediated by intermolecular relaxation.[9–11] The relaxation data were quantitatively compared to the Torrey model[12] introduced for Fickian diffusion of a spin system. However, reproduction of different $T_1(T)$ traces was not fully satisfying, although the temperature dependence of the time constant now agreed with that of the diffusion coefficient. Also, Fiorito and Meister[13] stated that the Torrey model is satisfactory for describing the relaxation of viscous liquids including glycerol, although in an earlier paper by Favret and Meister, Gaussian distribution was successfully applied, yet for relaxation data measured only at two frequencies.[14]

No significant progress was made ever since to fully understand the proton relaxation dispersion of viscous low molar mass liquids. The results of Noack and co-workers were obtained by conventional NMR relaxometry. Reviewing the NMR relaxation data on viscous liquids in 1986, Noack stated "With the improved experimental facilities now available for field-cycling (FC), this somewhat neglected subject should be studied more systematically."[15] The situation could have changed in the late nineties with the availability of a first commercial FC relaxometer,[16] which allows us to measure $R_1(T,\omega)$ routinely in the range 10 kHz–30 MHz. Indeed, the field has received new impetus,[17–22] also by new home-built FC machines.[20,23–29] However, a full analysis of the proton relaxation of glycerol down to the glass transition temperature T_g is still missing. We mention that starting with the work of Drake and Meister (1971)[30] and Kintzinger and Zeidler (1972)[31] on glycerol, several viscous liquids[32–36] were investigated by conventional deuteron NMR relaxometry. In this case, because of the dominance of the quadrupolar interaction,[3] the relaxation reflects purely molecular re-orientation. A successful interpretation in terms of a non-Lorentzian spectral density, specifically a Cole-Davidson (CD)[37] function applied before by DS, was achieved, yet only in a limited temperature range. For example, Sillescu and co-workers,[32,33,35,36] assuming isotropic re-orientation with a CD spectral density, established the proportionality between

the extracted τ_{rot} and viscosity η—as already suggested by BPP. In addition, Kintzinger and Zeidler applied isotope dilution experiments in order to isolate intra- and intermolecular proton relaxation and demonstrated that a CD spectral density describes the intramolecular rate.[31] Moreover, in the case of intermolecular relaxation, they stated failure of the Torrey model.

Glycerol was a natural choice by BPP as it is a viscous liquid at ambient conditions and well-known from daily life. Crystallization only rarely occurs, and hence, viscosity can be changed over several orders of magnitudes by varying temperature. Such liquids are called glass formers as their viscosity can be increased up to the limit of that of a solid body without significantly changing the liquid's structure. They finally form a glass, an amorphous solid body. In the last decades, this phenomenon of "glass transition" was studied by a variety of different techniques,[38–45] and they provided a generic picture of the evolution of the re-orientational or density–density correlation function (or corresponding spectral density/susceptibility), starting from temperatures well above the melting point T_m down to T_g. (i) The correlation loss occurs along two steps, a picosecond decay and a final slow decay (α-process). (ii) The latter is nonexponential (stretched), leading to a non-Lorentzian spectral density. (iii) Frequency–temperature superposition (FTS) applies, that is, the spectral shape of susceptibility does not significantly change with temperature. (iv) The characteristic correlation time τ_α follows a super-Arrhenius dependence. It is important to note that such "glassy dynamics" establishes already above T_m and hence is a property of the thermodynamically stable liquid.[45] Clearly, the dynamics in dense liquids is of cooperative nature, yet a full theoretical understanding of glass transition is missing.

Recently, our group investigated several molecular glass formers including (partly deuterated) glycerol by applying the Stelar FFC 2000 relaxometer.[18,19,22] Preliminary results on fully protonated glycerol are reported in refs 46 and 47. In contrast to previous studies, here, we present a full quantitative analysis of $R_1(T,\omega)$ covering temperatures down to T_g = 191 K and a frequency range 10 kHz–20 MHz. In addition, we included the so-far most complete data set of Noack and co-workers.[7] Instead of assuming a single relaxation channel—molecular rotation or translation—the present FC data are described by both contributions which, importantly, are spectrally well separated in the case of glycerol. Consequently, rotational and translational time constants are extracted and can be compared to those from DS and diffusion experiments, respectively. The rotational part of the spectral density shows high similarity with that reported by broadband DS or photon correlation spectroscopy (PCS). Regarding the full frequency range, it cannot be described by a CD function. As the accessible frequency range of the commercial FC relaxometer is still narrow, our analysis relies on the construction of master curves, that is, we apply FTS.[18,22,48,49] Moreover, we are able to confirm this assumption experimentally. In contrast to deuteron relaxation for which nonexponential relaxation sets in close to T_g and analyses become ambiguous,[33,50,51] proton relaxation remains exponential because of effective spin diffusion and thus can be easily analyzed. However, we will demonstrate that also deuteron relaxation can be interpreted consistently by the outcome of proton relaxometry. All in all, we think our analysis is paradigmatic for a full understanding of NMR relaxation in simple viscous liquids.

■ THEORETICAL BACKGROUND

Proton relaxation in molecular systems is dominated by the magnetic dipole−dipole interaction. The proton spin−lattice relaxation rate, $R_1(\omega)$, with $\omega = \gamma B$ being the Larmor angular frequency, is a sum of two contributions[3,17,21]

$$R_1(\omega) = R_{1,\text{intra}}(\omega) + R_{1,\text{inter}}(\omega) \qquad (2)$$

The intramolecular relaxation rate $R_{1,\text{intra}}(\omega)$ reflects interactions between protons belonging to the same molecule and thus probes molecular rotation. The intermolecular rate, $R_{1,\text{inter}}(\omega)$, originates from interactions between protons of different molecules. It is caused by translational and rotational dynamics. Equation 1 implies exponential magnetization recovery characterized by a single, well-defined relaxation rate, that is, the spin system is describable by a common spin temperature and satisfies to the Redfield limit.[3,52]

Regarding the intramolecular relaxation, the spectral density $J_{\text{intra}}(\omega) = J_{\text{rot}}(\omega)$ enters eq 1. It is the Fourier transform of the rotational correlation function $C_{\text{intra}}(t) = C_{\text{rot}}(t)$ defined in terms of spherical harmonics $Y_{2m}[\theta(t), \varphi(t)]$ where the angles $\theta(t)$ and $\varphi(t)$ specify the orientation of the internuclear vector. In liquids, the correlation function $C_{\text{rot}}(t)$ is identical to the correlation function of the second Legendre polynomial $C_2(t)$. The coupling constant $K = K_{\text{intra}}$ is related to the intramolecular second moment, reflecting the molecular structure in terms of proton−proton distances.[3] As discussed, it is well established that the correlation function describing the overall re-orientation of a molecule in a liquid is nonexponential even above the melting point except for temperatures close to the boiling point.[45] Moreover, the often-applied CD function holds only in a limited frequency range, and we assume that the full $J_{\text{rot}}(\omega)$ or $C_2(t)$ is given by empirical expressions provided by the results from broadband techniques like DS or PCS (see Results).

The intermolecular correlation function reflects both changes of the orientation as well as interspin distance $r(t)$[3,17,21]

$$C_{\text{inter}}(t) \propto \left\langle \frac{Y_{2m}(t)}{r^3(t)} \frac{Y_{2-m}(0)}{r^3(0)} \right\rangle \qquad (3)$$

Only spin pairs with spins from different molecules contribute. There are several approaches to calculate $C_{\text{inter}}(t)$.[21] Avoiding certain deficiencies of previous approaches, the "force-free hard sphere" (FFHS) assumes spins located in the center of hard spheres (representing the molecule), and diffusion is assumed to be "force-free". In the FFHS model, a distance of closest approach d (twice the hard spheres radius) is introduced, and the internuclear vector, $\vec{r}$, is entirely modulated by translational dynamics, and the (normalized) spectral density, $J_{\text{trans}}(\omega)$, takes the form[53,54]

$$J_{\text{trans}}(\omega) = \frac{54}{\pi} \int_0^\infty \frac{u^2}{81 + 9u^2 - 2u^4 + u^6} \frac{u^2 \tau_{\text{trans}}}{u^4 + (\omega \tau_{\text{trans}})^2} du \qquad (4)$$

The corresponding time constant τ_{trans} reads

$$\tau_{\text{trans}} = \frac{d^2}{D_{12}} = \frac{d^2}{2D} \qquad (5)$$

where $D_{12} = D_1 + D_2$ is the relative diffusion coefficient. For identical molecules (neat liquids), $D_{12} = 2D$ with D being the self-diffusion coefficient. An analogue of eq 1 connects

$R_{1,\text{inter}}(\omega)$ to $J_{\text{trans}}(\omega)$. The corresponding coupling constant K_{inter} is given by

$$K_{\text{inter}} = \left(\frac{\mu_0}{4\pi}\right)^2 \frac{8\pi}{15} \frac{n}{d^3} I(I+1) \hbar^2 \gamma^4 \qquad (6)$$

where n denotes the spin density which is calculated from the mass density and the number of protons in the molecule. Regarding the analysis of deuteron relaxation to be carried out, we give the connection between the quadrupolar coupling constant C_Q (in Hz) and the coupling constant K_Q—see eq 1[3]

$$K_Q = \frac{3}{10} \pi^2 C_Q^2 \qquad \text{with } C_Q = e^2 qQ/h \qquad (7)$$

where eq denotes the field gradient and eQ the quadrupolar moment.

For real molecules, of course, the assumption of hard spheres carrying a single proton in their centers does not hold. Actually, the intermolecular interaction is modulated by both translational and rotational dynamics—this is referred to as the eccentricity effect.[55−58] The effect was recently demonstrated for partially deuterated glycerol-h_5 mixed with fully deuterated glycerol by isotope dilution which allows isolating intra- and intermolecular relaxation contributions.[59] In addition to a low-frequency contribution originating from translation, there is also a high-frequency contribution in $R_{1,\text{trans}}(\omega)$, which covers essentially the same frequency range as the intramolecular relaxation caused by rotational dynamics.

Accounting for the eccentricity effect leads to quite involved expressions of the spectral density, depending on the extent of eccentricity in the particular molecule.[55−57] As a heuristic, but tractable approach, we assume that the spectral shape of $R_{1,\text{inter}}^{\text{rot}}(\omega)$ is similar to that of $R_{1,\text{intra}}(\omega)$.[22,58,59] Hence, we assume that the total relaxation rate can be described by a sum of rotational and translational contribution, specifically

$$R_1(\omega) \cong R_{1,\text{intra}}(\omega) + R_{1,\text{inter}}^{\text{rot}}(\omega) + R_{1,\text{inter}}^{\text{trans}}(\omega)$$

$$\cong R_1^{\text{rot}}(\omega) + R_{1,\text{inter}}^{\text{trans}}(\omega) \qquad (8)$$

Here, $R_1^{\text{rot}}(\omega)$ will be described by a spectral density qualitatively similar to that observed by DS or PCS and $R_{1,\text{inter}}^{\text{trans}}(\omega)$ by the FFHS model. Clearly, eq 8 contains an uncontrolled approximation. However, as will be demonstrated, this approach allows a perfect interpolation of the NMR master curves which extend over 15 decades.

Independent of any microscopic details of translational motion, at long times, the molecules in a liquid undergo Fickian diffusion, implying a mean square displacement linear in time $\langle \Delta r^2 \rangle = 6Dt$. In this limit, the translational correlation function displays a power-law behavior, $C_{\text{trans}}(t) \propto t^{-3/2}$, which leads to square root dispersion at low frequencies,[10,11,22,53,54,59−61]

$$R_{1,\text{inter}}(\omega) = R_{1,\text{inter}}(0) - \frac{B}{D^{3/2}} \cdot \sqrt{\omega} + \dots \qquad (9)$$

with $B = \left(\frac{\mu_0}{4\pi} \hbar \gamma^2\right)^2 \left(\frac{1 + 4\sqrt{2}}{30}\right) \pi n$. As the power-law decay of $C_{\text{inter}}(t)$ always wins at long times over the more or less exponential correlation function of $C_{\text{rot}}(t)$ together with the condition $\tau_{\text{trans}} \gg \tau_{\text{rot}}$ (see below), eq 9 provides a universal low-frequency dispersion law also for the total relaxation rate. It allows us to determine the diffusion coefficient and can be cast in the form of a master curve[22,58,62]

$$R_1(\omega)/R_1(0) = 1 - \sqrt{\omega\tau_{\text{res}}} + \dots \tag{10}$$

with a rescaled time constant

$$\tau_{\text{res}} = \left(\frac{B}{D^{3/2}R_1(0)}\right)^2 \tag{11}$$

and the total relaxation rate at zero frequency, $R_1(0)$. When constructing master curves in this spectral density representation, both the rate and the frequency are rescaled. We emphasize that eq 10 is an exact low-frequency expansion of the total relaxation rate, in contrast to constructing master curves by assuming FTS which applies in simple liquids and encompasses the full susceptibility (see below).

The spectral density of the FFHS model can be expanded up to the second order explicitly[53]

$$J_{\text{inter}}(\omega) = \frac{4\tau_{\text{trans}}}{9}\left[1 - \frac{3\sqrt{2}}{8}(\omega\tau_{\text{trans}})^{1/2} + \frac{1}{12\sqrt{2}}\right.$$
$$\left.(\omega\tau_{\text{trans}})^{3/2} + \dots\right] \tag{12}$$

Regarding the total relaxation, this leads to

$$\frac{R_1(\omega)}{R_1(0)} = 1 - (\omega\tau_{\text{res}})^{0.5} + \frac{800(1 + 8\sqrt{2})}{81(1 + 4\sqrt{2})^3}$$
$$\left(1 + \frac{R^{\text{intra}}(0)}{R^{\text{inter}}(0)}\right)^2 (\omega\tau_{\text{res}})^{3/2} \dots \tag{13}$$

provided dispersion by rotation can still be neglected. The numerical prefactor in eq 13 yields 0.41. Here, $R^{\text{intra}}(0)$ and $R^{\text{inter}}(0)$ are the intra- and inter molecular relaxation rate at zero frequency, respectively. This calculation provides another relation for the rescaled time explicitly

$$\tau_{\text{res}} = \frac{9(1 + 4\sqrt{2})^2}{160\left(1 + \frac{R_1^{\text{intra}}(0)}{R_1^{\text{inter}}(0)}\right)}\tau_{\text{trans}} \tag{14}$$

The ratio $\frac{R_1^{\text{intra}}(0)}{R_1^{\text{inter}}(0)}$ is not universal and depends on molecular details. An estimate can be given by considering the individual relaxation contributions

$$R_{1,\text{inter}}(0) = \frac{40\pi}{9}\left(\frac{\mu_0}{4\pi}\right)^2 (\gamma^2\hbar)^2 \frac{n}{dD}$$
$$= \frac{80}{9}\left(\frac{\mu_0}{4\pi}\right)^2 (\gamma^2\hbar)^2 \frac{n}{d^3}\tau_{\text{trans}} \tag{15}$$

$$R_{1,\text{intra}}(0) = \frac{15}{4}\left(\frac{\mu_0}{4\pi}\right)^2 (\gamma^2\hbar)^2 \frac{1}{r_{12}^6}\tau_{\text{rot}} \tag{16}$$

$$\frac{R_{1,\text{intra}}(0)}{R_{1,\text{inter}}(0)} \cong \frac{27}{64\pi}\frac{d^3}{r_{12}^6 n}\frac{\tau_{\text{rot}}}{\tau_{\text{trans}}} < \frac{3}{64\pi}\left(\frac{d}{r_{12}}\right)^6 \tag{17}$$

Here, r_{12} denotes a typical intramolecular proton−proton distance, and d, as before, the distance of the closest approach of two molecules in the liquid. In the second last step, we assumed $\tau_{\text{rot}} \leq 1/9\tau_{\text{trans}}$ and in the last, $n = 1/d^3$. Such an estimate will be done for glycerol (see Discussion).

Proton FC NMR relaxometry allows us to determine both D and τ_{rot}. Assuming Stokes−Einstein−Debye relation (SED), their product is a measure of the hydrodynamic radius R_H[3,63,64]

$$D\tau_{\text{rot}} = \frac{2}{9}R_H^2 \tag{18}$$

In the frame of the FFHS model, which does not imply the validity of SED, the time constant τ_{trans} is related to distance d (eq 5). The ratio $r = \tau_{\text{trans}}/\tau_{\text{rot}}$ is a measure of the separation of translation and rotation in a liquid, and one gets[64]

$$r = \frac{\tau_{\text{trans}}}{\tau_{\text{rot}}} = \frac{d^2}{2D\tau_{\text{rot}}} \tag{19}$$

Assuming further SED with $d = 2R_H$, one arrives at $r = 9$.[3] In other words, within the hydrodynamic approach, the spectral separation of translational and rotational relaxation contributions is independent of size—and small. However, in certain liquids (like glycerol), the ratio r is much larger, thus indicating a failure of SED, which goes along with unphysically small values of R_H—as will be demonstrated.

The relaxation dispersion can also be analyzed in the susceptibility representation based on the connection of the linear response theory and the fluctuation−dissipation theorem. Equilibrium fluctuations described by $J(\omega)$ are connected to the response represented by a (normalized) dynamic susceptibility $\chi''(\omega)$ along $\chi''(\omega) = \omega J(\omega)$. This is advantageous when comparing FC NMR results with dielectric or rheological results, for instance, and also for constructing master curves (see below).[48,49] Consequently, one can rewrite eq 1 for the spin−lattice rate

$$\omega R_1(\omega) = K[\chi''(\omega) + 2\chi''(2\omega)] \cong 3K\chi''_{\text{FC}}(\omega)$$
$$\equiv \chi''_{\text{NMR}}(\omega) \tag{20}$$

where K denotes the coupling constant K_{intra} or K_{inter}, respectively. We note that $\chi''_{\text{NMR}}(\omega)$ is only slightly broader than $\chi''(\omega)$, yet shifted by a factor of about 0.6 to lower frequencies.

In liquids as well as in polymers with their cooperative dynamics, usually FTS applies,[40,45] at least at high temperatures, that is, the dynamic susceptibility can be expressed by $\chi''(\omega\tau)$, where τ is a characteristic time constant, for instance τ_{rot}. This leads to the possibility to construct master curves by shifting the individual $\chi''(\omega)$ collected at different temperatures solely along the ω-axis until they overlap. Assuming that the NMR coupling constant K does not significantly change with temperature, master curves are obtained for $\chi''_{\text{NMR}} = \omega R_1(\omega)$ too.[48,49] The application of FTS is an important tool to effectively extend the still-narrow frequency window of FC NMR.

■ EXPERIMENTAL SECTION

High-purity glycerol was purchased from Aldrich, Germany. The NMR samples were thoroughly degassed before sealing the NMR tubes. For details regarding the FC NMR measurement done by employing the commercial Stelar FFC 2000 relaxometer, we refer to refs 46 and 47. Fourier transformation was accomplished by applying a program based on a Filon algorithm.[65]
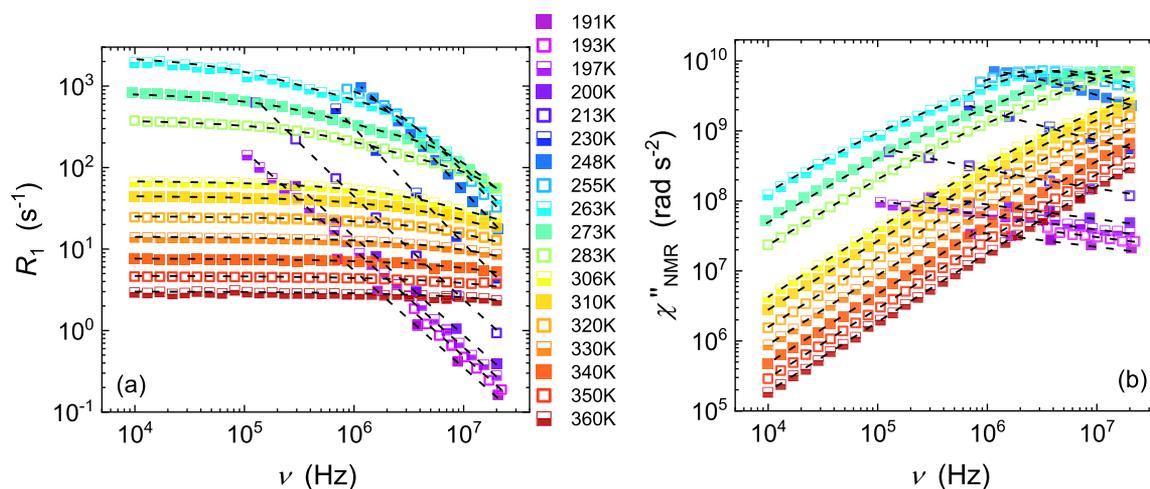
Figure 1. (a) Proton relaxation rates R_1 of glycerol as a function of frequency ν. (b) Data of (a) are shown in the susceptibility representation $\chi_{NMR}''(\omega) = \omega/T_1$. Dashed lines: predictions from applying parameters of the master curve (see text).

■ RESULTS

In Figure 1a, we reproduce the relaxation rates compiled for fully protonated glycerol covering temperatures from 360 K down to about $T_g = 186$ K as first published in ref 47. A little more than three decades in frequency are covered, specifically 10 kHz–20 MHz. The lower limit is given by approaching the earth field and the upper limit by the possibilities of choosing an appropriate magnet coil system. Whereas at low temperatures, pronounced dispersion is observed, which displays a power-law character, dispersion appears to vanish at high temperatures. However, a closer look shows that even at the highest temperature, still weak dispersion is recognizable. This indicates that the extreme narrowing condition is not yet reached. As will be demonstrated below, this is explained by the dominance of translational dynamics mediated by the intermolecular relaxation. At lowest temperatures, T_1 becomes rather long at high frequencies, and long times are needed to polarize the spin system. In order keep measuring time down, only a few frequencies were measured at most temperatures. Concerning the limitation of the current FC instrument, another feature is of relevance: at low temperatures, the rates reach values on the order of the reciprocal switching time which is a few milliseconds, that is, rates higher than 1000 s^{-1} are not reliably accessible.

In Figure 1b, we display the data of Figure 1a in the susceptibility representation, that is, $\chi_{NMR}''(\omega) = \omega/T_1$ is plotted versus frequency. Upon cooling, a broad relaxation maximum moves to lower frequencies as expected for a slow-down of a relaxation process. Regarding the low-frequency flank of the relaxation peak, some (weak) indication of a bimodal spectral shape is found (see below). At low temperatures approaching T_g, the high-frequency flank displays a power-law behavior with an extremely small exponent by magnitude. Such behavior cannot be described by a CD function with a constant width parameter. We note that in our previous FC NMR relaxation analysis of several liquids, a description with a single CD function was sufficient as no low temperatures close to T_g were involved.[18,22,46]

For a full exploration of the spectral density reflecting translational and rotational dynamics, we took recourse to constructing master curves which effectively enlarge the frequency range covered, that is, we applied FTS. Regarding the slow dynamics (α-process), underlying FTS is the fact that

the (normalized) susceptibility can be expressed in terms of temperature-independent susceptibility function χ'' of a temperature-dependent argument $\omega\tau$, where $\tau = \tau_{rot}(T) \cong \tau_\alpha(T)$ is the corresponding time constant. We will test how well FTS works.

Figure 2a presents the master curve $\chi_{NMR}''(\omega\tau_{rot})$. It is obtained by shifting the individual susceptibility data $\chi_{NMR}''(\omega)$ measured at different temperatures (191–273 K, see Figure 1b) solely along the frequency axis until best overlap. It is thus further assumed that the coupling constants K_i do not significantly change with temperature. The transformation to the reduced frequency axis $\omega\tau_{rot}$ will be explained below; for the following discussion of the spectral shape, the absolute scale is of no relevance. In extension to our previous analysis,[47] we optimized the master curve construction by relying also on the master curve construction in the spectral density representation (Figure 2b), where the reduced rate $R_1(\omega)/R_1(0)$ is plotted against the reduced frequency $\omega\tau_{rot}$—see eq 10. Only the low-frequency part obtained from data at high temperatures is displayed. This representation is particularly suited for guaranteeing best overlap of the master curve at lowest frequencies. Such an obtained master curve from the high-temperature data ($T > 273$ K) is transferred to the susceptibility representation in Figure 2a (grey symbols).

The master curve $\chi_{NMR}''(\omega\tau_{rot})$ (Figure 2a) shows particularities on each flank, at low and high frequencies. Starting with the low-frequency side, a weak shoulder is observed. The feature is also recognized when the data in spectral density representation Figure 2c are inspected at low frequencies (Figure 2b). This relaxation feature disappears when glycerol is diluted with its deuterated counterpart as is documented in ref 59. Hence, it is of intermolecular nature. This is demonstrated by inspecting the dipolar correlation function $C(t/\tau_{rot})$ (Figure 2d), which shows a long-time power-law behavior $t^{-3/2}$ characteristic of translational diffusion (Theoretical Background), while the exponential tail of the rotational contribution dominating at short times dies out at long times (see below); or when plotting the relaxation rate versus the root of the frequency along eq 10 (see Figure 7 and Discussion).

Second, considering the high-frequency flank of the susceptibility master curve (Figure 2a), a cross-over from a
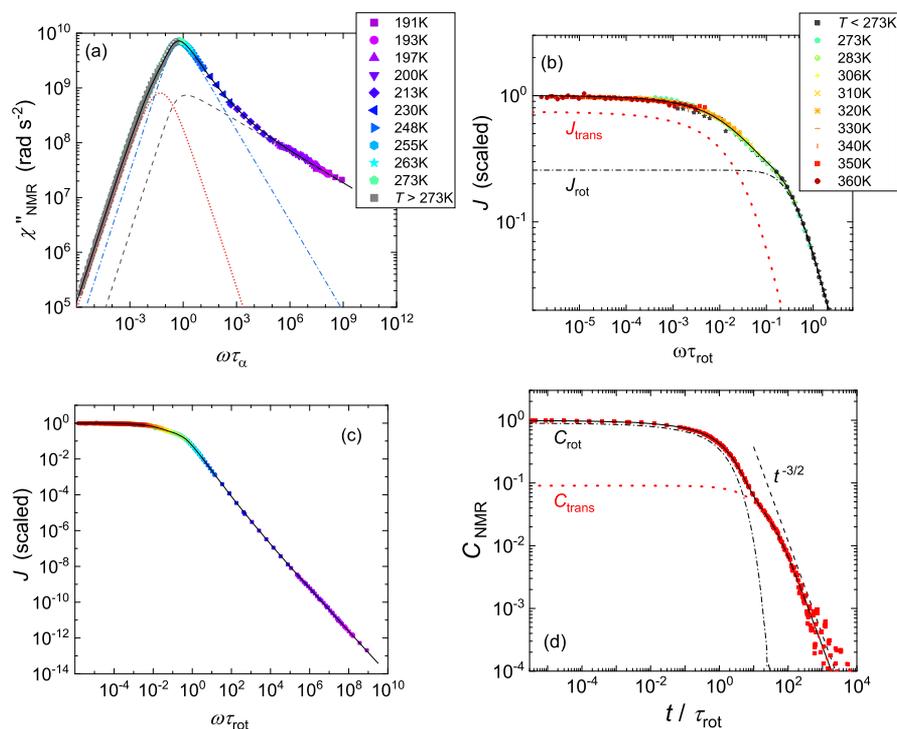
Figure 2. (a) Susceptibility master curve of glycerol obtained from the data in Figure 1 (191 K < T < 360 K); solid-line: fit by a double CD function representing the rotational relaxation and the FFHS model describing translational relaxation contribution, dashed, dash-dotted, and dotted lines represent the three subspectra. (b) Master curve in the spectral density representation displaying the low-frequency part; solid line: corresponding interpolation as in (a); dash-dotted line: rotational relaxation contribution, dotted line: translational contribution. (c) Full spectral density; solid-line: corresponding interpolation as in (a). (d) Normalized correlation function C_{NMR} vs reduced time t/τ_{rot}; solid-line: corresponding interpolation as in (a); dotted line: $C_{trans}(t)$, dash-dotted line: $C_{rot}(t)$, dashed straight line: power-law reflecting long-time behavior of $C_{trans}(t)$.

first power-law flank close to the peak to a second power-law at higher frequencies with a much smaller exponent is observed. This so-called excess wing feature is well known from dielectric as well as from light-scattering (LS) spectra of glass-forming liquids.[41,45,66] For example, we show in Figure 3a a direct comparison of the susceptibility data of glycerol compiled by DS,[66] PCS,[45]—and by proton NMR. The NMR susceptibility exhibits its maximum by a factor of about 0.6 at lower frequencies, as a contribution from the double frequency enters eq 20. Therefore, we shifted the NMR data to agree with the maximum of the other susceptibility curves. The slight broadening of the NMR curve can be neglected on the logarithmic scales considered here. In the case of DS and NMR data, master curves are displayed, whereas in the case of PCS, the Fourier transformation of a time domain fit of PCS data is shown. Clearly, a similar excess wing is observed by the three techniques; however, its amplitudes appear to be smaller in the dielectric spectrum, while the curves for PCS and NMR agree well. Similar results are observed in the case of *m*-tricresyl phosphate[45,67]—see Figure 3b. As the excess wing scales with τ_{rot}, it is interpreted as a genuine part of the main α-process in viscous liquids—although its molecular nature is still controversially discussed (see Discussion). Clearly, a low-frequency shoulder is missing in the dielectric and PCS susceptibility, again demonstrating its translational origin in the case of proton NMR susceptibility.

Summarizing the results compiled so far, we can state that the NMR susceptibility/spectral density contains three contributions: an intramolecular part, $R_{1,intra}(\omega)$, an intermolecular contribution, $R_{1,inter}^{rot}(\omega)$ resulting from rotation

(eccentricity effect), and a intermolecular part, $R_{1,inter}^{trans}(\omega)$ originating from translational diffusion. As a heuristic approach (cf. Theoretical Background), we assume that the total relaxation rate can be described by a sum of rotational and translational contribution, specifically[22,58,59]

$$R_1(\omega) \cong R_{1,intra}(\omega) + R_{1,inter}^{rot}(\omega) + R_{1,inter}^{trans}(\omega)$$
$$\cong R_1^{rot}(\omega) + R_{1,inter}^{trans}(\omega) \qquad (8)$$

Here, $R_1^{rot}(\omega)$ will be described by a spectral density qualitatively similar to that observed by DS or PCS, and $R_{1,inter}^{trans}(\omega)$ by the FFHS model.

Regarding the spectral shape of $\chi_{rot}''(\omega)$, in addition to DS and PCS, the rotational dynamics was investigated in terms of the corresponding pulse response function (the negative derivative of the step response) by the optical Kerr effect technique.[39,42,68] After converting the PCS decay into the pulse response representation, a direct comparison of PCS and Kerr effect data yielded satisfying agreement.[69,70] Both techniques probe the fluctuations of anisotropy of molecular polarizability, which is given by the second-order re-orientational correlation function $C_2(t)$. In addition, dielectric results converted to the step-response function representation agree qualitatively, either, as demonstrated in the frequency domain in Figure 3. In all the cases, the long-time decay of the step response can be interpolated by a sum of two power laws damped by an exponential function. Explicitly, we write for the pulse-response function of the α-process[71,72]
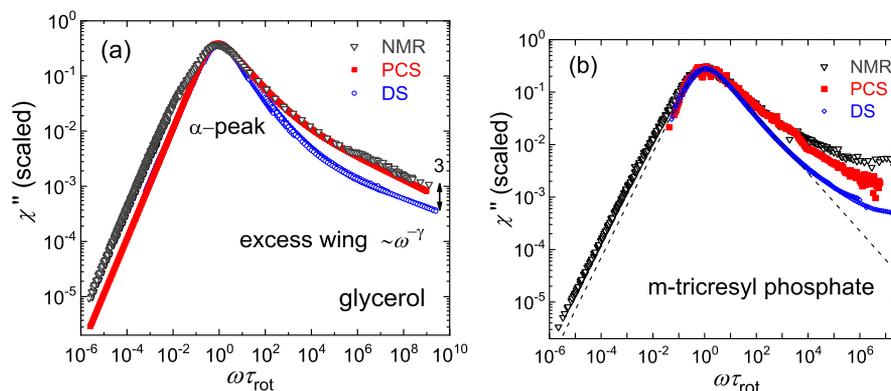
Figure 3. (a) Susceptibility master curves of glycerol as obtained from proton NMR (shifted by a factor 0.6), from PCS (fit of experimental data), and from DS relaxation; double arrow denotes factor 3, indicating the difference in the amplitude of the excess wing in the DS and PCS/NMR data, respectively. (b) Corresponding master curves of m-tricresyl phosphate (dashed line: Cole-Davidson fit).

$$-\frac{dC_2(t)}{dt} = [A_{ex}(t/\tau_{CD})^{\gamma_{CD}-1} + A_{CD}(t/\tau_{CD})^{\beta_{CD}-1}]$$
$$\exp(t/\tau_{CD}) \qquad (21)$$

Here, A_{ex} and A_{CD} are constants. In the susceptibility (frequency) domain, this is equivalent to applying a superposition of two CD functions[37] with different exponents, β_{CD} and γ_{CD}, respectively, but the same time constant τ_{CD}. Thus, we stick to this interpolation also for the rotational part of $\chi''_{NMR}(\omega\tau_{rot})$. As said, regarding the translational contribution $R_1^{trans}(\omega)$, we apply the FFHS model given by eq 4. In total, this description involves seven fit parameters. To further reduce the number of parameters, we took $\gamma_{CD} = 0.19$ as the experimental log−log slope provided by the FC measurement at the lowest temperature, for which the influence of the relaxation peak is smallest.
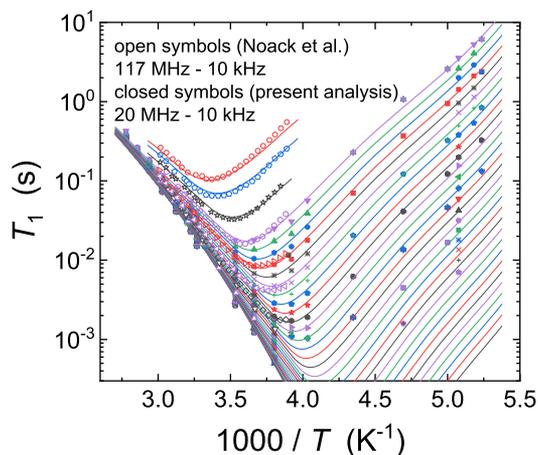

Figure 4. Proton relaxation rate at different frequencies as a function of temperature (double-log plot); present data (full symbols); data from Noack and co-workers (open symbols).[7] Solid lines: predictions from applying parameters of the master curve.

As demonstrated in Figure 2a−d, an almost perfect interpolation of the master curves in the three different representations is achieved. The rotational and translational relaxation contributions are indicated by dashed and dotted lines, respectively. In particular, the long-time power-law behavior $t^{-3/2}$ of $C_{NMR}(t/\tau_{rot})$ attributed to translational diffusion mediated by intermolecular relaxation is well

reproduced in Figure 2d. The fit together with the master curve construction provides two time constants, $\tau_{rot}(T) = \beta_{CD}\tau_{CD}$ and $r = \tau_{trans}/\tau_{rot} = 56$. The time constant $\tau_{rot}(T)$ also allows us to fix the reduced frequency axis in Figure 2. The temperature-independent "separation parameter" r quantifies the extent of separation of rotational and translational dynamics in the liquid, whereas $\tau_{rot}(T)$ can be compared to the data provided by other techniques including deuteron relaxometry. The comparison is shown in Figure 6. Satisfying agreement is observed. At low temperatures, τ_{rot} by proton NMR is somewhat shorter than τ_{DS}. In addition, the fit provides the coupling constants $A_{rot}^{CD} = 5.81 \times 10^9$ s^{-2}, $\beta_{CD} = 0.55$, $A_{ex}^{CD} = 1.3 \times 10^9$ s^{-2}, $\gamma_{CD} = 0.19$, and $K_{trans} = 7.29 \times 10^8$ s^{-2}. Using a spin density $N_H = 5 \times 10^{28}$ m^{-3} together with K_{trans}, we derive $d = 0.40$ nm for the distance of the closest approach. This value is physically reasonable and agrees within 20% with previously reported values (see Discussion).[46] We estimate an error of d of 2% (d enters K_{trans} by the third power). We note that including an excess wing in the description of the full susceptibility changes the actual value of β_{CD} in comparison to a single CD fit.

Given the successful interpolation of the master curve, we can take its parameters, specifically, the time constant $\tau_{rot}(T)$ (Figure 6), the coupling constants, and the spectral shape parameters β_{CD} and γ_{CD} in order to predict $R_1(\nu)$ or $\chi''(\nu)$ for each temperature. The results are included in Figure 1. An almost perfect reproduction is provided on log scales. Finally, we display in Figure 4 the relaxation data in terms of $T_1(T)$ for different frequencies. We added the results form Noack and co-workers.[7] Both data sets are well reproduced on log-scales by our approach. In the case of reproducing the Noack data, we assumed the temperature dependence given by the present analysis of the present FC data (cf. Figure 6).

Two observations are still worth to be discussed. First of all, one recognizes that the extreme narrowing condition, that is, the frequency independence of the relaxation time, is not reached even at highest temperatures. The reason, as said, is the dominance of the intermolecular relaxation contribution dominated by translational dynamics at low frequencies (eq 9). Second, as said before, relaxation times shorter than about 1 ms are not accessible because of the finite switching times of the FC relaxometer.

As already mentioned in the Introduction section, glycerol was also studied by conventional deuteron NMR relaxometry,[35,50] and a comparison with the results from proton
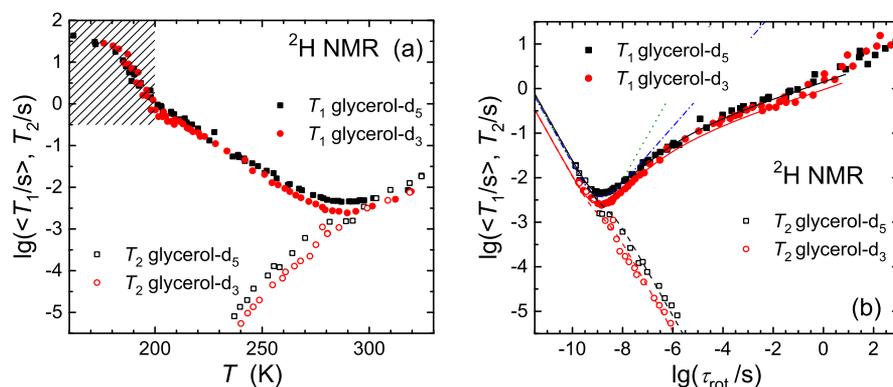
Figure 5. (a) Mean deuteron spin−lattice relaxation time $\langle T_1 \rangle$ and spin−spin relaxation time T_2 of glycerol-d_3 and glycerol-d_5 as a function of temperature (data taken from refs 35 and 50); shaded area: temperature interval for which nonexponential relaxation shows up. (b) Data of (a) as function of τ_{rot} (taken from ref 41); solid lines: expectations for $\langle T_1 \rangle$ (solid lines) and T_2 (dashed lines) taking the proton FC NMR results from the master curve description, together with appropriate quadrupolar coupling constants (see text). For comparison, we included the prediction assuming a Lorentzian (dotted line) and CD spectral density (dash-dotted line).

relaxation is of interest. One expects that the rotational contributions of proton relaxation compares to that of deuteron relaxation. The results as measured are reproduced in Figure 5a, for both glycerol-d_3 and glycerol-d_5. As the quadrupolar coupling constant C_Q is higher for glycerol-d_3 as compared to that of glycerol-d_5, the T_1 value of glycerol-d_3 at the minimum is shorter. We note that the minimum position is located at a very similar temperature, indicating that the glycerol molecule re-orients as an entity, that is, it behaves as being effectively rigid.

Demonstrated by DS or PCS and by the present proton FC NMR results, FTS applies in the sense that the variables ω and τ_{rot} in $\chi''(\omega\tau_{rot})$ are equivalent, and hence, plotting T_1 as a function of $\tau_{rot}(T)$ (as given by some literature data) is expected to directly yield the (temperature independent) shape of the susceptibility (disregarding the slight broadening because of the fact that two spectral densities enter eq 1). In the case of deuteron relaxation, because of dynamic heterogeneities, the magnetization recovery is not exponential any longer close to T_g. In order to allow a comparison with proton relaxation, which because of fast spin-diffusion measures the rate average $\langle 1/T_1 \rangle$ in the case of dynamic heterogeneities, it would be necessary to determine the initial slope of the nonexponential deuteron relaxation function.[73] However, this is not easily possible, and usually, the mean relaxation time $\langle T_1 \rangle$ is reported in the literature—and is also shown in Figure 5a. In the region of the onset of nonexponential deuteron relaxation around 200 K,[50] the relation $\langle T_1 \rangle > 1/\langle 1/T_1 \rangle$ holds, and one expects a kind of step-like further increase of the temperature dependence with respect to that extrapolated from higher temperatures where the relaxation is still exponential. Indeed, this is anticipated in Figure 5a where we indicated the temperature interval for which the crossover from exponential to nonexponential relaxation takes place (shaded area).

In Figure 5b, we display the deuteron relaxation times[35,50] as a function of the correlation time $\tau_{rot}(T)$ as reported by Lunkenheimer et al.[41] As said, this yields directly the reciprocal susceptibility function. Indeed, taking the proton rotational spectral density together with the quadrupolar coupling constant C_Q as the single fit parameter, we arrive at a very satisfying prediction of the deuteron T_1 and T_2 data of glycerol-d_5. The fit yields $C_Q = 164$ kHz compared to $C_Q = 165$

± 3 kHz from line shape analysis.[50] Likewise, we are able to interpolate the relaxation data of glycerol-d_3 (a shift of $\Delta\log_{10} \tau = -0.15$ is applied, indicating a slightly faster re-orientation of the OH group with respect to the paraffinic groups). We find $C_Q = 206$ kHz which compares to $C_Q = 212 \pm 4$ kHz from solid-state NMR.[50] Thus, the spectral density is the same for both molecular groups of glycerol as expected for an effectively rigid molecule. At $\log_{10}(\tau_{rot}) > -1$, the prediction somewhat underestimates the T_1 data. This is not surprising because here deuteron spin−lattice relaxation sets in to become non-exponential and $\langle T_1 \rangle > 1/\langle 1/T_1 \rangle$ holds, as said. For comparison, we added the result for assuming a Debye and a CD function. Clearly, the CD function often applied does not provide good interpolation at low temperatures/high frequencies.

Returning to proton relaxation, our analysis interpreted the measured susceptibility in terms of translational and rotational relaxation pathways. In particular, the (temperature independ-
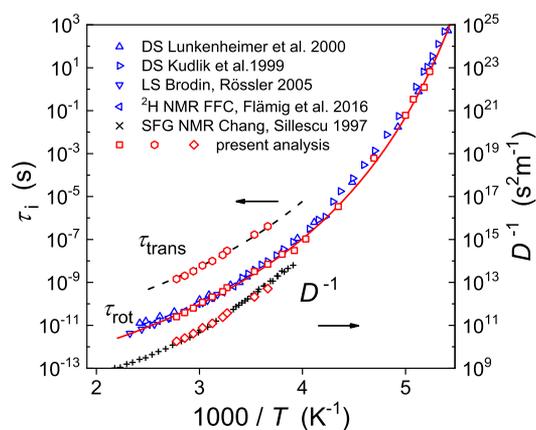

Figure 6. Time constants (left scale) of glycerol obtained from proton FC NMR (open squares and circles). In addition, rotational time constants from depolarized LS,[74] DS,[38,75] and from deuteron FC NMR relaxometry of glycerol-d_5[76] are displayed. The translational times τ_{trans} (hexagons, left scale) are calculated from the experimental D values obtained from an analysis of low-frequency dispersion along eq 10 (open diamonds, right scale); dashed line represents prediction from $r = \tau_{trans}/\tau_{rot} = 56$. For comparison, diffusion data from static field gradient diffusometry are added (crosses, right scale).[63]

ent) separation parameter r is directly revealed from fitting the master curve. Given $\tau_{rot}(T)$, the corresponding temperature dependence of $\tau_{trans} = r\tau_{rot}$ is known either, and represented by the dashed line in Figure 6. Within the FFHS model, $\tau_{trans} = d^2/2D$ holds, and knowing the distance d of closest approach from the master curve fit, the diffusion coefficient $D(T)$ can be calculated. Another possibility is to determine $D(T)$ directly from the low-frequency expansion of the (total) relaxation rate along eq 9. The latter results are included in Figure 6 and compared to D values reported from field gradient NMR.[63] Very satisfying agreement is found. We note the results also well agree with those reported in another study on glycerol.[61] In order to check consistency, one can now calculate individual $\tau_{trans}(T)$ values from $d = 0.40$ nm and $D(T)$. Again, such calculated data points fit to the dashed line in Figure 6. Finally, we calculate the hydrodynamic radius along $D\tau_{rot} = 2/9R_H^2$. At $T = 273$ K, we find $\tau_{rot} = 7.0 \times 10^{-9}$ s and $D = 2.0 \times 10^{-13}$ m^2 s^{-1} which leads to $R_H = 0.079$ nm. This is an unphysically small value, an experimental fact also reported by other studies for glycerol.[61] We will come back to this point in the Discussion section.

■ DISCUSSION

The present analysis of the proton relaxation rate $R_1(T,\omega)$ of glycerol provides its full understanding down to T_g which was not achieved so far. In contrast to previous approaches of assuming a single relaxation channel—molecular rotation or translation—the present relaxation data are described by both contributions which are spectrally well separated in the case of glycerol. The first dominates at high frequencies, the second at low frequencies, a feature already known since long and predicted by the SED relation.[3,10,11] Relying on the construction of master curves (in different representations) by exploiting FTS, the obtained master curves extend over 15 decades in frequency/time. The extracted time constant $\tau_{rot}(T)$ agrees well with those from other techniques probing rotational dynamics, and the diffusion coefficient $D(T)$ derived from the low-frequency expansion of the intermolecular relaxation rate is confirmed by that obtained from field gradient NMR studies. Moreover, from the parameters of the master curve, we are able to quantitatively interpolate $R_1(T,\omega)$ even including the so far most complete relaxation data set compiled by Noack and co-workers.[7] A posteriori, this confirms the possibility of constructing master curves over the full temperature range by assuming FTS to hold. In other words, the spectral shape of susceptibility of both rotation and translational contribution does not change with temperature, and, in addition, its mutual separation is constant at least at high temperatures ($T > 260$ K). Thus, nature providing a spectrally not-changing susceptibility in the (pure) liquid state helps overcoming the narrow frequency range of the FC technique. However, FTS may fail if further relaxations come into play.

Here, one comment is worthwhile. The data by Noack and co-workers cover a wider frequency range (but a smaller temperature range) compared to that of the present FC study performed by the commercial relaxometer FFC 2000. Thus, it appears that regarding the frequency range experimentally, no progress has been achieved since the seventies. Noack et al. measured relaxation using conventional multichannel NMR spectrometers. Such conventional relaxation studies are very tedious, and multichannel facilities covering four decades in frequency are sophisticated machines and, actually, do not exist

any longer. Hence, NMR relaxometry relies on the FC technique which allows much faster dispersion measurements. Moreover, recent experimental progress[20,27,28] reaching frequencies down to 10 Hz and up to 40 MHz offers new perspectives. Of course, the high-frequency range can always be extended by performing relaxation experiments in standard high-field magnets. Then, covering frequencies in the range $10-10^9$ Hz, NMR relaxometry may even compete with DS. However, a severe limitation of FC NMR relaxometry remains: relaxation rates larger than 1000 s^{-1} are not accessible because of switching times on the order of ms, a limitation which is even more severe in the case of deuteron FC with its significantly higher quadrupolar coupling.[76]

The CD function often applied to describe NMR rotational relaxation data in viscous liquids is not a sufficient description of the full spectral density. This is only discovered when FC NMR master curves are constructed including relaxation data down to T_g. At low temperatures and high frequencies, respectively, appears an "excess wing" on the high-frequency flank of susceptibility, a feature well established by DS, OKE, and PCS studies. Any relevant anisotropic re-orientation of the molecule can be ruled out as already concluded in refs.[33,35,77] However, this may change at high temperatures close to the boiling point.[76] Investigating the partially deuterated glycerol-d_3 and glycerol-d_5, Schnauss et al.[35] already concluded "... that the glycerol "molecule" moves as an entity as far as the α-process is concerned", although, obviously, the molecule is not rigid. It appears that isotropy and "rigidity" of an actually flexible molecule is a feature of cooperative dynamics in dense liquids.[77] A strong coupling between conformational and overall tumbling seems to appear. A completely different scenario is observed in the case of mono-alcohols where the differently deuterated molecule exhibits significantly different $T_1(T)$ traces.[78]

In previous proton NMR works, it was often argued that intermolecular relaxation can be ignored because of the strong dependence of the dipolar coupling on the internuclear spin distance. Our analysis proofs the contrary. For example, from Figure 2b, we extract a ratio $R_{1,trans}(0)/R_{1,rot}(0) = 3.0$ which, on the one hand, clearly demonstrates the relevance of the intermolecular relaxation pathway at low frequencies. On the other hand, from Figure 2d, the contribution at shortest times yields the ratio of the coupling constants, that is, $C_{trans}(0)/C_{rot}(0) = K_{trans}/K_{rot}$. We extract $C_{trans}(0)/C_{rot}(0) = 0.101$, whereas $K_{trans}/K_{rot} = 0.102$ is calculated from the analysis of the master curve, which is a very satisfying agreement. Clearly, the rotational coupling (including the eccentricity effect) is much stronger and it determines the relaxation at high frequencies. Consequently, the ratios $R_{1,trans}(\omega)/R_{1,rot}(\omega)$ and $R_{1,inter}(\omega)/R_{1,intra}(\omega)$ depend strongly on the considered frequency range. The rotational relaxation contribution contains intra- and intermolecular contributions (eccentricity) which cannot be separated without performing an isotope dilution experiment. Actually, in the case of glycerol, the eccentricity effect is larger than the translational contribution.[18] Taking the simple estimate from eq 15 together with $r = \tau_{trans}/\tau_{rot} = 56$, $d = 0.40$ nm, and $r_{12} = 0.176$ nm (assuming the proton–proton distance of the methylene groups as the most relevant distance in glycerol which is calculated from the structure of methane), we find
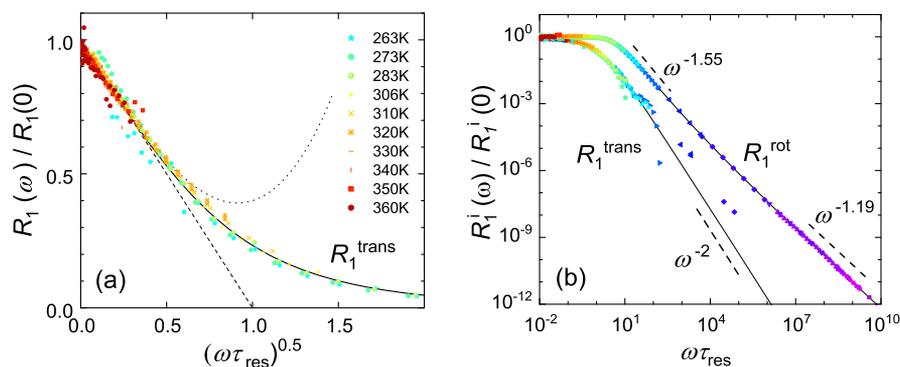
Figure 7. (a) Isolated translational relaxation rate plotted vs the square root of the rescaled frequency (initial part); different colors refer to different temperatures; solid line: interpolation by the FFHS model; in addition, the expansion up to the first (dashed line, see eq 10) and second order (dotted line, see eq 13) is shown. (b) Translational relaxation and rotational relaxation spectrum shown over the full frequency range; solid line gives interpolation by FFHS model (R_1^{rot}) and double CD spectral density (R_1^{trans}), respectively; note the different high-frequency power laws (see text).

$$\frac{R_{1,inter}(0)}{R_{1,intra}(0)} \cong \frac{64\pi}{27}\left(\frac{r_{12}}{d}\right)^6 r = 3.04$$

This reproduces perfectly the experimental result reported above. Of course, because of the higher power of six, the actual (average) value of the ratio r_{12}/d sensitively influences the outcome of the estimate. We emphasize that the estimate neglects the rotational contribution via the intermolecular relaxation pathway.

As discussed in the Theoretical Background section, direct evidence of the dominance of the translational relaxation contribution at low frequency may be demonstrated by displaying part of the reduced spectral density $R_1(\omega)/R_1(0)$ against the square root of the reduced frequency where the time constant τ_{res} is given by eq 11. In Figure 7a, we plot the isolated translational relaxation (as given by the fit of the master curve in Figure 2b) against $\sqrt{\omega\tau_{res}}$. The translational data are well fitted by the FFHS model (solid line) with an initial slope of −1, representing the first term of the expansion of eq 13 (dashed line). In addition, we included the prediction for the second term (dotted line) which, however, provides only a small extension of the interpolation. In Figure 7b, we display the full spectral densities in a double-log plot. One recognizes a different high-frequency behavior. The translational data follow a power law with exponent −2 up to highest frequencies as expected by the FFHS model, whereas the rotational part displays a power law with an exponent $-1.55 = -(1 + \beta_{CD})$ which crosses over to another power law with an exponent $-1.19 = -(1 + \gamma_{CD})$ at highest frequencies.

Extending our approach with the full rotational spectral density obtained from proton relaxation, we are able to reproduce the deuteron data of glycerol down to T_g, either (see Figure 6). We think our approach is paradigmatic for viscous liquids as is further demonstrated for the relaxation data of m-tricresyl phosphate (Figure 3b), for example. Assuming generic behavior of molecular glass formers in terms of a double CD function describing the rotational susceptibility of the α-process, any deviation from this behavior should signal the existence of internal relaxation. The additional relaxation could be due to a methyl group (if present) or a kind of β-process, the latter often found in molecular glass formers. Here, the case of o-terphenyl is of interest, as one still finds statements in the literature that o-terphenyl exhibits a strong β-process as first reported by Johari and Goldstein.[79] Because of its low dipole

moment, reliable dielectric spectra including high frequencies are missing as well as proton FC NMR relaxation data down to T_g so far. This situation can be improved by taking recourse to deuteron relaxation. In Figure 8, we show $T_1(T)$ and $T_2(T)$[33] plotted as a function of τ_{rot} as given by a depolarized LS study[80] which, as discussed, directly yields the (reciprocal) susceptibility function. A free fit with a double CD function yields very similar shape parameters as in the case of glycerol, and the quadrupolar coupling constant $C_Q = 187$ kHz well agrees with that obtained from a spectral analysis at low temperature ($C_Q = 182$ kHz[33]). Clearly, there is no indication of a β-process as also reported by Wagner and Richert.[81] However, here, there is a problem: the LS experiments so far were unable to clearly identify an excess wing in the case of o-terphenyl.[80] Therefore, we are looking forward to proton FC relaxation data measured down to T_g.
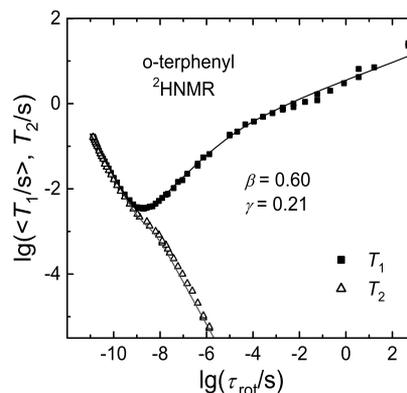

Figure 8. Deuteron spin−lattice $\langle T_1 \rangle$ and spin−spin relaxation time T_2 of o-terphenyl-d$_{14}$ as a function of correlation times taken from the literature;[80] solid lines: free fit with a double CD function describing the rotational spectral density.

There is one feature, however, which makes glycerol (and its homologues[82]) special. The extent of separation of molecular rotation and translation given by the separation parameter $r \cong 56$ does not conform to SED which predicts $r_{SED} = 9$. Consequently, the hydrodynamic radius extracted by assuming SED becomes unphysically small (cf. below). Actually, it was the large r value and concomitantly the recognizable bimodal structure of the NMR susceptibility that demonstrated the

relevance of both contributions, inter- and intramolecular relaxation in the case of glycerol. Smaller r values close to the SED limit are found in nonassociated liquids like o-terphenyl or m-tricresyl phosphate, for example, and the bimodal structure of susceptibility is hardly visible.[58,64] However, regarding o-terphenyl, we demonstrated by isotope dilution experiments that translational relaxation dominates at lowest frequencies also in this case.[58] Thus, applying proton NMR relaxometry, an important advantage is that both translation and rotation can be probed in a single experiment.

Chang and Sillescu measured the diffusion coefficient of several molecular glass formers down to values $D \cong 10^{-14}$ m^2 s^{-1} by NMR diffusometry.[63] While an enhancement of translational diffusion was found in comparison with rotational diffusion and shear viscosity in most systems at low temperatures, the situation regarding glycerol was less clear. For example, testing the SED relations $D\eta/T$ and $D\tau_{diel}$, no enhancement was observed at $T > 250$, whereas $\eta/(T\tau_{diel})$ showed weak increases at lowest temperatures close to T_g. Interestingly, a value $D\tau_{diel} \cong 1.6 \ 10^{-21} = 2/3R_H^2$ was found, which was anomalously low compared to those of the other systems, resulting in an unphysically low hydrodynamic radius $R_H = 0.049$ nm compared to the van der Waals radius R_{vdW} = 0.27 nm.[83] Similarly low values, $R_H = 0.08$ nm from $\eta/(T\tau_{diel})$, $R_H = 0.16$ nm from $D\eta/T$, and $R_H = 0.096$ from deuteron NMR, were reported.[62] These results agree with those from the present study. Because of the large separation parameter r, a hydrodynamic radius of $R_H = 0.09$ nm is calculated. The fit by the FFHS model, however, which does not assume SED to hold one, gets $d/2 = 0.20$ nm, which is close to R_{vdW}. An X-ray study reported a distance between next neighbors of 0.506 nm (at 250 K).[84] A comparatively low value, $R_H = 0.12$ nm, was also found in propylene glycol. Moreover, adding aprotic chloroform reduces the r value until a value close to that of o-terphenyl ($r \cong 10$) is found below a threshold concentration $x = 0.65$.[64] We suggested that the strong failure of SED in the case of glycerol and its homologues might find its explanation by the presence of a 3d hydrogen bond network, which makes glycerol a strongly associated liquid. Possibly, the ratio r/r_{SED} may be taken as a measure of molecular association in a liquid.[22]

As seen in Figure 6, close to T_g, the extracted correlation time τ_{rot} takes values up to seconds, and the NMR line is essentially given by its rigid body limit, that is, $|H_{DD}|\tau_{rot} \gg 1$, where $|H_{DD}|$ is the magnitude of the ensemble-averaged dipolar Hamiltonian, the fluctuations of which are responsible for the relaxation. Discussing the limit of the relaxation theory concerning T_1 and T_2, Abragam's textbook states that the condition $|H_{DD}| \tau \ll 1$ must be applied in order to derive eq 1.[3] Regarding T_2, clearly, the criterion is violated in the present case as the spin−spin relaxation close to T_g becomes essentially a Gaussian, that is, "BPP" fails, and the usual T_2 analysis stops well above T_g. Regarding T_1, the situation apparently is different as we do not see any indication of Gaussian recovery, which might indicate failure of "BPP", and the time constant $\tau_{rot}(T)$ extracted still follow that from the other techniques. In his textbook, Kimmich formulated the "Redfield limit", defining the application limit of the BPP approach in terms of $T_1, T_2 \gg \tau$.[85] Moreover, this is violated in the present case also, if we take τ_{rot} for τ, because τ_{rot} close to T_g becomes longer than T_1.

The situation may be understood by the result from deuteron relaxation which displays a nonexponential spin−lattice relaxation close to T_g where $|H_Q| \tau_{rot} \gg 1$ holds, and a solid-state (Pake) spectrum is observed, whereas exponential relaxation together with a Lorentzian spectrum is found at higher temperatures.[48,51] A nonexponential relaxation is found provided τ_{rot} is longer than the measured T_1. In terms of Zimmerman and Brittin,[86] the exchange time (given by τ_{rot}) among the different sites with different T_1 in the almost rigid glass former is too slow. Consequently, the actually short T_1 is not any longer determined by the overall tumbling of the molecules with time τ_{rot}, instead a faster process must control the relaxation which displays some extent of dynamic heterogeneity. The candidate is, of course, the excess wing which has been interpreted as a small-angle wobbling of the molecular axis which predates the main α-relaxation process.[47,87] This interpretation appears to be supported by the fact that in the dielectric spectra ($l = 1$ probe), the excess wing displays an amplitude which is roughly by a factor 3 smaller than that of the NMR or PCS susceptibility ($l = 2$ probes)—see Figure 3. Assuming small-angle motion, $\chi_2''(\omega) = 3\chi_1''(\omega)$ holds,[47,88,89] which leads to a corresponding relation between the susceptibilities at high frequencies, $\omega\tau_{rot} \gg 1$. However, we note that this argument was recently challenged.[90] We emphasize that the slow wobbling motion reflected by the excess wing must not be confused with the kind of motion on the picosecond time scale which is associated with the "rattling in the cage" motion discussed within the mode-coupling theory,[91] for example.

Referring to the Supporting Information, we can give a more precise formulation of the Redfield limit in the case of spin−lattice relaxation which is actually different from that of the spin−spin relaxation due to differences in the microscopic mechanism by which the relaxations occurs. As long as the time scale of the fluctuations yielding dispersion effects is short with respect to T_1, the Redfield is not violated. Taking $1/\omega$ as a measure of the time scale the probed fluctuations, the Redfield limit reads $T_1 \ll 1/\omega$ or $R_1 \ll \omega$. Inspecting Figure 1a, this condition is fulfilled at all temperatures in the case of glycerol.

There is a second NMR-intrinsic limit of the FC method. Generally, the external magnetic field applied should be significantly larger compared to the static local field. For example, some kind of anisotropic re-orientation occurs in a plastic crystal, and the corresponding solid-state spectrum exhibits a certain width reflecting the time-independent part of the Hamiltonian. Then, applying Larmor frequencies below the width of the spectrum lead to erroneous results. In the case of a liquid, specifically for glycerol close to T_g, the spectrum is controlled by the (full) static dipolar interaction which may be on the order of, for example, 50 kHz. Thus, relaxation data below 50 kHz would violate the criterion. However, inspecting Figure 2a, no such data are compiled first of all because of the fact that the relaxation rate becomes too high at such low frequencies.

■ CONCLUSIONS

For the first time, a full description of the dispersion of proton spin−lattice relaxation rate $R_1(T,\omega)$ from 360 K down to T_g is achieved, which also includes the so-far complete data set taken by Noack and co-workers from 1971. Taking recourse to different master curve constructions by exploiting FTS, 15 decades in frequency/time are covered, which allow a quantitative description in terms of rotational and translational relaxation contributions. The rotational part of the spectral density/susceptibility shows high similarity with those reported

by other techniques probing rotational dynamics. In addition to a Cole-Davidson-like peak, a high-frequency "excess wing" has to be accounted for. The translational contribution is reproduced by applying the FFHS model designed to describe diffusion of dipolarly coupled spin systems. Such quantitatively fitted master curves allows us to describe all the individual $R_1(T,\omega)$ data sets. The extracted time constant $\tau_{\rm rot}(T)$ agrees well with those from other techniques probing re-orientational dynamics, while the diffusion coefficient $D(T)$ derived from the low-frequency expansion of the intermolecular relaxation rate is confirmed by that from gradient NMR studies. In other words, the advantage of doing proton relaxation results from the possibility to access molecular rotation and translation in the same experiment.

We think our approach is paradigmatic for the analysis of spin−lattice relaxation in glass-forming liquids. It allows us also to solve the long-standing deficiencies of analyses regarding deuteron relaxation close to T_g. It is of no surprise that the same rotational spectral density as found for proton relaxation applies also in the case of deuterons. There is one feature which makes glycerol (and its homologues) special. The extent of separation of molecular rotation and translation directly extracted from the master curve is rather large compared to that of molecular liquids like *m*-tricresyl phosphate or *o*-terphenyl and thus does not conform to SED. This goes along with nonphysically low hydrodynamic radius well known also from the literature. We suggest explaining this peculiarity of glycerol by its capability to form a 3D hydrogen bond network, possibly leading to a strong coupling of conformational jumps and overall tumbling, challenging the applicability of the SED relationship.

ASSOCIATED CONTENT

SI **Supporting Information**

The Supporting Information is available free of charge at https://pubs.acs.org/doi/10.1021/acs.jpcb.9b11770.

Redfield limit in the case of the spin−lattice relaxation and spin−spin relaxation (PDF)

AUTHOR INFORMATION

Corresponding Author

E. A. Rössler − *Nordbayerisches NMR-Zentrum, Universität Bayreuth, 95440 Bayreuth, Germany;* orcid.org/0000-0001-5586-973X; Email: ernst.roessler@uni-bayreuth.de

Authors

M. Flämig − *Nordbayerisches NMR-Zentrum, Universität Bayreuth, 95440 Bayreuth, Germany*

M. Hofmann − *Nordbayerisches NMR-Zentrum, Universität Bayreuth, 95440 Bayreuth, Germany;* orcid.org/0000-0001-9330-2742

N. Fatkullin − *Nordbayerisches NMR-Zentrum, Universität Bayreuth, 95440 Bayreuth, Germany; Institute of Physics, Kazan Federal University, 420008 Kazan, Tatarstan, Russia*

Complete contact information is available at:
https://pubs.acs.org/10.1021/acs.jpcb.9b11770

Notes

The authors declare no competing financial interest.

REFERENCES

(1) Bloembergen, N.; Purcell, E. M.; Pound, R. V. Relaxation Effects in Nuclear Magnetic Resonance Absorption. *Phys. Rev.* **1948**, *73*, 679−712.

(2) Kubo, R.; Tomita, K. A General Theory of Magnetic Resonance Absorption. *J. Phys. Soc. Jpn.* **1954**, *9*, 888−919.

(3) Abragam, A. *The Principles of Nuclear Magnetism*; Clarendon Press; Oxford, 1961.

(4) Slichter, C. P. *Principles of Magnetic Resonance*, 3rd ed.; Springer; Berlin, Heidelberg, New York, 1992.

(5) Mehring, M. *Principles of High Resolution NMR in Solids*, 2nd ed.; Springer: Berlin, Heiderberg, New York, 1983.

(6) Noack, F.; Preissing, G. Magnetische Relaxation in Glycerin. *Z. Naturforsch.* **1969**, *24*, 143−153.

(7) Preissing, G.; Noack, F.; Kosfeld, R.; Gross, B. Zur Deutung der Protonenspinrelaxation in Glycerin. *Z. für Physik A Hadrons Nucl.* **1971**, *246*, 84−90.

(8) Luszczynski, K.; Kail, J. A. E.; Powles, J. G. Molecular Motion in Liquid Glycerol by Proton Magnetic Relaxation. *Proc. Phys. Soc.* **1960**, *75*, 243−256.

(9) Engel, G.; Hertz, H. On the Negative Hydration. A Nuclear Magnetic Relaxation Study. *Ber. Bunsenges. Phys. Chem.* **1968**, *72*, 808−834.

(10) Harmon, J. F.; Muller, B. H. Nuclear Spin Relaxation by Translational Diffusion in Liquid Ethane. *Phys. Rev.* **1969**, *182*, 400−410.

(11) Harmon, J. F. Low Frequency Spin Lattice Relaxation in Glycerol. *Chem. Phys. Lett.* **1970**, *7*, 207−208.

(12) Torrey, H. C. Nuclear Spin Relaxation by Translational Diffusion. *Phys. Rev.* **1953**, *92*, 962−969.

(13) Fiorito, R. B.; Meister, R. Pressure and Temperature Studies of NMR Translational Relaxation in Hydrogen Bonded Liquids. *J. Chem. Phys.* **1972**, *56*, 4605−4619.

(14) Favret, A. G.; Meister, R. Nuclear Magnetic Resonance Relaxation in Associated Liquids. *J. Chem. Phys.* **1964**, *41*, 1011−1018.

(15) Noack, F. NMR field-cycling spectroscopy: principles and a]lications. *Prog. NMR Spectrosc.* **1986**, *18*, 171−276.

(16) STELAR Company. www.stelar.it, 2020.

(17) Kimmich, R.; Anoardo, E. Field-cycling NMR Relaxometry. *Prog. Nucl. Magn. Reson. Spectrosc.* **2004**, *44*, 257−320.

(18) Kruk, D.; Herrmann, A.; Rössler, E. A. Field-cycling NMR Relaxometry of Viscous Liquids and Polymers. *Prog. Nucl. Magn. Reson. Spectrosc.* **2012**, *63*, 33−64.

(19) Meier, R.; Kruk, D.; Rössler, E. A. Intermolecular Spin Relaxation and Translation Diffusion in Liquids and Polymer Melts: Insight from Field-Cycling ^{1}H NMR Relaxometry. *ChemPhysChem* **2013**, *14*, 3071−3081.

(20) Fujara, F.; Kruk, D.; Privalov, A. F. Solid State Field-cycling NMR Relaxometry: Instrumental Improvements and New Applications. *Prog. Nucl. Magn. Reson. Spectrosc.* **2014**, *82*, 39−69.

(21) Kimmich, R.; Fatkullin, N. Self-Diffusion Studies by Intra- and Intermolecular Spin-lattice Relaxometry Using Field-cycling: Liquids, Plastic Crystals, Porous Media, and Polymer Segments. *Prog. Nucl. Magn. Reson. Spectrosc.* **2017**, *101*, 18−50.

(22) Rössler, E. A.; Hofmann, M.; Fatkullin, N. Application of Field-cycling NMR Relaxometry to the Study of Translational and Rotational Dynamics in Liquids and Polymers. In *New Developments of NMR Field-Cycling NMR Relaxometry*; Kimmich, R., Ed.; Royal Society of Chemistry: Cambridge, England, 2019; pp 181−206.

(23) Sousa, D. M.; Marques, G. D.; Cascais, J. M.; Sebastião, P. J. Desktop Fast-field Cycling Nuclear Magnetic Resonance Relaxometer. *Solid State Nucl. Magn. Reson.* **2010**, *38*, 36−43.

(24) Kruber, S.; Farrher, G. D.; Anoardo, E. Air Core Notch-coil Magnet with Variable Geometry for Fast-field-cycling NMR. *J. Magn. Reson.* **2015**, *259*, 216−224.

(25) Zampetoulas, V.; Lurie, D. J.; Broche, L. M. Correction of Environmental Magnetic Fields for the Acquisition of Nuclear Magnetic Relaxation Dispersion Profiles Below Earth's Field. *J. Magn. Reson.* **2017**, *282*, 38−46.

(26) Chou, C.-Y.; Abdesselem, M.; Bouzigues, C.; Chu, M.; Guiga, A.; Huang, T.-H.; Ferrage, F.; Gacoin, T.; Alexandrou, A.; Sakellariou, D. Ultra-wide Range Field-dependent Measurements of the Relaxivity of Gd 1− x Eu x VO 4 Nanoparticle Contrast Agents Using a Mechanical Sample-shuttling Relaxometer. *Sci. Rep.* **2017**, *7*, 44770.

(27) Kresse, B.; Privalov, A. F.; Herrmann, A.; Hofmann, M.; Rössler, E. A.; Fujara, F. Simultaneous Measurement of Very Small Magnetic Fields and Spin-lattice Relaxation. *Solid State Nucl. Magn. Reson.* **2014**, *59−60*, 45−47.

(28) Kresse, B.; Becher, M.; Privalov, A. F.; Hofmann, M.; Rössler, E. A.; Vogel, M.; Fujara, F. 1H NMR at Larmor Frequencies Down to 3 Hz by Means of Field-cycling Techniques. *J. Magn. Reson.* **2017**, *277*, 79−85.

(29) Zhukov, I. V.; Kiryutin, A. S.; Yurkovskaya, A. V.; Grishin, Y. A.; Vieth, H.-M.; Ivanov, K. L. Field-Cycling NMR Experiments in an Ultra-wide Magnetic Field Range: Relaxation and Coherent Polarization Transfer. *Phys. Chem. Chem. Phys.* **2018**, *20*, 12396−12405.

(30) Drake, P. W.; Meister, R. Rotational Spin-lattice and Spin-spin Quadrupole Relaxation in Perdeuterated Glycerol. *J. Chem. Phys.* **1971**, *54*, 3046−3050.

(31) Kintzinger, J. P.; Zeidler, M. D. Nuclear Magnetic Relaxation Study of Glycerol. *Ber. Bunsen Ges. Phys. Chem.* **1973**, *77*, 98−103.

(32) Rössler, E.; Sillescu, H. 2H NMR Study of Supercooled Toluene. *Chem. Phys. Lett.* **1984**, *112*, 94−98.

(33) Dries, T.; Fujara, F.; Kiebel, M.; Rössler, E.; Sillescu, H. 2H-NMR Study of the Glass Transition in Supercooled Ortho-terphenyl. *J. Chem. Phys.* **1988**, *88*, 2139−2147.

(34) Wolfe, M.; Jonas, J. Reorientational Motions in Compressed Viscous Fluids: Selectively Deuterated Glycerol. *J. Chem. Phys.* **1979**, *71*, 3252−3262.

(35) Schnauss, W.; Fujara, F.; Sillescu, H. The Molecular Dynamics Around the Glass Transition and in the Glassy State of Molecular Organic Systems: A 2H − Nuclear Magnetic Resonance Study. *J. Chem. Phys.* **1992**, *97*, 1378−1389.

(36) Döß, A.; Hinze, G.; Böhmer, R.; Sillescu, H.; Kolshorn, H.; Vogel, M.; Zimmermann, H. Deuteron and Carbon Magnetic Resonance Studies of Supercooled Liquid and Glassy Salol. *J. Chem. Phys.* **2000**, *112*, 5884−5892.

(37) Böttcher, C. J. F.; Bordewijk, P. *Theory of Electric Polarization*; Elsevier Scientific Polarization: Amsterdam, The Netherlands, 1978.

(38) Cummins, H. Z.; Li, G.; Hwang, Y. H.; Shen, G. Q.; Du, W. M.; Hernandez, J.; Tao, N. J. Dynamics of Supercooled Liquids and Glasses: Comparison of Experiments With Theoretical Predictions. *Z. Phys. B* **1997**, *103*, 501−519.

(39) Torre, R.; Bartolini, P.; Pick, R. Time-resolved Optical Kerr effect in a Fragile Glass-forming Liquid, Salol. *Phys. Rev. E* **1998**, *57*, 1912−1920.

(40) Götze, W. Recent Tests of the Mode-coupling Theory for Glassy Dynamics. *J. Phys.: Condens. Matter* **1999**, *11*, A1−A45.

(41) Lunkenheimer, P.; Schneider, U.; Brand, R.; Loid, A. Glassy Dynamics. *Contemp. Phys.* **2000**, *41*, 15−36.

(42) Hinze, G.; Brace, D. D.; Gottke, S. D.; Fayer, M. D. A Detailed Test of Mode-coupling Theory on All Time Scales: Time Domain Studies of Structural Relaxation in a Supercooled Liquid. *J. Chem. Phys.* **2000**, *113*, 3723−3733.

(43) Tölle, A. Neutron Scattering Studies of the Model Glass Former Ortho-terphenyl. *Rep. Prog. Phys.* **2001**, *64*, 1473−1532.

(44) Wolynes, P. G.; Lubchenko, V. *Structural Glasses and Supercooled Liquids*; Wiley: Oxford, 2012.

(45) Petzold, N.; Schmidtke, B.; Kahlau, R.; Bock, D.; Meier, R.; Micko, B.; Kruk, D.; Rössler, E. A. Evolution of the Dynamic Susceptibility in Molecular Glass Formers: Results From Light

Scattering, Dielectric Spectroscopy, and NMR. *J. Chem. Phys.* **2013**, *138*, 12A510.

(46) Kruk, D.; Meier, R.; Rössler, E. A. Translational and Rotational Diffusion of Glycerol by Means of Field Cycling 1H NMR Relaxometry. *J. Phys. Chem. B* **2011**, *115*, 951−957.

(47) Gainaru, C.; Lips, O.; Troshagina, A.; Kahlau, R.; Brodin, A.; Fujara, F.; Rössler, E. A. On the Nature of the High-frequency Relaxation in a Molecular Glass Former: A Joint Study of Glycerol by Field Cycling NMR, Dielectric Spectroscopy, and Light Scattering. *J. Chem. Phys.* **2008**, *128*, 174505.

(48) Kariyo, S.; Gainaru, C.; Schick, H.; Brodin, A.; Rössler, E. A. From a Simple Liquid to a Polymer Melt: NMR Relaxometry Study of Polybutadiene. *Phys. Rev. Lett.* **2006**, *97*, 207803. Kariyo, S.; Herrmann, A.; Gainaru, C.; Schick, H.; Brodin, A.; Rössler, E. A. Erratum From a Simple Liquid to a Polymer Melt: NMR Relaxometry Study of Polybutadiene. *Phys. Rev. Lett.* **2008**, *100*, 109901.

(49) Kariyo, S.; Brodin, A.; Gainaru, C.; Herrmann, A.; Schick, H.; Novikov, V. N.; Rössler, E. A. From Simple Liquid to Polymer Melt. Glassy and Polymer Dynamics Studied by Fast Field Cycling NMR Relaxometry: Low and High Molecular Weight Limit. *Macromolecules* **2008**, *41*, 5313−5321.

(50) Fujara, F.; Petry, W.; Diehl, R. M.; Schnauss, W.; Sillescu, H. Localized Motion in Supercooled Glycerol as Measured by 2H-NMR Spin-Lattice Relaxation and Incoherent Neutron Scattering. *Europhys. Lett.* **1991**, *14*, 563−568.

(51) Böhmer, R.; Diezemann, G.; Hinze, G.; Rössler, E. Dynamics of Supercooled Liquids and Glassy Solids. *Prog. Nucl. Magn. Reson. Spectrosc.* **2001**, *39*, 191−267.

(52) Wolf, D. *Spin-Temperature and Nuclear-Spin Relaxation in Matter: Basic Principles and Applications*; Clarendon Press: Oxford, 1979.

(53) Hwang, L.-P.; Freed, J. H. Dynamic Effects of Pair Correlation Functions on Spin Relaxation by Translational Diffusion in Liquids. *J. Chem. Phys.* **1975**, *63*, 4017−4025.

(54) Ayant, Y.; Belorizky, E.; Aluzon, J.; Gallice, J. Calcul des Densites Spectrales Resultant dun Mouvement Aleatoire de Translation en Relaxation par Interaction Dipolaire Magnetique Dans les Liquids. *J. Phys.* **1975**, *36*, 991−1004.

(55) Ayant, Y.; Belorizky, E.; Fries, P.; Rosset, J. Effet des Interactions Dipolaires Magnetiques Intermoleculaires sur la Relaxation Nucleaire de Molecules Polyatomiques Dans les Liquides. *J. Phys.* **1977**, *38*, 325−337.

(56) Fries, P.; Belorizky, E. Effect des Fonctions de Correlation de Paire sur la Relaxation Nucleaire Intermoleculaire par Diffusion Translationelle et Rotationelle Dans les Liquides. *J. Phys.* **1978**, *39*, 1263−1282.

(57) Albrand, J. P.; Taieb, M. C.; Fries, P.; Belorizky, E. Effects of Eccentricity on Nuclear Magnetic Relaxation by Intermolecular Dipole-dipole Interactions: 13C Relaxation of Neopentane. *J. Chem. Phys.* **1981**, *75*, 2141−2146.

(58) Meier, R.; Kruk, D.; Bourdick, A.; Schneider, E.; Rössler, E. A. Inter- and Intramolecular Relaxation in Molecular Liquids by Field Cycling 1H NMR Relaxometry. *Appl. Magn. Reson.* **2013**, *44*, 153−168.

(59) Meier, R.; Kruk, D.; Gmeiner, J.; Rössler, E. A. Intermolecular Relaxation in Glycerol as Revealed by Field Cycling 1H NMR Relaxometry Dilution Experiments. *J. Chem. Phys.* **2012**, *136*, 034508.

(60) Sholl, C. A. Nuclear Spin Relaxation by Translational Diffusion in Liquids and Solids: High-and Low-Frequency Limits. *J. Phys. C: Solid State Phys.* **1981**, *14*, 447−464.

(61) Kruk, D.; Meier, R.; Roessler, E. A. Nuclear Magnetic Resonance Relaxometry as a Method of Measuring Translational Diffusion Coefficients in Liquids. *Phys. Rev. E* **2012**, *85*, 020201.

(62) Meier, R.; Herrmann, A.; Hofmann, M.; Schmidtke, B.; Kresse, B.; Privalov, A. F.; Kruk, D.; Fujara, F.; Rössler, E. A. Iso-frictional Mass Dependence of Diffusion of Polymer Melts Revealed by 1H NMR Relaxometry. *Macromolecules* **2013**, *46*, 5538−5548.

(63) Chang, I.; Sillescu, H. Heterogeneity at the Glass Transition: Translational and Rotational Self-diffusion. *J. Phys. Chem. B* **1997**, *101*, 8794−8801.

(64) Meier, R.; Schneider, E.; Rössler, E. A. Change of Translational-rotational Coupling in Liquids Revealed by Field-Cycling ¹H NMR. *J. Chem. Phys.* **2015**, *142*, 034503.

(65) Blochowicz, T. Broadband Dielectric Spectroscopy in Neat and Binary Glass Formers. Ph.D. Thesis, Bayreuth University, Logos Verlag, Berlin, 2003.

(66) Blochowicz, T.; Tschirwitz, C.; Benkhof, S.; Rössler, E. A. Susceptibility Functions for Slow Relaxation Processes in Supercooled Liquids and the Search for Universal Relaxation Patterns. *J. Chem. Phys.* **2003**, *118*, 7544−7555.

(67) Adishchev, S.; Bock, D.; Gainaru, C.; Kahlau, R.; Micko, B.; Petzold, N.; Pötzschner, B.; Rössler, E. A. Reorientational Dynamics of Organophosphate Glass Formers − a Joint Study by ³¹P NMR, Dielectric Spectroscopy and Light Scattering. *Z. Phys. Chem.* **2012**, *226*, 1149−1168.

(68) Gottke, S. D.; Brace, D. D.; Hinze, G.; Fayer, M. D. Time Domain Optical Studies of Dynamics in Supercooled O-terphenyl: Comparison to Mode Coupling Theory on Fast and Slow Time Scales. *J. Phys. Chem. B* **2001**, *105*, 238−245.

(69) Brodin, A.; Rössler, E. A. Depolarized Light Scattering Versus Optical Kerr Effect Spectroscopy of Supercooled Liquids: Comparative Analysis. *J. Chem. Phys.* **2006**, *125*, 114502.

(70) Brodin, A.; Rössler, E. A. Depolarized Light Scattering Versus Optical Kerr Effect. II. Insight Into the Dynamic Susceptibility of Molecular Liquids. *J. Chem. Phys.* **2007**, *126*, 244508.

(71) Cang, H.; Novikov, V. N.; Fayer, M. D. Logarithmic Decay of Orientational Correlation Function in Supercooled Liquids on the ps to ns Time Scale. *J. Chem. Phys.* **2003**, *118*, 2800−2807.

(72) Brodin, A.; Gainaru, C.; Porokhonskyy, V.; Rössler, E. A. Evolution of Dynamic Susceptibility in Molecular Glass Formers—a Critical Assessment. *J. Phys.: Condens. Matter* **2007**, *19*, 205104.

(73) Diezemann, G. Dipolar Interactions in Deuteron Spin Systems. I. Spin Diffusion. *J. Chem. Phys.* **1995**, *103*, 6368−6384.

(74) Brodin, A.; Rössler, E. A. Depolarized Light Scattering Study of Glycerol. *Eur. Phys. J. B* **2005**, *44*, 3−14.

(75) Kudlik, A.; Benkhof, S.; Blochowicz, T.; Tschirwitz, C.; Rössler, E. The Dielectric Response of Simple Organic Glass Formers. *J. Mol. Struct.* **1999**, *479*, 201−218.

(76) Flämig, M.; Becher, M.; Hofmann, M.; Körber, T.; Kresse, B.; Privalov, A. F.; Willner, L.; Kruk, D.; Fujara, F.; Rössler, E. A. Perspectives of Deuteron Field-cycling NMR Relaxometry for Probing Molecular Dynamics in Soft Matter. *J. Phys. Chem. B* **2016**, *120*, 7754−7766.

(77) Rössler, E. Corresponding States Concept for Simple Supercooled Liquids Identifying a Change of Diffusion Mechanism Above the Glass Transition Temperature. *Ber. Bunsenges. Phys. Chem.* **1990**, *94*, 392−399.

(78) Gainaru, C.; Meier, R.; Schildmann, S.; Lederle, C.; Hiller, W.; Rössler, E. A.; Böhmer, R. Nuclear Magnetic Resonance Measurements Reveal the Origin of the Debye Process in Monohydroxy Alcohols. *Phys. Rev. Lett.* **2010**, *105*, 258303.

(79) Johari, G. P.; Goldstein, M. Viscous Liquids and the Glass Transition. II. Secondary Relaxations in Glasses of Rigid Molecules. *J. Chem. Phys.* **1970**, *53*, 2372−2388.

(80) Petzold, N.; Rössler, E. A. Light Scattering Study on the Glass Former O-terphenyl. *J. Chem. Phys.* **2010**, *133*, 124512.

(81) Wagner, H.; Richert, R. Equilibrium and Non-equilibrium Type β-relaxations: D-sorbitol Versus O-terphenyl. *J. Phys. Chem. B* **1999**, *103*, 4071−4077.

(82) Meier, R.; Kahlau, R.; Kruk, D.; Rössler, E. A. Comparative Studies of the Dynamics in Viscous Liquids by Means of Dielectric Spectroscopy and Field Cycling NMR. *J. Phys. Chem. A* **2010**, *114*, 7847−7855.

(83) Edward, J. T. Molecular Volumes and the Stokes-Einstein Equation. *J. Chem. Educ.* **1970**, *47*, 261−270.

(84) Soltwisch, M.; Steffen, B. The X-Ray Structure Factor of Liquid Glycerol. *Z. Naturforsch.* **1981**, *36*, 1045−1051.

(85) Kimmich, R. *NMR, Tomography, Diffusometry, Relaxometry*; Springer: Berlin, 1997.

(86) Zimmerman, J. R.; Brittin, W. E. Nuclear Magnetic Resonance Studies in Multiple Phase Systems: Lifetime of a Water Molecule in an Adsorbing Phase on Silica Gel. *J. Phys. Chem.* **1957**, *61*, 1328−1333.

(87) Vogel, M.; Medick, P.; Rössler, E. A. Secondary Relaxation Processes in Molecular Glasses Studied by Nuclear Magnetic Resonance Spectroscopy. *Annu. Rep. NMR Spectrosc.* **2005**, *56*, 231−299.

(88) Lebon, M. J.; Dreyfus, C.; Guissani, Y.; Pick, R. M.; Cummins, H. Z. Light Scattering and Dielectric Susceptibility Spectra of Glassforming Liquids. *Z. Phys. B* **1997**, *103*, 433−439.

(89) Blochowicz, T.; Kudlik, A.; Benkhof, S.; Senker, J.; Rössler, E.; Hinze, G. The Spectral Density in Simple Organic Glassformers: Comparison of Dielectric and Spin-lattice Relaxation. *J. Chem. Phys.* **1999**, *110*, 12011−12022.

(90) Gabriel, J. P.; Zourchang, P.; Pabst, F.; Helbling, A.; Weigl, P.; Böhmer, T.; Blochowicz, T. Intermolecular Cross-correlations in the Dielectric Response of Glycerol. **2019**, arXiv:1911.10976. arXiv preprint.

(91) Götze, W. *Complex Dynamics of Glass-Forming Liquids*; Oxford University Press: Oxford, 2009.

Publication 2

Perspectives of Deuteron Field-Cycling NMR Relaxaometry for Probing Molecular Dynamics in Soft Matter

Flämig, M.; Becher, M.; Hofmann, M.; Körber, T.; Kresse, B.; Privalov, A. F.; Willner, L.; Kruk, D.; Fujara, F.; Rössler, E. A.
J. Phys. Chem. B, **2016**, *120*, 7754

Perspectives of Deuteron Field-Cycling NMR Relaxometry for Probing Molecular Dynamics in Soft Matter

M. Flämig,[†] M. Becher,[‡] M. Hofmann,[†] T. Körber,[†] B. Kresse,[‡] A. F. Privalov,[‡] L. Willner,[§] D. Kruk,[∥] F. Fujara,[‡] and E. A. Rössler*,[†]

[†]Experimentalphysik II, Universität Bayreuth, 95440 Bayreuth, Germany
[‡]Institut für Festkörperphysik, TU Darmstadt, Hochschulstrasse 6, 64289 Darmstadt, Germany
[§]Institute of Complex Systems, Forschungszentrum Jülich, D-52425 Jülich, Germany
[∥]Faculty of Mathematics and Computer Science, University of Warmia & Mazury, Słoneczna 54, 10-710 Olsztyn, Poland

ABSTRACT: Due to the single-particle character of the quadrupolar interaction in molecular systems, ^{2}H NMR poses a unique method for probing reorientational dynamics. Spin−lattice relaxation gives access to the spectral density, and its frequency dependency can be monitored by field-cycling (FC) techniques. However, most FC NMR studies employ ^{1}H; the use of ^{2}H is still rare. We report on the application of ^{2}H FC NMR for investigating the dynamics in molecular liquids and polymers. Commercial as well as home-built relaxometers are employed accessing a frequency range from 30 Hz to 6 MHz. Due to low gyromagnetic ratio, high coupling constants, and finite FC switching times, current ^{2}H FC NMR does not reach the dispersion region in liquids (toluene and glycerol), yet good agreement

with the results from conventional high-field (HF) relaxation studies is demonstrated. The pronounced difference at low frequencies between ^{2}H and ^{1}H FC NMR data shows the relevance of intermolecular relaxation in the case of ^{1}H NMR. In the case of the polymers polybutadiene and poly(ethylene-*alt*-propylene), very similar relaxation dispersion is observed and attributed to Rouse and entanglement dynamics. Combination with HF ^{2}H relaxation data via applying frequency−temperature superposition allows the reconstruction of the full spectral density reflecting both polymer as well as glassy dynamics. Transformation into the time domain yields the reorientational correlation function $C_2(t)$ extending over nine decades in time with a long-time power law, $C_2(t) \propto t^{-0.45\pm0.05}$, which does not conform to the prediction of the tube-reptation model, for which $\propto t^{-0.25}$ is expected. Entanglement sets in below $C_2(t = \tau_e) \cong S^2 = 0.001$, where τ_e is the entanglement time and S the corresponding order parameter. Finally, we discuss the future prospects of the ^{2}H FC NMR technique.
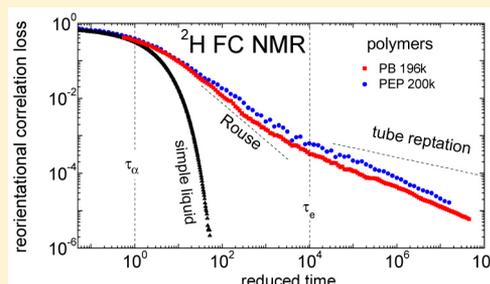
INTRODUCTION

NMR relaxometry, i.e., measuring the spin−lattice relaxation time T_1 or the spin−spin relaxation time T_2, is a well established method for probing the dynamics in condensed matter. In particular, with the availability of a commercial field-cycling (FC) relaxometer since about 2000, NMR relaxometry received new momentum, as it is now routinely possible to measure the dispersion of the spin−lattice relaxation in a frequency range of 10 kHz to 30 MHz (^{1}H).[1−5] With the use of a home-built relaxometer, even frequencies down to, say, 10 Hz are nowadays accessible.[6,7] The technique "cycles" the magnetic field produced by a resistive electromagnet from a (high) polarization field down to a (low) relaxation field and back to a (high) detection field. As in the case of dielectric spectroscopy (DS), relaxation spectra are collected for various temperatures and motional models in terms of their spectral density or susceptibility, respectively, are tested.

Most of the FC studies employed ^{1}H NMR. Due to the rather low detection field (about half a Tesla), protons with their high gyromagnetic ratio provide the most convenient way to get relaxation profiles within a reasonable time. Without

taking recourse to isotope labeling, ^{1}H FC NMR is well suited to study in particular the collective dynamics in soft matter, for example, in polymers, dendrimers, or liquid crystals. Here, collective dynamics is governed by frequency−temperature superposition (FTS); that is, the spectral shape of the dynamic susceptibility virtually does not change with temperature.[8−12] As in the case of shear stress relaxation,[13,14] collecting NMR relaxation data at different temperatures allows master curves to be constructed, which significantly extend the still narrow frequency range of the FC technique. Regarding polymers, different power-law dispersions were identified,[2−4,15−23] allowing the tube-reptation model to be tested,[24] for instance. The high similarity of such "broad band" NMR relaxation spectra with the corresponding shear relaxation spectra may establish FC NMR as a method of molecular rheology.[25]

The relaxation mechanism of ^{1}H NMR is provided by the fluctuation of the magnetic dipole−dipole interaction, which by

its very nature is a many-particle interaction.[26] For example, there is an intra- as well as an intermolecular relaxation pathway, and it is not easy to attribute both contributions in the total relaxation. For simple liquids and polymers, it is well-known that intermolecular contribution caused by translational dynamics (molecular diffusion) dominates the low-frequency dispersion of the total relaxation and allows the diffusion coefficient to be extracted,[26−29] while reorientational dynamics yields the dispersion at higher frequencies. However, this fact was only recently exploited in a systematic way[30−36] and also verified by molecular dynamics simulations.[37,38] However, molecular reorientations also yield an intermolecular ^{1}H relaxation contribution (the so-called eccentricity effect).[32,39] An ultimate approach to disentangle both intra- and intermolecular relaxation is given by the isotope dilution technique; first FC experiments were reported only recently.[35,40−43] Here, by dilution with the same but deuterated molecule, the intermolecular relaxation is suppressed. However, such FC experiments are time-consuming, as one has to measure the relaxation spectra for different concentrations (and temperatures). In the case of polymers, there are additional problems due to the necessity of having at hand deuterated and protonated polymers with the same molar mass and glass transition temperature T_g. Moreover, polymer blends tend to demix. Nevertheless, such experiments provide the intermolecular relaxation contribution, in addition to the intramolecular part. From the former, the mean square displacement as a function of time can be extracted in addition to that from field gradient NMR experiments.[44−47] Combining both methods discloses all the diffusion regimes of long-chain polymers predicted by the tube-reptation model.[43]

With its multiparticle interaction, another problem is inherent to ^{1}H NMR, in particular, to ^{1}H FC NMR with its low spectral resolution. It is not easily possible to distinguish between the relaxation of chemically different groups, for example, between the methyl group and chain protons in a polymer. In the worst case, the simple Bloch equations do not apply and nonexponential relaxations result, rendering it difficult to define a relaxation time.[48,49] Fortunately, in many cases, the different groups are strongly coupled due to fast cross relaxation and relax with a common time constant, yet the quantitative interpretation may still not be straightforward. These problems led many researchers to investigate the relaxation of other nuclei like ^{13}C or ^{2}H, for instance, where a single-particle interaction dominates. However, here relaxation rates for only a few frequencies were accessible, so far.

Applying ^{2}H NMR on (labeled) compounds does not suffer from many of the problems mentioned above, and the power of the techniques, in particular, regarding multidimensional solid-state investigations has been demonstrated in innumerous publications.[50−53] First of all, the relaxation is controlled by the quadrupolar interaction, which in molecular systems is of purely intramolecular origin; for example, the reorientation of the C−[2]H bond is probed. Each chemical group exhibits its own relaxation rate, and by appropriate (partial) isotope labeling, the dynamics of a specific group can be singled out. Even in the case when, e.g., two chemically different groups are deuterated and spectral resolution is lost due to molecular slowdown, the resulting (total) relaxation becomes biexponential and can be well measured in conventional high-frequency (HF) spectrometers. Thus, extending the FC technique to include also the ^{2}H nuclei is highly desired, yet several challenges have to be

mastered. Due to the by a factor of 6 lower gyromagnetic ratio, the detection field of the employed commercial electromagnets is below 5 MHz, and thus, the signal-to-noise ratio is very low. Moreover, the quadrupolar interaction is stronger than the ^{1}H dipolar coupling, and faster relaxation results. This may interfere with the switching time of the FC magnet, even more than in the case of ^{1}H FC NMR. Nevertheless, first ^{2}H FC NMR studies on polymers were used to check the reliability of the isotope dilution ^{1}H FC NMR experiments.[22,40−42,54,55] Intramolecular ^{1}H and ^{2}H relaxation are expected to essentially display the same dispersion. Indeed, this was found experimentally.

Performing experiments on a commercial as well as on a home-built relaxometer, in the present contribution, we further explore the potential of ^{2}H FC NMR for studying the dynamics in liquids and polymers. Provided that crystallization does not interfere, liquids like glycerol or toluene undergo the glass transition upon cooling, which results in a strong molecular slowdown. As shown by ^{1}H FC NMR (as well as by conventional high-field ^{2}H relaxation studies), strong dispersion is expected at low temperatures approaching T_g. As will be demonstrated, ^{2}H FC NMR with the current technical possibilities does not reach the dispersion region, but a comparison with results from high-field (HF) relaxation experiments on simple liquids yields good agreement. A direct comparison between the results of ^{2}H and ^{1}H FC NMR will confirm the relevance of intermolecular relaxation in the case of ^{1}H NMR, often ignored in conventional ^{1}H NMR studies. Considering polymers like poly(ethylene-*alt*-ethylene) (PEP) and polybutadiene (PB) collective, polymer-specific dynamics lead to pronounced dispersion well above T_g. By applying FTS, the full spectral density or reorientational correlation function, extending over many decades in frequency or time, respectively, can be revealed. The results will be discussed in the frame of the tube-reptation model describing Rouse and entanglement dynamics of long chain polymers.[2,15,24,56] Finally, we will discuss the future prospects of ^{2}H FC NMR relaxometry.

■ THEORETICAL BACKGROUND

Field-cycling NMR is applied to monitor the frequency dependence of the spin−lattice relaxation time T_1. The latter is determined by the evolution of the nuclear magnetization toward its equilibrium value. The frequency is given by the Larmor frequency depending on the magnetic relaxation field B via $\omega = \gamma B$, where γ denotes the gyromagnetic ratio of the nucleus. In the case of ^{2}H NMR, fluctuations of the quadrupolar interaction cause the relaxation, which in molecular systems is strictly of intramolecular origin.[50−53] Specifically, the present study focuses on the motional narrowing regime where the NMR spectrum of a more or less viscous liquid (or polymer melt) is given by a Lorentzian line shape with its width reflecting the inverse of the spin−spin relaxation time T_2. In the case of (high molar mass) polymers, due to slow polymer specific dynamics, some very small residual coupling may still be present. The ^{2}H spin−lattice relaxation rate $R_1 = 1/T_1$ of an ensemble of chemically identical deuterons reorienting presumably isotropically is connected to the spectral densities $J_m(\omega)$ by a "BPP-type" equation[26,56]

$$R_1(\omega) = K[J_1(\omega) + 4J_2(2\omega)] \tag{1}$$
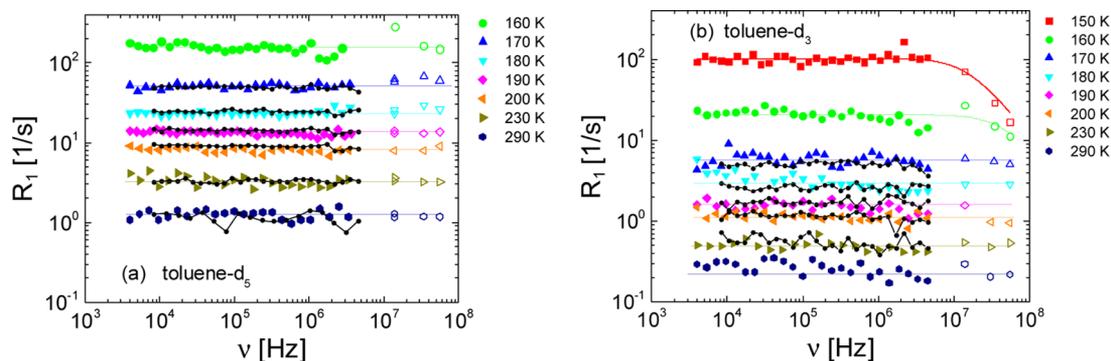
where K is given by

Figure 1. (a) ^{2}H spin−lattice relaxation rate R_1 of toluene-d_5 as a function of frequency at various temperatures as revealed by FC NMR. Conventional, high-field data measured at 14 MHz (present work), 13.8 MHz,[75] 34.4 MHz,[75] and 55.8 MHz[75] are included (open symbols). (b) Corresponding ^{2}H relaxation rate of toluene-d_3: HF data measured at 14 MHz (present work), 30.7 MHz,[77] 34.4 MHz,[70] and 55.2 MHz[59] are added (open symbols). For the two lowest temperatures, we show an interpolation with a Cole−Davidson spectral density. In both figures, the connected black points show the results of toluene-d_8 and the straight lines denote the average rate (cf. text).

$$K = \frac{3\pi^2}{10}\left(\frac{e^2Qq}{h}\right)^2 \qquad (2)$$

Here $\frac{e^2Qq}{h}$ = QCC is the ^{2}H quadrupolar coupling constant, a quantity easily accessible from the solid-state spectrum of a liquid, i.e., in the glass state $T < T_g$ when all large-angle motion has ceased. For the systems investigated, the coupling constant is known (cf. below). In the case of isotropic systems, all the quadrupolar spectral densities are m-independent and $J_m(\omega) = J(\omega)$ is the Fourier transform of the second order reorientational correlation function $C_2(t)$, i.e., the correlation function of the second Legendre polynomial. We note that DS probes $C_1(t)$ in good approximation, i.e., the first Legendre polynomial correlation function.[57]

In liquids or polymers, due to the collective nature of molecular dynamics, quite generally, the shape of the fluctuation spectrum in terms of the susceptibility representation $\chi''(\omega) = \omega J(\omega)$ virtually does not change with temperature; i.e., frequency−temperature superposition (FTS) applies. One can write the susceptibility as a function of a reduced frequency, explicitly $\chi''(\omega\tau)$, where τ denotes a characteristic correlation time, which drives the temperature dependence of the dynamics, for example, the time τ_α determined by the glass transition phenomenon (α-process). Thus, measuring at different temperatures, one can construct master curves, which effectively extend the covered frequency range. Actually, this is quite important for FC NMR as the currently accessible frequency range is still narrow (3−5 decades). In order to allow for such master curve construction, we rewrite eq 1 in the susceptibility representation[3,4,17−19]

$$\omega R_1(\omega) = K[\chi''(\omega) + 2\chi''(2\omega)] \equiv 3K\chi''_Q(\omega) \qquad (3)$$

Although $\chi''_Q(\omega)$ is a weighted sum of two susceptibilities, both quantities are essentially indistinguishable for broad relaxation dispersion monitored on logarithmic scales. We note that the susceptibility representation of NMR relaxation data was already used by Cohen-Addad and co-workers.[58] In many cases, for example, in rheological studies as well as in ^{2}H FC NMR studies, the time constant τ_α cannot be obtained directly, since the susceptibility maximum linked to the main relaxation (α-) process is not observable; i.e., the condition $\omega\tau_\alpha \cong 1$ is difficult to match experimentally. However, the temperature dependence of the shift factor a_T is that of τ_α.

Assuming isotropic reorientation in the extreme narrowing, the simple relation $R_1 = 5K\tau_2$ holds, which yields $\tau_2(T)$ from $R_1(T)$ provided that K is known from the solid-state spectrum accessible at low temperatures. Here, τ_2 is the time constant of the second Legendre correlation function.

In viscous liquids not too close to T_g, the reorientational spectral density is well interpolated by a Cole−Davidson (CD)[57] distribution of correlation times $G(\ln \tau)$ (or equivalently by a Kohlrausch decay in the time domain), a fact extensively demonstrated by dielectric and light scattering studies[8−12] as well as by many ^{2}H HF NMR relaxation investigations, which jointly analyzed $T_1(T)$ and $T_2(T)$.[59−62] This distribution will also be applied in the case of toluene and glycerol-d_5. Actually, choosing $G(\ln \tau)$ is nothing else than introducing a nonexponential correlation function $C_2(t)$ reflecting the collective dynamics.

■ EXPERIMENTAL SECTION

Parts of the ^{2}H spin−lattice relaxation experiments (toluene: methyl deuterated: -d_3, phenyl deuterated: -d_5, fully deuterated: -d_8 and PEP-d_{10}) were carried out on a home-built FC NMR relaxometer located at the Technische Universität Darmstadt. For the measurements on PEP-d_{10}, a home-built main current source[5−7] was used with a polarization field of 4.5 MHz and a detection frequency of about 6 MHz for deuterons. The earth and other stray magnetic fields from the surrounding laboratory equipment were compensated, and the evolution fields were calibrated carefully.[6,7,63] The temperature was stabilized by a thermally controlled gas flow across the probe. The measurements on toluene-d_3, -d_5, and -d_8 were performed using a commercial gradient pulse amplifier instead of the home-built one, namely, the model Avanto SQ from Siemens. All three channels of this amplifier were used in parallel to set up a detection field of 2 T (12 MHz), but for purposes of a stable coil temperature, the polarization field was kept at 4.5 MHz. In order to reach also lower temperatures (down to 80 K), a commercial cryostat was used. This cryostat contains unavoidable metal parts in which during field switching eddy currents are induced so that the switching time is about 4 ms and the minimum evolution field is limited to 4 kHz. The absolute accuracy of temperature is ± 1.5 K and its stability ± 1 K.

The measurements for glycerol-d_5 were carried out on a STELAR relaxometer FFC 2000 located in Bayreuth, which

allows measurements in the temperature range from 180 to 420 K and in a ^{2}H Larmor frequency range 800 Hz $\leq \nu \leq$ 3 MHz. The temperature is maintained by evaporating liquid nitrogen, which passes through a glass Dewar carrying the NMR coil with the sample; accuracy and stability of temperature is comparable with that of the home-built relaxometer.

■ RESULTS AND DISCUSSION

1. Molecular Liquids Undergoing the Glass Transition. High-field ^{2}H NMR relaxation studies are well established for investigating the dynamics in liquids, in particular in such systems which undergo the glass transition. Here, a strong molecular slowdown is observed upon cooling, provided that crystallization is avoided. Prominent examples are glycerol,[61,64-67] propylene carbonate,[68] salol,[69,70] o-terphenyl,[60,61,71] and toluene.[59,72-78] Typically, the spin–lattice relaxation rate is monitored as a function of temperature and at a few frequencies. The major aim is to extract correlation times which characterize the glass transition. In order to achieve this goal, an appropriate spectral density has to be assumed. As discussed (cf. Theoretical Background), a CD spectral density is well suited to describe $R_1(T)$ (and $R_2(T)$) in the modestly viscous regime of the liquid; it provides correlation times which agree with those reported by other methods. At lower temperatures close to T_g, secondary processes become relevant, and a straightforward analysis relying solely on HF NMR relaxation data is elusive. This, of course, makes ^{2}H FC NMR a promising tool for overcoming the limits of conventional (HF) NMR studies. Here, we discuss the ^{2}H FC NMR results for differently deuterated toluene (-d_3, -d_5, -d_8) and glycerol-d_5. As mentioned, ^{2}H NMR solely probes a single-particle reorientational correlation function which can easily be interpreted.

In Figure 1, we show a few examples of the ^{2}H relaxation dispersion of toluene-d_5 (Figure 1a) and toluene-d_3 (Figure 1b), respectively, as revealed by FC NMR. They were measured with a home-built relaxometer covering a ^{1}H frequency range of 4–4500 kHz (cf. Experimental Section). Note that, due to the different gyromagnetic ratio, for ^{2}H NMR, the frequencies available are by a factor of 6 lower than those for ^{1}H FC NMR. All relaxation decays are exponential and thus provide a well-defined relaxation rate $R_1(\nu)$. Starting with toluene-d_5, no frequency dependence is observed down to the lowest temperature (160 K). Even including results from HF NMR experiments taken from refs 59 and 75, no dispersion is found, yet the agreement between the results from FC and HF experiments is very satisfactory. In the case of the toluene-d_3 (Figure 1b), data down to somewhat lower temperature (150 K) can be collected due to the fact that the fast methyl group reorientation reduces the effective QCC (cf. eq 2 and below) and thus decreases the relaxation rate compared to that of toluene-d_5. Again, no dispersion is recognized for the FC NMR data; however, the HF data[59,70,77] clearly show the onset of dispersion. The onset can be reproduced by a CD spectral density with a stretching parameter of β = 0.32 (taken from refs 59 and 75) and included in Figure 1b. For completeness, in Figure 2, the currently available ^{2}H relaxation rates for toluene are displayed as a function of temperature.

We also measured the spin–lattice relaxation of toluene-d_8. Figure 3 shows the normalized relaxation function plotted versus a rescaled time $t\langle R_1 \rangle$ for some frequencies and temperatures measured. Here, $\langle R_1(\omega) \rangle$ denotes the initial slope, i.e., the average rate. Essentially, master curves are found; however, small deviations occur for the different temperatures,
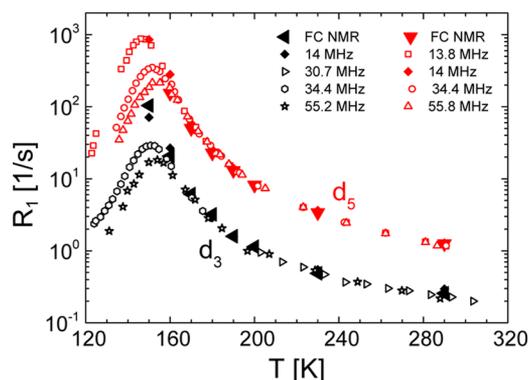

Figure 2. ^{2}H spin–lattice relaxation rate of toluene as a function of temperature. Closed symbols, present work; open symbols, literature data (13.8, 34.4,[75] 30.7,[77] 34.4,[70] 55.2,[59] and 55.8 MHz[75]).
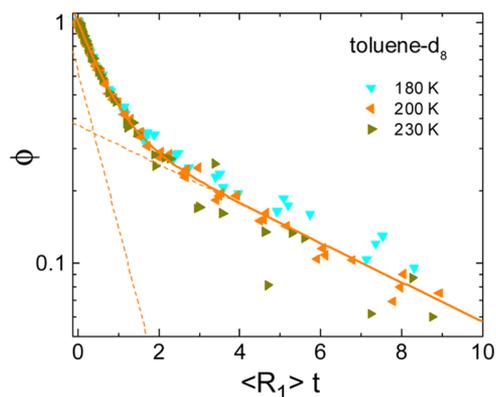

Figure 3. Normalized magnetization decay ϕ of toluene-d_8 for selected frequencies and temperatures displayed as a function of the rescaled time. A biexponential fit is shown for 200 K (straight line) as well as the decomposition in its monoexponential components (dashed lines).

since the ratio of the two relaxation times is not constant (cf. below). The nonexponential relaxation can be well fitted to a sum of two exponentials with weighting factors of 5/8 and 3/8, respectively, reflecting the number of different deuterons in the molecule. Here, we note that the correct weighting factors can only be retained in a limiting temperature range. While at low temperatures, due to the not ignorable switching time, the fast relaxation gets partly lost, at high temperatures and long relaxation times (∼ seconds), the stability of the detection field due to thermal expansion of the main coil decreases. The resulting relaxation rates $R_1^{d_3}(\nu)$ and $R_1^{d_5}(\nu)$ are included in parts a and b of Figure 1, respectively (black connected symbols). Satisfying agreement is observed with the data obtained for toluene-d_5 and toluene-d_3.

Given the rigid-lattice QCC values for toluene-d_5 as well as for toluene-d_3 and taking $R_1(\omega) = 5K\tau_2$ (cf. Experimental Section), one can extract the correlation time $\tau_2(T)$ from both data sets in Figure 1. For toluene-d_5, a value of QCC_{d_5} = 180 kHz was reported,[59,79] and for toluene-d_3, with its fast reorienting methyl group, the motionally averaged coupling is QCC_{d_3} = 52 kHz ($T < T_g$).[59] In Figure 4, the extracted correlation times are compared to a compilation of time constants collected by other techniques like DS and depolarized light scattering.[80] Overall, satisfying agreement is found; at high temperatures, some deviations are observed. As discussed below, they may be explained by some extent of anisotropic
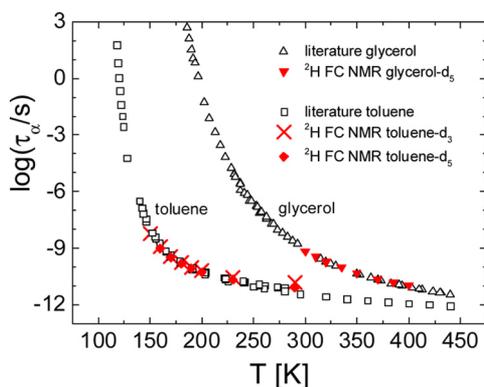
Figure 4. Reorientational correlation times τ_α for toluene and glycerol as a function of temperature as determined from ^{2}H FC NMR (closed symbols) and from several other techniques (open symbols[80]).

reorientation. As typical of the glass transition in molecular liquids, reorientational time constants revealed by the various methods agree well, i.e., $\tau_2(T) \equiv \tau_\alpha(T)$.

As discussed, collective dynamics in condensed matter usually exhibits FTS; i.e., the shape of the susceptibility virtually does not change with temperature, and it can be expressed as a system specific susceptibility function $\chi''(\omega\tau_\alpha)$. However, when measurements cover a very large temperature range, including temperatures close to T_g FTS may fail. In the present case, we stick to high temperatures only. The simplest way to construct master curves is by transforming the data to the susceptibility representation ωR_1 (cf. Theoretical Background) and taking $\tau_\alpha(T)$ from independent experiments. Another possibility is to produce susceptibility master curves by shifting different data sets solely along the ω-axis and check the extracted shift factor in terms of $\tau_\alpha(T)$ against independent measurements of the latter. Shifting along the frequency axis without any vertical shift conserves the integral over the susceptibility; the latter is given by the QCC, which is temperature independent in good approximation. Such susceptibility master curves are easily compared to results from DS, for instance.

In Figure 5, we constructed a master curve $\chi''(\omega\tau_\alpha)$ for the toluene-d_5 data (NMR and DS) by taking recourse to the time constants plotted in Figure 4. The maximum of $\chi''(\omega\tau_\alpha)$ is
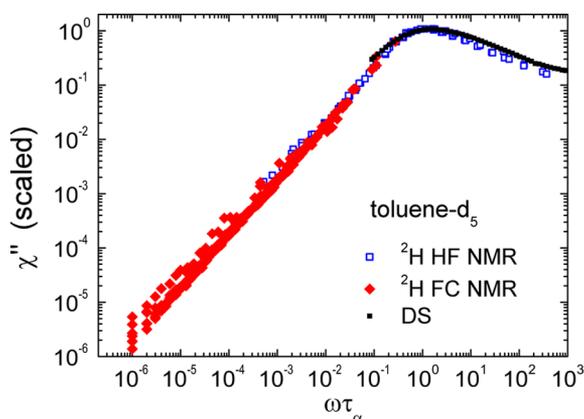
scaled to one. First, we discuss the ^{2}H FC NMR results, which are extended by HF data.[75] In the latter case, $R_1(T)$ data, measured at a single frequency, is taken, and in order to get the reduced frequency $\omega\tau_\alpha$ for each temperature, the time constant $\tau_\alpha(T)$ is picked off from Figure 4. For both data sets (FC and HF data), the same scaling factor of the amplitude is applied. While the ^{2}H FC data follow a straight line, i.e., $\omega R_1 \propto \omega^1$, as expected as a consequence of the dispersion-free data of the spectral density representation in Figure 1, the HF data exhibit a relaxation maximum which fits into the trend of the ^{2}H FC data. We added also the dielectric curve $\chi''(\omega\tau_\alpha)$ of toluene (unpublished results, see also ref 9). Good agreement between DS and ^{2}H NMR is revealed. In the case of toluene with its low electric dipole moment, DS can only probe a small amplitude range on the low-frequency side of the relaxation maximum. In addition, in most dielectric spectra of liquids (and polymers), the low-frequency flank is spoiled by the presence of parasitic contribution of a dc conductivity. Here, FC experiments provide access to a much larger susceptibility range, and dynamics slower than the α-process (for instance, polymer dynamics, see below) contributes here.

The master curve in Figure 5 can be interpolated by a CD susceptibility[57] (not shown), as typically done for dielectric spectra of glass forming liquids.[10,12] Moreover, the master curves demonstrate that in the temperature range (160−290 K) investigated by ^{2}H NMR no influence of another process like the β-process is recognized. Actually, from analyzing the dielectric spectra close to T_g = 117 K,[9] it is known that a pronounced β-process emerges at low temperatures. In other words, the α- and β-process have merged at temperatures, say, above 160 K, a phenomenon well-known in glass forming liquids.[9,81] We repeat that ^{2}H FC NMR with its current instrumentation cannot reach lower temperatures, as the rate becomes too high to be resolved. The master curve displayed in Figure 5 can be Fourier transformed to yield the reorientational correlation function $C_2(t/\tau_\alpha)$, which is included in Figure 11, for comparison (cf. below).

As already mentioned in the context of discussing the data in Figure 4, when extracting correlation times from the relaxation rates, one implicitly assumes isotropic reorientation. However, the deviations observed at high temperatures with respect to the literature data may originate from anisotropic reorientation of the toluene molecule. For example, given that the methyl group rotation is fast[77] and assuming overall isotropic reorientation, the ratio of the relaxation times $R_1^{d_5}(\nu)/R_1^{d_3}(\nu) = r$ is expected to be $r = (\mathrm{QCC}_{d_5}/\mathrm{QCC}_{d_3}) = (180/52)^2 = 12.0$, thus independent of temperature. Actually, the ratio decreases above 160 K reaching values around 6 at ambient temperature, and this may be explained by the presence of anisotropic reorientation as suggested in the literature.[82−84] Taking the Woessner model of anisotropic reorientation,[85] in the Appendix, we extract from $r(T)$ the anisotropy parameter $\delta = D_\parallel/D_\perp$.

Next, we consider the liquid glycerol-d_5; the corresponding relaxation rate $R_1(\omega)$, measured with the commercial relaxometer FFC 2000, is displayed for different temperatures in Figure 6. Compared to Figure 1, the frequency range extends to somewhat lower frequencies, but also the upper limit is smaller (800 Hz to 3 MHz). Again, no dispersion is revealed in the frequency range covered by ^{2}H FC NMR, and good agreement is found with HF relaxation data. For completeness, we note that at the highest temperatures a very weak dispersion
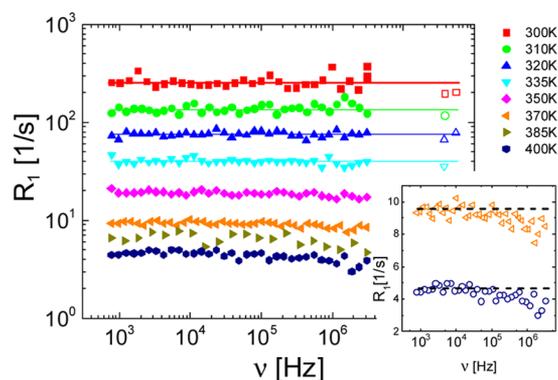

Figure 5. Susceptibility master curve for toluene-d_5 as obtained from ^{2}H FC and high field (HF) NMR relaxometry;[75] in addition, the corresponding dielectric spectrum (DS) is included (unpublished results, cf. also ref 9).

Figure 6. ^{2}H spin−lattice relaxation rates of glycerol-d_5 from FC NMR (closed symbols) and for comparison high field NMR data (55[61] and 38 MHz[67]). Inset: dispersion at high temperatures on linear scale.

is found (cf. inset in Figure 6), which is actually close to the error margin of the measurement and for which we currently have no explanation. Possibly, the finding is related to hydrogen exchange processes, like those found by ^{1}H FC NMR in water.[1] Taking the average rate from the ^{2}H FC data and QCC$_{glyc}$ = 165 kHz,[61] we again get very satisfying agreement with the time constants reported by other techniques (cf. Figure 4).

Figure 7 shows a master curve constructed by taking recourse to $\tau_\alpha(T)$, as given in Figure 4. For the ^{2}H FC and HF NMR
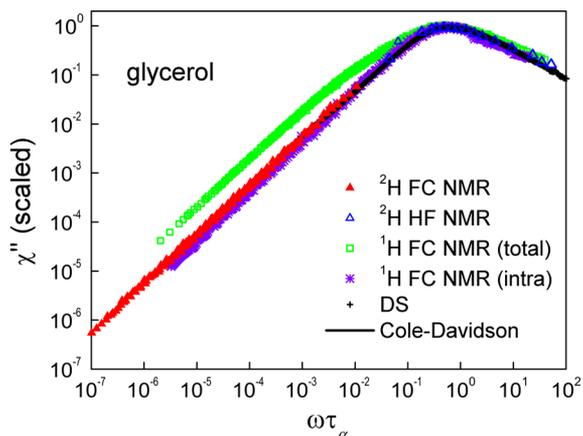
Figure 7. Susceptibility master curve constructed from taking $\tau_2 = \tau_\alpha$ in Figure 4: High field (HF) NMR,[61] ^{1}H FC NMR (total and intra),[30] and data from dielectric spectroscopy (DS)[86] were added for comparison. Solid line: interpolation by the Cole−Davidson function.

data (cf. ref 61), again the same scaling factor for the relaxation values is applied. While the ^{2}H FC NMR data follows a straight line, i.e., $\omega R_1 \propto \omega^1$, the HF NMR data exhibits a relaxation maximum which fits into the ^{2}H FC NMR data. We included the curve provided by our DS measurement,[86] which follows the HF ^{2}H NMR data. Moreover, comparing the ^{2}H NMR results with those from the intramolecular ^{1}H relaxation dispersion studies obtained by performing isotope dilution experiments,[30] complete agreement is recognized. As in the case of ^{2}H NMR, the ^{1}H intramolecular rate probes solely the reorientational dynamics. Thus, ^{2}H, ^{1}H(intra), and DS all probe essentially the same susceptibility, which can be well interpolated by the same CD function. In contrast, the total ^{1}H relaxation (taken from ref 30 and included in Figure 5) exhibits a low-frequency shoulder, which thus has to be

attributed to the intermolecular relaxation contribution. As established long ago,[27−29] the intermolecular correlation function shows a long-time power-law behavior, $C(t) \propto t^{-d/2}$, with d being the spatial dimension. With respect to the more or less exponential decay of $C_2(t)$ in liquids, this long-time power law in $d = 3$ will always dominate the response at long times or at low frequencies, respectively. This implies that for the total ^{1}H relaxation the extreme narrowing condition (R_1 becoming frequency independent) never applies, while in the ^{2}H case it is essentially found at high temperatures, as demonstrated in Figures 1 and 7. For $d = 3$, a square root frequency dependence is predicted for $R_1(\omega)$ at low frequencies, which directly allows the translational diffusion coefficient to be determined in liquids as well as polymers.[4,31−36]

2. Polymer Dynamics. High-field ^{2}H spin−lattice relaxation studies on polymer melts were conducted by several groups.[87−95] Focus was on characterizing the "local" segmental relaxation (α-process) determined by the glass transition phenomenon. In contrast, ^{2}H FC NMR investigations are still rare. For example, in the case of poly(butadiene) (PB) and poly(ethylene oxide) (PEO), first results were reported by the Kimmich group[2,15,41,54] and by our group.[22,42] In these systems, the ^{2}H spin−lattice relaxation is exponential, and in contrast to simple liquids, ^{2}H FC NMR probes pronounced dispersion at high temperature well above T_g, reflecting polymer-specific (collective) dynamics. They were interpreted in terms of Rouse and entanglement dynamics. Below we will discuss these results on PB in the context of new measurements performed on fully deuterated poly(ethylene-*alt*-propylene) (PEP) with molar mass $M = 200$ k ($\gg M_e$) and $T_g = 206$ K.

The low-T_g polymer PEP is well suited to probe the collective dynamics of linear chain polymers over a large temperature interval, as it provides a good compromise between avoiding crystallization and introducing minimal structural complexity. In contrast, structurally simpler polymers like poly(ethylene), poly(ethylene oxide), or poly-(dimethylsiloxane) show a strong tendency to crystallize, and thus do not allow the dynamics to be probed from high temperatures down to T_g. In the case of PB, the microstructure strongly influences T_g as well as the polymer-specific dynamics. Hence, any study has to rely on identically prepared polymer samples, which is actually not an easy task.

Poly(ethylene-*alt*-propylene) with a narrow molar mass distribution is synthesized via hydrogenation from standard polyisoprene; the latter is obtained from anionic polymerization.[96] Concerning the deuterated samples, we had only access to the fully deuterated polymer PEP-d_{10}, which at first glance complicates the situation, as methyl group dynamics as well as chain dynamics are probed by ^{2}H NMR. However, this is actually not the case, as the methyl and the chain deuterons yield different ^{2}H relaxation rates which can be resolved when the total relaxation is measured as is done in a FC NMR experiment. In other words, the total ^{2}H relaxation is biexponential, which was first tested by HF ^{2}H relaxation (unpublished results). The relaxation dispersion was measured by employing the home-built relaxometer in Darmstadt. However, in comparison to the toluene measurements, we are able to measure to higher relaxation rates R_1 by using a different home-built power supply with a shorter switching time, which covered a frequency range of 30 Hz to 6 MHz (cf. Experimental Section).

In Figure 8, the normalized ^{2}H relaxation decay plotted as a function of the reduced time $t\langle R_1 \rangle$ is presented for different
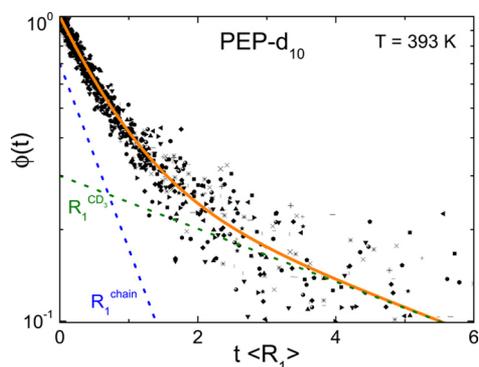
Figure 8. Normalized relaxation decay of PEP-d_{10} as a function of reduced time at $T = 393$ K for all frequencies investigated; $\langle R_1 \rangle$ is the mean relaxation rate derived from the initial slope of the relaxation decay. Decomposition into two exponentials is shown (dotted lines).

frequencies. Here, again, $\langle R_1 \rangle$ is the mean relaxation time taken from the initial slope of the relaxation curve. Comprising the relaxation functions measured at all frequencies, a master curve is found. The scatter for the long-time decay is rather high. Nonetheless, this result indicates that the ratio of these rates as well as the relative weight of the two exponentials are frequency independent—and temperature independent as confirmed by HF measurements (unpublished results). The decay can be fitted to a sum of two exponentials with the relative weights fixed by the ratio 3/10 and 7/10 as given by the numbers of the chemically different deuterons (solid line in Figure 8). The two extracted relaxation rates $R_1^{methyl}(\nu)$ and $R_1^{chain}(\nu)$ are shown in Figure 9a. Clearly, pronounced dispersion is identified for both rates, which reflects polymer-specific relaxation. The ratio $R_1^{chain}/R_1^{methyl} = 6.5 \pm 0.3$ is found, as said, independent of temperature, yet it is smaller than expected from the ratio of the QCCs. We note that in addition to the fast methyl group reorientation a nonmerging secondary (β-) relaxation process has to be taken into account (unpublished results). For the present discussion, these details are irrelevant.

As revealed by the ^{2}H FC data (red symbols), two dispersion regimes (I and II, as indicated) can be identified in Figure 9a. Rather similar dispersion is observed for PB which is plotted in Figure 9b, for comparison. In addition, we added our HF NMR results of PEP-d_{10} (unpublished results), which were converted from the temperature axis to the frequency axis by assuming

FTS. As discussed, collective dynamics in polymers (and liquids) usually follows FTS.[13,14] Showing an even stronger dispersion, the HF relaxation data reflects a third relaxation regime (regime 0), namely, the local dynamics (α-process). Furthermore, we included our results for the intramolecular ^{1}H relaxation rate of PEP and PB, respectively, obtained from an isotope dilution experiment, and which cover a much larger frequency range (again, a result of applying FTS; unpublished results). In contrast to ^{2}H, the magnetization recovery is exponential, yielding a single relaxation rate. Regarding the spectral shape, the ^{1}H (intra) and ^{2}H data are expected to agree, as was demonstrated above for glycerol. Indeed, the data, appropriately scaled in amplitude (due to different coupling constants), agree so well that the ^{1}H (intra) data can serve as a guide for the eye interpolating the ^{2}H dispersion of PEP. Only at lowest frequency some difference appears. Here one has to keep in mind that the nominal "intramolecular" relaxation data are obtained from measuring a sample with 10% protonated PEP in a deuterated matrix and we refrained to extrapolate to zero concentration. Very good agreement is also found for PB; however, HF ^{2}H relaxation data are missing here. More than nine decades in frequencies are effectively covered and encompassing all the different relaxation regimes of polymer melts, which are discussed in detail next.

In the rate representation (Figure 9), a plateau characteristic of the terminal relaxation is expected at lowest frequencies; this frequency range constitutes the terminal relaxation regime IV in the tube-reptation (TR) model. The plateau value was calculated with the help of the terminal relaxation time, which was determined from shear stress relaxation experiments (unpublished results). For high-M polymers, this regime cannot be covered by ^{2}H FC NMR but shows up for short chains, as seen for PB in Figure 9b. At higher frequencies, two regimes II and I (with increasing frequency) are well recognized. Presently, it is unclear whether another dispersion regime (reptation in terms of the TR model; III) shows up between regimes II and IV (cf. ref 43). In the frame of the TR model, regime II is attributed to entanglement dynamics, more precisely to the constraint Rouse regime for which a power law $R_1 \propto \nu^{-3/4}$ is predicted; however, a behavior close to $R_1 \propto \nu^{-1/2}$ is actually observed for both PEP and PB, while for the Rouse regime $R_1 \propto \ln(1/\nu)$ is predicted.[2,15,18,97−99] The latter is difficult to distinguish from a power-law behavior with a rather small exponent, what we could rather attribute. The crossover
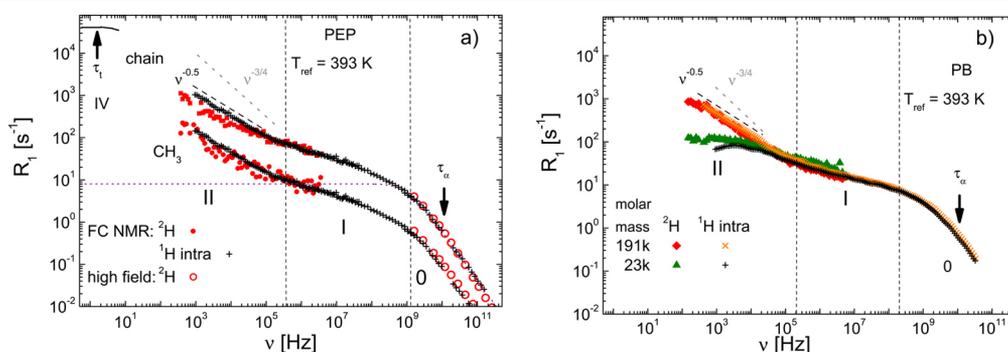

Figure 9. (a) Spin−lattice relaxation rates of PEP (200k) as a function of frequency at 393 K: ^{2}H FC data (solid symbols) comprising rates for the methyl and the polymer chain; intramolecular ^{1}H FC data (crosses, shifted; unpublished results), high field data (open symbols); relaxation regimes are indicated; the plateau value at the lowest frequencies (regime IV) is estimated from rheological experiments (unpublished results), dotted line: α-process. (b) Corresponding relaxation rates for polybudadiene (PB) with two molar masses. In both figures, the expectation of the TR model for regime II is indicated as a gray dotted line.

between the two regimes defines the entanglement time τ_e, which is a measure at which time the reorientational fluctuations of the segments "feel" the "tube",[24] and which can thus be extracted easily from FC NMR relaxation spectra. The Rouse regime (I) continues to high frequencies until at highest frequencies the local dynamics with its strong dispersion sets in (regime 0). At even higher frequencies not covered by our experiments, secondary relaxation processes will appear as proven for both PEP and PB by dielectric spectroscopy and HF ^{2}H NMR (unpublished results and ref 8).

As already demonstrated for toluene and glycerol, instead of the rate representation, the susceptibility representation of data may be of interest for polymers, too—see Figure 10. As
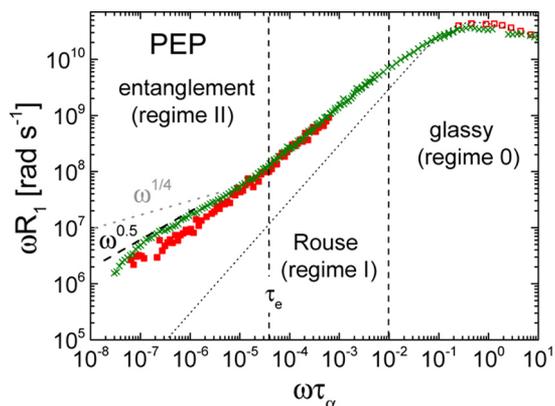
Figure 10. Susceptibility master curve of the chain dynamics of PEP-d_{10} obtained from ^{2}H FC NMR (filled squares) as well as intramolecular ^{1}H FC NMR data (crosses, scaled in amplitude); in addition, we added high-field data (open squares; unpublished results); dashed line: Cole–Davidson function representing the glassy relaxation. Gray dotted line: expectation of the TR model for regime II.

discussed, this representation is the starting point for constructing master curves by exploiting FTS. The dispersion profiles measured at different temperatures are solely shifted along the frequency axis to achieve best overlap. In Figure 10, the relaxation peak reflects the α-process, while at lower frequencies ($\omega\tau_\alpha \ll 1$) the polymer-specific contributions starting with the Rouse contribution (regime I) and followed at lower frequencies by another power law reflecting constraint reptation (regime II) is recognized. The dotted line represents a CD function interpolating solely the α-process as it appears in simple liquids. As mentioned before, in the case of the high-M PEP, the terminal relaxation leading to $\chi''(\omega) \propto \omega^1$ is only expected at even lower frequencies not covered by ^{2}H NMR, yet it shows up for shorter polymer chains. In the susceptibility representation, it is directly seen that ^{2}H FC NMR data does not cover the relaxation regime 0 ("local" or "glassy" dynamics), which leads to the relaxation maximum at high frequencies. Upon cooling, the value of T_1 quickly becomes too short to be resolved in a ^{2}H FC NMR experiment, a boundary which limits the analysis in the case of simple liquids as demonstrated above.

Finally, we show in Figure 11, the reorientational correlation function $C_2(t/\tau_\alpha)$ of PEP as well as of PB as obtained from Fourier transformation of the spectral density in Figure 9. The ^{1}H FC (intra) data were taken for interpolating the ^{2}H data. We added the corresponding function for toluene-d_5 and glycerol-d_5 (from Figures 5 and 7). This representation of the relaxation data, covering six decades in amplitude and nine
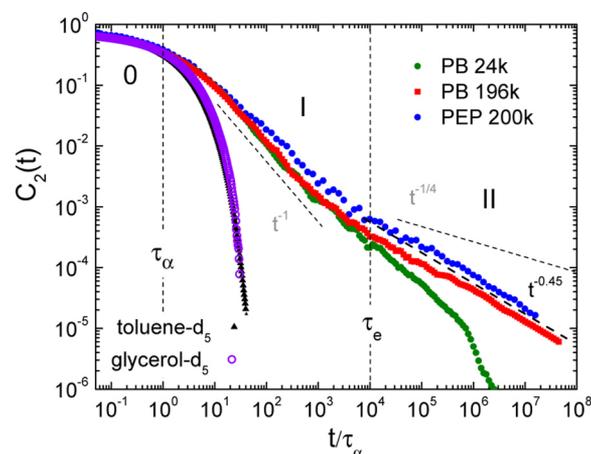

Figure 11. Segmental reorientational correlation function $C_2(t)$ of PEP and PB vs reduced time t/τ_2 as obtained from Fourier transforming relaxation master curves in Figure 9; relaxation regimes are indicated; numbers give the molar mass of polymers; gray dotted lines: prediction of the tube-reptation model;[15,19,100,101] for comparison, the decay for two simple liquids toluene and glycerol is given.

decades in time, is actually most convenient to illustrate the different relaxation regimes of a high-M polymer melt. Comparing polymer and simple liquid, a strong retardation of $C_2(t/\tau_\alpha)$ is obvious for the polymers. Moreover, the decays for PEP and PB are virtually indistinguishable, which emphasizes the conclusion that generic, polymer-specific relaxation is observed. While for the simple liquids $C_2(t/\tau_\alpha)$ can be interpolated by a Kohlrausch function (the time domain equivalent to the CD function), in the case of the polymers, at least two power-law decays are observed for the high-M samples, in addition to the short-time behavior attributed to glassy dynamics. In regime I, a power-law decay is recognized which closely follows the Rouse prediction, $C_2(t) \propto t^{-1}$. At the longest time, in regime II, a power-law behavior, $C_2(t) \propto t^{-0.45\pm0.05}$, is found which does not conform to the TR prediction for the constraint Rouse regime for which one expects a power-law exponent $\alpha = 0.25$. Possibly, the strong rotational–translational coupling assumed in the TR model in terms of the so-called return-to-origin hypothesis[15,100,101] does not apply in real polymers. Here, atomistic simulations will deliver further insight provided that they reach the entanglement regime which is still difficult with the current computer power.[102] In the case of PB, we added also our results for shorter chains, yet still entangled ($M > M_e$). Here the terminal relaxation appears within the frequency window of ^{2}H FC NMR featuring an essentially exponential cutoff of the power-law regime II. We note that entanglement dynamics sets in below $C_2(t_e) = S^2 \cong 0.001$, where τ_e is the entanglement time and S the corresponding order parameter, which is on the order of a few percent and thus very small.

■ CONCLUSION

As shown by the novel examples of ^{2}H FC NMR relaxometry studying molecular motions in glass forming liquids and polymers, the technique constitutes another dynamic susceptibility method thereby complementing traditional ones such as dielectric spectroscopy, dynamic light scattering, quasi-elastic neutron scattering, and rheology, for example. In the case of dielectric spectroscopy with its broad frequency window, however, only in favorable cases, i.e., for so-called type A

polymers,[103] the polymer-specific dynamics is accessible in the form of a normal mode relaxation.

Thus, the whole toolbox of susceptibility analyses (e.g., FTS allowing for the construction of master curves) can fruitfully be applied to FC relaxometry irrespective of which nuclear spin species is used. At the same time, one profits from the selectivity of NMR which in many cases allows data to be interpreted in a much more specific way compared to other methods. As this and some of our previous papers demonstrated,[17−22] there may be a lot of important physics hidden in the FC dynamic range, i.e., at frequencies below the range of typical high field NMR spectrometers. The simplest case (e.g., toluene), when ^{2}H FC relaxometry yields dispersion-less rates, gives the nontrivial information that there is no slow process. Another case discussed in this paper dealt with glycerol and the time scale separation of molecular rotation and translation, which is revealed when ^{2}H and ^{1}H relaxation dispersion is compared. We recall that in ^{1}H FC NMR translational dynamics leads to a characteristic low-field behavior of the rates.[29−33] In even other cases, e.g., in network forming monoalcohols,[104,105] there are dynamics reflecting the reorganization of the hydrogen bonding network, which exhibits characteristic dynamics slower than the structural relaxation. Thus, FC relaxometry should be ideally applicable to address this problem; characteristic low field dispersion is anticipated. A prominent case, discussed in some detail in this paper, is long chain polymer motion. FC relaxometry has been able, partly in concert with other methods, to test grand theories of polymer dynamics.[19,22,23,25,42] Not too much prophecy is required that more physical cases of slow molecular dynamics, e.g., hydrogen exchange processes[1] or the dynamics of supramolecular structures, wait for being detected by ^{2}H FC NMR.

As the title tells, this paper is meant to draw the attention of the reader to the perspectives of ^{2}H FC NMR relaxometry for studying molecular motions in soft matter. The central question is, why should one use deuterons? By dealing with selected experimental examples, our paper really has proposed some answers, which here we will try to recall in order to finally formulate a couple of summarizing take-home messages. A critical comparison of ^{1}H and ^{2}H FC relaxometry with respect to certain key properties may be instructive. The first two properties to be mentioned render ^{2}H FC relaxometry a very attractive method:

Reorientations measured exclusively: The dominant relaxation mechanism is the fluctuation of quadrupolar interaction, i.e., in the case of organic systems with covalent CD bonds: molecular reorientations only. Translational motions, which in the case of ^{1}H NMR contribute at low frequencies, do not contribute. In consequence, theoretical understanding as well as computer simulation is less demanding.

No cross relaxation effects: Deuteron quadrupolar interactions are much stronger than dipole−dipole interactions. This implies that cross relaxation effects, that in the case of ^{1}H NMR always tend to couple all system protons to each other, do not interfere. Thus, each subgroup of deuterons represents its own thermodynamic system and relaxes independently, and specific isotope labeling allows highly selective studies.

Of course, ^{2}H FC also encounters limitations:

Sensitivity problems: Due to the ^{2}H Larmor frequency being about a factor of 6 below that of the ^{1}H one is more seriously confronted with a poor signal-to-noise ratio. This stresses the point that high detection fields are essential for a broader application of the method. Currently, the most advanced home-built relaxometers may reach a detection field of about 12 MHz.

Short relaxation times: Due to the relatively strong (as compared to dipole−dipole interactions among protons) quadrupole interaction, the relaxation times are correspond-ingly short. This may lead to a limitation for low fields, especially in FC where field switching times are notoriously long anyway. Thus, even if evolution fields down to 10^{-6} T[6] (corresponding to ^{2}H frequencies of less than 10 Hz) may have become feasible, they cannot always be made use of.

Phase sensitive pulses: Even if in this paper we have not encountered a situation where we would have desired to apply phase sensitive high-frequency pulses and detection, we would like to use the occasion to stress that meeting the slow motion regime (nonaveraged static quadrupole interaction) one will have to measure solid-echo amplitudes. This will then require a highly stable detection field. At present, we have achieved a ^{2}H frequency drift in the detection field of about 500 Hz. This gradually starts to be sufficient for the first applications, and is a work in progress.

Concluding the conclusions: In view of the great potential of applying ^{2}H FC NMR relaxometry, especially at low fields, one should continue to invest in further instrumental improve-ments, i.e., among others, improving signal-to-noise ratio, increasing and stabilizing detection fields, and shortening field switching times.

■ APPENDIX

Here we discuss the ratio $r(T) = R_1^{d_5}(\nu)/R_1^{d_3}(\nu)$ in the case of toluene which allows one to estimate the extent of anisotropic reorientation. Given that the methyl group reorientation is fast with respect to the overall tumbling of the molecule,[77] a naïve picture would assume isotropic rotation, which would yield a ratio $R_1^{d_5}(\nu)/R_1^{d_3}(\nu) = r = 12.0$ (cf. above and eq 8). Figure 12
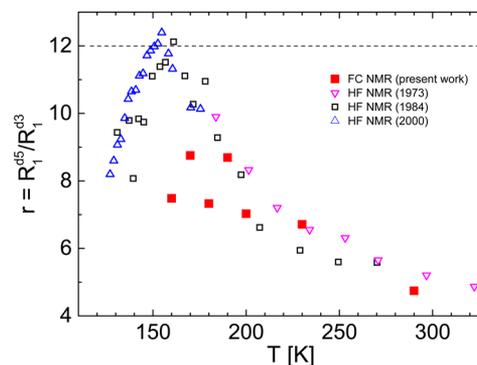

Figure 12. Ratio $r = R_1^{d_5}/R_1^{d_3}$ for toluene plotted versus temperature; conventional high-field (HF) data were taken from the literature: 1973,[77] 1984,[59] 2000;[70] dashed line: isotropic reorientation.

presents the experimentally observed value $r(T)$ taken from the present FC as well as from different HF NMR relaxation data (cf. Figure 2). The expected value (dashed line) is only reached around 160 K; below 160 K as well as above, the ratio drops. As the toluene-d_5 and toluene-d_3 relaxation rates are usually measured at different temperatures, some interpolation is necessary and may explain the scatter of the ratio. In addition, since the temperature coefficient of the relaxation rates is high at low temperatures, small differences in the absolute temperature may enhance the scatter. We also stress that the

comparison is now done on a linear scale, while in Figures 2 and 4 a logarithmic scale was chosen.

The strong temperature dependence of the ratio r above 160 K is explained by assuming that the reorientation of toluene becomes significantly anisotropic, an indication of which was already reported in the literature,[75,82−84] where the Woessner model of anisotropic diffusion[85] was applied. The decrease observed below 160 K is probably due to the emergence of the β-process. While the extension of the Woessner approach to viscous liquids with their nonexponential reorientational correlation functions is not straightforward, the situation under extreme narrowing conditions is more favorable—and it holds for the present analysis of the toluene data at $T > 160$ K.

The toluene molecule is an asymmetric top molecule described by three rotational diffusion coefficients, yet as our experiments cannot discriminate between the rotation around the two axes perpendicular to the C_2 axis, we approximate the molecular reorientation by assuming a symmetric top molecule with only two diffusion constants, $D_\parallel$ and $D_\perp$, and an anisotropy parameter given by $\delta = D_\parallel/D_\perp$. The quantity $D_\parallel$ represents the rotation around and $D_\perp$ the reorientation perpendicular to the pseudo C_2 axis. Then, given that the methyl group rotation is very fast,[77] and assuming extreme narrowing conditions, the spectral density of toluene-d_3—as well as that of the para (p) deuteron in toluene-d_5—reflects solely $\tau_\perp = 1/6D_\perp$; one gets

$$J_{d_3} = J_p = \tau_\perp \tag{4}$$

For the deuterons in ortho (o) and meta (m) position in toluene-d_5, it follows[85]

$$J_{o,m} = A(\cos\vartheta)(6D_\perp)^{-1} + B(\cos\vartheta)(D_\parallel + 5D_\perp)^{-1}$$
$$+ C(\cos\vartheta)(4D_\parallel + 2D_\perp)^{-1} \tag{5}$$

where the coefficients A, B, and C depend on the cosine of the angle ϑ between the C−D bond and the C_2 axis, which is 60° in the case of toluene. These deuterons are sensitive to both $D_\parallel$ and $D_\perp$, while the para (p) deuteron—like the methyl group deuterons—reflects only $D_\perp$. As the spin−lattice relaxation rates of o, m, and p deuterons are not expected to be largely different, we assume that the essentially exponential relaxation of toluene-d_5 is described by an average rate and a uniform coupling for each relaxation for o and m, and p, respectively. Thus, we can write

$$J_{d_5} = 0.8J_{o,m} + 0.2J_p \tag{6}$$

With eq 5, this leads to

$$J_{d_5} = 0.8\tau_\perp\left[\frac{1}{64} + \frac{81}{64(2\delta+1)} + \frac{27}{8(\delta+5)}\right] + 0.2\cdot\tau_\perp \tag{7}$$

Here, the anisotropy parameter δ appears. It can be extracted from the ratio r of the relaxation rates.

$$r(\delta) \equiv \frac{R_1^{d_5}}{R_1^{d_3}} = \frac{J_{d_5}QCC_{d_5}{}^2}{J_{d_3}QCC_{d_3}{}^2} = \frac{QCC_{d_5}{}^2\cdot(17\delta^2 + 350\delta + 353)}{QCC_{d_3}{}^2\cdot(80\delta^2 + 440\delta + 200)} \tag{8}$$

Figure 13 presents $r(\delta)$. As the dependence of r on δ becomes very flat for low r values, the uncertainty of δ becomes quickly large at high temperatures.
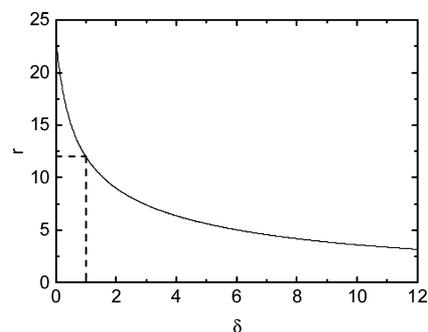

Figure 13. Ratio of the relaxation rates $r = R_1^{d_5}/R_1^{d_3}$ of toluene as a function of δ (cf. eq 8). The isotropic case $r = 1$ is indicated (dashed lines).

Figure 14 displays the anisotropy ratio δ as a function of temperature. While at low temperatures the toluene molecule
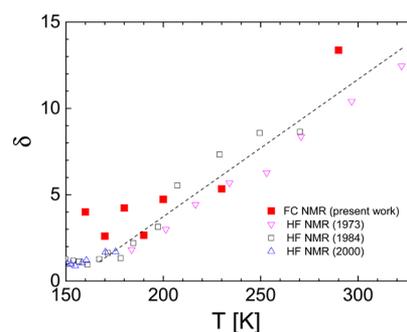

Figure 14. Anisotropy parameter δ versus temperature as given by ^{2}H FC NMR as well as by HF NMR from the literature: 1973,[77] 1984,[59] 2000.[70] Dashed line: guide for the eye.

essentially reorients isotropically, in the high temperature range, anisotropic reorientation is observed, the extent of which grows upon heating. In the literature, δ values between 2 and 3 were reported for ambient temperature;[75,82,83] the present study reveals values around 10 at room temperature. A completely different scenario was reported in ref 84 and thus can be questioned. As said, concerning the δ value, the error bars become quickly large when low r values are involved (cf. Figure 12). Importantly, the anisotropy disappears when the glass transition sets in. Hence, the suppression of anisotropic reorientation may be taken as a signature of glassy dynamics becoming strongly cooperative at low temperatures approaching T_g, a phenomenon already suggested a while ago.[106]

■ **AUTHOR INFORMATION**

Corresponding Author
*E-mail: ernst.roessler@uni-bayreuth.de. Phone: +49 921 553 164.

Notes
The authors declare no competing financial interest.

■ **ACKNOWLEDGMENTS**

■ REFERENCES

(1) Noack, F. NMR Field-Cycling Spectroscopy: Principles and Applications. *Prog. Nucl. Magn. Reson. Spectrosc.* **1986**, *18*, 171–276.

(2) Kimmich, R.; Anoardo, E. Field-Cycling NMR Relaxometry. *Prog. Nucl. Magn. Reson. Spectrosc.* **2004**, *44*, 257–320.

(3) Kruk, D.; Herrmann, A.; Rössler, E. A. Field-Cycling NMR Relaxometry of Viscous Liquids and Polymers. *Prog. Nucl. Magn. Reson. Spectrosc.* **2012**, *63*, 33–64.

(4) Meier, R.; Kruk, D.; Rössler, E. A. Intermolecular Spin Relaxation and Translation Diffusion in Liquids and Polymer Melts: Insight from Field-Cycling 1H NMR Relaxometry. *ChemPhysChem* **2013**, *14*, 3071–3081.

(5) Fujara, F.; Kruk, D.; Privalov, A. F. Solid state Field-Cycling NMR relaxometry: Instrumental improvements and new applications. *Prog. Nucl. Magn. Reson. Spectrosc.* **2014**, *82*, 39–69.

(6) Kresse, B.; Privalov, A. F.; Fujara, F. NMR Field-Cycling at Ultralow Magnetic Fields. *Solid State Nucl. Magn. Reson.* **2011**, *40*, 134–137.

(7) Kresse, B.; Privalov, A. F.; Herrmann, A.; Hofmann, M.; Rössler, E. A.; Fujara, F. Simultaneous measurement of very small magnetic fields and spin-lattice relaxation. *Solid State Nucl. Magn. Reson.* **2014**, *59–60*, 45–47.

(8) Götze, W. J. Recent tests of the mode-coupling theory for glassy dynamics. *J. Phys.: Condens. Matter* **1999**, *11*, A1.

(9) Kudlik, A.; Benkhof, S.; Tschirwitz, T.; Blochowicz, T.; Rössler, E. The dielectric response of simple organic glass formers. *J. Mol. Struct.* **1999**, *479*, 201–218.

(10) Lunkenheimer, P.; Schneider, U.; Brand, R.; Loidl, A. Glassy dynamics. *Contemp. Phys.* **2000**, *41*, 15–36.

(11) Wolynes, P. G.; Lubchenko, V. *Structural Glasses and Supercooled Liquids*; Wiley: Oxford, 2012.

(12) Petzold, N.; Schmidtke, B.; Kahlau, R.; Bock, D.; Meier, R.; Micko, B.; Kruk, D.; Rössler, E. A. Evolution of the Dynamic Susceptibility in Molecular Glass Formers: Results from Light Scattering, Dielectric Spectroscopy, and NMR. *J. Chem. Phys.* **2013**, *138*, 12A510.

(13) Rubinstein, M.; Colby, R. H. *Polymer Physics*; Oxford University: New York, 2003.

(14) Graessley, W. W. *Polymeric Liquids & Networks: Dynamics and Rheology*; Taylor and Francis: New York, 2008.

(15) Kimmich, R.; Fatkullin, N. Polymer Chain Dynamics and NMR. *Adv. Polym. Sci.* **2004**, *170*, 1–113.

(16) Kariyo, S.; Stapf, S. Restricted Molecular Dynamics of Polymer Chains y means of NMR Field Cycling Relaxometry. *Macromol. Chem. Phys.* **2005**, *206*, 1300–1310.

(17) Kariyo, S.; Gainaru, C.; Schick, H.; Brodin, A.; Rössler, E. A. From a Simple Liquid to a Polymer Melt: NMR Relaxometry Study of Polybutadiene. *Phys. Rev. Lett.* **2006**, *97*, 207803. Erratum: Kariyo, S.; Herrmann, A.; Gainaru, C.; Schick, H.; Brodin, A.; Rössler, E. A. *Phys. Rev. Lett.* **2008**, *100*, 109901.

(18) Kariyo, S.; Brodin, A.; Gainaru, C.; Herrmann, A.; Schick, H.; Novikov, V. N.; Rössler, E. A. From Simple Liquid to Polymer Melt. Glassy and Polymer Dynamics studied by Fast Field Cycling NMR Relaxometry: low and high Molecular Weight Limit. *Macromolecules* **2008**, *41*, 5313–5321.

(19) Herrmann, A.; Kariyo, S.; Abou Elfadl, A.; Meier, R.; Gmeiner, J.; Novikov, V.; Rössler, E. A. Universal Polymer Dynamics Revealed by Field Cycling 1H NMR. *Macromolecules* **2009**, *42*, 5236–5243.

(20) Herrmann, A.; Kresse, B.; Gmeiner, J.; Privalov, A. F.; Kruk, D.; Fujara, F.; Rössler, E. A. Protracted Crossover to Reptation Dynamics: A Field Cycling 1H NMR Study Including Extremely Low Frequencies. *Macromolecules* **2012**, *45*, 1408–1416.

(21) Hofmann, M.; A; Herrmann, A.; Abou Elfadl, A.; Kruk, D.; Wohlfahrt, M.; Rössler, E. A. Glassy, Rouse, and entanglement dynamics as revealed by field cycling 1H NMR relaxometry. *Macromolecules* **2012**, *45*, 2390–2401.

(22) Hofmann, M.; Kresse, B.; Privalov, A.; B; Willner, L.; Fatkullin, N.; Fujara, F.; Rössler, E. A. Field-Cycling NMR Relaxometry Probing the Microscopic Dynamics in Polymer Melts. *Macromolecules* **2014**, *47*, 7917–7929.

(23) Fatkullin, N.; Stapf, S.; Hofmann, M.; Meier, R.; Rössler, E. A. Proton Spin Dynamics in Polymer Melts: New Perspectives for Experimental Investigations of Polymer Dynamics. *J. Non-Cryst. Solids* **2015**, *407*, 309–317.

(24) Doi, M.; Edwards, S. F. *The Theory of Polymer Dynamics*; Oxford Sci. Publication: Hoboken, New Jersey, 1986.

(25) Hofmann, M.; Gainaru, C.; Cetinkaya, B.; Valiullin, R.; Fatkullin, N.; Rössler, E. A. Field-Cycling Relaxometry as a Molecular Rheology Technique: Common Analysis of NMR, Shear Modulus and Dielectric Loss Data of Polymers vs Dendrimers. *Macromolecules* **2015**, *48*, 7521–7534.

(26) Abragam, A. *The Principles of Nuclear Magnetism*; Clarendon Press: Oxford, U.K., 1961.

(27) Torrey, H. C. Nuclear Spin Relaxation by Translational Diffusion. *Phys. Rev.* **1953**, *92*, 962.

(28) Harmon, J. F.; Muller, B. H. Nuclear Spin Relaxation by Translational Diffusion in Liquid Ethane. *Phys. Rev.* **1969**, *182*, 400.

(29) Sholl, C. A. Nuclear Spin Relaxation by Translational Diffusion in Liquids and Solids: High-and Low-Frequency Limits. *J. Phys. C: Solid State Phys.* **1981**, *14*, 447.

(30) Meier, R.; Kruk, D.; Gmeiner, J.; Rössler, E. A. Intermolecular relaxation in glycerol as revealed by field cycling 1H NMR relaxometry dilution experiments. *J. Chem. Phys.* **2012**, *136*, 034508.

(31) Kruk, D.; Meier, R.; Rössler, E. A. Nuclear Magnetic Resonance Relaxometry as a Method of Measuring Translational Diffusion Coefficients in Liquids. *Phys. Rev. E* **2012**, *85*, 020201.

(32) Meier, R.; Kruk, D.; Bourdick, A.; Schneider, E.; Rössler, E. A. Inter-and Intramolecular Relaxation in Molecular Liquids by Field Cycling 1H NMR Relaxometry. *Appl. Magn. Reson.* **2013**, *44*, 153–168.

(33) Meier, R.; Herrmann, A.; Hofmann, M.; Schmidtke, B.; Kresse, B.; Privalov, A. F.; Kruk, D.; Fujara, F.; Rössler, E. A. Iso-Frictional Mass Dependence of Diffusion of Polymer Melts Revealed by 1H NMR Relaxometry. *Macromolecules* **2013**, *46*, 5538–5548.

(34) Kruk, D.; Meier, R.; Rössler, E. A. Determining Diffusion Coefficients of Ionic Liquids by Means of Field Cycling Nuclear Magnetic Resonance Relaxometry. *J. Chem. Phys.* **2014**, *140*, 244509.

(35) Meier, R.; Schneider, E.; Rössler, E. A. Change of Translational-Rotational Coupling in Liquids Revealed by Field-Cycling 1H NMR. *J. Chem. Phys.* **2015**, *142*, 034503.

(36) Ordikhani Seyedlar, A.; Stapf, S.; Mattea, C. Dynamics of the Ionic Liquid 1-Butyl-3-Methylimidazolium Bis (Trifluoromethylsulphonyl) Imide Studied by Nuclear Magnetic Resonance Dispersion and Diffusion. *Phys. Chem. Chem. Phys.* **2015**, *17*, 1653–1659.

(37) Odelius, M.; Laaksonen, A.; Levitt, M. H.; Kowalewski, J. Intermolecular dipole-dipole relaxation. A molecular dynamics simulation. *J. Magn. Reson., Ser. A* **1993**, *105*, 289–294.

(38) Henritzi, P.; Bormuth, A.; Vogel, M. Interpretation of 1 and 2 H Spin–Lattice Relaxation Dispersions: Insights from Molecular Dynamics Simulations of Polymer Melts. *Solid State Nucl. Magn. Reson.* **2013**, *54*, 32–40.

(39) Ayant, Y.; Belorizky, E.; Fries, P.; Rosset, J. Effet des Interactions Dipolaires Magnétiques Intermoléculaires sur la Relaxation Nucléaire de Molécules Polyatomiques dans les Liquides. *J. Phys. (Paris)* **1977**, *38*, 325–337.

(40) Kehr, M.; Fatkullin, N.; Kimmich, R. Molecular Diffusion on a Time Scale between Nano-and Milliseconds Probed by Field-Cycling NMR Relaxometry of Intermolecular Dipolar Interactions: Application to Polymer Melts. *J. Chem. Phys.* **2007**, *126*, 094903.

(41) Kehr, M.; Fatkullin, N.; Kimmich, R. Deuteron and Proton Spin-Lattice Relaxation Dispersion of Polymer Melts: Intrasegment, Intrachain, and Interchain Contributions. *J. Chem. Phys.* **2007**, *127*, 084911.

(42) Herrmann, A.; Kresse, B.; Wohlfart, M.; Bauer, I.; Privalov, A. F.; Kruk, D.; Fatkullin, N.; Fujara, F.; Rössler, E. A. Mean Square Displacement and Reorientational Correlation Function in Entangled

Polymer Melts Revealed by Field Cycling 1H and 2H NMR Relaxometry. *Macromolecules* **2012**, *45*, 6516−6526.

(43) Kresse, B.; Hofmann, M.; Privalov, A. F.; Fujara, F.; Fatkullin, N.; Rössler, E. A. All Polymer Diffusion Regimes Covered by Combining Field-Cycling and Field-Gradient 1H NMR. *Macromolecules* **2015**, *48*, 4491−4502.

(44) Fischer, E.; Kimmich, R.; Fatkullin, N. NMR field gradient diffusometry of segment displacements in melts of entangled polymers. *J. Chem. Phys.* **1996**, *104*, 9174−9178.

(45) Fischer, E.; Kimmich, R.; Fatkullin, N. Spin Diffusion in Melts of Entangled Polymers. *J. Chem. Phys.* **1997**, *106*, 9883−9888.

(46) Pahl, S.; Fleischer, G.; Fujara, F.; Geil, B. Anomalous Segment Diffusion in Polydimethylsiloxane Melts. *Macromolecules* **1997**, *30*, 1414−1418.

(47) Komlosh, M. E.; Callaghan, P. T. Segmental motion of entangled random coil polymers studied by pulsed gradient spin echo nuclear magnetic resonance. *J. Chem. Phys.* **1998**, *109*, 10053−10067.

(48) Solomon, I. Relaxation Processes in a System of two Spins. *Phys. Rev.* **1955**, *99*, 559.

(49) Kowalewski, J.; Maler, L. *Nuclear Spin Relaxation in Liquids: Theory, Experiments, and Applications*; CRC Press: Boca Raton, FL, 2006.

(50) Spiess, H. W. Molecular Dynamics of Solid Polymers as Revealed by Deuteron NMR. *Colloid Polym. Sci.* **1983**, *261*, 193−209.

(51) Hoatson, G. L.; Vold, R. L. 2H-NMR Spectroscopy of Solids and Liquid Crystals. In *Solid-State NMR III Organic Matter*; Blümich, B., Ed.; Springer: Berlin, 1994; pp 1−67.

(52) Schmidt-Rohr, K.; Spiess, H. W. *Multidimensional Solid-State NMR and Polymers*; Academic Press: Mainz, Germany, 1994.

(53) Böhmer, R.; Diezemann, G.; Hinze, G.; Rössler, E. A. Dynamics of Supercooled Liquids and Glassy Solids. *Prog. Nucl. Magn. Reson. Spectrosc.* **2001**, *39*, 191−267.

(54) Kimmich, R.; Fatkullin, N.; Seitter, R. O.; Gille, K. Chain Dynamics in Entangled Polymers: Power Laws of the Proton and Deuteron Spin-Lattice Relaxation Dispersions. *J. Chem. Phys.* **1998**, *108* (5), 2173−2177.

(55) Kariyo, S.; Stapf, S.; Blümich, B. Site specific Proton and Deuteron NMR Relaxation Dispersion in Selectively Deuterated Polyisoprene Melts. *Macromol. Chem. Phys.* **2005**, *206*, 1292−1299.

(56) Kimmich, R. *Principles of Soft-Matter Dynamics*; Springer Science & Business Media: Heidelberg, Germany, 2012.

(57) Böttcher, C. J. F.; Bordewijk, P. *Theory of Electric Polarization*; Elsevier Scientific Polarization: Amsterdam, The Netherlands, 1978.

(58) Cohen-Addad, J. P.; Messa, J. P. Concentration Frequency Dependence of Short Range Chain Fluctuations Observed in Concentrated Polymer Solutions from Nuclear Magnetic Resonance Rates. *J. Phys., Lett.* **1976**, *37*, 193.

(59) Rössler, E.; Sillescu, H. 2 H NMR Study of Supercooled Toluene. *Chem. Phys. Lett.* **1984**, *112*, 94−98.

(60) Dries, T.; Fujara, F.; Kiebel, M.; Rössler, E.; Sillescu, H. 2H-NMR Study of the Glass Transition in Supercooled ortho-Terphenyl. *J. Chem. Phys.* **1988**, *88*, 2139−2147; *J. Chem. Phys.* **1989**, *90*, 7613.

(61) Schnauss, W.; Fujara, F.; Sillescu, H. The Molecular Dynamics around the Glass Transition and in the Glassy State of Molecular Organic Systems: A 2H− Nuclear Magnetic Resonance Study. *J. Chem. Phys.* **1992**, *97*, 1378−1389.

(62) Rössler, E. A.; Eiermann, P. Reorientational Dynamics in Supercooled m-Tricresyl Phosphate: Its Relation to Main and Secondary Relaxation—31P Nuclear Magnetic Resonance Study of Relaxation, Line Shape, and Stimulated Echo. *J. Chem. Phys.* **1994**, *100* (7), 5237−5248.

(63) Lips, O.; Privalov, A. F.; Dvinskikh, S. V.; Fujara, F. Magnet Design with high B 0 Homogeneity for Fast-Field-Cycling NMR Applications. *J. Magn. Reson.* **2001**, *149*, 22−28.

(64) Drake, P. W.; Meister, R. Rotational Spin−Lattice and Spin−Spin Quadrupole Relaxation in Perdeuterated Glycerol. *J. Chem. Phys.* **1971**, *54*, 3046−3050.

(65) Wolfe, M.; Jonas, J. Reorientational Motions in Compressed Viscous Fluids: Selectively Deuterated Glycerol. *J. Chem. Phys.* **1979**, *71*, 3252−3262.

(66) Diehl, R.; Fujara, F.; Sillescu, H. 2H-NMR-Stimulated Echo Study of Ultraslow Reorientational Motion in Viscous Glycerol near its Glass Transition Temperature. *Europhys. Lett.* **1990**, *13*, 257−262.

(67) Friedrich, A.; Dölle, A.; Zeidler, M. D. Reorientational Dynamics of Glycerol Derived from Temperature-Dependent Multi-Nuclear Magnetic Resonance Relaxation Data. *Magn. Reson. Chem.* **2003**, *41*, 813−818.

(68) Qi, F.; Böhmer, R.; Sillescu, H. The Methyl Group as a built-in Probe of the Glassy Dynamics in Propylene Carbonate. *Phys. Chem. Chem. Phys.* **2001**, *3* (18), 4022−4028.

(69) Döß, A.; Hinze, G.; Böhmer, R.; Sillescu, H.; Kolshorn, H.; Vogel, M.; Zimmermann, H. Deuteron and Carbon Magnetic Resonance Studies of Supercooled Liquid and Glassy Salol. *J. Chem. Phys.* **2000**, *112*, 5884−5892.

(70) Qi, F.; Hinze, G.; Böhmer, R.; Sillescu, H.; Zimmermann, H. Slow and Fast Methyl Group Rotations in Fragile Glass-Formers Studied by NMR. *Chem. Phys. Lett.* **2000**, *328*, 257−262.

(71) Jörg, T.; Böhmer, R.; Sillescu, H.; Zimmermann, H. Isotope Effects on the Dynamics of a Supercooled van der Waals Liquid. *Europhys. Lett.* **2000**, *49* (6), 748.

(72) Woessner, D. E.; Snowden, B. S., Jr. Magnetic Relaxation under Hindered Rotation in Fluids. *Adv. Mol. Relax. Processes* **1972**, *3*, 181−197.

(73) Parker, R. G.; Jonas, J. Spin-Lattice Relaxation in Several Molecules Containing Methyl Groups. *J. Magn. Reson.* **1972**, *6*, 106−116.

(74) Wilbur, D. J.; Jonas, J. Fourier Transform NMR in Liquids at High Pressure. III. Spin−Lattice Relaxation in Toluene-d8. *J. Chem. Phys.* **1975**, *62*, 2800−2807.

(75) Hinze, G.; Sillescu, H. 2H Nuclear Magnetic Resonance Study of Supercooled Toluene: Slow and Fast Processes above and below the Glass Transition. *J. Chem. Phys.* **1996**, *104*, 314−319.

(76) Hinze, G.; Sillescu, H.; Fujara, F. Anisotropic Motion of Toluene above and below the Glass Transition Studied by 2 H NMR. *Chem. Phys. Lett.* **1995**, *232*, 154−158.

(77) Spiess, H. W.; Schweitzer, D.; Haeberlen, U. Molecular Motion in Liquid Toluene from a Study of 13 C and 2 D Relaxation Times. *J. Magn. Reson.* **1973**, *9*, 444−460.

(78) NaNagara, B.; O'Connor, R. D.; Blum, D. Mobility of Toluene in Polystyrene-Toluene Solutions: A NMR Study. *J. Phys. Chem.* **1992**, *96*, 6417−6423.

(79) Barnes, R. G. Deuteron Quadrupole Coupling Tensors in Solids. *Advances in Nuclear Quadrupole Resonance* **1972**, *1*, 335−355.

(80) Schmidtke, B.; Petzold, N.; Kahlau, R.; Rössler, E. A. Reorientational Dynamics in Molecular Liquids as Revealed by Dynamic Light Scattering: from Boiling Point to Glass Transition Temperature. *J. Chem. Phys.* **2013**, *139*, 084504.

(81) Ngai, K. L.; Paluch, M. Classification of Secondary Relaxation in Glass-Formers based on Dynamic Properties. *J. Chem. Phys.* **2004**, *120*, 857−873.

(82) Sturz, L.; Dölle, A. Anisotropic Reorientational Dynamics of Toluene in Neat Liquid. A 13C Nuclear Magnetic Relaxation Study. *J. Phys. Chem. A* **2001**, *105*, 5055−5060.

(83) Lambert, J. B.; Nienhuis, R. J.; Finzel, R. B. The Influence of Anisotropic Motion on the Barrier to Methyl Rotation in p-Toluenes. *J. Phys. Chem.* **1981**, *85*, 1170−1172.

(84) Bauer, D. R.; Alms, G. R.; Brauman, J. I.; Pecora, R. Depolarized Rayleigh Scattering and 13C NMR Studies of Anisotropic Molecular Reorientation of Aromatic Compounds in Solution. *J. Chem. Phys.* **1974**, *61*, 2255−2261.

(85) Woessner, D. E. Nuclear Spin Relaxation in Ellipsoids undergoing Rotational Brownian Motion. *J. Chem. Phys.* **1962**, *37*, 647−654.

(86) Blochowicz, Th.; Tschirwitz, Ch.; Benkhof, St.; Rössler, E. A. Susceptibility Functions for Slow Relaxation Processes in Supercooled

Liquids and the Search for Universal Relaxation Patterns. *J. Chem. Phys.* **2003**, *118*, 7544−7555.

(87) Rössler, E. A.; Sillescu, H.; Spiess, H. W. Deuteron NMR in relation to the glass transition in polymers. *Polymer* **1985**, *26*, 203−207.

(88) Litvinov, V. M.; Spiess, H. W. 2H NMR Study of Molecular Motions in Polydimethylsiloxane and its Mixtures with Aerosils. *Makromol. Chem.* **1991**, *192*, 3005−3019.

(89) Pschorn, U.; Rössler, E.; Sillescu, H.; Kaufmann, S.; Schaefer, D.; Spiess, H. W. Local and Cooperative Motions at the Glass Transition of Polystyrene: Information from one- and two-dimensional NMR as Compared with other Techniques. *Macromolecules* **1991**, *24*, 398−402.

(90) Rössler, E. A.; Sokolov, A. P.; Eiermann, P.; Warschewske, U. Dynamical Phase Transition in Simple Supercooled Liquids and Polymers − an NMR Approach. *Phys. A* **1993**, *201*, 237−256.

(91) Hansen, M. T.; Kulik, A. S.; Prins, K. O. Effect of High Hydrostatic Pressure on the Phenylene Motion in Polycarbonate as Revealed by 2H Spin-Lattice Relaxation. *Polymer* **1992**, *33*, 2231−2233.

(92) Döss, A.; Hinze, G.; Diezemann, G.; Böhmer, R.; Sillescu, H. Spatial heterogeneity in glassy polystyrene detected by deuteron NMR relaxation. *Acta Polym.* **1998**, *49*, 56−58.

(93) O'Connor, R. D.; Ginsburg, E. J.; Blum, F. D. Solid-State Deuterium Nuclear Magnetic Resonance of the Methyl Dynamics of Poly(Alpha-methylstyrene) and Polymethylphenylsilane. *J. Chem. Phys.* **2000**, *112*, 7247−7259.

(94) Lutz, T. R.; He, Y.; Ediger, M. D.; Cao, H. H.; Lin, G. X.; Jones, A. A. Rapid Poly(ethylene oxide) Segmental Dynamics in Blends with Poly(methyl methacrylate). *Macromolecules* **2003**, *36*, 1724−1730.

(95) Nozirov, F.; Nazirov, A.; Jurga, S.; Fu, R. Q. Molecular Dynamics of Poly(l-lactide) Biopolymer Studied by Wide-Line Solid-State 1 and 2 H NMR Spectroscopy. *Solid State Nucl. Magn. Reson.* **2006**, *29*, 258−266.

(96) Perez Aparicio, A.; Arbe, A.; Colmenero, J.; Frick, B.; Willner, L.; Richter, D.; Fetters, L. J. Quasielastic Neutron Scattering Study on the Effect of Blending on the Dynamics of Head-to-Head Poly-(propylene) and Poly(ethylene-propylene). *Macromolecules* **2006**, *39*, 1060−1072.

(97) Khazanovich, T. N. Theory of Nuclear Magnetic Relaxation in Liquid-Phase Polymers. *Polym. Sci. U.S.S.R.* **1963**, *4*, 727−736.

(98) Ullman, R. Nuclear Magnetic Relaxation of Polymer Solutions. *J. Chem. Phys.* **1965**, *43*, 3161−3177.

(99) Kariyo, S.; Brodin, A.; Gainaru, C.; Herrmann, A.; Hintermeyer, J.; Schick, H.; Novikov, V. N.; Rössler, E. A. From Simple Liquid to Polymer Melt. Glassy and Polymer Dynamics Studied by Fast Field Cycling NMR Relaxometry: Rouse Regime. *Macromolecules* **2008**, *41*, 5322−5332.

(100) deGennes, P. G. Reptation of a Polymer Chain in the Presence of Fixed Obstacles. *J. Chem. Phys.* **1971**, *55*, 572−579.

(101) Ball, R. V.; Callaghan, P. T.; Samulski, E. T. A Simplified Approach to the Interpretation of Nuclear Spin Correlations in Entangled Polymeric Liquids. *J. Chem. Phys.* **1997**, *106*, 7352−7361.

(102) Bormuth, A.; Hofmann, M.; Henritzi, P.; Vogel, M.; Rössler, E. A. Chain-Length Dependence of Polymer Dynamics: A Comparison of Results from Molecular Dynamics Simulations and Field-Cycling 1H NMR. *Macromolecules* **2013**, *46*, 7805−7811.

(103) Kremer, F.; Schönhals, A. *Broad Band Dielectric Spectroscopy*; Springer: Berlin, 2002.

(104) Gainaru; Gainaru, C.; Meier, R.; Schildmann, S.; Lederle, C.; Hiller, W.; Rössler, E. A.; Böhmer, R. Nuclear-Magnetic-Resonance Measurements Reveal the Origin of the Debye Process in Monohydroxy Alcohols. *Phys. Rev. Lett.* **2010**, *105*, 258303.

(105) Gainaru, C.; Figuli, R.; Hecksher, T.; Jakobsen, B.; Dyre, J. C.; Wilhelm, M.; Böhmer, R. Shear-Modulus Investigations of Monohydroxy Alcohols: Evidence for a Short-Chain-Polymer Rheological Response. *Phys. Rev. Lett.* **2014**, *112*, 098301.

(106) Rössler, E. A. Corresponding States Concept for Simple Supercooled Liquids Identifying a Change of Diffusion Mechanism Above the Glass Transition Temperature. *Ber. Bunsenges. Phys. Chem.* **1990**, *94*, 392−399.

Publication 3

Dielectric Relaxation and Proton Field-Cycling NMR Relaxometry Study of Dimethyl Sulfoxide/Glycerol Mixtures Down to Glass-Forming Temperatures

Flämig, M.; Gabrielyan, L.; Minikejew, R.; Markarian, S.; Rössler, E. A.

Dielectric relaxation and proton field-cycling NMR relaxometry study of dimethyl sulfoxide/glycerol mixtures down to glass-forming temperatures [Q2]

Max Flämig,[a] Liana Gabrielyan,[b] Rafael Minikejew,[a] Shiraz Markarian[b] and Ernst A. Rössler [ID] *[a]

Mixtures of glycerol and dimethyl sulfoxide (DMSO) are studied by dielectric spectroscopy (DS) and by ^{1}H field-cycling (FC) NMR relaxometry in the entire concentration range and down to glass-forming temperatures (170–323 K). Molecular dynamics is accessed for $0 < x_{DMSO} \leq 0.64$, at higher concentration phase separation occurs. The FC technique provides the frequency dependence of the spin–lattice relaxation rate which is transformed to the susceptibility representation and thus allows comparing NMR and DS results. The DS spectra virtually do not change with x_{DMSO} and T, only the relaxation times become shorter. This is in contrast to the non-associated mixture toluene/quinaldine for which strong spectral changes occur. The FC relaxation spectra of glycerol in solution with DMSO or (deuterated) DMSO-d_6 display a bimodal structure with a high-frequency part reflecting rotational and a low-frequency part reflecting translational dynamics. Regarding the rotational contribution in the glycerol/DMSO-d_6 mixtures, no spectral change with x_{DMSO} and T is observed. Yet, the non-deuterated mixture reveals a broader relaxation spectrum. Time constants $\tau_{rot}(T)$ probed by the two techniques complement each, a range 10^{-11} s $< \tau < 10$ s is covered. The glass transition temperature $T_g(x_{DMSO})$ is determined, yielding $T_g = 149.5 \pm 1$ K of pure DMSO by extrapolation. Analysing the low-frequency FC NMR spectra allows to determine the diffusion coefficient D_{trans}. Its logarithm shows a linear x_{DMSO}-dependence as does lg τ_{rot}. The ratio D_{trans}/D_{rot} is independent of x_{DMSO} and its low value indicates large separation of translation and rotation. The corresponding unphysically small hydrodynamic radius indicates strong failure of Stokes–Einstein–Debye relation. Such anomaly is taken as characteristics of a 3d hydrogen-bonded network. We conclude, although DMSO is an aprotic liquid the molecule is continuously incorporated in the hydrogen network of glycerol. Both molecules display common dynamics, i.e., no decoupling of the component dynamics is found in contrast to quinaldine/toluene with a similar T_g difference of its components.

1. Introduction

The dynamics of pure molecular (mostly non-associated) liquids was extensively investigated in the last decades particularly when being strongly super-cooled and thus approaching the glass transition temperature T_g. The evolution of dynamic susceptibilities reflecting, for instance, density or reorientational fluctuations was unravelled by various techniques covering times scales from picoseconds up to minutes.[1–6] The next challenge is to characterize and understand the dynamics of binary glass forming systems. Of special interest are non-polymeric systems with a high T_g contrast of the

components.[7,8] Such systems may be taken as model systems for binary glass formers with significant size (or mass) disparity of their components.[9] With up-to-date spectroscopic methods, the dynamics not only in the super-cooled (viscous) regime but also in the stable liquid can be accessed, and this research encompasses the important field of understanding dynamics in multi-component liquids. The outstanding properties of multi-component liquids are pronounced dynamical heterogeneities reflected by anomalously broad or bimodal dielectric spectra, for example, which in the case of binary liquids may even allow to identify two glass transition temperatures, albeit they are fully miscible.[7,8,10–16] Similar results were reported for polymer–plasticizer systems.[3,17–22]

In the case of associated liquids, which in some cases can also be super-cooled and finally become a highly viscous liquid approaching the glass state at low temperatures, additional

[a] Nordbayerisches NMR-Zentrum, Universität Bayreuth, 95440 Bayreuth, Germany.
E-mail: ernst.roessler@uni-bayreuth.de
[b] Chair of Physical Chemistry, Yerevan State University, 0025 Yerevan, Armenia

This journal is © the Owner Societies 2020

Phys. Chem. Chem. Phys., 2020, **00**, 1–15 | 1

phenomena may show up. For example, understanding the appearance of the so-called Debye relaxation (in addition to the α-relaxation) in mono-alcohols, prototypes of associated liquids, is currently thoroughly investigated.[23,24] Here, one assumes the formation of transient chains of alcohol molecules providing a further slow relaxation path. Innumerable associated mixtures were studied but usually in the stable and low-viscosity state, and the role of the T_g contrast of the components was not given much attention. In a recent rheological study of glycerol–water mixtures[25] it was demonstrated that in addition to the main relaxation a weak relaxation feature at low frequencies is found similar to what is observed in mono-alcohols. Adding water, the feature disappears abruptly at equimolar composition. The authors speculated that the water acts as a lubricant for softening the glycerol–glycerol hydrogen-bonded network. In all the cases, the fundamental question is how the hydrogen-bond network transforms upon adding a second component.

In the present contribution we investigate the mixtures of glycerol with aprotic dimethyl sulfoxide (DMSO) up to high viscosities over a large concentration range. Liquid glycerol forms a strong 3d hydrogen bonded network, and is one of the most studied glass formers;[1,6,25,26] crystallization is rarely observed. In contrast, pure DMSO can only weakly be super-cooled T_m = 291 K). Its glass transition temperature was estimated by extrapolation from concentrated DMSO solutions and found to be T_g = 150 K[27] and T_g = 151 K,[28] respectively. Thus, given T_g = 186 K of glycerol,[2] a moderate T_g contrast of about 40 K characterizes the mixture. Pure DMSO is a polar aprotic solvent with high dipole moment and high dielectric permittivity.[29,30] The polar nature of the S–O bond underlies its self-association ability, which testifies to complex interactions between the hydrophilic and hydrophobic parts of molecular structure. Sulfoxides are known to form strong hydrogen bonds with various proton donors, such as water, acids and alcohols – and probably also with glycerol. Studying the dynamics of pure DMSO and its binary mixtures were the objects of many researchers, yet, in most cases they were not studied at high viscosities approaching T_g.[31–34] The properties of DMSO–glycerol mixtures were studied by various methods;[34] in particular, dielectric spectra in the micro wave range were analysed in ref. 35 and transport coefficients compiled in ref. 36.

Here, we combine dielectric spectroscopy (DS) and proton field-cycling (FC) nuclear magnetic resonance (NMR) relaxometry to probe reorientational and translational dynamics. The dielectric spectra of pure glycerol are paradigmatically simple, *i.e.*, the main (α-) relaxation peak can be described by a Cole–Davidson (CD) function.[37] In addition, there is a so-called excess wing on the high-frequency flank of the α-relaxation, but no discernible secondary relaxation peak is identified at $T \leq T_g$.[1,2] With the emergence of a commercial FC relaxometer since 1997[38] and recent instrumental progress made by home-built machines,[39–41] FC NMR relaxometry has become an important tool for studying viscous liquids and polymers.[42–46] Whereas DS probes the reorientation of all the molecular dipoles present in the mixture, NMR enables component-

selective studies provided that one component is isotope-labelled. Moreover, proton FC NMR relaxometry allows to monitor in addition to rotational also translational dynamics due to the dominance of the magnetic dipolar interaction providing an intra- as well as an intermolecular pathway. In a single experiment the ratio of the translational and rotational diffusion coefficient, D_{trans}/D_{rot} are accessible.[44,47] Very recently, a proton FC NMR study on pure glycerol demonstrated that in addition to the translational relaxation contribution the rotational spectral density is essentially the same as that probed by light scattering experiments.[48] Moreover, the ratio D_{trans}/D_{rot} turned out to be unphysically small compared to the situation in molecular liquids like *o*-terphenyl, and thus indicating strong failure of Stokes–Einstein–Debye (SED) relation.[47] Here, the question appears whether this anomalously large separation of molecular translation and rotation prevails in mixtures.

2. Theoretical background

In (super-cooled) liquids like glycerol the main dielectric (α-) relaxation peak, reflecting reorientational dynamics, is often described by a Cole–Davidson (CD) function together with the high-frequency dielectric constant ε_∞, explicitly[37]

$$\varepsilon^*(\omega) = \varepsilon_\infty + \frac{\Delta\varepsilon}{[1 + (i\omega\tau_{CD})]^{\beta_{CD}}} \qquad (1)$$

where $\Delta\varepsilon$ is the amplitude of the relaxation process, $\tau_{rot} = \tau_{CD}\beta_{CD}$ is the relaxation time, and β_{CD} the stretching parameter with $0 \leq \beta_{CD} \leq 1$.

Proton NMR relaxation in molecular systems is dominated by the magnetic dipole–dipole interaction. The ^{1}H spin–lattice relaxation rate, $R_1(\omega)$ with $\omega = \gamma B$ being the Larmor frequency, B the magnetic field and γ the gyromagnetic ratio, is a sum of two contributions:[44,45]

$$R_1(\omega) = R_{1,intra}(\omega) + R_{1,inter}(\omega) \qquad (2)$$

The intramolecular relaxation rate is given by the Bloembergen, Purcell, and Pound (BPP) type of expression[44,45]

$$R_{1,intra}(\omega) = K_{intra}[J_{intra}(\omega) + 4J_{intra}(2\omega)] \qquad (3)$$

where $J_{intra}(\omega)$ denotes the rotational spectral density, and K_{intra} the intramolecular coupling constant. In liquids the (normalized) rotational correlation function $C_{rot}(t) \equiv C_{intra}(t)$ is identical to that of the second Legendre polynomial $C_2(t)$. We note that dielectric spectroscopy probes the first Legendre polynomial correlation function usually in good approximation.[37] The spectral density $J_{intra}(\omega) \equiv J_{rot}(\omega)$ is given by

$$J_{rot}(\omega) = \frac{1}{2}\int_{-\infty}^{\infty} C_{rot}(t)e^{-i\omega t}dt$$

with

$$\int_0^\infty J_{rot}(\omega)d\omega = \frac{\pi}{2} \qquad (4)$$

2 | *Phys. Chem. Chem. Phys.*, 2020, **00**, 1–15

This journal is © the Owner Societies 2020

and the correlation time τ_{rot} by

$$\tau_{rot} \equiv \int_0^\infty C_{rot}(t)\mathrm{d}t = J_{rot}(0) \qquad (5)$$

The correlation function in liquids is non-exponential even above the melting point except for temperatures close to the boiling point,[6] and $J_{rot}(\omega)$ may phenomenologically be described again by CD function (eqn (1)) as in the case of DS.

The correlation function for intermolecular relaxation reflects both, changes of the orientation as well as the inter-spin distance $r(t)$:[44,45]

$$C_{inter}(t) \propto \left\langle \frac{Y_{2m}(t)}{r^3(t)} \frac{Y_{2-m}(0)}{r^3(0)} \right\rangle \qquad (6)$$

In a simple approach the molecules are taken as hard spheres with a distance of closest approach d (twice the hard spheres radius) leading to the "force-free hard sphere" (FFHS) model, and the (normalized) spectral density takes the form:[49–52]

$$J_{trans}(\omega) = \frac{54}{\pi} \int_0^\infty \frac{u^2}{81 + 9u^2 - 2u^4 + u^6} \frac{u^2 \tau_{trans}}{u^4 + (\omega\tau_{trans})^2} \mathrm{d}u \qquad (7)$$

where $\tau_{trans} = \frac{d^2}{2D_{trans}}$ defines the translational time constant, D_{trans} the self-diffusion coefficient, and d the distance of closest approach. An analogue of the BPP expression, eqn (3), connects $R_{1,inter}(\omega)$ to $J_{trans}(\omega)$. Within the FFHS model the corresponding coupling constant K_{inter} is given by[49–52]

$$K_{inter} = \left(\frac{\mu_0}{4\pi}\right)^2 \frac{8\pi}{15} \frac{n}{d^3} I(I+1)\hbar^2\gamma^4 \qquad (8)$$

where n denotes the spin density.

For real molecules (being no hard spheres), the intermolecular interaction is modulated by both, translational and rotational dynamic. Within a phenomenological model, we write[51,52]

$$R_1(\omega) \cong R_{1,intra}(\omega) + R_{1,inter}^{rot}(\omega) + R_{1,inter}^{trans}(\omega) \cong R_1^{rot}(\omega) + R_1^{trans}(\omega) \qquad (9)$$

$R_1^{rot}(\omega)$ may again be described by a CD spectral density, and $R_{1,inter}^{trans}(\omega)$ by the FFHS spectral density.

Independent of any details of translational motion, at long times the molecules in a liquid undergo Fickian diffusion, implying a mean square displacement $\langle \Delta r^2 \rangle = 6D_{trans}t$. In this limit the translational correlation function is given by a power law $C_{inter}(t) \propto t^{-3/2}$, and the low-frequency limit $J_{inter}(\omega)$ depends on the square root of the frequency,[44,45,53] what is re-found also in the total relaxation

$$R_1(\omega) = R_1(0) - \frac{B}{D_{trans}^{3/2}} \cdot \sqrt{\omega} \qquad (10)$$

since the power-law behaviour of $C_{inter}(t)$ dominates the total correlation function at longest times and thus the frequency dependences in the limit of low frequencies. Here, $R_1(0)$ contains both, an intra- as well as an intermolecular part, specifically $R_1(0) = R_{1,intra}(0) + R_{1,inter}(0)$. The constant is given by $B = \frac{\pi}{30}(1 + 4\sqrt{2})\left(\frac{\mu_0}{4\pi}\hbar\gamma_H^2\right)^2 n$. Hence, from the low-frequency

dispersion of $R_1(\omega)$ the diffusion coefficient D_{trans} of a (pure) liquid can be determined in a straightforward manner.[54,55] Field-cycling ^{1}H NMR relaxometry allows to determine both D_{trans} as well as τ_{rot} whereas DS provides only τ_{rot}.

Assuming the Stokes–Einstein–Debye relation (SED), i.e., assuming a sphere performing rotational and translational Brownian motion in a viscous medium, the ratio D_{trans}/D_{rot} is linked to the hydrodynamic radius R_H:[56,57]

$$D_{trans}/D_{rot} = D_{trans}\tau_l l(l+1) = \frac{4}{3}R_H^2 \qquad (11)$$

The diffusion coefficient D_{rot} is connected with the reorientational correlation time provided by DS (rank $l = 1$) or NMR (rank $l = 2$) via[56,58]

$$\tau_l = \frac{1}{D_{rot}l(l+1)} \qquad (12)$$

The ratio $r = \tau_{trans}/\tau_{rot}$ may be taken as a measure of the separation of translation and rotation in a liquid. Assuming SED, one arrives at $r = 9$,[59] however, in certain liquids, e.g., glycerol, the ratio r is much larger, thus indicating a failure of SED, which goes along with unphysically small values of R_H[47,48] as will be again demonstrated for the present mixture.

The NMR relaxation dispersion data may also be displayed in the generalized susceptibility representation. Consequently, one can re-write the BPP equation:[43,60]

$$\omega R_{1,i}(\omega) = K_i[\chi_{0i}''(\omega) + 2\chi_{0i}''(\omega)] \equiv \chi_i''(\omega) \qquad (13)$$

where K_i denotes the coupling constant K_{intra}, K_{inter} or $K_{NMR} = K_{total}$. The normalized susceptibility $\chi_i''(\omega)$ is only slightly broader than $\chi_{0i}''(\omega)$, yet shifted by a factor of about 0.6.

In liquids with their cooperative dynamics, frequency-temperature superposition (FTS) applies at least at high temperatures,[3,6,61] i.e., the (normalised) dynamic susceptibility can be expressed by an temperature independent function $\chi_{NMR}''(\omega) = \chi_{NMR}''(\omega\tau)$ of a temperature dependent argument $\omega\tau$, where τ is some characteristic time constant, for instance $\tau_{rot} = \tau_2$.

So far, we discussed translation in pure liquids. In binary mixtures as studied here (where both components carry protons) the relaxation rate $R_1(\omega)$ is sensitive to motions of both components. Still eqn (10) remains valid, however, an effective diffusion coefficient $\tilde{D}_{trans}$ is measured. Specifically,

$$R_1(\omega) = R_1(0) - \frac{\pi}{30}(1 + 4\sqrt{2})\left(\frac{\mu_0}{4\pi}\gamma_H^2\right)^2 \frac{n}{\tilde{D}_{trans}^{3/2}}\sqrt{\omega} + \cdots \qquad (14)$$

with

$$\tilde{D}_{trans} = \left(\frac{\phi_a^2}{D_a^{3/2}} + \frac{2\phi_a\phi_b}{\left(\frac{D_a + D_b}{2}\right)^{3/2}} + \frac{\phi_b^2}{D_b^{3/2}}\right)^{-2/3} \qquad (15)$$

Here $\phi_{a/b} = \frac{N_{a/b}}{N_a + N_b}$ are the fractions of the spin numbers of the component and $N_{a/b}$ the numbers of protons of the

This journal is © the Owner Societies 2020

Phys. Chem. Chem. Phys., 2020, 00, 1–15 | 3

component a/b, and $D_{a/b}$ are the diffusion coefficients of the individual components a and b. For $\phi_b = 0$, eqn (10) is revealed. Unless an assumption is made (for example: immobile component $D_a = 0$ or $D_a = D_b$), no direct access to the diffusion coefficients is possible. The spin density can be linearly interpolated from those of the neat components, n_a and n_b, respectively; explicitly, $n = x_a n_a + (1 - x_a) n_b$, where x_a and x_b are the corresponding mole fraction. The temperature dependence of $n(T)$ can be neglected.

Eqn (14) can be quickly derived. Consider a mixture of two type of spins "a" and "b" having same gyromagnetic ratio γ_H but belonging to different molecules with possibly different diffusion coefficients, D_a and D_b. Usually, in NMR relaxation experiments the Redfield limit is satisfied and the contribution to the relaxation rate is additive from each spin group. For sufficiently low frequencies and for normal diffusion, i.e., translation of the molecules can be described in terms of a time-independent self-diffusion coefficient, the relaxation rates of types "a" and "b" can be written as appears.

$$R_{1,a}(\omega) = R_{1,a}(0) - \frac{\pi}{30}\left(1 + 4\sqrt{2}\right)\left(\frac{\mu_0}{4\pi}\gamma_H^2\right)^2$$

$$\times \sqrt{\omega}\left[\frac{n_a}{\left(\frac{D_a + D_a}{2}\right)^{3/2}} + \frac{n_b}{\left(\frac{D_a + D_b}{2}\right)^{3/2}}\right] + \ldots \tag{16}$$

an analogue expression holds for $R_{1,b}(\omega)$. Here, n_a is the spin density of type "a" and n_b that of type "b". Note that for the intermolecular relaxation the relative motions of different molecules are of relevance. This is reflected by relative diffusion coefficients $D_a + D_a$, $D_b + D_b$ and $D_a + D_b$, respectively. The average relaxation rate is then given by the corresponding average $R_{1,a\nu}(\omega) = \phi_a R_{1a}(\omega) + \phi_b R_{1b}(\omega)$, from which eqn (15) follows.

3. Experimental details

Glycerol and DMSO with purity 99.9% were used as received from Sigma-Aldrich. Also the deuterated glycerol-h$_5$ as well as perdeuterated DMSO-d$_6$ were purchased from Sigma-Aldrich. The DMSO concentrations are specified in molar fractions x_{DMSO}. The following samples were investigated: x_{DMSO} = 0.10, 0.20, 0.30, 0.40, 0.50, 0.55, 0.60, 0.64, 0.70, 0.90, 1.0. The samples were prepared by weighting the calculated masses of the components using an analytical balance. Concentration error is estimated to be $\pm 0.2\%$. All samples were stored under dry nitrogen.

The complex dielectric permittivity spectra of the DMSO/glycerol mixtures were recorded for frequencies between 10^{-2} Hz and 10^7 Hz by means of a high resolution Alpha-A analyzer (Novocontrol Technologies). The solutions were filled into a gold-plating capacitor, which was attached to the measuring cell. Capacitor plates had a diameter of 20 mm and a distance of 50 µm. For temperature-dependent measurements from

170 K to 323 K, the sample was maintained into cryostat, which was cooled with liquid nitrogen. The temperature controller (Quatro-H, Novocontrol Technologies) allows to set a stability of 0.02 K. All measurements were done under cooling to avoid crystallization of the samples.

The dc conductivity was taken into account by subtracting its contribution from the total relaxation along $\varepsilon''(\omega) = \varepsilon_{tot}''(\omega) - \varepsilon_{cond}''(\omega) = \varepsilon_{tot}''(\omega) - \frac{\kappa}{\varepsilon_0 \omega}$, where κ is the specific conductivity and ε_0 is the permittivity of the empty space.

Field cycling ^{1}H NMR measurements were performed with a commercial relaxometer (STELAR Spinmaster FFC 2000). A ^{1}H frequency range from ν = 10 kHz to 30 MHz is covered. The switching time from high polarization field to relaxation field was about 3 ms. The spin–lattice relaxation was probed using a 90° rf-pulse with a pulse length of about 7.7 µs. The temperatures covered range from 223 K up to 313 K. Below room temperature a stream of evaporated nitrogen was used, above room temperature a stream of dry air heated using a VTC 90 (Stelar). We reached a temperature accuracy of about ± 1 K and a stability of about ± 0.5 K during a typical measurement, which took less than an hour.

4. Results

4.1 Dielectric relaxation

Fig. 1 presents the frequency dependences of the real $\varepsilon'(\omega)$ (a) and imaginary $\varepsilon''(\omega)$ part (b) of the complex dielectric spectra of a DMSO/glycerol mixture with a mole fraction x_{DMSO} = 0.50, measured at various temperatures, as an example. The spectra of the other mixtures within the concentration range 0.1 < x_{DMSO} < 0.6 show very similar spectral shapes (see below, Fig. 4). As said, the dc conductivity contribution was subtracted. The typical signature of the α-relaxation is observed: the relaxation peak shifts toward lower frequency upon decreasing temperature indicating molecular slowdown. The relaxation is broadened on the high-frequency flank. A simultaneous fit of $\varepsilon'(\omega)$ and $\varepsilon''(\omega)$ to a CD function (eqn (1)) yields a stretching parameter $\beta_{CD} = 0.60 \pm 0.04$. We note a weak systematic trend of β_{CD} ($0.54 \leq \beta_{CD} \leq 0.63$, see Fig. 12 in Appendix) is observed with temperature and concentration, yet, it can be ignored when $\varepsilon''(\omega)$ is plotted in a double-log plot (see also Fig. 4(a)). The corresponding time constant $\tau_\alpha(T)$ are displayed in Fig. 5 and discussed below together with the result from the other mixtures. The CD function does not cover the response at highest frequencies due to the occurrence of the excess wing which is a characteristic feature of the relaxation of viscous liquids.[1,6] As in neat glycerol, no secondary relaxation peak is observed in the mixtures.

Fig. 2 shows $\varepsilon''(\omega)$ measured at two temperatures of 215 K (a) and 200 K (b), and for different concentrations in the range 0 < x_{DMSO} < 0.7. Obviously, the position of the relaxation peak shifts toward higher frequencies with increasing DMSO content implying an acceleration of the dynamics, i.e., at first DMSO acts as a plasticizer. However, as seen from Fig. 2(a), at x_{DMSO} =

4 | Phys. Chem. Chem. Phys., 2020, 00, 1–15

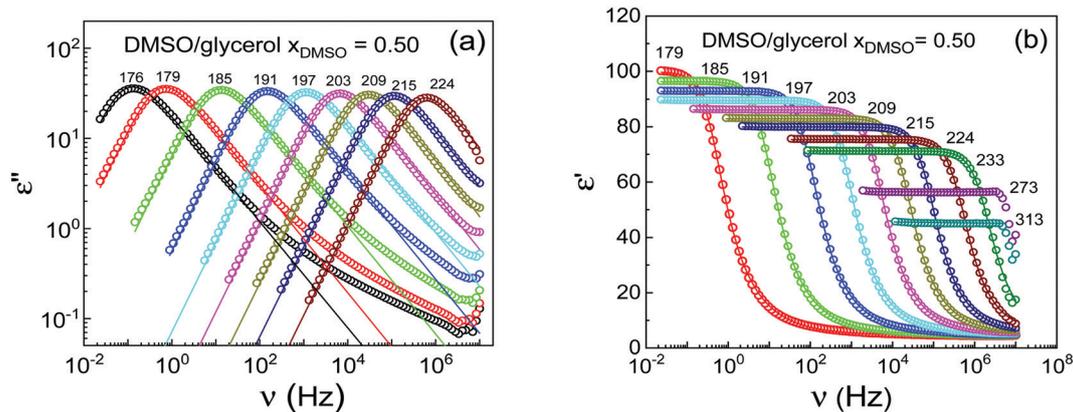This journal is © the Owner Societies 2020

Fig. 1 Frequency-dependent imaginary $\varepsilon''(\omega)$ (a) and real $\varepsilon'(\omega)$ (b) part of the dielectric permittivity of the mixture DMSO/glycerol with a mole fraction $x_{DMSO} = 0.50$ measured at various temperatures. Numbers indicate temperature in K. The dc conductivity is subtracted. Solid lines are fits using a Cole–Davidson function, eqn (1) with $\beta_{CD} = 0.60$.
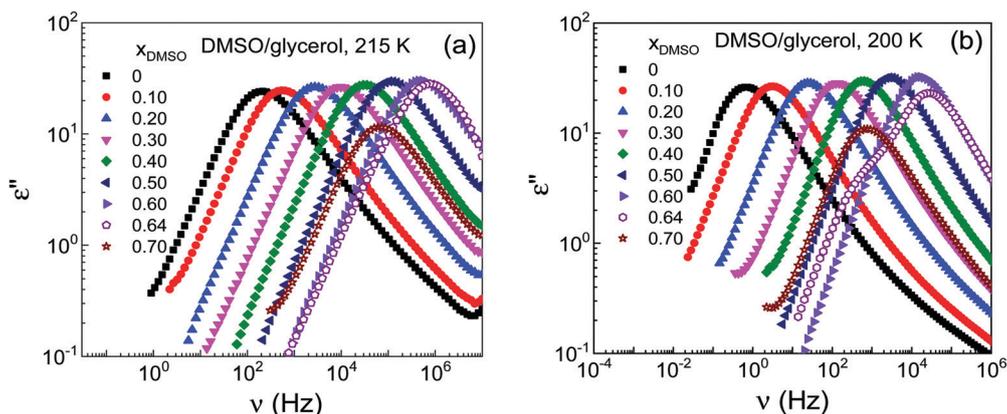

Fig. 2 (a) Comparison of the dielectric loss spectra of DMSO/glycerol mixtures at various concentrations ($0 < x_{DMSO} < 0.7$) measured at $T = 215$ K (a) and $T = 200$ K (b). Open symbols indicate data of phase separated systems.

0.70 the trend is reversed, *i.e.*, the relaxation shifts again to lower frequencies, and the signal significantly decreases. This is explained by the onset of partial crystallization ($T_m = 291$ K of neat DMSO) leading to the coexistence of a glycerol-rich liquid and a DMSO-rich crystalline phase. At $T = 200$ K (Fig. 2(b)) crystallization sets in already at $x_{DMSO} = 0.64$. At this
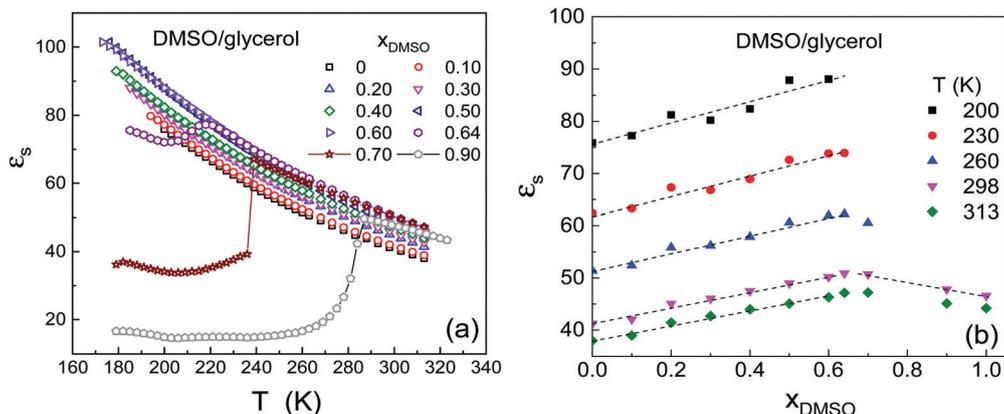
Fig. 3 (a) Temperature dependence of static dielectric constant ε_s of DMSO/glycerol mixtures at various concentrations. (b) Concentration dependences of ε_s of the mixtures at five temperatures.

This journal is © the Owner Societies 2020

Phys. Chem. Chem. Phys., 2020, **00**, 1–15 | **5**

concentration a bimodal spectrum is recognized, whereas at x_{DMSO} = 0.70 a mono-modal spectrum is found, yet, with lower amplitude and shifted again to lower frequencies.

The temperature dependence of the static dielectric constant ε_s, obtained from the analysis of the real part $\varepsilon'(\omega)$, provides another hint on the stability of the liquid mixtures. Note that ε_s can be determined up to room temperature although this is not possible for the spectrum $\varepsilon''(\omega)$ as the dynamics becomes too fast for the present instrument. As seen from Fig. 3(a), in the range of $0 < x_{DMSO} < 0.6$, ε_s increase monotonously with decreasing of temperature as expected by Curie's law. The mixtures can be super-cooled down to T_g. In the concentration range $0.64 < x_{DMSO} < 1$, one observes at some temperature a sharp drop in $\varepsilon_s(T)$ which indicates (partial) crystallization. This drop occurs at the higher temperature, the higher x_{DMSO} is. Therefore, this concentration range was excluded from the discussion below. Fig. 3(b) presents the concentration dependences of ε_s at five temperatures. Up to $x_{DMSO} \cong 0.6$, $\varepsilon_s(x_{DMSO})$ increases linearly whereas at larger x_{DMSO} it decreases again confirming the data reported by Angulo et al.,[36] whereas in ref. 35 the authors found a monotonous trend $\varepsilon_s(x_{DMSO})$. The maximum of $\varepsilon_s(x_{DMSO})$ can only be resolved at high temperatures due to crystallization at low temperature. We note that the here collected values ε_s of pure DMSO are somewhat smaller (by about 1–2%) than those reported in the literature.[30,33,62,63]

In order to compare the dielectric spectra of the mixtures measured at different temperatures and concentrations, we construct master curves by plotting of $\varepsilon''/\Delta\varepsilon$ versus the ν/ν_{max} (see Fig. 4(a)). Clearly, the spectral shape does not change in any way. Thus, mixing of the two liquids DMSO and glycerol leads to a change of the relaxation time, only. For comparison, in Fig. 4(b) we show the dielectric spectra for the mixture quinaldine/toluene, a mixture of non-associating liquids.[16] Clearly, the spectra significantly broaden with respect to the spectra of the neat components. There are even indications that the relaxation becomes bimodal and two time constants can be defined, a phenomenon which becomes even more pronounced when the T_g contrast of the components gets larger.[7,13–15]

One of the important parameters obtained from the analysis of the dielectric spectra is the relaxation time $\tau_{DS}(T) = \tau_{rot}(T)$. Fig. 5(a) reveals that $\tau_{rot}(T)$ of the DMSO/glycerol mixtures decreases with increasing DMSO content. This indicates an acceleration of dynamics, a plasticization effect, as said. The temperature dependency of the relaxation time of all investigated mixtures is well interpolated by a Vogel–Fulcher–Tammann (VFT) equation (solid line for glycerol). Clearly, the data for x_{DMSO} = 0.70 does not fit into the trend of the concentration dependence. As discussed, this is due to phase separation/crystallization. We anticipate that the time constants extracted from DS are well continued by those obtained from ^{1}H FC NMR relaxometry at higher temperatures (open symbols) except for a small offset of about a factor 3 hardly observable in a logarithmic plot (see below). We included the time constant of pure DMSO at ambient temperature obtained from ref. 62 and that at some lower temperature extrapolated from the linear behaviour of lg τ_{rot} vs. x_{DMSO} – see inset of Fig. 5(b). Regarding the correlation times at 298 K, similar values as in ref. 35 are found. Fig. 5(b) presents the time constant as a function of the reduced temperature T_g/T. A master curves is revealed up to highest temperatures. Clearly, the fragility index, $m = \left.\dfrac{\partial \log \tau}{\partial (T_g/T)}\right|_{T_g}$, of the mixtures does not alter, it is virtually the same as for pure glycerol.

The VFT fits are also taken to determine the glass transition temperatures $T_g(x_{DMSO})$ by applying the conventional definition $\tau_{rot}(T_g) = 100$ s – see Fig. 6. As expected, T_g decrease upon adding DMSO to glycerol. The data point at x_{DMSO} = 0.70 corresponds to a phase separated systems. Assuming that the volume fraction of the separated phases (liquid mixture and crystalline phase) does not change much with temperature one can estimate the concentration of the liquid phase in equilibrium with the crystalline phase. As indicated by the horizontal
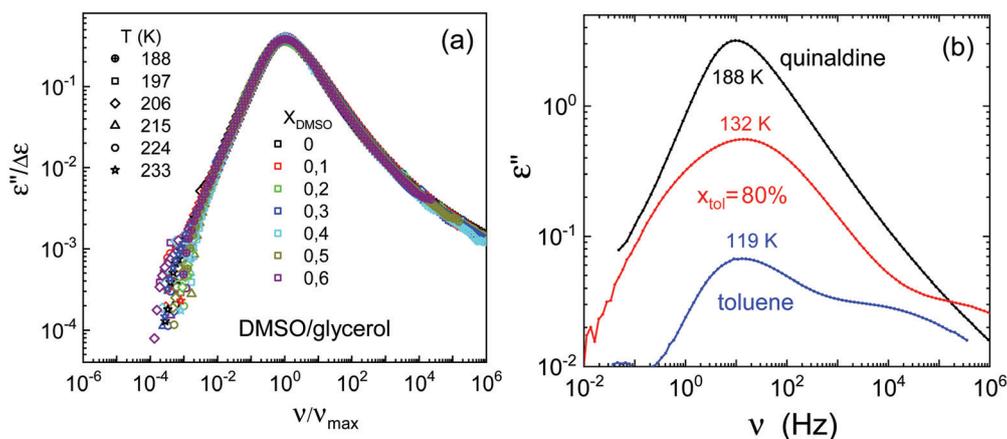

Fig. 4 (a) Normalized dielectric loss spectra $\varepsilon''/\Delta\varepsilon$ versus reduced frequency ν/ν_{max} for DMSO/glycerol mixtures at various concentrations ($0 \leq x_{DMSO} \leq$ 0.6) and temperatures ($188 \leq T \leq 233$ K). (b) Typical behaviour of dielectric spectra in a non-associated binary mixture: quinaldine (T_g = 180 K) mixed with toluene (T_g = 117 K).[16]
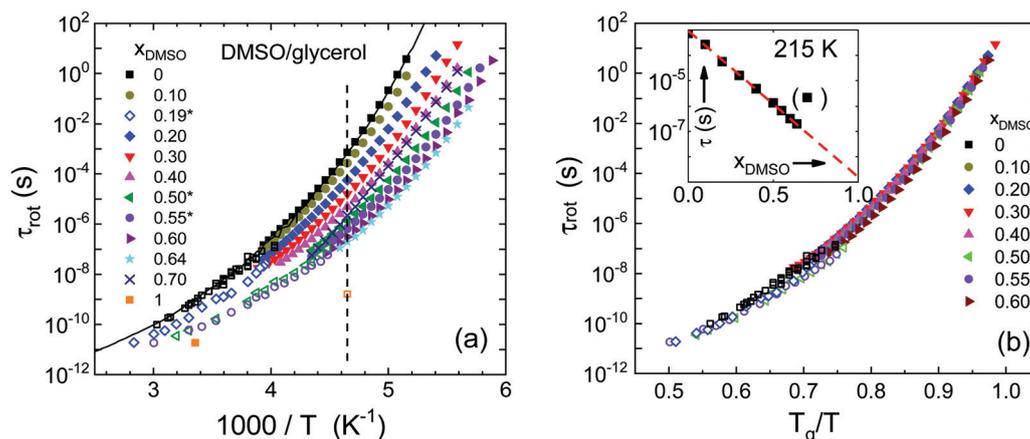
6 | Phys. Chem. Chem. Phys., 2020, 00, 1–15

This journal is © the Owner Societies 2020

Fig. 5 (a) Temperature dependences of the relaxation time τ_{rot} for DMSO/glycerol mixtures as obtained by dielectric spectroscopy (filled symbols) and by ^{1}H FC NMR relaxometry (open symbols, concentration entry marked by stars; for x_{DMSO} = 0.50 and x_{DMSO} = 1 colour indicates the same concentration) complemented by literature data for pure glycerol[64] and pure DMSO.[62] The time constants for x_{DMSO} = 0.70 (nominal; crosses) correspond to a phase separated systems. By extrapolation (along dashed line in (a), see also inset of (b)) one gets $\tau(x_{DMSO} \rightarrow 0)$ = 1.6 × 10^{-9} s (open square). (b) Time constant τ_{rot} as a function of the reduced temperature T_g/T. Inset shows the linearity of lg(τ_{DS}) with x_{DMSO}.
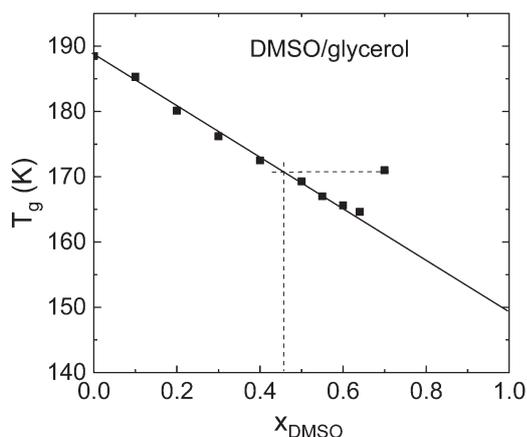
Fig. 6 Concentration dependence of the glass transition temperature $T_g(x_{DMSO})$ of the mixtures DMSO/glycerol. For the mixture x_{DMSO} = 0.70 (nominally) phase separation/crystallization occurs; dashed lines: estimate of the concentration of the DMSO-poor phase.

dotted line in Fig. 6, one finds $x_{DMSO} \cong 0.46$. Whereas T_g = 188.5 K of pure glycerol is close to the value reported in the literature,[1] that of pure DMSO is not directly accessible because the liquid cannot be significantly super-cooled below its melting point of T_m = 291 K. Anticipating a linear dependence, i.e., $T_g(x_{DMSO})$ = 188.5 − 39x_{DMSO}, we get by extrapolation T_g = 149.5 ± 1 K for pure DMSO. We note that deviations from linearity offer occur in associated liquids,[25,28] consequently, the present T_g value of DMSO remains preliminary, yet, the value well agrees with that is found in the literature (T_g = 150–151 K).[27,28] Concluding, the two components display a T_g contrast of 39 K, yet, the shape of the dielectric spectra in the mixtures do not show any broadening with respect to pure glycerol in contrast to the quinaldine (T_g = 180 K)[65]/toluene (T_g = 118 K)[1] mixtures.

4.2 Proton NMR relaxation

We turn to the results compiled by ^{1}H FC NMR relaxometry. Our experiments show exponential spin–lattice relaxation in the pure liquids as well as in the mixtures at all frequencies and temperatures. This allows to extract a well-defined relaxation rate $R_1 = 1/T_1$ as a function of the frequency $\nu = \omega/(2\pi)$. Fig. 7(a) displays $R_1(\nu)$ for DMSO/glycerol with x_{DMSO} = 0.50. About 3–4 decades are covered in frequency with a minimum frequency at 10 kHz and a maximum frequency at 30 MHz. The latter is somewhat higher than that of the present dielectric spectra (see Fig. 1). The lower the temperature and the higher the frequency, the stronger is the dispersion. This is the typical behaviour of a liquid in which the dynamics slows down. The data in the susceptibility representation $\chi_{NMR}''(\omega) = \omega/T_1$ are shown in Fig. 7(b). For several temperatures a relaxation maximum is recognized. As in the case of the dielectric spectra, the relaxation peak shifts to lower frequencies as temperature decreases. We note that the low-frequency flank of the relaxation maximum can be monitored down to rather low relative amplitudes since no parasitic dc conductivity interferes as is the case of the dielectric spectra.

Fig. 8(a) presents a direct comparison of an NMR and a dielectric spectrum of the x_{DMSO} = 0.50 mixture measured at the same temperature. The relaxation maximum occurs at similar frequencies; however, the spectral shape is different. The FC NMR spectrum exhibits a significant low-frequency broadening. This is obvious when attempting a fit with a CD function: The dielectric spectrum is well interpolated whereas inserting a CD function into the BPP equation (eqn (3)) does not reproduce the low-frequency flank. Restricting the CD fit to the high-frequency region provides a correlation time τ_{rot} = 3 × 10^{-8} s compared to τ_{rot} = 9 × 10^{-8} s by dielectric spectroscopy. This is exactly the ratio expected assuming rotational diffusion to occur. However, given the low precision of the temperature control and the strong temperature dependence of the time
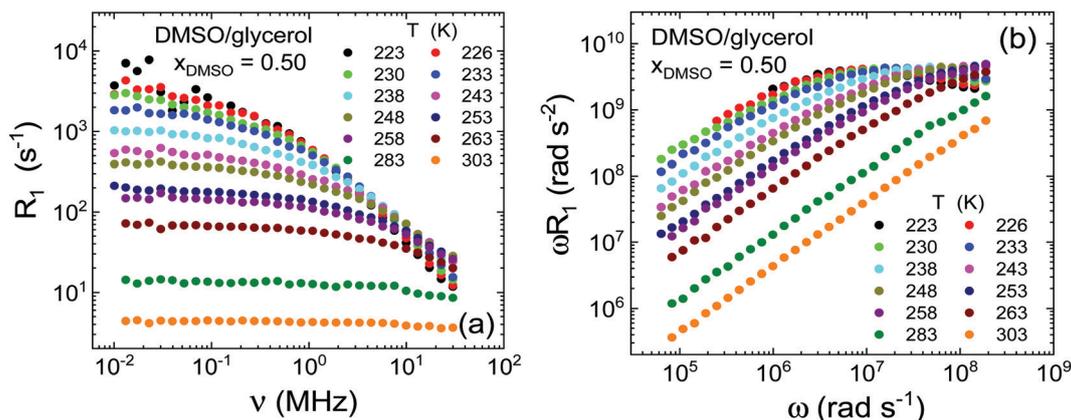
This journal is © the Owner Societies 2020

Phys. Chem. Chem. Phys., 2020, 00, 1–15 | 7

Fig. 7 (a) Frequency dependence of the spin–lattice relaxation rate R_1 of DMSO/glycerol mixtures with $x_{DMSO} = 0.50$ at different temperatures. (b) Relaxation data of (a) displayed in the susceptibility representation and plotted *vs.* angular frequency.
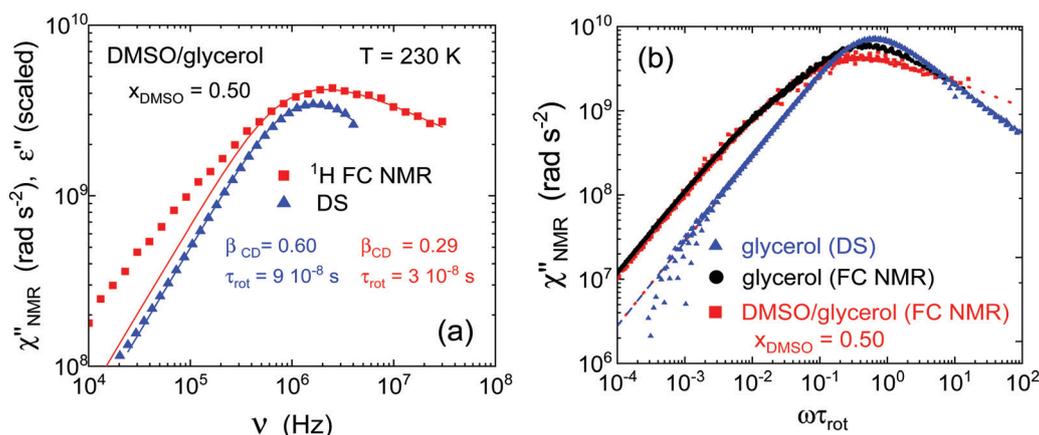

Fig. 8 (a) Dielectric and ^{1}H FC NMR relaxation spectrum of the mixture DMSO/glycerol with $x_{DMSO} = 0.50$ in the susceptibility representation; solid lines: Cole–Davidson (CD) fits with stretching parameter β_{CD} as indicated. (b) Susceptibility master curve (on absolute scale) of ^{1}H FC NMR data of the mixture (red circles) compared to that of pure glycerol (black squares) and to the DS master curve (blue diamonds, shifted by a factor 0.6 to lower frequencies); dashed red and blue line: CD fits.

constants this agreement may be incidental. We note that there is a long discussion in the literature attempting to explain the fact that this ratio is not observed in many cases.[66] Whatsoever, the difference found in the present study is merely recognizable when plotting correlation times of DS and NMR on logarithmic scales, as done in Fig. 5. We note that the high-frequency flank of the relaxation spectra is different between DS and NMR.

As demonstrated above in the case of the dielectric spectra (*cf.* Fig. 4), FTS applies well in the DMSO/glycerol mixtures, and this we expect to hold also for the FC NMR relaxation spectra. Thus, we plotted in Fig. 8(b) the quantity $\chi_{NMR}''(\omega\tau_{rot})$, which was obtained by shifting the individual FC profiles collected at the different temperatures solely along the frequency axis to get best overlap with the spectrum at some reference temperature. Then, a CD fit to the high-frequency part of the master curve (reflecting rotational dynamics) yields the time constant at the reference temperature and from the shift factors one finally gets $\tau_{rot}(T)$. Indeed, such master curve construction works well.

We added the FC master curve of pure glycerol,[67] and that from DS (the latter scaled in amplitude and horizontally shifted by a factor 0.6, see eqn (3)). Three observations are made. (i) The ^{1}H FC NMR master curves of DMSO/glycerol (red squares) as well as those of pure glycerol (black circles) are very similar on the low-frequency side ($\omega\tau_{rot} \ll 1$), but they are significantly broadened compared to the DS spectrum (blue triangles); a kind of shoulder is observed. (ii) On the high-frequency flank ($\omega\tau_{rot} \gg 1$), the spectrum of pure glycerol is less broad than that of the mixture. A CD fit yields $\beta_{CD} = 0.29$ for the mixture and $\beta_{CD} \cong 0.47$ for glycerol. (iii) The time constants obtained from constructing the NMR master curves are included in Fig. 5(a) (open symbols). They overlap with those from DS (filled symbols) in a small temperature interval and continue to significantly higher temperatures. As said, the small difference among the two methods is merely recognizable in a logarithmic plot. (iv) Clearly, the FC NMR curves cannot be described by a CD function, however, this is possible in the case

8 | *Phys. Chem. Chem. Phys.*, 2020, **00**, 1–15

This journal is © the Owner Societies 2020

of the dielectric spectrum, at least for the relaxation peak (solid line in Fig. 1).

The difference among the NMR and DS spectra at low frequencies is well understood:[44,46,51,55] Proton NMR relaxation is determined by both, rotational as well as translational dynamics. As described in Theoretical background, the low-frequency dispersion is dominated by intermolecular relaxation which mirrors translational dynamics, whereas the high-frequency relaxation reflects rotational dynamics. A measure of the time scale separation of translation and rotation is given by the "separation parameter" $r = \tau_{trans}/\tau_{rot}$ which can be specified by applying the FFHS model as will be demonstrated below. Since the FC NMR data in Fig. 8(b) agree on the low-frequency flank but not at high frequencies and show the same position of the relaxation peak, this suggests that the separation parameter r remains essentially the same when mixing glycerol with DMSO. Yet, the stretching of the rotational correlation function, i.e., the parameter β_{CD} determining the high-frequency part of the master curves, changes with respect to that of glycerol.

NMR offers another opportunity: it allows probing the dynamics component-selectively. We measured two mixtures ($x_{DMSO} = 0.19$ and $x_{DMSO} = 0.55$) of partially deuterated glycerol-h_5 with fully deuterated DMSO-d_6. We used glycerol-h_5 in analogy to our previous isotope dilution experiments of glycerol-h_5/glycerol-d_8.[51] This enables to monitor solely the dynamics of glycerol in the mixtures in contrast to the previous experiment which probes some average over the dynamics of both glycerol and DMSO. Two things are induced by such dilution experiments: first, the intermolecular interaction is reduced as the proton spin density goes down. Second, the time constant change as proven by the DS experiments. The corresponding two FC master curves together with that of pure glycerol-h_5 are displayed in Fig. 9(a). Whereas the rates close to the relaxation peak and its high-frequency flank decrease only minorly (due to a weak eccentricity effect), the low-frequency contribution strongly decreases along the dilution

of glycerol-h_5 with DMSO-d_6 – as expected due to the reduced intermolecular coupling. One expects a completely vanished low-frequency shoulder when reaching $x_{DMSO} = 1.0$ as was reported for glycerol-h_5 in perdeuterated glycerol for which a systematic isotope dilution experiment was carried out.[51] The rotational (high-frequency) relaxation contribution of all three samples can be fitted by a CD function with an average stretching parameter $\beta_{CD} = 0.47 \pm 0.02$, which is significantly higher than $\beta_{CD} = 0.29$ observed for the fully protonated mixture with $x_{DMSO} = 0.50$. The corresponding time constants $\tau_{rot}(T)$ obtained from constructing the master curves are included in Fig. 4(a). The time constants for the mixture DMSO-d_6/glycerol-h_5 and those of DMSO/glycerol (fully protonated) at $x_{DMSO} = 0.55$ and $x_{DMSO} = 0.50$, respectively, agree indicating that both components display the same dynamics, i.e., essentially no decoupling of the dynamics is found as already suggested by dielectric spectra not broadening upon mixing (cf. Fig. 4(a)).

In order to allow a coherent description of all the FC NMR master curves we applied a further scaling procedure which transforms the CD spectral shape of the rotational relaxation contribution at high frequencies into a Debye shape,[44,67] i.e., one applies a factor $f(\omega\tau_\alpha, \beta_\alpha)$ defined as:

$$f(\omega\tau_{rot}, \beta_{CD}) = \frac{\chi_D''(\omega\tau_{rot})}{\chi_{CD}''(\omega\tau_{rot}, \beta_{CD})} \tag{17}$$

Here, $\chi_{CD}''(\omega\tau_{rot}, \beta_{CD})$ is a CD function obtained by fitting an individual NMR susceptibility master curve in the high-frequency regime ($\omega\tau_{rot} \gg 1$), and $\chi_D''(\omega\tau_{rot})$ a Lorentzian (Debye) spectrum. This eliminates the effect of a varying broadening of the high-frequency part of the spectra of the different liquids. In other word, we assume that the different broadening of the relaxation peak of the various liquids is only caused by different stretching of the rotational correlation function and, in the case of the fully protonated DMSO/glycerol mixture, not by a broadening due to somewhat different time constants of the two components. This interpretation is suggested by the
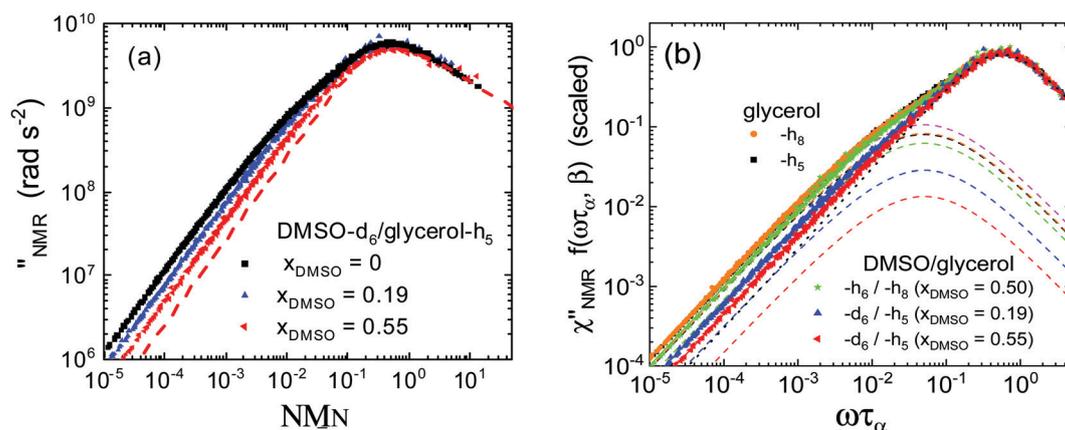

Fig. 9 (a) Susceptibility master curves for glycerol-h_5 and for the mixtures DMSO-d_6/glycerol-h_5 with $x_{DMSO} = 0.19$ and $x_{DMSO} = 0.55$. Relaxation peak and high-frequency flank are described by a CD function with $\beta_{CD} = 0.47 \pm 0.02$ (dashed line). (b) Susceptibility master curves of (a) scaled by a factor $f(\omega\tau_{NMR}, \beta_{CD})$ (cf. eqn (15)) transforming the high-frequency relaxation contribution into a Debye spectral shape. Solid line: fit by a sum of a Debye and a FFHS function (eqn (7)) with a common value $r = 58$, dashed line: FFHS contribution; dotted line: Debye function.

This journal is © the Owner Societies 2020

Phys. Chem. Chem. Phys., 2020, 00, 1–15 | 9

single peak structure of the dielectric spectrum and the extracted time constant of DS and NMR all agree. The such rescaled master curves are shown in Fig. 9(b) for the liquids considered here. In this representation of the data the only difference among the master curves is found at low-frequencies due to different relative intermolecular relaxation contributions mediated by translational diffusion.

In order to quantitatively describe the FC NMR master curves in Fig. 9(b), we take recourse to eqn (9) and describe the rotational relaxation $R_{1,rot}(\omega)$, by a Debye function and $R_{1,trans}(\omega)$ by the FFHS model (eqn (7)), respectively, entering the BPP equation. Three parameters are optimised: the amplitudes of the FFHS and the rotational contributions and the r value. We ignored the weak heteronuclear proton/deuteron relaxation. A satisfying interpolation is achieved (see Fig. 9(b)), which yields the separation parameter $r = \tau_{trans}/\tau_{rot}$ and the effective rotational and translational coupling constants. A free fit yields $r = 58 \pm 5$; a fit with a common value $r = 58$ for all curves works as well. Thus we conclude that the separation parameter in all the investigated liquids does not change – and a value $r = 58$ is much larger than expected in the SED model ($r_{SED} = 9$).[59] We come back to this point in the Discussion.

Independent of analyzing the FC NMR data in terms of master curves which yield an r value, the low-frequency dispersion of the individual relaxation spectra measured at a given temperature allows to extract the diffusion coefficient D_{trans} along eqn (10). This was demonstrated for several pure liquids in comparison with the results from field gradient NMR;[44,55] the latter technique is well-established for measuring the self-diffusion in liquids. As discussed in Theoretical background, in the mixtures eqn (10) still applies, however, one probes a kind of effective diffusion coefficient $\tilde{D}_{trans}$ given by eqn (15). In Fig. 10(a) the relaxation rate of the mixture DMSO/glycerol ($x_{DMSO} = 0.50$) is plotted vs. the square root of the frequency. From the limiting slope at low frequencies together with the

spin density n the diffusion coefficient $\tilde{D}_{trans}$ is extracted and displayed as a function of temperature in Fig. 10(b). We also included the results for pure glycerol[51] and pure DMSO (taken from ref. 70) as well as the results for the two mixtures DMSO-d_6/glycerol-h_5: in the latter case, as only one protonated species is present, $D_{trans} = D_{glyc}$ values of the glycerol molecule are obtained. As in the case of $\lg[\tau_{rot}(x_{DMSO})]$ (cf. Fig. 5(b)), a linear change of $\lg D_{trans}$ with x_{DMSO} is revealed, and the value $\tilde{D}_{trans}(x_{DMSO} = 0.50)$ essentially agrees with $D_{glyc}(x_{DMSO} = 0.55)$ (see inset of Fig. 10(b)). This, together with the fact that a common r value suffices to describe all the master curves (Fig. 9(b)), we take as a strong hint that $D_{glyc} \cong D_{DMSO}$ in the mixtures. Accordingly, $\lg[D_{glyc(x_{DMSO})}]$ follows that of the viscosity $\lg[\eta(x_{DMSO})]$ (see inset of Fig. 10(b); viscosity data taken from ref. 36).

Given the diffusion coefficients from the preceding analysis and the rotational correlation times from the construction of the FC master curves, one can determine the ratio D_{trans}/D_{rot}. Thereby the effective hydrodynamic radius R_H along eqn (11) is obtained. In Fig. 11 the ratio is found to be very similar for all systems investigated; moreover, it is independent of temperature. This is consistent with the result from the FC master curves which a temperature independent parameter $r = \tau_{trans}/\tau_{rot}$. We included data of pure DMSO taken from the literature,[70] which yields a ratio significantly above those of the mixtures. For comparison, we added the FC NMR results for propylene glycol and o-terphenyl.[47] The corresponding R_H values are listed in Table 1 and compared to the van der Waals radii R_{vdW} found in the literature.[71] As reported in our previous study[47] as well as in the work by Chang and Sillescu,[57] the value R_H of glycerol is significantly lower than the van der Waals radius R_{vdW}; unphysically low values around 1.0 Angstrom are found (see Table 1). Physically more reasonable values are found for DMSO and o-terphenyl, still, the radii are by about a factor 2 too small.
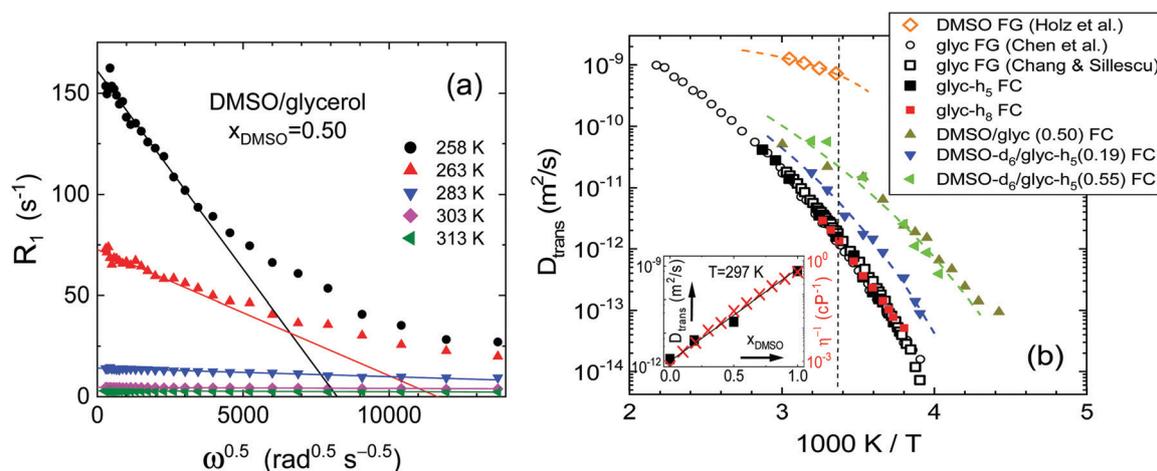

Fig. 10 (a) Spin–lattice relaxation rate versus square root of the frequency for DMSO/glycerol mixture with $x_{DMSO} = 0.50$ at different temperatures. The diffusion coefficient $\tilde{D}_{trans}$ is extracted along eqn (14) from a linearly extrapolation at small frequencies (straight lines). (b) Diffusion coefficient D_{glyc} for $x_{DMSO} = 0.19$ and 0.55, and $\tilde{D}_{trans}$ for $x_{DMSO} = 0.50$ as measured by ^{1}H FC NMR; we added $D_{trans}(T)$ of pure glycerol (-h_8 and -h_5) obtained by FC NMR (filled symbols)[68] as well as by FG NMR (open symbols),[56,69] and of pure DMSO obtained from FG NMR (open diamonds).[70] Inset: Diffusion coefficient and viscosity (taken from ref. 36) as a function of x_{DMSO} at room temperature.
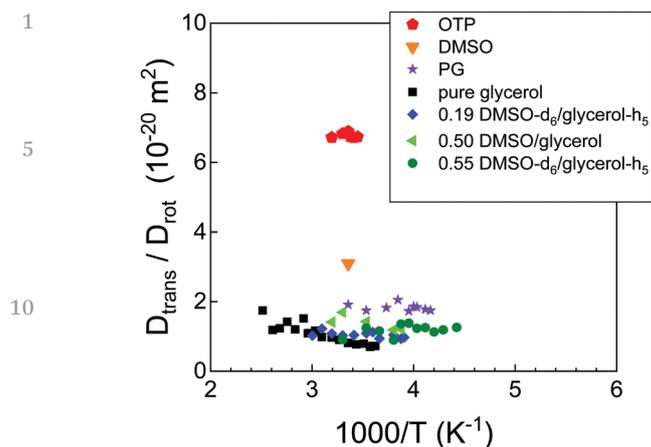
10 | Phys. Chem. Chem. Phys., 2020, **00**, 1–15

This journal is © the Owner Societies 2020

Fig. 11 Ratio D_{trans}/D_{rot} in pure DMSO,[62,70] pure glycerol,[47] and its mixtures (present work). For comparison, we added data of propylene glycol (PG)[47] and of o-terphenyl (OTP).[47]

5. Discussion

For the mixtures DMSO/glycerol in the concentration range $0 \leq x_{DMSO} \leq 0.64$, we find that the two components, glycerol and DMSO, virtually show the same rotational time constant as well as the same diffusion coefficient in the mixtures. This is in contrast to the situation for the non-associated binary liquid quinaldine/toluene, for example, for which the components display rather different transport coefficients. The difference of the T_g values of DMSO and glycerol is about 40 K, whereas that of quinaldine and toluene is 60 K, thus is rather similar. The logarithm of both, rotational time and diffusion coefficient display a linear concentration dependence as does the viscosity.[36] Also $T_g(x_{DMSO})$ is a linear function in the investigated concentration range which allows to determine T_g of pure DMSO *via* extrapolation. A value $T_g = 149.5 \pm 1$ K is obtained in excellent agreement with literature data. Fragility does not change, *i.e.*, the corresponding plot $\tau_{rot}(T_g/T)$ shows a unique trace. Regarding the concentration range for which the dynamics was accessible by DS and FC NMR ($x_{DMSO} \leq 0.64$), the static susceptibility ε_s increases linearly with x_{DMSO}, however, at $x_{DMSO} > 0.6$ it drops again. As phase separation occurs at such concentrations (and low temperatures) our experiments are unable to decide whether the linearity in the transport coefficients prevails in the high-concentration range. We note that deviations from linearity leading to excess parameters (*e.g.*, excess permittivity, excess relaxation time) were observed for DMSO–water and DMSO–alcohol mixtures over the entire concentration range at

ambient temperatures.[33–35,62,63,72,73] The non-linear dielectric behavior of these mixtures was explained by the formation of intermolecular hydrogen bonds between DMSO and water, or DMSO and alcohols. A maximum of the dielectric constant at 293 K for DMSO/glycerol[36] and DMSO/ethylene glycol[73] mixtures was found at $x_{DMSO} \cong 0.7$. The hydrogen bonding ability of the S–O bond can result in the formation of DMSO/alcohol various hetero-associates: dimers, multimers.[35,36,63,73]

Regarding the rotational part of the FC NMR susceptibility, the stretching parameter β_{CD} of glycerol-h_5 in deuterated DMSO is virtually the same as that of pure glycerol. In contrast, β_{CD} becomes smaller for the fully protonated system DMSO/glycerol whereas the time constants essentially agree with those from DS. In this case FC NMR probes some average over the dynamics of both components which yields an enhanced stretching. Thus, the broadening of the rotational FC NMR spectrum cannot be explained by some decoupling of the component's rotational dynamics.

In the case of glycerol as well as for its homologues like propylene glycol, xylitol, threitol, and sorbitol[67] the separation parameter is found to be rather large ($r \cong 60–80$)[44] which goes along with a low ratio D_{trans}/D_{rot} indicating a strong failure of the SED relation ($r_{SED} = 9$). This leads to unphysically small hydrodynamic radii, a phenomenon well known for glycerol in the literature.[57] A similarly high value $r = 58$ is also found for the DMSO/glycerol mixtures. In accordance with previous works,[46–48] we suggest that the large separation of rotational and translational dynamics originates from the 3d hydrogen bond network of glycerol which apparently is not destroyed by adding DMSO. For example, destroying the network by adding a solvent not capable of hydrogen bonding leads to a decrease of the r value as was demonstrated for propylene glycol diluted with chloroform.[47] At a threshold concentration of $x_{PG} \cong 0.5$ the r value becomes close to the value reported for the non-associated liquid o-terphenyl ($r \cong 10$). Actually, it was the finding of a large r value in glycerol and its homologues, which allowed to fully understand ^{1}H FC NMR relaxation spectrum in (viscous) liquids. In the case of a non-associating liquid like o-terphenyl r values close to $r_{SED} = 9$ are reported and it is difficult to determine r unambiguously.[47,52] In passing we note that the r value may become large in plastically crystalline solids like cyano adamantane.[74] In this case the translational dynamics is controlled by vacancy diffusion and one does not expect a coupling of both types of motions as in the case of liquids.

We emphasize that usually the ratio D_{trans}/D_{rot} is difficult to determine with high precision as different techniques have to

Table 1 Rotational time constant τ_{rot}, translational diffusion coefficient D_{trans}, separation parameter $r = \tau_{trans}/\tau_{rot}$, ratio of translational over rotational diffusion coefficient D_{trans}/D_{rot}, experimental hydrodynamic radius R_{exp}, and van der Waals radius R_{vdW}

Sample	τ_{rot} (ps)	D_{trans} (10^{-9} m^2 s^{-1})	r	D_{trans}/D_{rot} (Å^2)	R_{exp} (Å)	R_{vdW}[71] (Å)
Glycerol			58	1.1	0.91 (FC)[47]/0.8[56]	2.7
DMSO/glycerol $x_{DMSO} = 0.50$			58	1.4	1.02 (FC)	2.7/2.5
DMSO-d$_6$/glycerol-h$_5$ $x_{DMSO} = 0.19$			58	1.0	0.87 (FC)	2.7/2.5
DMSO-d$_6$/glycerol-h$_5$ $x_{DMSO} = 0.55$			58	1.2	0.95 (FC)	2.7/2.5
DMSO	$\tau_1 = 21.1$ (298 K)[62]	0.73 (298 K)[70]		3.1	1.52	2.5
PG			35	1.8 (FC)[47]	1.16[47]	2.6
OTP			10	5.9 (FC)[47]	2.1 (FC)[47]/2.3[56]	3.7

be applied. In the case of the ^{1}H FC NMR relaxometry one can directly access D_{trans}/D_{rot} in a single experiment. Yet, given the still narrow frequency range of the commercial FFC 2000 relaxometer, both values cannot be determined at the same temperature and one has to take recourse to the master curve construction. However, with recent instrumental progress the frequency range is extended,[39,40] which in future may allow to determine D_{trans} and D_{rot} at the same temperature. As the FC techniques currently stops at some ten MHz, the r value can only be determined for viscous liquids, so far.

Recently, Angulo *et al.* reported density, dielectric constant, viscosity and diffusion coefficient for DMSO/glycerol around ambient temperatures.[36] The logarithm of the viscosity was found to essentially display a linear behaviour with x_{DMSO}, a behaviour also observed for $D(x_{DMSO})$ and $\tau_{rot}(x_{DMSO})$ in the present contribution, as said. The D_{trans} values reported by the authors are close to those revealed by ^{1}H FC NMR relaxometry. The authors also tested the Stokes–Einstein (SE) relation by plotting double logarithmically D_{exp} *vs.* D_{SE}, the latter calculated from the van der Waals volume and the measured viscosity. Including data of a variety of organics liquids, D_{exp} and D_{SE} were found to agree within significant scatter produced by including data of many liquids. They concluded "there are no deviations from the continuum solvent picture in these mixtures." While we go fully conform with this statement, the subtle features regarding the unphysically low hydrodynamic radii (discussed above) are not resolved when plotting the diffusion data on a double logarithmic scale. As suggested by Angulo *et al.* and by the present study, the absence of different "micro-environments" in DMSO/glycerol mixtures, a notion for some kind of preferential solvation or some decoupling of the component dynamics, is at variance with the conclusions drawn by Ghosh and co-workers studying the solvation dynamics of coumarin dyes,[34] who speak about "inhomogeneity" of the DMSO/glycerol mixture and the "presence of micro-domains."

The situation in DMSO/glycerol is different from that in the mixture water/glycerol for which the shape of the dielectric spectra changes as a function of x and temperature.[75] In other words, water appears to change the hydrogen bond network of glycerol in contrast to DMSO. As mentioned in the Introduction, a recent rheological study demonstrated that in addition to the main relaxation a weak relaxation feature at low frequencies is found similar to what is observed in mono-alcohols.[25] Adding water, the feature disappears abruptly at equimolar composition. The authors argued that the water softens the glycerol–glycerol hydrogen-bonded network.

6. Conclusion

Mixtures of glycerol with DMSO are studied by dielectric spectroscopy (DS) in the frequency range 10^{-2}–10^7 Hz and by ^{1}H field-cycling (FC) NMR relaxometry down to glass-forming temperatures. The dynamics of the components is monitored in the concentration range $x_{DMSO} < 0.64$; higher concentrations cannot be covered because of phase separation. The FC technique

provides the frequency dependence of the spin–lattice relaxation rate which is transformed to the susceptibility representation and allows comparing NMR and DS results. Rotational time constants $\tau_{rot}(T)$ probed by the two techniques complement each, a range 10^{-11} s $< \tau_{rot} <$ 10 s is covered. The glass transition temperature $T_g(x_{DMSO})$ is determined, yielding $T_g =$ 149.5 $\pm$ 1 K of pure DMSO by extrapolation. The DS spectra do not change with x_{DMSO} and T, only the relaxation times become shorter. The FC NMR relaxation spectra of glycerol in solution with DMSO or DMSO-d$_6$ display a bimodal structure with a high-frequency part reflecting rotational and a low-frequency part reflecting translational dynamics. Regarding the rotational contribution in the glycerol/DMSO-d$_6$ mixtures, again no spectral change with x_{DMSO} and T is observed. Analysing the low-frequency FC NMR spectra allows to determine the diffusion coefficient D_{trans}. Its logarithm shows a linear x_{DMSO}-dependence as does lg τ_{rot}. The ratio D_{trans}/D_{rot} is independent of x_{DMSO} and displays an anomalously low value indicating large separation of molecular translation and rotation. The corresponding unphysically small hydrodynamic radius indicates strong failure of Stokes–Einstein–Debye relation. Such anomaly is taken as characteristic of a 3d hydrogen bond network.

Regarding the concentration range accessed ($x_{DMSO} < 0.64$), we conclude that the dynamics of the components does not decouple in contrast to the case of the non-associated binary liquid. The system behaves like an ideal mixture. As DMSO is an aprotic liquid, which allows to form hydrogen bonds *via* the S–O group, the molecule appears to be continuously incorporated in the hydrogen network of glycerol.

Conflicts of interest

There are no conflicts to declare.

Appendix

Fig. 12 displays the temperature and concentration dependence of the stretching parameter β_{CD} of the mixture DMSO/glycerol.
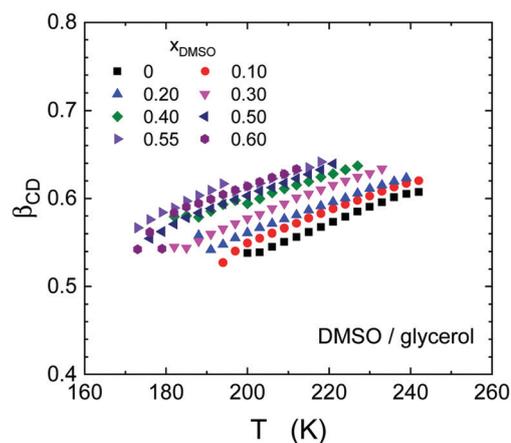

Fig. 12 Stretching parameter β_{CD} of DMSO/glycerol mixtures for different concentrations as a function of temperature.

12 | *Phys. Chem. Chem. Phys.*, 2020, **00**, 1–15

This journal is © the Owner Societies 2020

Acknowledgements

References

1 A. Kudlik, S. Benkhof, T. Blochowicz, C. Tschirwitz and E. Rössler, The dielectric response of simple organic glass formers, *J. Mol. Struct.*, 1999, **479**, 201–218.

2 P. Lunkenheimer, U. Schneider, R. Brand and A. Loidl, Glassy dynamics, *Contemp. Phys.*, 2000, **41**, 15–36.

3 A. Tölle, Neutron scattering studies of the model glass former ortho-terphenyl, *Rep. Prog. Phys.*, 2001, **64**, 1473–1532.

4 G. Floudas, M. Paluch, A. Grzybowski and K. L. Ngai, *Molecular Dynamics of Glass-forming Systems*, Springer, Berlin, Germany, 2011.

5 *Structural Glasses and Supercooled Liquids*, ed. P. G. Wolynes and V. Lubchenko, Wiley, Hoboken, New Jersey, 2012.

6 N. Petzold, B. Schmidtke, R. Kahlau, D. Bock, R. Meier, B. Micko, D. Kruk and E. A. Rössler, Evolution of the dynamic susceptibility in molecular glass formers: results from light scattering, dielectric spectroscopy, and NMR, *J. Chem. Phys.*, 2013, **138**, 12A510.

7 B. Pötzschner, F. Mohamed, C. Bächer, E. Wagner, A. Lichtinger, R. Minikejew, K. Kreger, H. W. Schmidt and E. A. Rössler, Non-polymeric asymmetric binary glass-formers. I. Main relaxations studied by dielectric, ^{2}H NMR, and ^{31}P NMR spectroscopy, *J. Chem. Phys.*, 2017, **146**, 164503.

8 D. Bock, T. Körber, F. Mohamed, B. Pötzschner and E. A. Rössler, Dynamic heterogeneities in binary glass-forming systems, in *The Scaling of Relaxation Processes*, Springer, Cham, 2018, pp. 173–201.

9 A. J. Moreno and J. Colmenero, Relaxation scenarios in a mixture of large and small spheres: dependence on the size disparity, *J. Chem. Phys.*, 2006, **125**, 164507.

10 D. Cangialosi, A. Alegría and J. Colmenero, Dielectric relaxation of polychlorinated biphenyl/toluene mixtures: component dynamics, *J. Chem. Phys.*, 2008, **128**, 224508.

11 S. Capaccioli, K. Kessairi, M. S. Thayyil, D. Prevosto and M. Lucchesi, The Johari–Goldstein β-relaxation of glass-forming binary mixtures, *J. Non-Cryst. Solids*, 2011, **357**, 251–257.

12 B. Micko, C. Tschirwitz and E. A. Rössler, Secondary relaxation processes in binary glass formers: emergence of "islands of rigidity", *J. Chem. Phys.*, 2013, **138**, 154501.

13 T. Blochowicz, S. Schramm, M. Lusceac, B. Vogel, B. Stühn, P. Gutfreund and B. Frick, Signature of a Type-A glass transition and intrinsic confinement effects in a binary glass forming system, *Phys. Rev. Lett.*, 2012, **109**, 035702.

14 S. Valenti, S. Capaccioli and K. L. Ngai, Contrasting two different interpretations of the dynamics in binary glass forming mixtures, *J. Chem. Phys.*, 2018, **148**, 054504.

15 B. Pötzschner, F. Mohamed, C. Bächer, E. Wagner, A. Lichtinger, R. Minikejew, K. Kreger, H.-W. Schmidt and E. A. Rössler, Non-polymeric asymmetric binary glass-formers. I. Main relaxations studied by dielectric, 2H NMR, and ^{31}P NMR spectroscopy, *J. Chem. Phys.*, 2017, **146**, 164503.

16 Th. Körber, R. Minikejew, B. Pötzschner, D. Bock and E. A. Rössler, Dynamically asymmetric binary glass-formers studied by dielectric and NMR spectroscopy, *Eur. Phys. J. E: Soft Matter Biol. Phys.*, 2019, **42**, 143.

17 M. Scandola, G. Ceccorulli and M. Pizzoli, Composition dependence of the glass transition of polymer-diluent mixtures: 2. Two concomitant glass transition processes as a general feature of plasticized polymers, *Polymer*, 1987, **28**, 2081–2084.

18 M. Nakazawa, O. Urakawa and K. Adachi, Effect of local heterogeneity on dielectric relaxation spectra in concentrated solutions of poly(vinyl acetate) and poly(vinyl octanoate), *Macromolecules*, 2000, **33**, 7898–7904.

19 D. Cangialosi, A. Alegría and J. Colmenero, "Self-concentration" effects on the dynamics of a polychlorinated biphenyl diluted in 1,4-polybutadiene, *J. Chem. Phys.*, 2007, **126**, 204904.

20 D. Bingemann, N. Wirth, J. Gmeiner and E. A. Rössler, Decoupled dynamics and quasi-logarithmic relaxation in the polymer–plasticizer system poly(methyl methacrylate)/tri-m-cresyl phosphate studied with 2D NMR, *Macromolecules*, 2007, **40**, 5379–5388.

21 G. Goracci, A. Arbe, A. Alegria, Y. Su, U. Gasser and J. Colmenero, Structure and component dynamics in binary mixtures of poly(2-(dimethylamino) ethyl methacrylate) with water and tetrahydrofuran: a diffraction, calorimetric, and dielectric spectroscopy study, *J. Chem. Phys.*, 2016, **144**, 154903.

22 D. Bock, R. Kahlau, B. Pötzschner, T. Körber, E. Wagner and E. A. Rössler, Dynamics of asymmetric binary glass formers. II. Results from nuclear magnetic resonance spectroscopy, *J. Chem. Phys.*, 2014, **140**, 094505.

23 C. Gainaru, R. Meier, S. Schildmann, C. Lederle, W. Hiller, E. A. Rössler and R. Böhmer, Nuclear-magnetic-resonance measurements reveal the origin of the Debye process in monohydroxy alcohols, *Phys. Rev. Lett.*, 2010, **105**, 258303.

24 C. Gainaru, R. Figuli, T. Hecksher, B. Jakobsen, J. C. Dyre, M. Wilhelm and R. Böhmer, Shear-modulus investigations of monohydroxy alcohols: evidence for a short-chain-polymer rheological response, *Phys. Rev. Lett.*, 2014, **112**, 098301.

25 M. H. Jensen, C. Gainaru, C. Alba-Simionesco, T. Hecksher and K. Niss, Slow rheological mode in glycerol and glycerol–water mixtures, *Phys. Chem. Chem. Phys.*, 2018, **20**, 1716–1723.

26 C. Gainaru, O. Lips, A. Troshagina, R. Kahlau, A. Brodin, F. Fujara and E. A. Rössler, On the nature of the high-

frequency relaxation in a molecular glass former: a joint study of glycerol by field cycling NMR, dielectric spectroscopy, and light scattering, *J. Chem. Phys.*, 2008, **128**, 174505.

27 E. J. Sare and C. A. Angell, Glass-forming composition regions and glass transition temperature in nonaqueous electrolyte solutions, *J. Solution Chem.*, 1973, **2**, 53–57.

28 S. S. N. Murthy, Some insight into the physical basis of the cryoprotective action of dimethyl sulfoxide and ethylene glycol, *Cryobiology*, 1998, **36**, 84–96.

29 T. Clark, J. S. Murray, P. Lane and P. Politzer, Why are dimethyl sulfoxide and dimethyl sulfone such good solvents?, *J. Mol. Model.*, 2008, **14**, 689–697.

30 L. S. Gabrielian and S. A. Markarian, Temperature dependence of the dielectric relaxation of liquid dimethyl- and diethylsulfoxides, *J. Mol. Liq.*, 2004, **112**, 137–140.

31 S. S. N. Murthy, Phase behavior of the supercooled aqueous solutions of dimethyl sulfoxide, ethylene glycol, and methanol as seen by dielectric spectroscopy, *J. Phys. Chem. B*, 1997, **101**, 6043–6049.

32 S. A. Lusceac, C. Gainaru, D. A. Ratzke, M. F. Graf and M. Vogel, Secondary water relaxation in a water/dimethyl sulfoxide mixture revealed by deuteron nuclear magnetic resonance and dielectric spectroscopy, *J. Phys. Chem. B*, 2011, **115**(40), 11588–11596.

33 Z. Lu, E. Manias, D. D. Macdonald and M. Lanagan, Dielectric relaxation in dimethyl sulfoxide/water mixtures studied by microwave dielectric relaxation spectroscopy, *J. Phys. Chem. A*, 2009, **113**(44), 12207–12214.

34 S. Koley, H. Kaur and S. Ghosh, Probe dependent anomalies in the solvation dynamics of coumarin dyes in dimethyl sulfoxide–glycerol binary solvent: confirming the local environments are different for coumarin dyes, *Phys. Chem. Chem. Phys.*, 2014, **16**, 22352–22363.

35 Q. Jie and J. Guo-Zhu, Dielectric constant of polyhydric alcohol–DMSO mixture solution at the microwave frequency, *J. Phys. Chem. A*, 2013, **117**, 12983–12989.

36 G. Angulo, M. Brucka, M. Gerecke, G. Grampp, D. Jeannerat, J. Milkiewicz, Y. Mitrev, C. Radzewicz, A. Rosspeintner, E. Vauthey and P. Wnuk, Characterization of dimethylsulfoxide/glycerol mixtures: a binary solvent system for the study of "friction-dependent" chemical reactivity, *Phys. Chem. Chem. Phys.*, 2016, **18**, 18460–18469.

37 C. J. F. Böttcher, *Theory of Dielectric Polarization, V.1*, Elsevier, Amsterdam, 1973.

38 Homepage STELAR, 2020.

39 F. Fujara, D. Kruk and A. F. Privalov, Solid state field-cycling NMR relaxometry: instrumental improvements and new applications, *Prog. Nucl. Magn. Reson. Spectrosc.*, 2014, **82**, 39–69.

40 B. Kresse, M. Becher, A. F. Privalov, M. Hofmann, E. A. Rössler, M. Vogel and F. Fujara, ^{1}H NMR at Larmor frequencies down to 3 Hz by means of Field-Cycling techniques, *J. Magn. Reson.*, 2017, **277**, 79–85.

41 *Field-cycling NMR relaxometry: Instrumentation, model theories, applications*, ed. R. Kimmich, RSC, London, 2019, pp. 1–41.

42 R. Kimmich and E. Anoardo, Progress in nuclear magnetic resonance spectroscopy, *Prog. Nucl. Magn. Reson. Spectrosc.*, 2004, **44**, 257–320.

43 D. Kruk, A. Herrmann and E. A. Rössler, Field-cycling NMR relaxometry of viscous liquids and polymers, *Prog. Nucl. Magn. Reson. Spectrosc.*, 2012, **63**, 33–64.

44 R. Meier, D. Kruk and E. A. Rössler, Intermolecular spin relaxation and translation diffusion in liquids and polymer melts: insight from field-cycling ^{1}H NMR relaxometry, *Chem. Phys. Chem.*, 2013, **14**, 3071–3081.

45 R. Kimmich and N. Fatkullin, Self-diffusion studies by intra- and inter-molecular spin-lattice relaxometry using field-cycling: liquids, plastic crystals, porous media, and polymer segments, *Prog. Nucl. Magn. Reson. Spectrosc.*, 2017, **101**, 18–50.

46 E. A. Rössler, M. Hofmann and F. Fatkullin, in *Field-cycling NMR relaxometry, Instrumentation, model theories, applications*, ed. R. Kimmich, RSC, London, 2019, pp. 181–206.

47 R. Meier, E. Schneider and E. A. Rössler, Change of translational-rotational coupling in liquids revealed by field-cycling ^{1}H NMR, *J. Chem. Phys.*, 2015, **142**, 034503.

48 M. Flämig, N. Fatkullin and E. A. Rössler, NMR Relaxometry: the canonical case of glycerol, *J. Phys. Chem.*, 2020, **124**, 1557–1570.

49 L. P. Hwang and J. H. Freed, Dynamic effects of pair correlation functions on spin relaxation by translational diffusion in liquids, *J. Chem. Phys.*, 1975, **63**, 4017–4025.

50 Y. Ayant, E. Belorizky, J. Aluzon and J. Gallice, Calcul des densités spectrales résultant d'un mouvement aléatoire de translation en relaxation par interaction dipolaire magnétique dans les liquids, *J. Phys.*, 1975, **36**, 991–1004.

51 R. Meier, D. Kruk, J. Gmeiner and E. A. Rössler, Intermolecular relaxation in glycerol as revealed by field cycling ^{1}H NMR relaxometry dilution experiments, *J. Chem. Phys.*, 2012, **136**, 034508.

52 R. Meier, D. Kruk, A. Bourdick, E. Schneider and E. A. Rössler, Inter- and intramolecular relaxation in molecular liquids by field cycling ^{1}H NMR relaxometry, *Appl. Magn. Reson.*, 2013, **44**, 153–168.

53 C. A. Sholl, Nuclear spin relaxation by translational diffusion in liquids and solids: high-and low-frequency limits, *J. Phys. C: Solid State Phys.*, 1981, **14**, 447.

54 J. F. Harmon and B. H. Muller, Nuclear spin relaxation by translational diffusion in liquid ethane, *Phys. Rev.*, 1969, **182**, 400.

55 D. Kruk, R. Meier and E. A. Roessler, Nuclear magnetic resonance relaxometry as a method of measuring translational diffusion coefficients in liquids, *Phys. Rev. E: Stat., Nonlinear, Soft Matter Phys.*, 2012, **85**, 020201.

56 J.-P. Hansen and I. R. McDonald, *Theory of simple liquids*, Academic Press, Amsterdam, 3rd edn, 2006.

57 I. Chang and H. Sillescu, Heterogeneity at the glass transition: translational and rotational self-diffusion, *J. Phys. Chem.*, 1997, **101**, 8794–8801.

58 J. Kowalewski and L. Mädler, *Nuclear spin relaxation in liquids: Theory, experiments, and applications*, Taylor & Francis, Boca Raton, 2006.

14 | *Phys. Chem. Chem. Phys.*, 2020, **00**, 1–15

This journal is © the Owner Societies 2020

59 A. Abragam, *The principles of nuclear magnetism*, Clarendon Press, Oxford, 1961.

60 S. Kariyo, C. Gainaru, H. Schick, A. Brodin, V. N. Novikov and E. A. Rössler, *Phys. Rev. Lett.*, 2006, **97**, 207803 Erratum: A. Herrmann, C. Gainaru, H. Schick, A. Brodin, V. N. Novikov and E. A. Rössler, *Phys. Rev. Lett.*, 2008, **100**, 109901.

61 M. Flämig, M. Hofmann and E. A. Rössler, Field-cycling NMR relaxometry: the benefit of constructing master curves, *Mol. Phys.*, 2019, **117**, 877.

62 U. Kaatze, R. Pottel and M. Schaefer, Dielectric spectrum of dimethyl sulfoxide/water mixtures as a function of composition, *J. Phys. Chem.*, 1989, **93**, 5623–5627.

63 P. W. Khirade, A. Chaudhari, J. B. Shinde, S. N. Helambe and S. C. Mehrotra, Static dielectric constant and relaxation time measurements on binary mixtures of dimethyl sulfoxide with ethanol, 2-ethoxyethanol, and propan-1-ol at 293, 303, 313, and 323 K, *J. Chem. Eng. Data*, 1999, **44**, 879–881.

64 B. Schmidtke, N. Petzold, R. Kahlau and E. A. Rössler, Reorientational dynamics in molecular liquids as revealed by dynamic light scattering: from boiling point to glass transition temperature, *J. Chem. Phys.*, 2013, **139**, 084504.

65 R. Kahlau, T. Gnutzmann, F. Emmerling, K. Rademann and E. A. Rössler, Quinaldine: accessing two crystalline polymorphs via the supercooled liquid, *J. Chem. Phys.*, 2012, **137**, 054505.

66 G. Diezemann, H. Sillescu, G. Hinze and R. Böhmer, Rotational correlation functions and apparently enhanced translational diffusion in a free-energy landscape model for the relaxation in glass-forming liquids, *Phys. Rev. E: Stat. Phys., Plasmas, Fluids, Relat. Interdiscip. Top.*, 1998, **57**, 4398–4410.

67 R. Meier, R. Kahlau, D. Kruk and E. A. Rössler, Comparative studies of the dynamics in viscous liquids by means of dielectric spectroscopy and field cycling NMR, *J. Phys. Chem. A*, 2010, **114**, 7847–7855.

68 D. Kruk, R. Meier and E. A. Rössler, Translational and rotational diffusion of glycerol by means of field cycling ^{1}H NMR relaxometry, *J. Phys. Chem. B*, 2011, **115**, 951–957.

69 B. Chen, E. E. Sigmund and W. P. Halperin, Stokes-Einstein relation in supercooled aqueous solutions of glycerol, *Phys. Rev. Lett.*, 2006, **96**, 145502.

70 M. Holz, S. R. Heil and A. Sacco, Temperature-dependent self-diffusion coefficients of water and six selected molecular liquids for calibration in accurate ^{1}H NMR PFG measurements, *Phys. Chem. Chem. Phys.*, 2000, **2**, 4740–4742.

71 J. T. Edward, Molecular volumes and the Stokes-Einstein equation, *J. Chem. Educ.*, 1970, **47**, 261.

72 L. S. Gabrielyan and S. A. Markaryan, Dielectric relaxation spectroscopy study of the structure and dynamics of dialkyl sulfoxide solutions, *Russ. J. Phys. Chem. A*, 2018, **92**, 205–213.

73 P. B. Undrea, P. W. Khirade, V. S. Rajenimbalkar, S. N. Helambe and S. C. Mehrotra, Dielectric relaxation in ethylene glycol-dimethyl sulfoxide mixtures as a function of composition and temperature, *J. Korean Chem. Soc.*, 2012, **56**, 416–423.

74 M. Flämig, N. Fatkullin and E. A. Rösssler, The dynamics of the plastically crystalline phase of cyano adamantane revisited by NMR line shape analysis and field-cycling relaxometry, *J. Chem. Phys.*, 2019, **151**, 224507.

75 Y. Hayashi, A. Puzenko, I. Balin, Y. E. Ryabov and Y. Feldman, Relaxation dynamics in glycerol–water mixtures. 2. Mesoscopic feature in water rich mixtures, *J. Phys. Chem. B*, 2005, **109**, 9174–9177.

This journal is © the Owner Societies 2020

Phys. Chem. Chem. Phys., 2020, **00**, 1–15 | **15**

Publication 4

Field-Cycling NMR relaxometry: the benefit of constructing master curves

Flämig, M.; Hofmann, M.; Fatkullin, N.; Rössler, E. A.

Mol. Phys., **2019**, *117*, 887

Taylor & Francis
Taylor & Francis Group

## NMR RELAXOMETRY AND RELATED METHODS

Check for updates

Field-cycling NMR relaxometry: the benefit of constructing master curves

M. Flämig[a], M. Hofmann[b] and E. A. Rössler[a]

[a]Experimentalphysik II, Universität Bayreuth, Bayreuth, Germany; [b]Department of Chemistry, Louisiana State University, Baton Rouge, LA, USA

ABSTRACT

The currently available field-cycling NMR relaxometers still suffer from a rather narrow frequency range; they facilitate measurements of the ^{1}H spin–lattice relaxation rate in the frequency of 10 kHz–30 MHz. This limit may be overcome by constructing master curves via exploiting frequency-temperature superposition, the latter being an intrinsic feature of the collective dynamics in many soft matter systems. It states that the shape of the motional time-correlation function is essentially temperature independent over a large temperature interval. As will be demonstrated, master curves may be built in the susceptibility or the spectral density representation of spin–lattice relaxation data. As a result, the effective frequency range is expanded up to ten decades, and the applied shift factors provide the temperature dependence of the corresponding correlation time. Three examples are presented: cyano adamantane in its plastically crystalline phase, the liquid glycerol, and the melt of poly(ethylene propylene). Advantages and limitations of the approach are discussed.
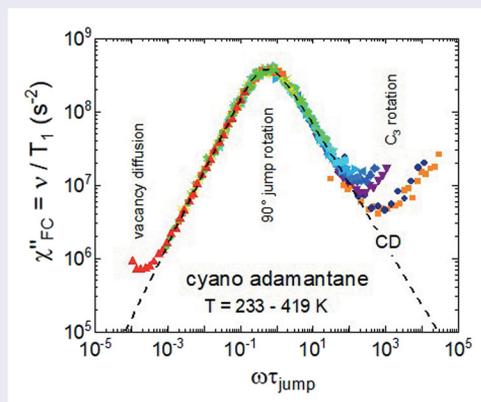
1. Introduction

Ever since the pioneering work of Bloembergen, Purcell, and Pound (BPP) [1], measuring the frequency (field) dependence of the spin–lattice relaxation rate $R_1(\omega) = 1/T_1(\omega)$ has been an important tool for studying the molecular dynamics in condensed matter as it allows to directly probe the underlying spectral density. Early studies monitored the relaxation mainly as a function of temperature, yet, only for a few frequencies due to the low sensitivity of NMR at low fields. This limitation is overcome by the field-cycling (FC) technique, i.e. the relaxation performed at different fields is decoupled from polarisation and detection by rapidly switching

('cycling') the external magnetic field. First FC relaxation studies were restricted to a few groups applying a home-built relaxometer [2]. This changed with the availability of a commercial electronic FC relaxometer since 1997 [3]. It is now routinely possible to measure $R_1(\omega)$ in a frequency range of 10 kHz $< \omega/2\pi <$ 30 MHz (^{1}H) [4–7]. Taking recourse to home-built instruments and compensating for earth and stray field, frequencies down to 100 Hz are accessible [8–10]. Very recently, experiments even down to 3 Hz were reported [11], and further instrumental developments are ongoing [12–17].

Still, compared to competing methods such as dielectric spectroscopy, a frequency range of 3–4 decades of

---

the commercial FC relaxometer is rather narrow. Characterising the salient features of the dielectric response of a viscous liquid like glycerol requires more than ten decades [18–20]. Thus, many studies interpreting $R_1(\omega)$ measured at a few temperatures relied on model assumptions and were not always fully compelling. Here, nature provides a way out. In many cases, collective dynamics in condensed matter is governed by frequency-temperature superposition (FTS) [19, 20]. That is, by collecting relaxation dispersion data at different temperatures and transforming such to the susceptibility representation $\chi''_{FC}(\omega) \equiv \omega R_1$, master curves $\chi''_{FC}(\omega\tau)$ are constructed. Here, τ is some reference time constant. Thereby, the frequency window of the FC technique is effectively extended significantly [8, 9, 21]. The procedure is well established in rheology [22, 23] which covers only a few decades in frequency, as well. Moreover, transforming the NMR relaxation data to the susceptibility representation allows to identify different relaxation processes and to directly compare the results to the dielectric susceptibility, for example. Extending the pioneering works of Kimmich and co-workers [4, 24–28], we applied this approach to molecular [21, 29–33] and ionic liquids [34], polymers [8, 9, 35–41] as well as dendrimers [42].

Most of the FC studies employ ^{1}H NMR, although other nuclei like ^{19}F, ^{13}C, ^{7}Li or ^{2}H are accessible, too [24, 26, 34, 43, 44]. Proton relaxation is dominated by the magnetic dipole–dipole interaction, and the relaxation rate $R_1(\omega)$ is a sum of two contributions originating from the intra- and intermolecular relaxation pathway [4, 27, 45]. The intramolecular rate, $R_{1,\text{intra}}(\omega)$, is caused by interactions between protons belonging to the same molecule. These couplings fluctuate due to the molecular rotation. The intermolecular rate, $R_{1,\text{inter}}(\omega)$, stems from interactions between protons of different molecules. Here, the internuclear distances undergo fluctuations that are caused by both translational as well as rotational dynamics.

Focussing on proton relaxation, we want to demonstrate the benefits of constructing master curves in terms of the susceptibility or the spectral density representation. Without performing an explicit spectral analysis, the characteristic time constants and/or the diffusion coefficient are obtained. Three examples will be presented: dynamics in a plastically crystalline phase (cyano adamantane), in a viscous liquid (glycerol) and in a polymer melt (poly(ethylene-propylene)).

2. Master curves – theoretical background

^{1}H NMR relaxation in molecular systems is dominated by the magnetic dipole–dipole interaction. Assuming a common spin temperature [46], the ^{1}H spin–lattice relaxation rate, $R_1(\omega)$, is a sum of two contributions [1, 4, 45]:

$$R_1(\omega) = R_{1,\text{intra}}(\omega) + R_{1,\text{inter}}(\omega), \quad (1)$$

The (angular) Larmor frequency is given by $\omega = \gamma B$ with B denoting the (variable) magnetic field and γ the gyromagnetic ratio. As said, the intramolecular relaxation, $R_{1,\text{intra}}(\omega)$, is caused by interactions between protons belonging to the same molecule and reflects molecular rotation or reorientational dynamics of segments in polymers, respectively. The intermolecular relaxation, $R_{1,\text{inter}}(\omega)$, originates from interactions between protons of different molecules and is caused by relative translational as well as rotational dynamics.

The frequency dependence of the relaxation rate is a linear combination of spectral densities $J(\omega)$. The latter is the Fourier transform of the rotational or translational correlation function $C(t)$. For intramolecular relaxation the BPP equation connects relaxation rate and spectral density [1, 4, 45]:

$$R_{1,\text{intra}}(\omega) = K_{\text{intra}}[J_{\text{intra}}(\omega) + 4J_{\text{intra}}(2\omega)] \quad (2)$$

Here, K_{intra} is the intramolecular coupling constant. The normalised spectral density $J_{\text{intra}}(\omega) \equiv J_{\text{rot}}(\omega)$ is given by

$$J_{\text{rot}}(\omega) = \frac{1}{2} \int_{-\infty}^{\infty} C_{\text{rot}}(t)e^{-i\omega t}dt \quad (3)$$

where the rotational time-correlation function $C_{\text{rot}}(t) \equiv C_{\text{intra}}(t)$ correlates molecular reorientation in terms of the spherical harmonics $Y_{2m}(\Omega)$ with $\Omega(t)$ denoting the orientation of inter-nuclear vector. In isotropic systems like liquids or polymer melts the correlation function is independent of m. One may define a correlation time τ_{rot} by

$$\tau_{\text{rot}} \equiv \int_0^{\infty} C_{\text{rot}}(t)dt = J_{\text{rot}}(0) \quad (4)$$

Due to the cooperative nature of the dynamics in dense fluids, the correlation function describing the overall reorientation of a molecule in a liquid and often in a plastically crystalline phase is non-exponential. Phenomenologically, the spectral density may be described by a Cole-Davidson (CD) function [47].

The correlation function for intermolecular relaxation reflects both, changes of orientation $\Omega(t)$, as well as inter-spin distance $r(t)$, explicitly [4, 27, 45]

$$C_{\text{inter}}(t) \propto \left\langle \frac{Y_{2m}(t)}{r^3(t)} \frac{Y_{2-m}(0)}{r^3(0)} \right\rangle \quad (5)$$

An analogue of the BPP Equation (5) connects $R_{1,\text{inter}}(\omega)$ with the translational spectral density $J_{\text{trans}}(\omega)$. In a simple model, the spins are located in the centre of the

molecule, diffusion is assumed to be 'force-free', and molecules in a liquid are modelled as hard spheres with a distance of closest approach d given by the molecular diameter. This refers to the 'force-free hard sphere' (FFHS) model and yields an explicit expression for $J_{\text{trans}}(\omega)$ [48, 49]. However, the inter-molecular interaction is modulated by both translational and rotational dynamics, the so-called excentricity effect [50]. Within a phenomenological model [32], the total rate $R_1(\omega)$ can be described by

$$R_1(\omega) \cong R_{1,\text{intra}}(\omega) + R_{1,\text{inter}}^{\text{rot}}(\omega) + R_{1,\text{inter}}^{\text{trans}}(\omega)$$
$$\cong R_1^{\text{rot}}(\omega) + R_1^{\text{trans}}(\omega) \quad (6)$$

where the spectral density for $R_1^{\text{rot}}(\omega)$ is represented by a CD function and that of $R_1^{\text{trans}}(\omega)$ by the FFHS model.

Independent of any details of translational motion, at long times molecules in a liquid undergo Fickian diffusion, implying a mean square displacement (msd) $\langle \Delta r^2 \rangle = 6D\,t$. In this limit, the translational correlation function is given by a power-law $C_{\text{inter}}(t) \propto t^{-3/2}$ and correspondingly, the low-frequency dispersion of $J_{\text{inter}}(\omega)$ follows a square root dependence and so does total rate [33, 48–53]

$$R_1(\omega) = R_{1,\text{intra}}(\omega) + R_{1,\text{inter}}(\omega)$$
$$= R_1(0) - \frac{B}{D^{3/2}} \cdot \sqrt{\omega} \quad (7)$$

as the power law, $C_{\text{inter}}(t) \propto t^{-3/2}$, always dominates the total correlation function at longest times. The constant B is given by $B = ((\mu_0/4\pi)\hbar\gamma^2)^2 \left(1 + 4\sqrt{(2)}/30\right) \pi n$, where n is the spin density.

It is of interest to display the relaxation dispersion also in the susceptibility representation based on the connection of linear response theory and the fluctuation-dissipation theorem (FDT). Equilibrium fluctuations described by $J(\omega)$ are connected to the response represented by a (normalised) dynamic susceptibility $\chi''(\omega)$ along $\chi''(\omega) = \omega J(\omega)$. Consequently, one can re-write the BPP equation [6, 8, 9, 21]:

$$\omega R_1(\omega) = K(\chi''(\omega) + 2\chi''(2\omega)) \equiv 2\pi \chi_{\text{FC}}''(\omega) \quad (8)$$

where K_i denotes the coupling constant K_{intra} or K_{inter}, respectively (the factor 2π appears since the experimentally shown data refer to $\chi_{\text{FC}}''(\omega) = \nu R_1(\omega)$). We note that $\chi_{\text{FC}}''(\omega)$ is only slightly broader than $\chi''(\omega)$, yet shifted along the frequency axes by a factor of about 0.6, due to the contribution of $\chi''(2\omega)$. In the susceptibility representation, relaxation processes show up as more or less distinguishable relaxation peaks shifting with temperature. As will be demonstrated, this feature will help to identify different relaxation processes, and $\chi_{\text{FC}}''(\omega)$

may be directly compared to the dielectric susceptibility. Moreover, this representation of the measured relaxation data allows to easily construct master curves (see next).

As discussed, in liquids as well as in polymers with their cooperative dynamics frequency-temperature superposition (FTS) applies, i.e. the dynamic susceptibility can be expressed as $\chi''(\omega) = \chi''(\omega\tau)$, where $\tau(T)$ is a characteristic time constant, τ_{rot}, for instance. This leads to the possibility to construct FC NMR master curves by shifting the individual susceptibility data, $\chi''(\omega)$, collected at different temperatures solely along the ω-axis until they overlap [6, 8, 9, 21], thereby retaining the normalisation of the susceptibility.

Another possibility arises from Equation (7) which represents the universal low-frequency dispersion of the total relaxation rate. All relaxation data of liquids can be cast in form of another master curve [39, 53]

$$R_1(\omega)/R_1(0) = 1 - \sqrt{\omega\tau_{\text{res}}} + \dots \quad (9)$$

with a rescaled time constant

$$\tau_{\text{res}} = \left(\frac{B}{D^{3/2}R_1(0)}\right)^2 \quad (10)$$

When constructing master curves in this way, i.e. by re-scaling the spectral density (instead of the susceptibility), both, the rate as well as the frequency are rescaled. Important to note, as in the low-frequency limit the intermolecular relaxation becomes dominant, the limiting low-frequency behaviour along Equation (7) is always exact even if FTS fails.

3. Experimental examples

3.1. Cyano adamantane

Plastically crystalline phases [54] may be considered as model systems for the glass transition phenomenon [55, 56]. In contrast to structural glass formers they show translational order but dynamic orientational disorder, i.e. the molecules reorient on fixed lattice sites. Often, the phase can be super-cooled and the reorientational dynamics slows down, finally leading to a glassy crystal below the glass transition temperature T_g [57]. In the glass state ($T < T_g$), the molecules' overall rotation is arrested. Like in liquids the dynamics at $T > T_g$ is of cooperative nature as the free volume needed to allow reorientation can only be accommodated by a concerted motion of many molecules. Here, we consider cyano adamantane which is a rigid globular molecule with a strong dipole moment [58–64] (see inset of Figure 2(b)). At room temperature, it forms a plastically crystalline phase of cubic symmetry which transforms to an ordered

crystalline phase at $T_c = 280$ K. Yet, the dynamically disordered phase can be super-cooled and forms a glassy crystal close to $T_g = 170$ K. In particular, NMR studies showed that three processes have to be distinguished: (i.) rotation around the C_3-axis (process I). (ii.) 90-degree jumps of this axis along the direction of the cubic lattice (process II); (iii.) Vacancy diffusion (process III) [58, 61, 64]. Here, we present ^{1}H NMR relaxation data measured with a Stelar FFC 2000 relaxometer.

Figure 1(a) displays the spin–lattice relaxation rate as a function of frequency for a large number of different temperatures in the range 153–419 K. For most temperatures, strong dispersion is observed which makes it rather difficult to identify different relaxation processes. At the highest temperature $T = 419$ K (red filled squares), a weak, plateau-like dispersion is found at high frequencies whereas stronger dispersion sets in at low frequencies. The level of the plateau rises with decreasing temperature and with dispersion setting in at high frequencies the plateau appears to shifts to lower frequencies (cf. $T = 353$ K and $T = 323$ K, orange and violet filled squares, respectively). Going to even lower temperatures the low-frequency plateau vanishes. Instead strong dispersion is observed at all frequencies which shifts to lower frequencies upon further cooling (see $T = 263$ K and $T = 233$ K, black and green filled squares, respectively). Finally, at even lower temperatures, another plateau emerges which moves to higher values at the lowest temperatures (cf. $T = 193$ K and $T = 153$ K, cyan and blue squares, respectively). Clearly, the relaxation behaviour is difficult to understand. However, this changes when turning to the susceptibility representation of the data.

Figure 1(b) shows the measured relaxation data in the susceptibility representation, i.e. we plotted $\nu \cdot R_1(\nu) = \chi''_{FC}(\nu)$ against frequency. High- (red symbols) and low-temperature data (blue symbols) are distinguished. The high-temperature data clearly display a relaxation maximum shifting to lower frequencies upon cooling. We tentatively attribute this relaxation peak to the overall rotational jumps of the molecule along the lattice directions (process II). At $T = 419$ K and low frequencies a minimum is recognised indicating the appearance of another dispersion regime attributed to the slowest dynamics in the system: translational diffusion of lattice vacancies (process III). The low-temperature data shows in addition to the high-frequency flank of relaxation II another dispersion regime first recognised at T = 244 K (solid blue symbol) where another minimum in the susceptibility appears. Finally, at lowest temperatures a second, higher relaxation maximum can be anticipated which is not fully covered, yet, due to the temperature limitation of the FC relaxometer. This relaxation regime originates from the fastest relaxation process, namely the C_3-rotation of the molecule (process I).

Next, regarding the high temperature data we attempt to construct a master curve by plotting the νR_1 vs the rescaled frequency $\omega \tau_{rot}$. Given a susceptibility maximum for some temperatures (cf. Figure 1(b): $T = 320$–380 K) an estimate of the time constant is provided by the condition $\omega \tau_{rot} = 0.616$. For the rest of the susceptibility data (with no maximum), the spectra are shifted solely along the frequency axis to achieve best overlap. The result is displayed in Figure 2(a). Within the temperature range 294 K–380 K perfect overlap results and a master curve is obtained. At higher and lower temperatures, respectively, the master curve construction clearly fails: Here, relaxation by translational vacancy diffusion and by the molecular C_3 rotation, respectively, become dominant. Around the relaxation peak of the
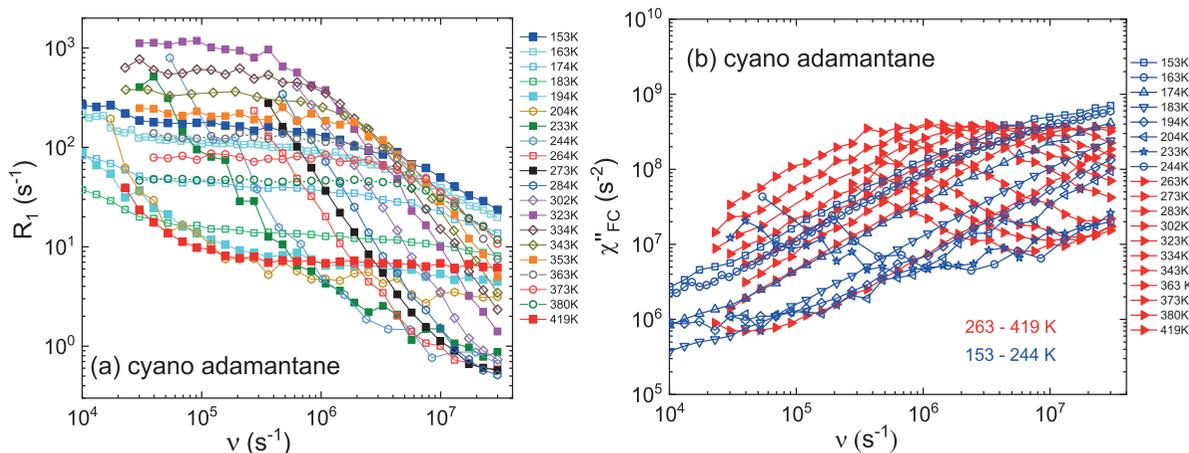

Figure 1. (a) Proton relaxation dispersion of cyano adamantane measured over a broad temperature range; data represented by filled symbols are discussed in the text. (b) Susceptibility representation of the data in (a), $\nu \cdot R_1 = \chi''_{FC}$; two temperature ranges are marked by a different colour.
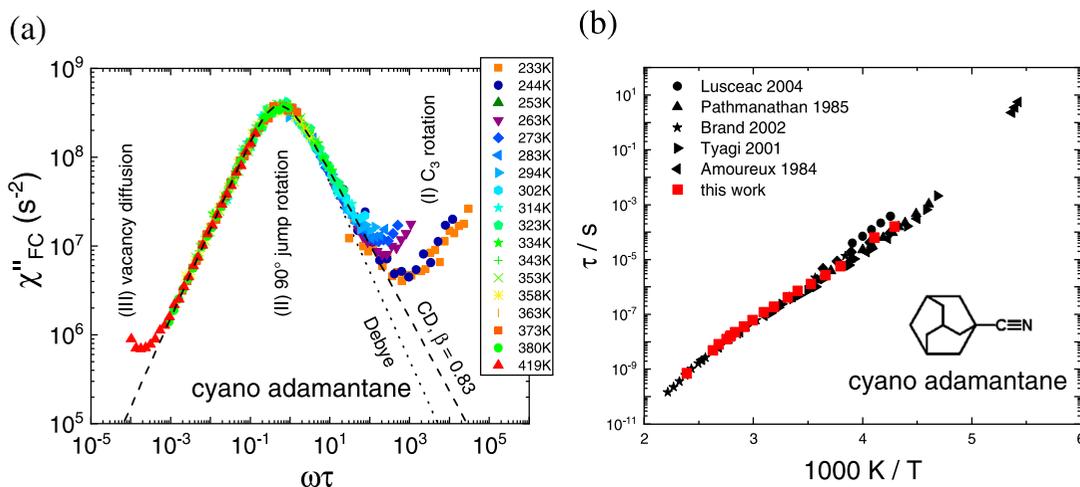
Figure 2. (a) Susceptibility master curve constructed from the high-temperature data displayed in Figure 1(b), different colours correspond to different temperatures; relaxation processes are indicated; the relaxation peak is described by a Cole-Davidson (CD) function, for comparison a Debye function is shown (dotted line). (b) Time constants of the overall rotational jump process in cyano adamantane as obtained by the ^{1}H FC NMR master curve construction (cf. (b)); for comparison, literature data from several sources are included [58–64].

master curve does not follow a Debye (Lorentzian) curve (dotted line) which is expected for an exponential correlation function. Instead, it can be modelled by a CD function with a stretching parameter $\beta_{CD} = 0.83$ (dashed line). Stimulated echo experiments by ^{2}H NMR revealed a very similar value of $\beta_{CD} = 0.82$ [61]. Therefore, the rotational correlation function is (weakly) stretched as it is typically observed for cooperative dynamics. In the course of constructing the master curve, the time constants $\tau_{rot}(T)$ are obtained. In Figure 2(b) they are compared to those reported by other techniques [54–63]. Perfect agreement is found. In particular, a ^{2}H study [61] clearly showed that molecular jumps along the six directions of the cubic lattice are the origin of the relaxation II.

3.2. Glycerol

Glycerol is a viscous liquid already studied by BPP [1]. It displays pronounced ^{1}H relaxation dispersion around ambient temperatures. Upon cooling glycerol undergoes the glass transition which leads to a glass at temperatures below $T_g \cong 180$ K. This slowing down of molecular motion was studied by various techniques [18, 65]. Figure 3(a) shows the proton relaxation rate in the susceptibility representation of (fully protonated) glycerol (see also ref. [31]). The relaxation maximum of $\chi''_{FC}(\omega)$ shifts to lower frequencies upon cooling as expected for dynamics getting slower. Compared to the susceptibility data of cyano adamantane (cf. Figure 1(b)) the relaxation is broader. Again, the susceptibility data collected at different temperatures are combined to
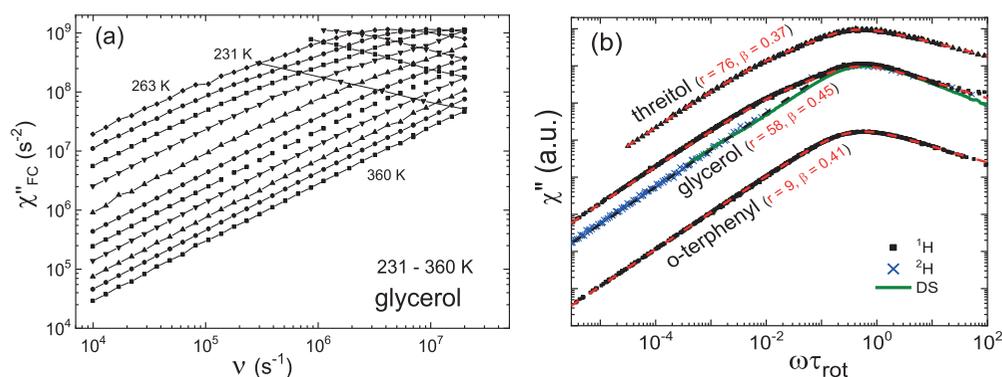

Figure 3. (a) Susceptibility representation of the ^{1}H spin-lattice relaxation data as a function of frequency for glycerol measured at different temperatures. (b) Susceptibility master curves for glycerol, threitol, and o-terphenyl as obtained from ^{1}H FC NMR relaxation data (black points, arbitrarily shifted vertically); in addition, data from ^{2}H FC NMR and dielectric spectroscopy (DS) for glycerol are added (blue crosses and green line, respectively); dashed black line: CD fit; red dashed line: fit along Equation (6), separation parameter $r = \tau_{trans}/\tau_{rot}$ and stretching parameter β_{CD} are indicated.

build a master curve $\chi''_{FC}(\omega\tau_{rot})$, which is directly compared to the dielectric susceptibility $\varepsilon''(\omega) = \chi''_{DS}(\omega\tau_{rot})$ in Figure 3(b). The latter solely probes the reorientation of the molecular electric dipole moment and can be well described by a CD function. In the time domain, this corresponds to a non-exponential rotational correlation function typical of dense fluids [19, 20]. Such an interpolation is not possible for $\chi''_{FC}(\omega\tau_{rot})$, as a low-frequency shoulder is recognised in addition to the main peak. We assign the low-frequency shoulder of the ^{1}H relaxation to intermolecular relaxation which was proven by isotope dilution experiments [32] and by ^{2}H FC NMR relaxation data included in Figure 3(b) [44]. In the latter case, relaxation is caused by fluctuation of the quadrupolar interaction, which is of purely intra-molecular origin in molecular systems [45].

In Figure 3(b) we included master curves of the two other viscous liquids, o-terphenyl and threitol. The relaxation spectrum of threitol looks quite similar to that of glycerol, whereas that of o-terphenyl is different; in the latter case, no low-frequency shoulder is recognised. As discussed (cf. Section 2) the master curves can be described by a sum of two contributions $R_1^{rot}(\omega)$ and $R_1^{trans}(\omega)$ along Equation (6). The rotational relaxation contribution from both, the intra- as well as the intermolecular pathway is contained in $R_1^{rot}(\omega)$. A spectral analysis applying a CD and the FFHS function yields the separation parameter $r = \tau_{trans}/\tau_{rot}$ and the stretching parameter β_{CD}. Fits with this two-compoent model (red dashed lines) together with the corresponding parameters are also given in Figure 3(b). Very satisfying interpolations are achieved. In the case of glycerol and threitol, the separation parameter r is large, i.e. the time scales of translation and rotation are separated by almost two decades, whereas in the case o-terphenyl the separation is significantly smaller. A large separation parameter is characteristic of hydrogen-bonded liquids. For example, the r value decreases when an aprotic solvent is added to the associated liquid [66].

As seen from Figure 3(b) the slope of the high-frequency flank of the peak reflecting the rotational relaxation contribution varies among the different liquids. In other words, the stretching parameter β_{CD} of the CD function is a liquid-specific property. This hampers a straightforward comparison of the NMR master curves of different liquids. Here, we just mention that a further scaling procedure can be applied to susceptibility master curves which transforms a CD spectral shape into a Debye shape, i.e. one applies a factor $f(\omega, \tau_\alpha, \beta_\alpha)$ defined as [30]:

$$f(\omega\tau_{rot}, \beta_{CD}) = \frac{\chi''_D(\omega\tau_{rot})}{\chi''_{CD}(\omega\tau_{rot}, \beta_{CD})} \quad (11)$$

Here, $\chi''_{CD}(\omega\tau_{rot}, \beta_{CD})$ is a CD function obtained by fitting an individual NMR susceptibility master curve, and $\chi''_D(\omega\tau_{rot})$ a Lorentzian (Debye) spectrum. In this way, the contribution to the main relaxation peak is transformed to a Debye spectral shape while conserving the normalisation. This eliminates the effect of a varying broadening of the high-frequency part of the spectra of the different liquids. Such rescaled master curves are shown in Figure 4. As a result, the high-frequency relaxation contributions coincide for all liquids, by construction. The hydrogen-bonded liquids show a pronounced low-frequency shoulder, whereas simple molecular liquids like o-terphenyl or tristyrene show a weak shoulder. This goes along with a large or small ratio r, respectively, as discussed.
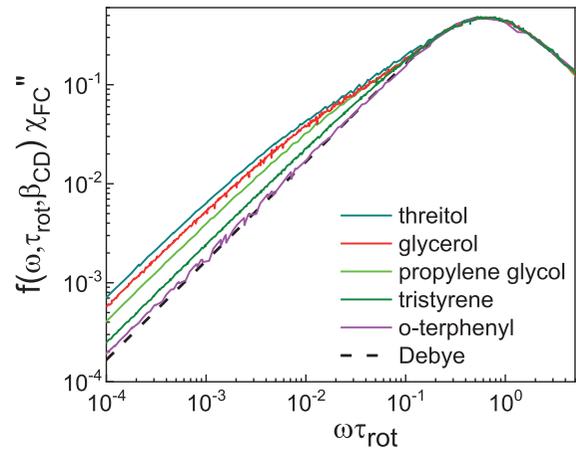

Figure 4. ^{1}H FC NMR susceptibility master curves of selected liquids after rescaling the high-frequency part according to Equation (11) to achieve a Debye-like (Lorentzian) spectral shape at high frequencies; dashed line: Debye spectrum.
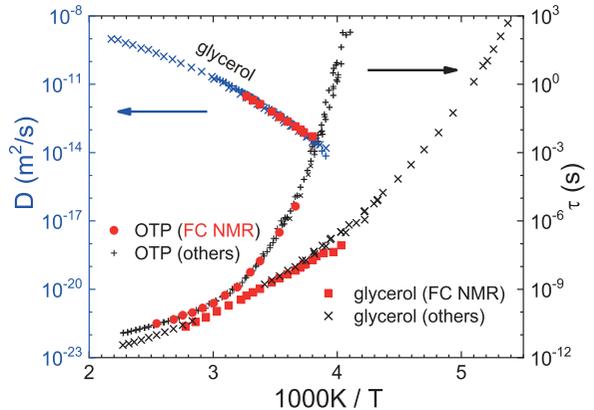

Figure 5. Reorientational time constants versus the reciprocal temperature as obtained from ^{1}H FC NMR (red circles) and by other techniques (black crosses) in the case of glycerol and of o-terphenyl (OTP) (right scale). In addition, for glycerol diffusion coefficient D (left scale) obtained from ^{1}H FC NMR (red circles) and from field gradient NMR (blue crosses) [30, 66].

From the frequency shift factors applied in the course of the master curve construction, the time constant $\tau_{\rm rot}(T)$ is extracted. This data is shown in Figure 5 for glycerol and o-terphenyl, together with the results from other methods (dielectric spectroscopy and light scattering [19]). Good agreement is found among all methods probing molecular rotation. The temperature dependence does not follow an Arrhenius behaviour. Instead, a 'super-Arrhenius' dependence is recognised as is characteristic for the dynamics in (super-cooled) liquids undergoing the glass transition. It turns out that $\tau_{\rm rot}(T)$ coincides with the time constant o the structural or α–relaxation, $\tau_{\rm rot}(T) \cong \tau_\alpha(T)$ [30].

The results discussed so far show that the low-frequency dispersion of the total relaxation rate $R_1(\omega)$ of a liquid is dominated by the translationally mediated inter-molecular relaxation. In Figure 6 we display spectral density master curves, i.e. we plot $R_1(\omega)/R_1(0)$ vs. rescaled frequency $\sqrt{\omega\tau_{\rm res}}$ according to Equation (9). A common linear low-frequency regime results (dashed line), while differences among the systems observed at higher frequencies originate from different inter- and intramolecular relaxation contributions. For glycerol (with a large separation parameter r) at high frequencies the curve deviates upwards from the projected linear low-frequency limit, whereas the one for o-terphenyl (with small r value) bends down staying below this projection (dashed line). As translational and rotational dynamics are usually coupled and thus FTS applies, this data representation reflects another type of master curves extending up to highest frequencies. We stress again that the low-frequency scaling is universal whereas a master curve results at higher frequencies only if FTS applies.
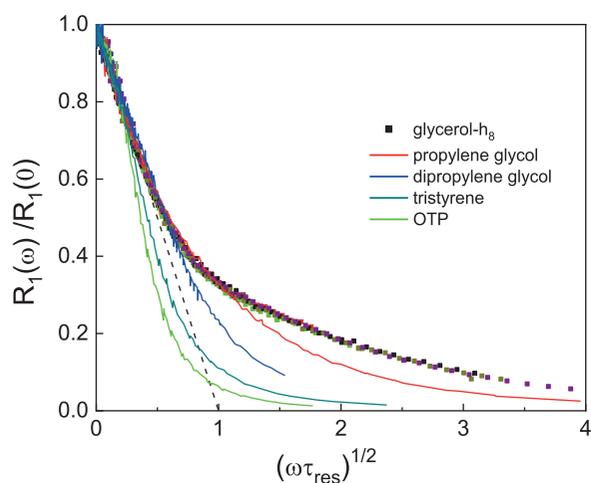

Figure 6. Spectral density master curves of several liquids: reduced relaxation rate vs. square root of rescaled frequency according to Equation (9). In the case of glycerol, the differently coloured symbols reflect data obtained at different temperatures in the range 276 K–398 K.

From the rescaling time $\tau_{\rm res}$ together with the proton density (cf. Equation (10)) one gets the diffusion coefficient $D(T)$. The FC NMR result for glycerol compared to that derived from field gradient NMR studies [67, 68] are included in Figure 5. A very good agreement is found.

Finally, we mention that with $D(T)$ obtained from the construction of the spectral density master curve and $\tau_{\rm rot}(T)$ from that of the susceptibility master curve one can estimate the hydrodynamic radius $R_{\rm H}$ of the molecule within a single experiment by assuming the Stokes–Einstein-Debye relationship $D\tau_{\rm rot} = \frac{2}{9} R_H^2$. Satisfying agreement with other methods is revealed [66].

3.3. Polymer melts

Polymer melts exhibit relaxation modes which are much slower than the segmental mode (τ_s) [28]. The latter is controlled by the glass transition phenomenon as observed also in simple liquids and one can set $\tau_s \cong \tau_\alpha$ (cf. Section 3 B). The mode spectrum strongly depends on the chain length, i.e. the molar mass M. Of particular importance is the appearance of entanglement effects when the critical molar mass, M_c, is exceeded. The dynamics in un-entangled melts, i.e. such with $M < M_c$, is well understood within the Rouse model [69]. For entangled polymers, the most accepted theoretical approach explaining this slow, collective dynamics offers the tube-reptation (TR) model developed by Edwards, DeGennes and Doi [70, 71]. A polymer chain 'reptates' in a virtual tube representing the topological constraints exerted by neighbouring chains. Before normal (Fickian) diffusion sets in at longest times (regime IV), three different sub-diffusive regimes are forecast for the segmental mean square displacement (msd) $r^2(t)$: Rouse regime (I), constraint Rouse regime (II), and reptation regime (III). Correspondingly, three characteristic times delimit the different regimes: entanglement time τ_e, Rouse time τ_R, and disengagement or terminal relaxation time τ_t. The latter two are strongly dependent on M.

Regarding the msd, the TR scenario was essentially verified by neutron scattering [72] – and recently by ^{1}H FC NMR experiments [41] as well as by simulations [73, 74]. The model predicts characteristic power-law regimes also for the NMR relaxation dispersion [27, 74–77], and FC NMR turned out to be very useful to identify them, thereby testing current polymer theories. Not included in most polymer theories is the glass relaxation regime (0) which governs the msd at shortest times [6, 8, 9, 21]. Here, we consider the linear polymer poly(ethylene-propylene) (PEP) [9].

As seen in Figure 7(a), for entangled PEP with $M = 29\,{\rm kg/mol} < M_c = 6\,{\rm kg/mol}$ there is strong dispersion
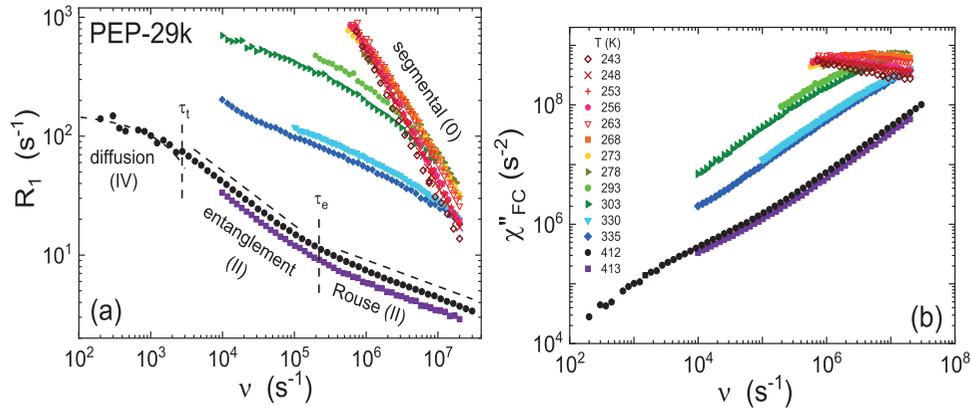
Figure 7. (a) Dispersion of the spin-lattice relaxation rate of poly(ethylene-propylene) (PEP) with molar mass $M = 29$ k measured at temperatures as indicated. Relaxation regimes (0-IV) are indicated. The dashed lines reflect power-law behaviour associated with polymer dynamics (regimes I and II) and the onset of the diffusion regime (IV) following Eq. 7, respectively. (b) Same data in the susceptibility representation.

even at high temperatures at which the segmental relaxation is much too fast to cause relaxation within the accessible frequency range. For such a high-M polymer, the extreme narrowing condition is not reached as the slow collective polymer dynamics controls the relaxation. In the low-temperature range even stronger dispersion is recognised and attributed to the segmental dynamics governed by glassy dynamics. We added ^{1}H FC NMR data from a home-built relaxometer which allows reaching frequencies of about 100 Hz [7, 10, 11]. This particular curve measured at 412 K not only displays two different power-laws regimes (I,II) associated with Rouse and entanglement dynamics, respectively, with a crossover at the entanglement time τ_e, but also the onset of the square root law Equation (7) at lowest frequencies reflecting diffusion already. The actual reptation regime III only appears for higher M [9].

Again, the situation becomes clearer when inspecting the susceptibility representation of the data – see Figure 7(b). Just as in simple liquids, at low temperatures one finds a relaxation maximum reflecting the segmental or a-relaxation (regime 0). The peak shifts toward lower frequencies when the temperature is decreased. Upon increasing the temperature the α–peak shifts out of the frequency window and again the two power-law regimes ascribed to Rouse (I) and entanglement dynamics (II), respectively, are recognised (dashed lines in Figure 7(b)), which reflect collective chain dynamics typical of high-M polymers, specifically Rouse (I) and entanglement dynamics (II) [8, 9, 28].

Assuming FTS again, susceptibility master curves are constructed. In Figure 8(a) we display such curves for five different M values; in addition, we show the data for dipropylene glycol (di-PG) as reference for a simple
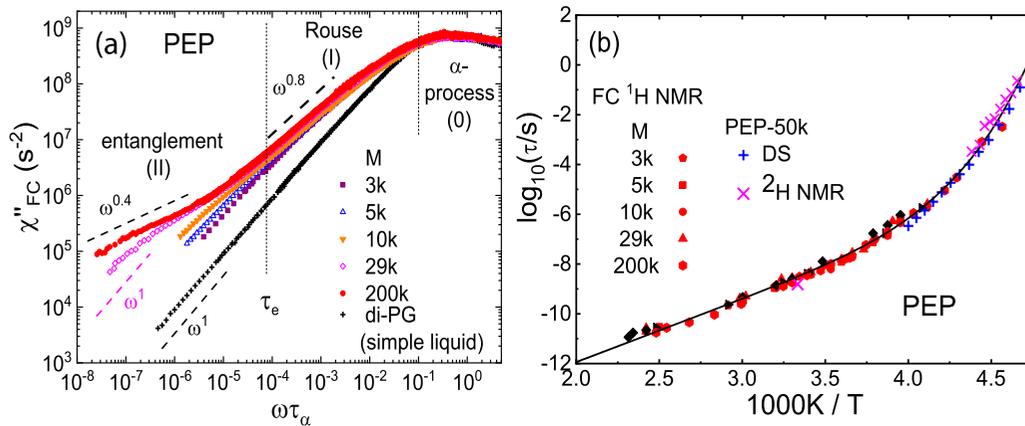

Figure 8. (a) Master curves $\chi''_{FC}(\omega\tau_s)$ for different 3 k $\leq M \leq 200$ k of poly(ethylene-propylene) (PEP), for comparison data of dipropylene glycol (di-PG) as reference for a simple liquid is shown; different relaxation regimes are indicated. In addition to the α–peak representing relaxation regime 0, two power-law regimes (I, II) are observed reflecting polymer-specific relaxation (dashed lines). (b) Segmental time constant obtained from master curve construction (cf. Figure (a)) compared to results from dielectric spectroscopy (DS) and ^{2}H NMR [78]; solid-line: guide for the eye.

liquid. All polymers display pronounced low-frequency relaxation contributions which are not observed in the case of simple liquids. For PEP with $M = 29$ k, the two polymer-specific power-law dispersion are recognised best. As said, the high-frequency one is attributed to the Rouse regime (I) and the second to the constraint Rouse regime (II). The crossover of both marks the entanglement time τ_e. For lower M values the curves at lowest frequencies bend over to an asymptotic behaviour close to $\chi''_{FC}(\omega < \tau_t^{-1}) \propto \omega^1$ which characterises the terminal relaxation. While for PEP-27k the diffusion regime (IV) is still observed (cf. Figure 7(a)), in the case of PEP-200k this longest relaxation is too slow to be accessible by the FC technique. Finally, the corresponding segmental time constants $\tau_s(T)$ are found in Figure 8(b). They are independent of M and agree well with those from dielectric spectroscopy and from high-field ^{2}H NMR [78].

4. Discussion and conclusions

Taking recourse to the susceptibility representation of spin–lattice relaxation data and constructing master curves by exploiting FTS, the rotational or segmental (in polymers) time constants can be estimated without performing an explicit spectral analysis. The approach works well in plastically crystalline phases as well as in viscous liquids and polymer melts. Moreover, the susceptibility representation allows distinguishing between different relaxation regimes what may be difficult in the rate representation, in particular, if the system displays several relaxation processes. Furthermore, the susceptibility representation also allows a direct comparison with that from dielectric spectroscopy, for example. Relying on the universal low-frequency square root dispersion caused by translational diffusion master curves can also be constructed in terms of the spectral density. Thereby, the diffusion coefficient is extracted again in a model-independent way. Finally, master curves at hand extending over many decades in frequency, the data can be transformed into the time domain to directly display the corresponding time-correlation function [5,6,8,9,44] which may be compared to that of double quantum NMR [76] or to that provided by rheological experiments [42].

Of course, master curve construction relies on the applicability of FTS, which, however, is a well-established fact in liquids and polymers, in particular at high temperatures [19–22]. The present approach must be reconsidered if the NMR coupling constant, or more precisely the pre-factors of the spectral density become frequency dependent as is the case for spin relaxation caused by chemical shift anisotropy or by paramagnetic relaxation enhancement [79]. Drastic changes in the density affect the intermolecular dipolar coupling and may spoil the

master curve construction as well. Also, in the case that the dynamics is governed by a distribution of activation energies $g(E)$, the approach fails. The presumably temperature independent distribution $g(E)$ transforms into a temperature dependent distribution of correlation times $G(ln\tau)$ along $G(ln\tau) = RTg(RT \, ln\tau/\tau_o)$, where τ_o denotes some attempt time and R the ideal gas constant [80, 81]. In other words, the width of the distribution $G(ln\tau)$ broadens with decreasing temperature and consequently the corresponding susceptibility function broadens either. For example, as demonstrated by ^{2}H NMR the C_3 rotation of cyano adamantane in the glassy crystal phase is controlled by a broad distribution $g(E)$ [64]. In this case, again a master curve may be constructed by appropriately rescaling the individual spectra measured at different temperatures [47, 82, 83]. Possibly, the low-temperature relaxation data of cyano adamantane reflecting the C_3 rotation in the glassy crystal can be described along these lines. Yet, this is a future task.

References

[1] N. Bloembergen, E.M. Purcell and R.V. Pound, Phys. Rev. **73**, 679 (1948).
[2] F. Noack, Prog. NMR Spectrosc. **18**, 171 (1986).
[3] STELAR Company: www.stelar.it.
[4] R. Kimmich and E. Anoardo, Progr. NMR Spectr. **44**, 257 (2004).
[5] D. Kruk, A. Herrmann and E.A. Rössler, Progr. NMR Spectr. **63**, 33 (2012).
[6] R. Meier, D. Kruk and E.A. Rössler, Chem. Phys. Chem. **14**, 3071 (2013).
[7] B. Kresse, A.F. Privalov, A. Herrmann, M. Hofmann, E.A. Rössler and F. Fujara, Solid State Nucl. Magn. Reson. **59**, 45 (2014).
[8] A. Herrmann, B. Kresse, J. Gmeiner, A. Privalov, D. Kruk, F. Fujara and E.A. Rössler, Macromolecules. **45**, 1408 (2012).

[9] M. Hofmann, B. Kresse, L. Heymann, A.F. Privalov, L. Willner, N. Fatkullin, N. Aksel, F. Fujara and E.A. Rössler, Macromolecules. **49**, 8622 (2016).

[10] F. Fujara, D. Kruk and A.F. Privalov, Prog. NMR Spectrosc. **82**, 39 (2014).

[11] B. Kresse, M. Becher, A.F. Privalov, M. Hofmann, E.A. Rössler, M. Vogel and F. Fujara, J. Magn. Reson. **277**, 79 (2017).

[12] V. Zampetoulas, D.J. Lurie and L.M. Broche, J. Magn. Reson. **282**, 38 (2017).

[13] D.M. Sousa, P.A.L. Fernandes, G.D. Marques, A.C. Ribeiro and P.J. Sebastiao, Solid State Magn. Reson. **25**, 160 (2010).

[14] S. Korchak, K. Ivanov, A. Yurkovskaya and H.-M. Vieth, J. Chem. Phys. **133**, 094502 (2012).

[15] S. Kruber, G.D. Farrher and E. Anoardo, J. Magn. Reson. **259**, 216 (2015).

[16] O. Neudert, C. Mattea and S. Stapf, J. Magn. Reson. **271**, 7 (2016).

[17] C.Y. Chou, M. Abdesselem, C. Bouzigues, M. Chu, A. Guiga, T.H. Huang, F. Ferrage, T. Gacoin, A. Alexandrou and D. Sakellariou, Scientific Reports. **7**, 44770 (2017).

[18] P. Lunkenheimer, U. Schneider, R. Brand and A. Loidl, Contemp. Phys. **41**, 15 (2000).

[19] N. Petzold, B. Schmidtke, R. Kahlau, D. Bock, B. Micko, R. Meier, D. Kruk and E.A. Rössler, J. Chem. Phys. **138**, 154501 (2013).

[20] W. Götze, J. Phys. Condens. Matter. **11**, A1 (1999).

[21] S. Kariyo, C. Gainaru, H. Schick, A. Brodin, V.N. Novikov and E.A. Rössler, Phys. Rev. Lett. **97**, 207803 (2006). Erratum: A. Herrmann, C. Gainaru, H. Schick, A. Brodin, V.N. Novikov, and E.A. Rössler:, Phys. Rev. Lett. **100**, 109901 (2008).

[22] J.D. Ferry, *Viscoelasticity Properties of Polymers* (John Wiley & Sons Ltd, New York, 1980).

[23] M. Rubinstein and R.H. Colby, *Polymer Physics* (Oxford University Press, Oxford, 2008).

[24] S. Stapf, R. Kimmich and R.O. Seiter, Phys. Rev. Lett. **75**, 2855 (1995).

[25] M. Kehr, N. Fatkullin and R. Kimmich, J. Chem. Phys. **126**, 094903 (2007).

[26] M. Kehr, N. Fatkullin and R. Kimmich, J. Chem. Phys. **127**, 084911 (2007).

[27] R. Kimmich and N. Fatkullin, Progr. NMR Spectrosc. **101**, 18 (2017).

[28] R. Kimmich and N. Fatkullin, Adv. Polym. Sci. **170**, 1 (2004).

[29] C. Gainaru, O. Lips, A. Troshagina, R. Kahlau, A. Brodin, F. Fujara and E.A. Rössler, J. Chem. Phys. **128**, 174505 (2008).

[30] R. Meier, R. Kahlau, D. Kruk and E.A. Rössler, J. Phys. Chem. A. **114**, 7847 (2010).

[31] D. Kruk, R. Meier and E.A. Rössler, J. Phys. Chem. B. **115**, 951 (2011).

[32] R. Meier, D. Kruk, J. Gmeiner and E.A. Rössler, J. Chem. Phys. **136**, 034508 (2012).

[33] D. Kruk, R. Meier and E.A. Roessler, Phys. Rev. E. **85**, 020201 (2012).

[34] D. Kruk, R. Meier, A. Rachocki, A. Korpała, R.K. Singh and E.A. Rössler, J. Chem. Phys. **140**, 244509 (2014).

[35] S. Kariyo, A. Brodin, C. Gainaru, A. Herrmann, J. Hintermeyer, H. Schick, V.N. Novikov and E.A. Rössler, Macromolecules. **41**, 5322 (2008).

[36] A. Herrmann, V.N. Novikov and E.A. Rössler, Macromolecules. **42**, 2063 (2009).

[37] A. Herrmann, S. Kariyo, A. Abou Elfadl, R. Meyer, V.N. Novikov and E.A. Rössler, Macromolecules. **42**, 5236 (2009).

[38] A. Herrmann, B. Kresse, M. Wohlfahrt, I. Bauer, A.F. Privalov, D. Kruk, N. Fatkullin, F. Fujara and E.A. Rössler, Macromolecules. **45**, 6516 (2012).

[39] R. Meier, A. Herrmann, M. Hofmann, B. Schmidtke, B. Kresse, A.F. Privalov, D. Kruk, F. Fujara and E.A. Rössler, Macromolecules. **46**, 5538 (2013).

[40] M. Hofmann, B. Kresse, A.F. Privalov, L. Willner, N. Fatkullin, F. Fujara and E.A. Rössler, Macromolecules. **47**, 7917 (2014).

[41] B. Kresse, M. Hofmann, A.F. Privalov, N. Fatkullin, F. Fujara and E.A. Rössler, Macromolecules. **48**, 4491 (2015).

[42] M. Hofmann, C. Gainaru, B. Cetinkaya, R. Vaiullin, N. Fatkullin and E.A. Rössler, Macromolecules. **48**, 7521 (2015).

[43] A.O. Seyedlar, S. Stapf and C. Mattea, Phys. Chem. Chem. Phys. **17**, 1633 (2015).

[44] M. Flämig, M. Becher, M. Hofmann, T. Körber, B. Kresse, A.F. Privalov and L. Willner, J. Phys. Chem. B. **120**, 7754 (2016).

[45] A. Abragam, *The Principles of Nuclear Magnetism* (Clarendon Press, Oxford, 1961).

[46] D. Wolf, *Spin-Temperature and Nuclear-Spin Relaxation in Matter: Basic Principles and Applications* (Clarendon Press, Oxford, 1979).

[47] C.J.F. Böttcher and P. Bordewijk, *Theory of Electric Polarization*, Vol. II (Elsevier Scientific, Amsterdam, 1978).

[48] L.P. Hwang and J.H. Freed, J. Chem. Phys. **63**, 4017 (1975).

[49] Y. Ayant, E. Beloritzky, J. Alizon and J. Gallice, J. Phys. (France). **36**, 991 (1975).

[50] Y. Ayant, E. Belorizky, P. Fries and J. RossetL, J. Phys. (France). **38**, 325 (1977).

[51] J.F. Harmon and B.H. Muller, Phys. Rev. **182**, 400 (1969).

[52] C.A. Sholl, J. Phys. C Solid State Phys. **14**, 447 (1981).

[53] R. Meier, D. Kruk, A. Bourdick, E. Schneider and E.A. Rössler, Appl. Magn. Reson. **44**, 153 (2013).

[54] J.N. Sherwood, *The Plastically Crystalline State* (Wiley, New York, 1979).

[55] M.D. Ediger, Annu. Rev. Phys. Chem. **51**, 99 (2000).

[56] A. Cavagna, Phys. Reports. **476**, 51 (2009).

[57] H. Suga, Pure Appl. Chem. **55**, 427 (1983).

[58] J.P. Amoureux, R. Decressain, M. Sahour and E. Cochon, J. Phys. France. **2**, 249 (1992).

[59] J.F. Willart, M. Descamps and J.C. Miltenburg, J. Chem. Phys. **112**, 10992 (2000).

[60] R. Brand, P. Lunkenheimer and A. Loidl, J. Chem. Phys. **116**, 10386 (2002).

[61] S.A. Lusceac, I. Roggatz, P. Medick, J. Gmeiner and E.A. Rössler, J. Chem. Phys. **121**, 4770 (2004).

[62] M. Tyagi and S.S.N. Murthy, J. Chem. Phys. **114**, 4640 (2001).

[63] K. Pathmanathan and G.P. Johari, J. Phys. C: Solid Stat. Phys. **18**, 6535 (1985).

[64] S.A. Lusceac, I. Roggatz, J. Gmeiner and E.A. Rössler, J. Chem. Phys. **126**, 014701 (2007).

[65] A. Kudlik, S. Benkhof, T. Blochowicz, C. Tschirwitz and E. Rössler, J. Mol. Struct. **479**, 201 (1999).

[66] R. Meier, E. Schneider and E.A. Rössler, J. Chem. Phys. **142**, 034503 (2015).

[67] I. Chang and H. Sillescu, J. Phys. Chem. **101**, 8794 (1997).

[68] B. Chen, E.E. Sigmund and W.P. Halperin, Phys Rev. Lett. **96**, 123 (2006).

[69] P.E.A. Rouse, J. Chem. Phys. **21**, 1272 (1953).

[70] P.G. deGennes, J. Chem. Phys. **55**, 572 (1971).

[71] M. Doi, M. and S and F. Edwards, *The Theory of Polymer Dynamics* (Oxford Sci. Publication, London, 1986).

[72] D. Richter, in *Dynamics of Soft Matter*, edited by V.G. Sakai, Ch. Alba-Simionesco, and S.-H. Chen (Springer, New York, 2012).

[73] K. Kremer and G.S. Greet, J. Chem. Phys. **92**, 5057 (1989).

[74] Z. Wang, A.E. Likhtman and R.G. Larson, Macromolecules. **45**, 3557 (2012).

[75] R.C. Ball, P.T. Callaghan and E.T. Samulski, J. Chem. Phys. **106**, 7352 (1997).

[76] F. Vaca Chávez and K. Saalwächter, Macromolecules. **44**, 1560 (2011).

[77] N. Fatkullin, S. Stapf, M. Hofmann, R. Meier and E.A. Rössler, J. Non-Cryst. Solids. **407**, 309 (2015).

[78] K. Nusser, G.J. Schneider and D. Richter, Macromolecules. **46**, 6263 (2013).

[79] D. Kruk, A. Korpała, A. Kubica, R. Meier, E.A. Rössler and J. Moscicki, J. Chem. Phys. **138**, 024506 (2013).

[80] H.A. Resing, J. Chern. Phys. **43**, 669 (1965).

[81] E. Rössler, J. Chem. Phys. **92**, 5847 (1990).

[82] R. Kahlau, T. Dörfler and E.A. Rössler, J. Chem. Phys. **139**, 134504 (2013).

[83] J. Wiedersich and E. Rössler, Phys. Rev. Lett. **84**, 2718 (2000).

Publication 5

The Dynamics of the Plastically Crystalline Phase of Cyanoadamantane Revisited by NMR Line Shape Analysis and Field-Cycling Relaxometry

Flämig, M.; Fatkullin, N.; Rössler, E. A.

J. Chem. Phys., **2019**, *151*, 224507

The dynamics of the plastically crystalline phase of cyanoadamantane revisited by NMR line shape analysis and field-cycling relaxometry

View Online   Export Citation   CrossMark

M. Flämig,[1] N. Fatkullin,[1,2] (iD) and E. A. Rössler[1,a] (iD)

AFFILIATIONS

[1] Nordbayerisches NMR-Zentrum, Universität Bayreuth, 95440 Bayreuth, Germany
[2] Institute of Physics, Kazan Federal University, Kremlevskaya 18, Kazan 420008, Tatarstan, Russia

[a] Author to whom correspondence should be addressed: ernst.roessler@uni-bayreuth.de

ABSTRACT

The dynamics of cyanoadamantane (CN-ADA) in its plastically crystalline phase encompasses three processes: overall tumbling of the rigid molecule, rotation around the molecular symmetry axis, and vacancy diffusion. This makes CN-ADA a prototypical case to be studied by field-cycling as well as by conventional NMR relaxometry. Data are collected from 430 K down to about 4 K and frequencies in the range of 10 kHz–56 MHz are covered. The overall tumbling is interpreted as a cooperative jump process preceding along the orthogonal axis of the cubic lattice and exhibiting a temperature independent non-Lorentzian spectral density. Consequently, a master curve is constructed, which yields model-independent correlation times, which agree well with those reported in the literature. It can be interpolated by a Cole-Davidson function with a width parameter $\beta_{CD} = 0.83$. The uniaxial rotation persisting in the glassy crystal ($T < T_g = 170$ K) is governed by a broad distribution of activation energies, $g(E)$. In this case, the standard master curve construction applied for the overall tumbling, for example, fails, as the actually probed distribution of correlation times $G(\ln \tau)$ strongly changes with temperature. We suggest a scaling method that generally applies for the case that a relaxation process is determined by a distribution of thermally activated processes. Frequency as well as temperature dependence of the relaxation rate can be used to reconstruct $g(E)$. In addition, $g(E)$ is extracted from the proton line-shape, which was measured down to 4 K. Vacancy diffusion governs the relaxation dispersion at highest temperatures; yet, a quantitative analysis is not possible due to instrumental limitations.

Published under license by AIP Publishing. https://doi.org/10.1063/1.5126953

I. INTRODUCTION

Plastically crystalline (PC) solids are often taken as model systems for studying the glass transition phenomenon.[1–3] In contrast to structural glasses, they show positional order but orientational disorder. Provided that the transition to an orientationally ordered crystalline phase is avoided, the dynamic disorder of the PC phase can be slowed down and finally be arrested by cooling below the glass transition temperature T_g yielding a so-called glassy crystal.[4,5] Many such systems were studied in the past by a variety of techniques,[6–11] and cyanoadamantane (CN-ADA) is a prototypical case.[9,12–21] The molecule is rigid and of globular shape [see the inset of Fig. 3(b)]. It forms a PC phase below the melting point $T_m = 462$ K. At $T_t = 280$ K,

a transition to an ordered monoclinic phase is observed. Supercooling the PC phase below T_t leads to a progressive slow-down of the overall molecular reorientation. As demonstrated among others by ^{2}H NMR spectroscopy,[16,18,21] the main molecular axis given by the CN direction reorients via 90° jumps among the six directions of the cubic lattice—an (isotropic) overall reorientation of the molecule characterized by a single correlation time. It shows an Arrhenius temperature dependence at high temperatures, whereas the apparent activation energy increases approaching $T_g = 170$ K.[10] Clearly, theses jumps can only take place provided that several molecules participate in a concerted action, i.e., a certain extent of cooperativity is needed to accommodate each jump. This is an important difference to the so-called rotor phases such as solid benzene, for example,

for which motional processes are observed, which are induced by the high symmetry of the molecule. The presence of some extent of cooperativity is the reason for considering plastic crystals as model systems for glass formation.

In addition to the overall reorientation of the molecule, a (faster) uniaxial reorientation around the main (C_3) axis of the molecule is found, which leads to partly averaged solid-state NMR spectra in the PC phase.[14,16,21] Only below 140 K, this motion becomes slow enough to broaden the NMR spectra. The uniaxial rotation is also observed in the ordered phase and an Arrhenius temperature dependence is observed, typical of a simple thermally activated process as expected for a noncooperative motion controlled by the symmetry of the molecule.[21] As demonstrated by neutron scattering[22] and by ^{2}H NMR,[21] the uniaxial rotation is described by an angular jump process of 12-fold and 3-fold symmetry, respectively. In addition, the ^{2}H NMR study revealed "two phase" spectra and strong nonexponential spin-lattice relaxation in the glassy PC phase, suggesting the presence of a broad distribution of jump times, i.e., heterogeneous dynamics is observed. It was assumed to be controlled by a temperature independent distribution of activation energies $g(E)$, in contrast to the ordered phase, showing a single and much higher activation barrier.[21] The reorientation of the C_3 axis itself, i.e., the overall tumbling of the molecule, is neither present in the ordered nor in the glassy crystalline phase.

Amoureux *et al.* studied CN-ADA in the dynamically disordered phase by ^{1}H NMR relaxometry.[14,16] Covering a temperature range from 360 K down to about 100 K and Larmor frequencies in the range of 30 MHz–400 MHz, the spin-lattice relaxation times T_1 (and T_{1rho}) were studied. In addition to the two aforementioned processes, the authors discussed vacancy diffusion, which determined the T_{1rho} data at highest temperatures. A jump model of the overall molecular reorientation reproduced the high-temperature relaxation data. Regarding the uniaxial rotation in the glassy crystal, a description by a distribution of "residence times" was suggested; however, no attempts were made to provide a quantitative interpolation of the low-temperature data. In a later study on chloroadamantane, the authors presented field-cycling (FC) ^{1}H as well as ^{13}C NMR relaxation data, essentially suggesting a similar motional scenario as in the case of CN-ADA.[23]

Regarding translational dynamics in plastic crystals, the first FC studies were published by Stapf and Kimmich and by Kimmerle *et al.*[7,24] Among other systems, cyclohexane was studied.[7] Measuring the dispersion of the proton relaxation time in dilution with deuterated cyclohexane, the low-frequency dispersion was identified to be dominated by intermolecular relaxation, whereas the high-frequency part was interpreted as predominantly of intramolecular origin. From the low-frequency part, the diffusion coefficient was extracted along the square root dispersion law to hold for 3D diffusion.[25] The values agreed well with those measured by field gradient NMR.[7]

In the present contribution, we report on a proton FC NMR study of CN-ADA, which covers the spin-lattice relaxation rate $R_1 = 1/T_1$ measured at Larmor frequencies (ω) in the range of 10 kHz–30 MHz and at temperatures from 430 K down to 150 K. Preliminary FC NMR results were reported in Ref. 26. The FC technique has gained a new momentum with the availability of commercial relaxometers since about 2000.[27–32] In addition, we measured T_1

at three Larmor frequencies with a standard high-field NMR spectrometer down to 4.1 K. Covering a much wider frequency and temperature range compared to previous studies, we are able to present a quantitative description of the $T_1(T, \omega)$ data or, in other words, the spectral density describing the overall molecular reorientation and the uniaxial rotation, respectively. In the case of the overall reorientation, frequency-temperature superposition (FTS) works well and allows us to overcome the still narrow frequency window of the FC relaxometer. In contrast to the previously assumed jump model,[16] we find indications that the spectral density has to be described by a non-Lorentzian shape—as expected for cooperative ("glassy") dynamics. In the case of the uniaxial rotation, we demonstrate that a distribution of activation energies described by a skewed Gaussian function allows us to reproduce the relaxation data in the glassy crystal down to lowest temperatures. In the case of thermally activated processes, FTS fails; yet, we suggest a scaling procedure that allows us to construct master curves.

II. THEORETICAL BACKGROUND

A. Relaxation, spectral density, and susceptibility representation

Proton relaxation in molecular systems is dominated by the magnetic dipole-dipole interaction. Generally, the spin-lattice relaxation rate, $R_1(\omega) = 1/T_1(\omega)$ with $\omega = \gamma B$ denoting the Larmor angular frequency, is a sum of two contributions,[31,33]

$$R_1(\omega) = R_{1,\text{intra}}(\omega) + R_{1,\text{inter}}(\omega). \quad (1)$$

The intramolecular relaxation rate $R_{1,\text{intra}}(\omega)$ reflects interactions between protons belonging to the same molecule and thus probes molecular rotation. The intermolecular rate, $R_{1,\text{inter}}(\omega)$, originates from the interactions between the protons of different molecules. It is caused by translational as well as by rotational dynamics. In crystals, in contrast to liquids, translational and rotational dynamics are usually well separated. Equation (1) implies an exponential magnetization recovery characterized by a single, well-defined relaxation rate, i.e., the spin system is describable by a common spin temperature.[34]

The frequency dependence of the relaxation rate is given by a linear combination of spectral densities $J(\omega)$. The latter is the Fourier transform of the rotational or the translational correlation function $C_i(t)$. The relaxation dispersion can also be analyzed in the susceptibility representation[23,28,36–38] based on the connection of linear response theory and the fluctuation-dissipation theorem. Equilibrium fluctuations described by $J(\omega)$ are connected to the response represented by a (normalized) dynamic susceptibility $\chi''(\omega)$ along $\chi''(\omega) = \omega J(\omega)$. This is advantageous when comparing with dielectric or rheological results, for instance, and also when constructing master curves (see below). Consequently, one can rewrite the Bloembergen, Purcell, and Pound (BPP) type equation,

$$\omega R_1(\omega) = K[\chi''(\omega) + 2\chi''(2\omega)] \cong 3K\chi''_{\text{FC}}(\omega) \equiv \chi''_{\text{NMR}}(\omega), \quad (2)$$

where K denotes the corresponding coupling constant, which can be expressed in terms of the relevant second moment. In this case, the integral over $\chi''_{\text{FC}}(\ln \omega)$ yields $\pi/2$, like the integral of $J(\omega)$. We note

that $\chi''_{\text{NMR}}(\omega\tau)$ is shifted by a factor of 0.616 to lower frequencies with respect to the dielectric susceptibility $\chi''_{\text{DS}}(\omega\tau)$, for example.

The CN-ADA molecules undergo an overall reorientation and a threefold rotation around the symmetry axis of the molecule, as said. The situation somewhat resembles that of the Woessner model, describing an isotropic small-step rotational diffusion of the molecule in addition to a rotational diffusion around some molecular axis.[39,40] However, the overall reorientation of CN-ADA is not a small-step rotational diffusion nor is it a simple single-particle jump process (as assumed by Amoureux *et al.*[16]). Instead, as revealed by the results from ^{2}H NMR mentioned in the Introduction, the jumps along the cubic lattice directions are part of a cooperative process.[20] Specifically, as the deuteron spin-lattice relaxation is essentially exponential and the corresponding line-shape changes can be described by a single time constant, the dynamics of the overall reorientation is of homogeneous nature with a weakly nonexponential reorientational correlation function or non-Lorentzian spectral density not expected to change its shape with temperature (as proven by ^{2}H stimulated echo experiments).[20] Such isotropic jumps completely average to zero the quadrupolar interaction just like in liquids.[20,21] We emphasize that from measuring the spectral densities alone one cannot distinguish between homogeneous and heterogeneous dynamics. That is why we took results from ^{2}H NMR as input for the modeling the proton relaxation.

Regarding the uniaxial rotation, it was demonstrated that a threefold jump occurs, the dynamics of which is governed by a broad distribution of correlation times.[21] As said in the Introduction, nonexponential relaxation and characteristic spectra are observed below T_g by ^{2}H NMR. In other words, pronounced dynamic heterogeneities are present, a fact not fully accounted for by Amoureux *et al.*, either. However, the molecular reorientation at a given site in the disordered crystal is determined by the symmetry of the molecule and is thus expected to be described by the Lorentzian spectral density.

A third process has to be considered. The full dipolar coupling, i.e., intra and intermolecular coupling, of the fast overall reorientation as well as of the fast uniaxial rotation do not completely average the intermolecular interaction. The latter is only relaxed by translational motion, i.e., by vacancy diffusion.

B. Description of the overall reorientation

In the case of an isotropic reorientation, the BPP equation is written as[33]

$$R_1(\omega) = 2/3\gamma^2\Delta M_{2,\text{iso}}\left[J_{\text{intra}}(\omega) + 4J_{\text{intra}}(2\omega)\right]. \quad (3)$$

The spectral density $J_{\text{intra}}(\omega)$ is the Fourier transform of the rotational correlation function $C_{\text{rot}}(t)$. There is also some intermolecular relaxation contribution caused by reorientation (so-called eccentricity effect),[35] which is difficult to access without isotope dilution experiments. Here, we assume that its spectral density is similar to that of $J_{\text{intra}}(\omega)$, and $\Delta M_{2,\text{iso}}$ is taken as an effective second moment "relaxed" by overall reorientation. As the latter displays cubic symmetry, we take Eq. (3) for describing the corresponding relaxation rate at high temperatures, i.e., $\Delta M_{2,\text{iso}}$ and $J_{\text{intra}}(\omega) \cong J_{\text{iso}}(\omega)$.

As the overall reorientation is part of a cooperative process, one expects a non-Lorentzian spectral density. As in the case of

supercooled liquids, we assume a Cole-Davidson (CD) spectral density[41]

$$J_{\text{iso}}(\omega) = J_{\text{CD}}(\omega) = \frac{\sin\left[\beta\arctan(\omega\tau_{\text{CD}})\right]}{\omega\left[1 + (\omega\tau_{\text{CD}})^2\right]^{\frac{\beta}{2}}} \quad (4)$$

with $\tau_{\text{iso}} = \tau_{\text{CD}}\beta = J_{\text{iso}}(0)$ and a stretching parameter $0 < \beta_{\text{CD}} \leq 1$. The intermolecular relaxation rate caused by molecular translation (vacancy diffusion) occurs on much longer time scales and can be omitted for the analysis of the overall reorientation.

An additional feature is characteristic of cooperative processes. The dynamic susceptibility does not change significantly with temperature except for its time constant. Hence, one can construct master curves by applying FTS.[23,37,38,42] In other words, the (normalized) susceptibility can be expressed in terms of a temperature independent susceptibility function χ'' of a temperature-dependent argument $\omega\tau$, where here $\tau = \tau_{\text{iso}}(T)$ is the characteristic time constant of the overall reorientation, explicitly $\chi''_{\text{NMR}}(\omega) = \omega R_1(\omega) = \chi''_{\text{iso}}(\omega\tau_{\text{iso}})$. Thereby, the spectral range effectively covered is significantly expanded. The approach is well established in the rheology of polymeric systems,[42] for example, and was recently applied to liquids and polymers by FC NMR relaxometry.[28,30,37,38] Actually, it was shown to be applicable regarding the dielectric spectra of CN-ADA, either.[10] Such FC master curves were also discussed in the case of chloroadamantane, yet, resulting from a narrow temperature interval.[23] We will document to which extent FTS works.

C. Description of the uniaxial rotation

The uniaxial rotation of CN-ADA is assumed to be governed by a temperature independent distribution of activation energies, $g(E)$ ($T < T_g$). In this case, FTS fails as the corresponding (normalized) distribution of correlation times $G(\ln\tau)$ strongly broadens upon lowering the temperature along

$$G(\ln\tau) = RTg\left(RT\ln\left(\frac{\tau}{\tau_0}\right)\right). \quad (5)$$

Here, we assume an Arrhenius temperature dependence for a given site in the amorphous matrix, specifically $\ln(\tau/\tau_0) = E/RT$, where τ_0 denotes an exponential prefactor or attempt time, which is taken to be temperature independent. Of course, assuming a constant attempt time may be a severe simplification. One can improve the description by assuming a kind of Meyer-Neldel rule connecting τ_0 (or equivalently the activation entropy) with E.[43,44] However, this introduces another parameter, and it cannot be easily implemented in the present scaling procedure described below.

As we considered proton relaxation, due to efficient spin diffusion, the spin-lattice relaxation is exponential even in the case of dynamic heterogeneities, and the relaxation rate averaged over the heterogeneous dynamics is given by the integral over $G(\ln\tau)$,

$$\left\langle\frac{1}{T_1}(T,\omega)\right\rangle = \frac{2}{3}\gamma^2\Delta M_{2,\text{uni}}\left[\int_{-\infty}^{\infty} G(\ln\tau)\left[\frac{\tau}{1 + (\omega\tau)^2}\right.\right.$$
$$\left.\left. + 4\frac{\tau}{1 + (2\omega\tau)^2}\right]d\ln\tau\right]. \quad (6)$$

Again, $\Delta M_{2,\text{uni}}$ is an effective second moment including also intermolecular rotational contributions. Together with $\Delta M_{2,\text{iso}}$, it provides the total rotational second moment, explicitly $M_{2,\text{rot}} = \Delta M_{2,\text{iso}} + \Delta M_{2,\text{uni}}$. Within a Frenkel model, the threefold jump process can be described by Eq. (6) with $\Delta M_{2,\text{uni}} = 0.747 M_{2,\text{rot}}$ yet, including only intramolecular relaxation contributions.[16,23] The quantity $M_{2,\text{rot}}$ has to be distinguished from $M_{2,\text{total}}$ measured at lowest temperatures, which includes the residual intermolecular coupling not averaged by the fast overall reorientation (see below). The corresponding second moment will be compared to what can be extracted from the independently measured $M_2(T)$ behavior as reported in the literature.[16]

Introducing the distribution of activation energies $g(E)$, one gets

$$\left\langle \frac{1}{T_1}(T,\omega) \right\rangle = K\left[\int_0^\infty g(E)\left[\frac{\tau(E)}{1+(\omega\tau(E))^2} + 4\frac{\tau(E)}{1+(2\omega\tau(E))^2} \right] dE \right] \tag{7}$$

with

$$K = \frac{2}{3}\gamma^2 M_{2,\text{uni}}. \tag{8}$$

It is worthwhile to discuss the temperature dependence of $\left\langle \frac{1}{T_1} \right\rangle$ assuming different (but simple) distribution functions $g(E)$, as the trace of $\left\langle \frac{1}{T_1} \right\rangle = f\left(\frac{1}{T}\right)$ depends sensitively on the details of $g(E)$. We compare a Gaussian distribution with a left-skewed or right skewed Gaussian. The definitions of the functions are given in the Appendix, the distributions are plotted in Fig. 1(a), and the corresponding curves, $1/\left\langle \frac{1}{T_1} \right\rangle$ vs temperature, are shown in Fig. 1(b). Although $g(E)$ does not differ strongly, the dependence of $1/\left\langle \frac{1}{T_1} \right\rangle$ with temperature displays quite a different behavior. In no case, an Arrhenius temperature dependence is observed in the limits $\omega\tau \ll 1$ and $\omega\tau \gg 1$, respectively; instead, a behavior resembling more a power-law behavior is found at low temperatures ($\omega\tau \gg 1$). For example, the right-skewed distribution displays higher amplitudes at high activation energies and corresponding $1/\left\langle \frac{1}{T_1} \right\rangle$ increases steeper with $1/T$ compared to a Gaussian. The left-skewed distribution features higher amplitudes at low energies and $1/\left\langle \frac{1}{T_1} \right\rangle$ grows much slower
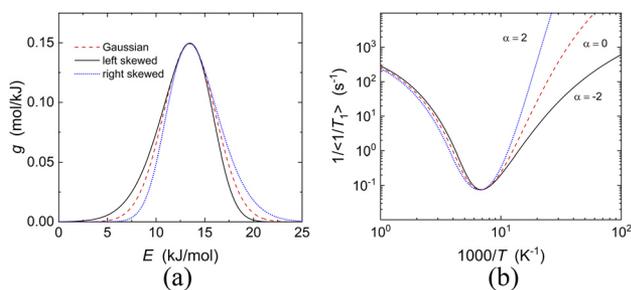

FIG. 1. (a) Distribution of activation energies: Gaussian, left skewed, and right skewed Gaussian with similar most probable activation energy; the parameter α defines the extent of skewness. (b) Corresponding $1/\left\langle \frac{1}{T_1} \right\rangle$ calculated along Eq. (7) vs inverse temperature in a double logarithmic plot.

with $1/T$. The differences at high temperatures are less pronounced as the distribution $G(\ln\tau)$ becomes narrow. At infinite high temperature, all distributions $G(\ln\tau)$ originating from different $g(E)$ would collapse to a delta function, i.e., differences among $g(E)$ become more and more unimportant at high temperature.

In order to further understand the temperature dependence of $1/\left\langle \frac{1}{T_1} \right\rangle$, we consider the extreme-narrowing condition and the slow-motion condition, i.e., the behavior at sufficiently high and at sufficiently low temperature, respectively,

$$\left\langle \frac{1}{T_1}(T,\omega) \right\rangle = 5K \int_{-\infty}^\infty G(\ln\tau)\tau\, d\ln\tau \quad \omega\tau \ll 1, \tag{9}$$

$$\left\langle \frac{1}{T_1}(T,\omega) \right\rangle = \frac{2K}{\omega^2} \int_{-\infty}^\infty G(\ln\tau)\frac{1}{\tau}\, d\ln\tau \quad \omega\tau \gg 1. \tag{10}$$

In other words, at $\omega\tau \ll 1$ (high temperatures), the temperature of the mean correlation $\langle\tau\rangle$ is probed, whereas at $\omega\tau \gg 1$ (low temperatures), the mean rate $\langle r \rangle = \langle 1/\tau \rangle$. Consequently, quite different aspects of the distribution $G(\ln\tau)$ are probed at low and high temperatures, respectively. Another feature is recognized in Eq. (10): In the slow-motion regime, the frequency dependence of the relaxation rate goes with $1/\omega^2$. This is not the case if a non-Lorentzian correlation function like a CD function, for example, describes the orientational correlation function.

D. Scaling the relaxation rates when governed by a distribution of activation energies

As introduced in Eq. (2), the relaxation data described by Eq. (6) transformed into the susceptibility representation ω/T_1 yield a relaxation peak due to the terms like $\frac{\omega\tau}{1+(\omega\tau)^2}$. In the case of a broad distribution $g(E)$ and thus a broad distribution $G(\ln\tau)$, the susceptibility directly reflects the distribution of correlation times $G(\ln\tau)$. As the evolution of $G(\ln\tau)$ is controlled by a temperature independent distribution $g(E)$, one can derive a scaling procedure of the susceptibility spectra. Such master curve construction was applied before in the case of dielectric or light scattering data rescaling the corresponding susceptibility.[45–48] The only difference is that the NMR relaxation is described by two susceptibility functions [cf. Eq. (2)]. Hence, under the condition of a broad $G(\ln\tau)$, the sum of the two Lorentzians in the "BPP function" can be approximated by a delta function at the position of the maximum of this function, which is given by $\tau_{\max} \approx 0.616/\omega \equiv 1/(\alpha\,\omega)$. Thus, we write

$$\frac{\omega\tau}{1+(\omega\tau)^2} + 4\frac{\omega\tau}{1+(2\omega\tau)^2} \cong \frac{3\pi}{2}\delta(\ln\tau - \ln(1/(\alpha\omega))). \tag{11}$$

Note that the factor $\pi/2$ results from the integral over the Lorentzian, and the factor 3 follows from the BPP equation [cf. Eq. (2)].

Introducing this into Eq. (6), we can calculate the mean relaxation rate,

$$\omega\left\langle \frac{1}{T_1}(\omega) \right\rangle = \omega R_1(\omega) = \frac{3}{2}\pi K\left[\int_{-\infty}^\infty G(\ln\tau)\delta(\ln\tau - \ln(1/(\alpha\omega)))\, d\ln\tau \right]$$

$$= \frac{3}{2}\pi K G(\ln(1/(\alpha\omega))). \tag{12}$$

Finally, introducing $g(E)$, we get

$$K \cdot g(E) = K \cdot g(RT(\ln(v_0/v) - 0.48)) \cong \frac{2}{3\pi RT} \omega \left\langle \frac{1}{T_1}(\omega) \right\rangle \quad (13)$$

with $v = \omega/(2\pi)$ and $v_0 = 1/(2\pi\tau_0)$. In other words, plotting the right hand side of Eq. (13) vs $RT(\ln(v_0/v) - 0.48)$ yields a master curve, which reveals the distribution $g(E)$. Here, the attempt frequency v_0 is assumed to be constant for all E. Generally, it can be obtained by bringing measurements at different T and v to best overlap. In the cases when only a few datasets are at hand, by varying v_0 one gets different values of K via integrating the left part of Eq. (13). The value of v_0 is fixed, when K is taken from an independent experiment.

E. Line-shape analysis of the uniaxial rotation

Again, we consider the case of a broad distribution of correlation times, $G(\ln \tau)$, which describes the uniaxial rotation in the glassy PC phase. Instead of observing a continuous transition from a spectrum in the limit of slow motion, $S_{\text{slow}}(\omega)$, to an "intermediate" spectrum and finally at high temperatures to a spectrum in the limit of fast motion, $S_{\text{fast}}(\omega)$, one expects the so-called "two-phase" spectra.[49–51] They are described by a sum of the two subspectra,

$$S(\omega, T) = S_{\text{fast}}(\omega) W(T) + S_{\text{slow}}(\omega)[1 - W(T)], \quad (14)$$

with the weighting factor given by[50]

$$W(T) = \int_{-\infty}^{\ln \tau^*} G(\ln \tau) d\ln \tau. \quad (15)$$

The factor $W(T)$ quantifies the fraction of molecules reorienting with correlation times shorter than the corresponding inverse dipolar coupling $1/\delta \cong \tau^*$. Due to the broad distribution, the contribution of intermediate spectra with $\tau \cong 1/\delta$ can be neglected as well as the effect of the reduction factor when applying a solid-echo pulse sequence. In the case of proton NMR on CN-ADA, the solid-state spectrum of rigid protons $S_{\text{slow}}(\omega)$ as well as the motionally averaged spectrum $S_{\text{fast}}(\omega)$ resemble more or less a Gaussian spectral shape. However, a quantitative description cannot be given easily. Therefore, in order to determine $W(T)$, we take the experimentally observed spectra $S_{\text{slow}}(\omega)$ and $S_{\text{fast}}(\omega)$ monitored at low and high temperatures, respectively. As before, the distribution $G(\ln \tau)$ is assumed to be the result of a temperature independent distribution

of activation energies, $g(E)$, and the derivative of $W(T)$ provides an estimate of $g(E)$ along[50]

$$g(E) = f^{-1} \partial W(T)/\partial T \quad \text{with} \quad f = R \ln(\tau^*/\tau_0). \quad (16)$$

The factor f converts the temperature scale into an energy scale and may be estimated from the condition $\tau^* \delta \approx 1$. The quantity f is relatively insensitive with respect to the numerical values of τ^* and τ_0 because f depends logarithmically on them. For a proton line with a half width of about 65 kHz as given by the low temperature spectrum of CN-ADA, a value $\tau^* = 2.5 \ 10^{-6}$ s is found. The value τ_0 is provided by the $T_1(T)$ analysis (see below). Thus, the such performed line-shape analysis provides a third way to get an estimate of $g(E)$, which governs the uniaxial rotation of CN-ADA.

III. EXPERIMENTAL

Cyanoadamantane was purchased from Sigma Aldrich, and the samples were carefully degassed and flame sealed under vacuum, without further treatment. The proton spin-lattice relaxation was measured in the frequency range of 10 kHz–30 MHz and in the temperature range of 150–430 K employing a FFC 2000 relaxometer (STELAR). The temperature error was below 1 K, and the stability was better than ±0.5 K. In addition, the spin-lattice relaxation at three Larmor frequencies $\omega/2\pi = 20.5$ MHz, 46 MHz, and 54.15 MHz was measured down to 4.1 K by using a high field spectrometer (CXP 200) equipped with an electromagnet.[51] A homebuilt probe head was immersed in an Oxford cryostat CFA 1200. A solid echo sequence with an interpulse distance $t_p = 10 \ \mu s$ was applied to monitor the recovery of the NMR signal following a saturation sequence. The temperature precision was below 0.1 K as well as the stability.

IV. RESULTS

Figure 2(a) shows the relaxation rate $R_1(\omega)$ as a function of the (Larmor) frequency for different temperatures in the range of 153 K–433 K. For most temperatures, strong dispersion is observed and it is rather difficult to identify different relaxation processes. At the highest temperature T = 433 K (red filled squares), a weak, plateaulike dispersion is found at high frequencies, whereas dispersion sets in at low frequencies. The level of the plateau rises with decreasing temperature and with dispersion setting in at
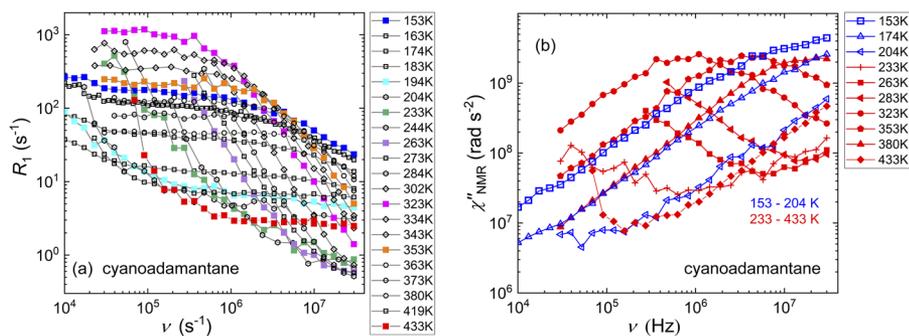

FIG. 2. (a) Proton relaxation rate of cyanoadamantane as a function of frequency measured by FC NMR over a broad temperature range; data points are connected by polygon lines. (b) Susceptibility representation of selected data in (a), $\chi''_{\text{NMR}}(v) = v \cdot R_1(v)$, relaxation curves reflecting the dominance of different relaxation processes are marked by different colors.

high frequencies the plateau appears to shift to lower frequencies (cf. $T = 353$ K and $T = 323$ K, orange and magenta filled squares, respectively). Going to even lower temperatures, the low-frequency plateau vanishes. Instead, strong dispersion is observed at all frequencies, which shifts to lower frequencies upon further cooling (see $T = 263$ K and $T = 233$ K, violet and green filled squares, respectively). Finally, at even lower temperatures, another plateau emerges, which moves to higher values at the lowest temperatures (cf. $T = 193$ K and $T = 153$ K, cyan and blue squares, respectively).

Clearly, the relaxation behavior in the rate representation (together with the many datasets) is difficult to interpret. However, this changes when turning to the susceptibility representation of the data—see Fig. 1(b), i.e., we plotted $\chi''_{\mathrm{NMR}}(\nu) = \nu \cdot R_1(\nu)$ against frequency for selected datasets. High- (red symbols) and low-temperature data (blue symbols) are distinguished. The high-temperature data clearly display a relaxation maximum shifting to lower frequencies upon cooling. Another dispersion regime is recognized around $T = 233$ K (crosses), where a minimum in the susceptibility appears. At even lower temperatures, a second, higher relaxation maximum can be anticipated, which is not fully covered, due to the temperature limitation of the FC relaxometer. Taking recourse to previous dielectric and deuteron NMR studies,[10,20,21] which identified a relatively slow overall orientation of the CN-ADA molecule and a relatively fast uniaxial rotation, we consequently attribute the high-temperature relaxation to the overall molecular reorientation and the low-temperature relaxation to the faster uniaxial rotation. This attribution will be further substantiated below.

There is another subtle feature observed at $T = 419$ K and $T = 433$ K, and at low frequencies in Fig. 2: A minimum is recognized at low frequencies in Fig. 2(b) and an onset of dispersion in Fig. 2(a) (see also Fig. 4), indicating the appearance of another dispersion regime attributed to the slowest dynamics in the system: translational diffusion due to lattice vacancies as already documented in previous $T_{1\rho}$ studies.[16] This relaxation is only reflected by proton spin-lattice relaxation (and not by deuteron NMR) due to the intra- and intermolecular character of the dipolar coupling, the

fluctuation of which causes the spin-lattice relaxation in the case of protons.

As justified by the results from deuteron spin-lattice relaxation and line-shape studies, the dynamics of the overall reorientation is of homogeneous nature with a weakly nonexponential reorientational correlation function.[20] In other words, we expect FTS to hold for the isotropic overall reorientation. Thus, as in the case of analyzing FC NMR data in liquids,[37,38] we first attempted to construct a master curve regarding the high-temperature data (reflecting the overall reorientation of CN-ADA). Explicitly, the susceptibility spectra at 433 K–233 K of Fig. 2 are shifted solely along the frequency axis to achieve the best overlap. The result is displayed in Fig. 3(a). Indeed, a master curve is obtained: Within the temperature range 294 K–380 K, a perfect overlap results. At higher and lower temperatures, the master curve construction clearly fails: here, relaxation by vacancy diffusion and by the uniaxial rotation becomes dominant, respectively. The spectral shape of the master curve does not follow a (symmetric) Debye curve (dotted line). Instead, it can be fitted by a CD function (dashed line) as is characteristic of cooperative dynamics with a stretching parameter $\beta_{CD} = 0.83 \pm 0.03$, revealing a weakly asymmetric peak shape. Thereby, the frequency axis is rescaled to provide $\chi''_{\mathrm{NMR}}(\omega\tau_{\mathrm{iso}})$ along $\tau_{\mathrm{iso}} = \beta_{CD}\,\tau_{CD}$. Thus, the corresponding rotational correlation function is (weakly) stretched as it is typically observed for cooperative (glassy) dynamics. From the integral over the susceptibility curve, an effective second moment $\Delta M_{\mathrm{iso}} = (3.75 \pm 0.09)\ 10^{-8}$ T^2 is extracted, which will be compared below to the value obtained from $M_2(T)$.

By constructing the master curve, the time constants $\tau_{\mathrm{iso}}(T)$ are obtained. In Fig. 3(b), they (red symbols) are compared to those reported by other techniques.[10,13,15,19,20] Very good agreement is found, which is the first confirmation that indeed FTS applies for the overall reorientation of the molecule. In the temperature range 220 K–300 K, the temperature dependence can be described by an Arrhenius law with an activation energy $E_{\mathrm{iso}} = 52$ kJ/mol (see the straight line in Fig. 4), whereas at higher temperatures, a crossover to another Arrhenius may be anticipated. Only at lowest temperatures, the apparent activation energy increases as is typical of "glassy dynamics" close to T_g. Given the parameters of the master curve,
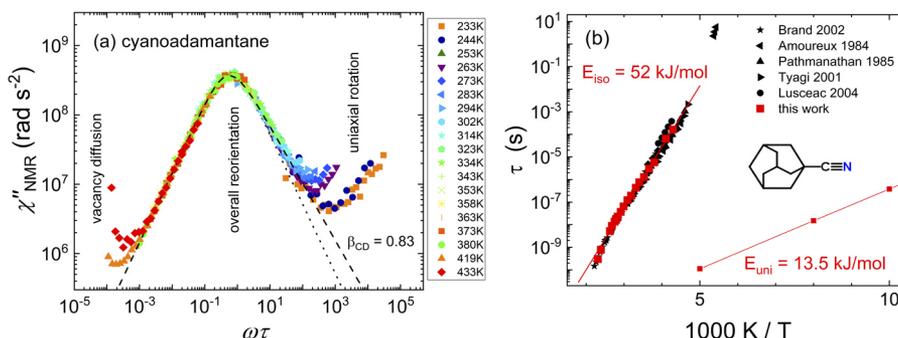

FIG. 3. (a) Susceptibility master curve of cyanoadamantane constructed from the high-temperature data displayed in Fig. 2. Different colors correspond to different temperatures; relaxation processes are indicated; the relaxation peak is described by a Cole-Davidson (CD) function (dashed line); for comparison, a Debye function is shown (dotted line). (b) Time constants of the overall reorientation as obtained by constructing the FC ^{1}H NMR master curve (red symbol); Arrhenius straight line is displayed; literature data from several sources are included.[10,13,15,19,20] We added the most probable time constant taken from the distribution $G(\ln \tau_{\mathrm{uni}})$ [Fig. 6(b)] and indicated the corresponding activation energy E_{uni} of the uniaxial rotation of the molecule.
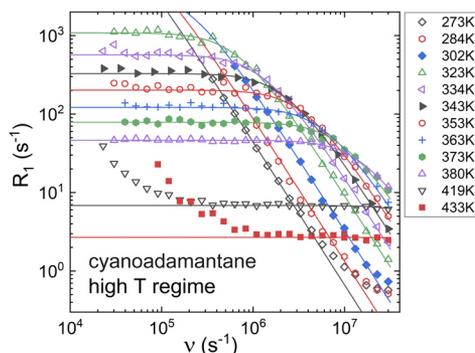
FIG. 4. Spin-lattice relaxation rate of cyanoadamantane in the high-temperature range as a function of frequency; solid lines: predictions calculated from the master curve [Fig. 3 (a)] together with $\tau_{iso}(T)$ from Fig. 3(b).

i.e., ΔM_{iso}, β_{CD}, and $\tau_{iso}(T)$, we show the prediction for the individual relaxation rates vs frequency in Fig. 4. Clearly, the master curve provides a satisfying interpolation of the rate dispersion at high-temperature.

In Fig. 4, at the highest temperatures 419 K and 433 K, one observes the onset of a further dispersion regime at low frequencies, which we attribute to vacancy diffusion, as mentioned before, and in accordance with the interpretation given by Amoureux *et al.*[16] Clearly, translation is significantly slower than the overall reorientation of the molecule. As 440 K is essentially the high-temperature limit of the current STELAR relaxometer, we were not able to fully cover this third dispersion regime. More importantly, at these temperatures close to the melting point $T_m = 460$ K, the sample started to sublimate and accumulated in the colder region at the top of the NMR tube being outside the receiver coil.

Instead of presenting dispersion spectra at the various temperatures, one can also display the temperature dependence of T_1 at different frequencies. This is done in Fig. 5(a) in a semilog and in Fig. 5(b) in a double-log plot, where we included, in the latter

figure, the results from conventional NMR measurements at three frequencies and low temperatures.[52] In addition, covering higher frequencies, we added the results from Amoureux *et al.*[16] (open symbols), which fit well into the scenario given by our results. For example, our FC NMR measurement with $\omega/2\pi = 30$ MHz well reproduces the result of Amoureux *et al.* at the same frequency. However, the result at $\omega/2\pi = 200$ MHz of Amoureux does not fit to the other low temperature data, a fact already noted by Amoureux *et al.*;[16] it was removed from the discussion. As expected, the relaxation data [Fig. 5(b)] exhibit two minima, which are attributed to the overall reorientation of the molecule (at high temperatures) and to the uniaxial rotation (at low temperatures). Corresponding to each relaxation process, two regimes are recognized for which the relaxation is essentially frequency independent (extreme narrowing condition). The temperature dependence of T_1 at low temperatures resembles more a power-law behavior with an exponent even decreasing at lowest temperatures. This leads to a situation that at 4.1 K the relaxation is still sufficiently short to be experimentally accessible. Surprisingly, the temperature dependence of T_1 does not change discontinuously around T_g as it may be expected.

Concerning the overall reorientation, in Fig. 5(a), we have included the prediction for $T_1(T)$ for each frequency given by the master curve and $\tau_{iso}(T)$ [see Fig. 3(b)]. Again, an almost perfect reproduction is achieved for the temperature range for which the dominance of the overall molecular tumbling can be anticipated. In the case of the data of Amoureux *et al.*, small systematic deviations are found, the higher the frequency, yet, the overall trend is reproduced well. This can easily be explained by a crossover to a higher activation energy at highest temperatures, which was not taken into account by our calculation. As the susceptibility function is described by an (asymmetric) CD function with a stretching parameter $\beta_{CD} = 0.83$ and given an Arrhenius temperature dependence of $\tau_{iso}(T)$ in the considered temperature interval, the relaxation minimum in this representation is not expected to be symmetric. Instead, the apparent high-temperature activation is given by E_{iso}, whereas the low-temperature value is given by $\beta_{CD}E_{iso}$ [cf. Fig. 5(a)]. As β_{CD} is close to one, the effect is small.
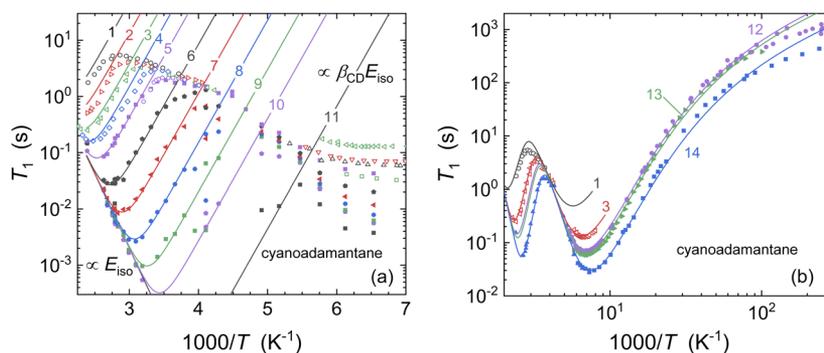

FIG. 5. (a) Proton spin-lattice relaxation time of cyanoadamantane as a function of reciprocal temperature; present FC data (full symbols, only selected frequencies are shown), data by Amoureux *et al.*[16] (open symbols), solid lines: calculated from the parameters of the master curve (cf. Fig. 3). (b) Relaxation times of (a) as a function of reciprocal temperature in a double-log plot; added are rates measured by conventional NMR;[52] solid lines: calculation including overall reorientation and uniaxial rotation (see text). Numbers 1–14 correspond to frequencies in MHz: 400, 200, 100, 60, 30, 9.9, 3.3, 1.1, 3.6, 0.12, 0.01, 54.15, 46.06, and 20.5.

Next, we turn our attention to the analysis of the low-temperature relaxation rate, which is solely determined by the uni-axial rotation of the CN-ADA molecule. As discussed in the Introduction, from ^{2}H NMR studies one knows that the reorientation in the glassy crystal, i.e., below $T_g = 170$ K, is described by a broad distribution of correlation times $G(\ln \tau_{uni})$ reflecting heterogeneous dynamics.[21] In the glassy PC phase, exchange (i.e., diffusion) among the different sites can safely be ruled out. The reorientation itself can be described by a C_3 jump process around the molecular symmetry axis, which at a given site in the glassy crystal is assumed to be determined by a single activation energy. Due to a disordered spatial distribution of the cyano groups, which is characteristic of the glassy phase, the local potentials vary significantly, and one expects a distribution of activation energies $g(E)$, which we assume to be temperature independent. The resulting distribution $G(\ln \tau_{uni})$, however, is not temperature independent; instead, it broadens with $1/T$ along Eq. (5). Thus, FTS does not apply in this case. Still, a master curve can be constructed by appropriately compensating the broadening with $1/T$. Referring to Theoretical Background [Eq. (13)], we show in Fig. 6(a) the such obtained master curve, which provides a first estimate of the distribution $g(E)$ (black points). Explicitly, we plotted $\frac{2}{3\pi\,RT}\omega\left\langle \frac{1}{T_1}(\omega)\right\rangle$ vs $RT(\ln(\nu_0/\nu) - 0.48)$. The integral over $g(E)$ yields the effective second moment $\Delta M_{2,uni}$, and the attempt frequency $\nu_0 = \frac{1}{2\pi\tau_0}$ is chosen such that the second moment takes the value $\Delta M_{2,uni} = \Delta M_{2,iso}/(1 - 0.747) = 14.8 \cdot 10^{-8}\ T^2$ as suggested by the Frenkel model. Here, $\Delta M_{2,iso} = 3.75 \cdot 10^{-8}\ T^2$ is taken from the high temperature T_1 analysis. The resulting value reads $\tau_0 = 3.3 \cdot 10^{-14}$ s.

A more advanced analysis follows Eq. (7) and attempts to find a distribution of activation energies $g(E)$, which simultaneously describes the $T_1(T)$ curves for all frequencies in Fig. 5(b). However, finding a simple analytical distribution function, which covers the salient features of the relaxation data in a quite broad temperature range of 10 K–200 K, is not an easy task. In particular, the choice of τ_0 influences the effective second moment $M_{2,uni}$ needed to cover the amplitude of the T_1 minimum. In addition, the low-energy flank of $g(E)$ sensitively determines $T_1(T)$ at lowest temperatures (see Theoretical Background). Vice versa, the high-energy flank influences the behavior at highest temperatures, and, of course, at high temperatures relaxation by the overall reorientations interferes. In order to
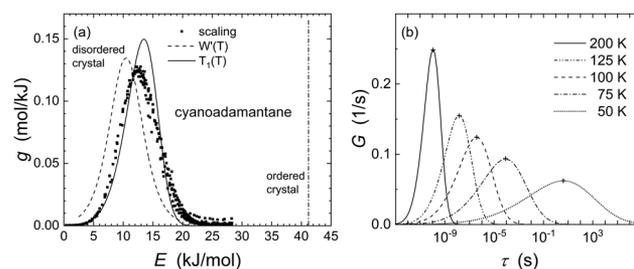

FIG. 6. (a) Distribution of activation energy $g(E)$ of the uniaxial reorientation of cyanoadamantane as given by different approaches: scaling the spin-lattice relaxation times along Eq. (13) (squares), fitting $T_1(T)$ as shown in Fig. 5(b) via Eq. (7) (solid line), analyzing the weighting factor $W(T)$ of the ^{1}H NMR spectra along Eq. (16) (dashed line). For comparison, we added the delta distribution of the ordered crystal.[21] (b) Distribution $G(\ln \tau_{uni})$ at some temperatures as calculated from $g(E)$ taken to interpolate the low-temperature relaxation data [cf. Fig. 5(b)].

proceed, we take the second moment $\Delta M_{2,uni} = 14.8 \cdot 10^{-8}\ T^2$ and $\tau_0 = 3.3 \cdot 10^{-14}$ s as done for the scaling analyses above. A left skewed Gaussian with $\mu = 15.6$ kJ/mol, $\sigma = 5.6$ kJ/mol and $\alpha = -2.0$ is able to reproduce the T_1 curves down to about 10–30 K as documented in Fig. 5(b). We included for the fit the description of the overall reorientation as additive contribution. The derived distribution $g(E)$ is included in Fig. 6(a) (solid line), demonstrating fair agreement with the data from the scaling procedure (solid squares). A subtle enhancement of $g(E)$ on the low-energy flank would provide even better agreement to lower temperatures. However, such tiny changes would not be discernible in Fig. 6(a). In addition, we cannot exclude that paramagnetic impurities control the relaxation at lowest temperatures, yet, the samples were carefully degassed. The corresponding evolution of $G(\ln \tau_{uni})$ as calculated from the fit of $T_1(T)$ is documented in Fig. 6(b). The distribution becomes extremely broad at low temperatures. The corresponding most probable time constant τ_{uni} is plotted in Fig. 3(b), providing its activation energy $E_{uni} = 13.5$ kJ/mol.

Finally, we present the result of analyzing the proton line-shape in the glassy crystal ($T < 140$ K). The solid-echo spectra measured are displayed in Fig. 7(a).[52] They are qualitatively different from
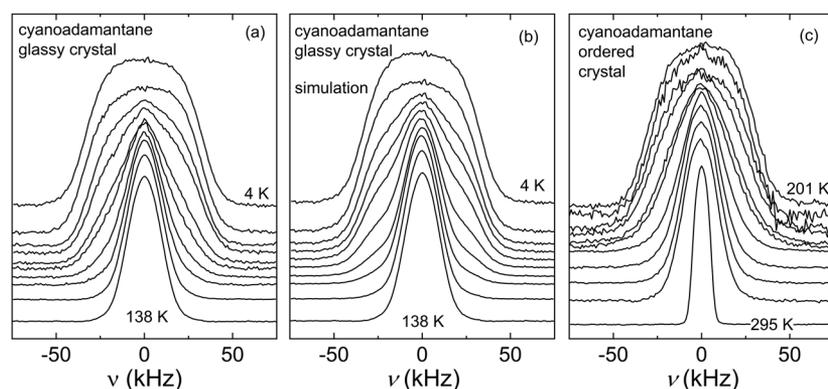

FIG. 7. Proton solid-echo spectra of the glassy PC phase (a) vs spectra of the orientationally ordered phase (c); simulation of the spectra in the glassy PC phase by assuming "two phase" spectra [(b), see text].

those acquired in the ordered phase, right column.[52] We recall that a uniaxial rotation is also observed in the ordered phase,[16,21] yet, governed by a single (and higher) activation energy, or equivalently, by $G(\ln \tau_{uni})$ or $g(E)$ being a delta function [cf. Fig. 6(a)]. The line shape transition spectra of the ordered phase, occurring at much higher temperatures compared to those of the disordered phase, display a continuous broadening with decreasing temperature. In contrast, the spectra in the glassy PC phase show the character of "two-phase" spectra in accordance with the findings of the ^2H NMR spectra.[21] They can be approximated by a weighted superposition of the spectrum acquired at the highest (138 K) and the one at low temperature (16 K) (middle column) [see Eq. (14)]. Such two-phase spectra are the fingerprint of a broad heterogeneous distribution of correlation times $G(\ln \tau_{uni})$.[50,51] In the case of the spectrum measured at 138 K, the rotation around the C_3 axis is fast ($\tau_{uni} \ll 1/\delta$) for all the molecules; at 16 K, the motion of the molecules is in the limit $\tau_{uni} \gg 1/\delta$.

The weighting factor $W(T)$ is shown in Fig. 8. It is obtained by analyzing the transition spectra of the PC phase [cf. Fig. 7(a)] along Eq. (14). The quantity $W(T)$ specifies the fraction of the subspectrum corresponding to the fast motion limit. A sigmoid curve is found starting from zero at lowest temperatures and reaching 1 at highest temperatures. As described in Theoretical Background, the derivative of $W(T)$ yields an estimate of the distribution of activation energies $g(E)$—see Eq. (15). Interpolating $W(T)$ by an error function and performing the derivative, the resulting distribution $g(E)$ is included in Fig. 6(a). Here, we assumed $\tau^* = 1/\delta = 1/(2\pi\,64.9\,kHz) = 2.5\,10^{-6}\,s^{-1}$ as given by the FWHM at low temperatures and $\tau_0 = 3.3\,10^{-14}$ given by the scaling procedure, which leads to $f = 151\,J\,K^{-1}\,mol^{-1}$ [Eq. (16)]. The distribution is close to the distributions provided by the other two approaches.

In Fig. 9, we display the full width at half maximum (FWHM) of the solid-echo spectra as a function of temperature (red filled squares) in the range of 4 K–140 K. Assuming a Gaussian line shape, we added the data calculated from the second moment data reported by Amoureux et al.[16] (open squares) at higher temperatures, explicitly FWHM = $2\sqrt{2\ln 2 M_2}\gamma/2\pi$. At intermediate temperatures (around 150 K), the such obtained FWHM values agree well with the present ones, indicating that indeed the spectrum can
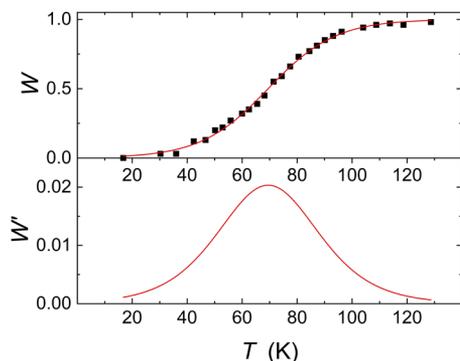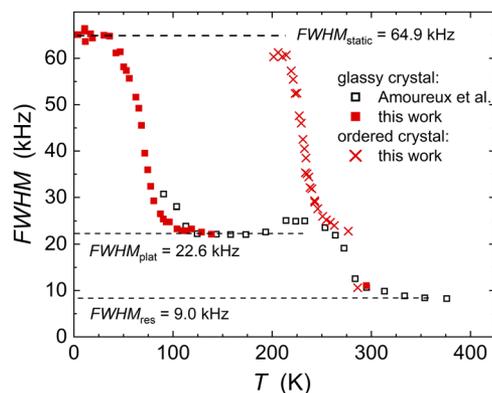

FIG. 9. Full width at half maximum (FWHM) of the solid-echo spectra as a function of temperature for the disordered (solid squares) and ordered (crosses) phase of cyanoadamantane; data from Amoureux et al.,[16] assuming Gaussian spectral shape are added (open squares).

be described by a Gaussian profile. Here, we note that a solid-echo spectrum only agrees with a CW spectrum (measured for obtaining the second moment) for an interpulse distance going to zero.[53] However, applying a short interpulse distance of $t_p = 10\,\mu s$, the difference is small and we neglect it for the following semiquantitative discussion. Starting from the lowest temperature, the spectral width sets in to decline above 40 K, due to the uniaxial rotation becoming fast with respect to the reciprocal spectral width of the low-temperature spectrum. A corresponding reduction is also observed in the ordered phase (red crosses); yet, it occurs at much higher temperatures. This again clearly demonstrates that the uniaxial rotation is significantly accelerated in the disordered phase.

In the supercooled PC phase, a further reduction of the width sets in above 240 K, which is due to the overall reorientation of the CN-ADA molecule becoming sufficiently fast. Such reduction at similar temperatures is also observed when monitoring the spectral width of the ordered phase. This is not surprising, since above $T_t = 280\,K$, the ordered phase transforms into the disordered phase. As seen from Fig. 4, at temperatures close to the melting point $T_m = 462\,K$, the dispersion data indicate additional dynamics in the megahertz range, which in accordance with previous work is attributed to the vacancy diffusion. This translational motion is expected to finally bring the residual M_2 down to zero.

It is of interest to compare the changes of the second moment with what is obtained by the relaxation analysis. From Amoureux et al.,[16] we extract a plateau value $M_{2,plat} = 5.3\,10^{-8}\,T^2$ at intermediate temperatures (corresponding to FWHM = 22.3 kHz in Fig. 9) and an estimate of $M_{2,res} \cong 0.7\,10^{-8}\,T^2$ (taken from the data point close to 360 K) for the residual dipolar coupling. The quantity $M_{2,res}$ reflects the remaining intermolecular coupling not averaged by the overall (isotropic) reorientation of the molecule. Thus, the effective second moment "relaxed" by the overall reorientation is $\Delta M_{2,iso} = M_{2,plat} - M_{2,res} = 4.6 \cdot 10^{-8}\,T^2$, which compares fairly well with the value $3.75 \cdot 10^{-8}\,T^2$ extracted from the relaxation analysis. We cannot extract the total second moment from the low-temperature limit value FWHM = 64.9 kHz as the corresponding line shape exhibits non-Gaussian spectral shape (see Fig. 7). From

FIG. 8. Weighting factor $W(T)$ describing the fraction of the subspectrum corresponding to the fast motion limit as given by the analysis of the "two-phase" spectra displayed in Fig. 7(b), together with its derivative $W'(T)$.

the relaxation analysis, we get $M_{2,rot} = \Delta M_{2,iso} + \Delta M_{2,uni} = (3.75 + 14.8) \cdot 10^{-8}$ T^2 $= 18.55 \cdot 10^{-8}$ T^2 and $M_{2,total} = \Delta M_{2,rot} + \Delta M_{2,res} = 19.25 \cdot 10^{-8}$ T^2. The latter value is not so far from the value $M_{2,total} = 23.2 \cdot 10^{-8}$ T^2 calculated from structural data[54] and reported by Amoureux et al.[55]

V. DISCUSSION AND CONCLUSION

Applying the FC technique, the dispersion of proton spin-lattice of CN-ADA was measured over a broader frequency and temperature range compared to previous studies.[16] Thereby, the full spectral density of the motional processes is obtained, an endeavor not made before. Including conventionally measured relaxation rates, the temperature range could be extended down to 4.1 K.

Our interpretation of the relaxation differs from the previous ones. The overall reorientation is described by a (weakly) non-Lorentzian spectral density given by a CD function with a width parameter $\beta_{CD} = 0.83$ instead of by a Lorentzian as done by Amoureux et al.[16] It reflects the cooperative nature of the overall rotation of the molecule. Our result agrees with that of a deuteron stimulated echo analysis, which reported a similar stretching of the reorientational correlation function described by a Kohlrausch function with $\beta_K = 0.82$[20] and with that of a dielectric study yielding $\beta_{CD} \cong 0.80$.[10] Generally, the extent of stretching appears to be smaller in plastic crystals compared to structural glass formers.[10] As often found for cooperative dynamics, the stretching does not change with temperature. Hence, one can apply frequency-temperature superposition (FTS) to construct master curves, which effectively enlarge the still narrow frequency window of the commercial FC relaxometer. The such extracted time constants agree well with those reported in the literature. However, the activation energy extracted ($E_{iso} = 52$ kJ/mol) is somewhat higher than the value reported by Amoureux et al. ($E_{iso} = 45.5$ kJ/mol). Moreover, taking the parameters of the master curve, we are able to quantitatively reproduce the individual relaxation data collected at different temperatures together with those from Amoureux et al.[16] This definitely demonstrates the validity of FTS. Moreover, the effective second moment relaxed by the overall molecular reorientation agrees reasonably well with the value obtained from the step in $M_2(T)$ provided by CW NMR measurements of Amoureux et al.[16]

Regarding the uniaxial rotation in the glassy PC phase ($T < T_g$), a broad temperature dependent distribution $G(\ln \tau)$ resulting from a temperature independent distribution of activation energies $g(E)$ is assumed. In other words, pronounced dynamic heterogeneities determine the relaxation behavior as is directly revealed by the "two-phase" character of the proton as well as the deuteron spectra reported in Ref. 21. The range of activation energies is significantly shifted to lower energies when compared to the single value in the ordered crystal, a behavior also found in structural glasses doped by molecules like benzene or adamantane when compared to the corresponding crystal of the guest molecule.[43] Probably, this reflects the lower density of the disordered phase. Actually, the temperature coefficient of the lattice parameter exhibits a significant change near T_g,[56] indicating that some free volume is "frozen in" below T_g—like in supercooled liquids. The presence of such a distribution visualizes the notion "glassy crystal": Every CN-ADA molecule senses a different local environment. Quantitatively, we describe $g(E)$ by a left-skewed Gaussian distribution. As the distribution $g(E)$ covers activation energies down to very low values, the spin-lattice relaxation remains comparatively short even at 4 K. Of course, one may speculate whether paramagnetic impurities or even tunneling effects become relevant at such low temperatures. As the distribution broadens with $1/T$, it becomes extremely broad at low temperatures. As a consequence, one cannot apply frequency-temperature superposition as done for the overall reorientation of CN-ADA. However, we propose a scaling procedure, which appropriately compensates for the broadening and directly provides an estimate of $g(E)$. Previously, the approach was successfully applied for constructing master curves for secondary relaxation in glasses, for example.[45–48] Importantly, the approach allows us to reconstruct the distribution not only from the susceptibility spectrum but also from the temperature dependence of the spin-lattice relaxation time, as demonstrated.

All in all, we showed that ^{1}H FC NMR relaxometry offers new insights into the dynamics of disordered solids, systems which have only been rarely investigated by FC NMR relaxometry so far.[7,23,57] The spectral density of the motional processes is directly accessed which is not the case for most other NMR techniques. Finally, we mention that a particular advantage of analyzing proton relaxation is given by the fact that due to the dominance of the magnetic dipole-dipole interaction, there is also an intermolecular relaxation pathway, which may provide access to translational motion, i.e., to the diffusion coefficient D. This was systematically exploited to measure $D(T)$ in liquids and polymers utilizing the FC method.[28,30,58,59] In the case of the PC phase of cyclohexane, this was first applied by Stapf and Kimmich[7] in order to probe the vacancy diffusion. In CN-ADA, the FC relaxation spectra at highest temperatures provide evidence that another relaxation regime enters the experimental frequency window, which, following the analysis of the T_{1rho} measurements of Ref. 16, we interpret as caused by the vacancy diffusion. It is well separated from the overall reorientation in contrast to what one observes in liquids.[28,30,58,59] However, the current performance of the relaxometer together with the onset of sublimation close to the melting does not allow a quantitative analysis of the full dispersion regime.

APPENDIX: SKEWED GAUSSIAN DISTRIBUTION DESCRIBING $g(E)$

Describing spin-lattice relaxation $\left\langle \frac{1}{T_1} \right\rangle (T)$ along Eq. (6), we needed to specify a distribution $g(E)$. In order to allow for some asymmetric distribution, we introduce the skewed Gaussian distribution along[60]

$$g(x) = \exp\left(-\left(\frac{x-\mu}{\sigma}\right)^2\right) \cdot \left[1 + \text{erf}\left(\alpha \frac{x-\mu}{\sigma}\right)\right]. \quad (A1)$$

Here, μ is connected to the mean, σ denotes the variance, and α the skewness of the distribution. For $\alpha < 0$, a left skewed Gaussian is obtained. For $\alpha > 0$, a right skewed Gaussian is obtained [cf. Fig. 1(a)]. For $\alpha = 0$, the Gaussian distribution is recovered.

REFERENCES

[1] J. Timmermans, J. Chem. Phys. **35**, 331 (1938).

[2] N. G. Parsonage and L. A. K. Staveley, *Disorder in Crystals* (Oxford University, Oxford, 1978).

[3] J. N. Sherwood, *The Plastically Crystalline State* (Wiley, New York, 1979).

[4] K. Adachi, H. Suga, and S. Seki, Bull. Chem. Soc. Jpn. **41**, 1073 (1968).

[5] H. Suga, Thermochim. Acta **245**, 69 (1994).

[6] M. Bee, *Quasielastic Neutron Scattering* (Adam Hilger, Bristol, 1988).

[7] S. Stapf and R. Kimmich, Mol. Phys. **92**, 1051 (1997).

[8] S. Benkhof, A. Kudlik, T. Blochowicz, and E. Rössler, J. Phys.: Condens. Matter **10**, 8155 (1998).

[9] M. Jimenez-Ruiz, A. Criado, F. J. Bermejo, G. J. Cuello, F. R. Trouw, R. Fernandez-Perea, H. Löwen, C. Cabrillo, and H. E. Fischer, Phys. Rev. Lett. **83**, 2757 (1999).

[10] R. Brand, P. Lunkenheimer, and A. Loidl, J. Chem. Phys. **116**, 10386 (2002).

[11] B. Micko, D. Kruk, and E. A. Rössler, J. Chem. Phys. **138**, 074503 (2013).

[12] J. L. Sauvajol, M. Bee, and J. P. Amoureux, Mol. Phys. **46**, 811 (1982).

[13] J. P. Amoureux, G. Noyel, M. Foulon, M. Bee, and L. Jorat, Mol. Phys. **52**, 161 (1984).

[14] M. Foulon, J. P. Amoureux, J. L. Sauvajol, J. P. Cavrot, and M. Muller, J. Phys. C: Solid State Phys. **17**, 4213 (1984).

[15] K. Pathmanathan and G. P. Johari, J. Phys. C: Solid State Phys. **18**, 6535 (1985).

[16] J. Amoureux, R. Decressain, M. Sahour, and E. Cochon, J. Phys. II Fr. **2**, 249 (1992).

[17] M. Descamps, J. F. Willart, and O. Delcourt, Physica A **201**, 346 (1993).

[18] B. Kuchta, M. Descamps, and F. Affouard, J. Chem. Phys. **109**, 6753 (1998).

[19] M. Tyagi and S. S. N. Murthy, J. Chem. Phys. **114**, 3640 (2001).

[20] S. A. Lusceac, I. Roggatz, P. Medick, J. Gmeiner, and E. A. Rössler, J. Chem. Phys. **121**, 4770 (2004).

[21] S. A. Lusceac, I. Roggatz, J. Gmeiner, and E. A. Rössler, J. Chem. Phys. **126**, 014701 (2007).

[22] M. Bee, J. P. Amoureux, and J. Dianoux, Mol. Phys. **41**, 325–339 (1980).

[23] L. Decressain, E. Carpenter, J. P. Cochon, and J. Amoureux, Eur. Phys. J. B **58**, 223 (2007).

[24] F. Kimmerle, G. Majer, U. Kaess, A. J. Maeland, M. S. Conradi, and A. F. McDowell, J. Alloys Compd. **264**, 63–70 (1998).

[25] C. A. Sholl, J. Phys. C: Solid State Phys. **14**, 447 (1981).

[26] M. Flämig, M. Hofmann, and E. A. Rössler, Mol. Phys. **117**, 877 (2019).

[27] R. Kimmich and E. Anoardo, Prog. Nucl. Magn. Reson. Spectrosc. **44**, 257–320 (2004).

[28] R. Meier, D. Kruk, and E. A. Rössler, ChemPhysChem **14**, 3071 (2013).

[29] F. Fujara, D. Kruk, and A. F. Privalov, Prog. Nucl. Magn. Reson. Spectrosc. **82**, 39 (2014).

[30] E. A. Rössler, M. Hofmann, and N. Fatkullin, *New Developments of NMR Field-Cycling NMR Relaxometry*, edited by R. Kimmich (RSC, Cambridge, England, 2019), p. 181.

[31] R. Kimmich and N. Fatkullin, Prog. NMR Spectrosc. **101**, 18 (2017).

[32] B. Kresse, M. Becher, A. F. Privalov, M. Hofmann, E. A. Rössler, M. Vogel, and F. Fujara, J. Magn. Reson. **277**, 79–85 (2017).

[33] A. Abragam, *The Principles of Nuclear Magnetism* (Clarendon Press, Oxford, 1961).

[34] D. Wolf, *Spin-Temperature and Nuclear-Spin Relaxation in Matter: Basic Principles and Applications* (Clarendon Press, Oxford, 1979).

[35] Y. Ayant, E. Belorizky, P. Fries, and J. Rosset, J. Phys. **38**, 325 (1977).

[36] A. Guillermo, R. Dupeyre, and J. P. Cohen-Addad, Macromolecules **23**, 1291 (1990).

[37] S. Kariyo, G. Gainaru, H. Schick, A. Brodin, and E. A. Rössler, Phys. Rev. Lett. **97**, 207803 (2006); Erratum, **100**, 109901 (2008).

[38] S. Kariyo, A. Brodin, C. Gainaru, A. Herrmann, H. Schick, V. N. Novikov, and E. A. Rössler, Macromolecules **41**, 5313 (2008).

[39] D. E. Woessner, J. Chem. Phys. **36**, 1–4 (1962).

[40] J. Kowalewski and L. Mäler, *Liquids: Theory, Experiments and Applications* (Taylor & Francis, New York, 2006).

[41] C. J. F. Böttcher and P. Bordewijk, *Theory of Electric Polarization* (Elsevier Scientific Polarization, Amsterdam, The Netherlands, 1978).

[42] J. D. Ferry, *Viscoelasticity Properties of Polymers* (John Wiley & Sons, New York, 1980).

[43] I. Roggatz, C. Karle, M. Taupitz, and E. Rössler, Ber. Bunsenges. Phys. Chem. **100**, 1554 (1996).

[44] A. Kudlik, C. Tschirwitz, T. Blochowicz, S. Benkhof, and E. Rössler, J. Non-Crystal. Solids **235-237**, 406 (1998).

[45] K. S. Gilroy and W. A. Phillips, Philos. Mag. B **43**, 735 (1981).

[46] E. Courtens, Phys. Rev. **33**, 2975–2978 (1986).

[47] J. Wiedersich, S. V. Adichtchev, and E. Rössler, Phys. Rev. Lett. **84**, 2718 (2000).

[48] R. Kahlau, T. Dörfler, and E. A. Rössler, J. Chem. Phys. **139**, 134504 (2013).

[49] H. A. Resing, J. Chem. Phys. **43**, 669 (1965).

[50] E. Rössler, M. Taupitz, K. Börner, M. Schulz, and H.-M. Vieth, J. Chem. Phys. **92**, 5847 (1990).

[51] R. Böhmer, G. Diezemann, G. Hinze, and E. Rössler, Prog. Nucl. Magn. Reson. **39**, 191 (2001).

[52] Unpublished results, N. Römer, Diploma Work, Bayreuth University, 1996.

[53] J. G. Powles and P. Mansfield, Phys. Lett. **2**, 58–59 (1962).

[54] J. P. Amoureux and M. Bee, Acta Cryst. B **35**, 2957–2962 (1979).

[55] J. P. Amoureux, M. Castelain, M. Bee, B. Arnaud, and M. L. Shouteenten, Mol. Phys. **42**, 119–127 (1981).

[56] M. Foulon, J. Lefebvre, J. P. Amoureux, M. Muller, and D. Magnier, J. Phys. **46**, 919–926 (1985).

[57] E. Carignani, C. Forte, E. Juszyńska-Gałązka, M. Gałązka, M. Massalska-Arodź, A. Mandoli, and L. Calucci, J. Phys. Chem. B **122**, 9792–9802 (2018).

[58] D. Kruk, R. Meier, and E. A. Röessler, Phys. Rev. E **85**, 020201 (2012).

[59] R. Meier, A. Herrmann, M. Hofmann, B. Schmidtke, B. Kresse, A. F. Privalov, D. Kruk, F. Fujara, and E. A. Roessler, Macromolecule **46**, 5538 (2013).

[60] A. Azzalini, Scand. J. Stat. **12**, 171–178 (1985).

Bibliography

1. Bloembergen, N.; Purcell, E. M.; Pound, R. V. Relaxation Effects in Nuclear Magnetic Resonance Absorption. *Phys. Rev.* **1948**, *73*, 679-712.

2. Kubo, R.; Tomita, K. A General Theory of Magnetic Resonance Absorption. *J. Phys. Soc. Jap.* **1954**, *9*, 888-919.

3. Abragam, A. *The Principles of Nuclear Magnetism* (Clarendon Press, Oxford, 1961).

4. Slichter, C.P., *Principles of Magnetic Resonance*, 3rd ed. (Springer, Berlin, Heidelberg, New York, 1992).

5. Mehring, M. *Principles of High Resolution NMR in Solids*, 2nd ed. (Springer, Berlin, Heiderberg, New York, 1983).

6. Kruk, D.; Herrmann, A.; Rössler, E.A. Field-cycling NMR relaxometry of viscous liquids and polymers. *Prog. Nucl. Magn. Reson. Spectrosc.* **2012,** *63*, 33-64.

7. Meier, R.; Kruk, D.; Rössler, E.A. Intermolecular Spin Relaxation and Translation Diffusion in Liquids and Polymer Melts: Insight from Field-Cycling ^{1}H NMR Relaxometry. *ChemPhysChem* **2013**, *14*, 3071−3081.

8. Rössler, E.A.; Hofmann, M.; Fatkullin, N. Application of Field-Cycling NMR Relaxometry to the Study of Translational and Rotational Dynamics in Liquids and Polymers, in: *New Developments of NMR Field-Cycling NMR Relaxometry*, ed. by Kimmich, R., RSC, Cambridge, England, 181- 206.

9. Kariyo, S.; Brodin, A.; Gainaru, C.; Herrmann, A.; Schick, H.; Novikov, V. N.; Rössler, E. A. From Simple Liquid to Polymer Melt. Glassy and Polymer Dynamics studied by Fast Field Cycling NMR Relaxometry: low and high Molecular Weight Limit. *Macromolecules* **2008**, *41*, 5313−5321.

10. Wolfe, M.; Jonas, J. Reorientational Motions in Compressed Viscous Fluids: Selectively Deuterated Glycerol. *J. Chem. Phys.* **1997**, *71*, 3252-3262.

11. Zwanzig, R., *Nonequilibrium Statistical Mechanics 3rd ed.* (Oxford University Press, New York, 2001).

12. STELAR Company: www.stelar.it

13. Fujara, F.; Kruk, D.; Privalov, A.F. Solid state Field-Cycling NMR relaxometry: Instrumental improvements and new applications. *Prog. Nucl. Magn. Reson. Spectrosc.* **2014**, *82*, 39−69.

14. Kresse, B.; Privalov, A. F.; Fujara, F. NMR field-cycling at ultralow magnetic fields. *Solid State Nucl. Magn. Reson.,* **2011**, *40*, 134-137.

15. Kresse, B.; Privalov, A. F.; Herrmann, A.; Hofmann, M.; Rössler, E. A.; Fujara, F. Simultaneous measurements of very small magnetic fields and spin-lattice relaxation. *Solid State Nucl. Magn. Reson.* **2014**, *59*, 45-47.

16. Ferry, J. D. *Viscoelastic Properties of Polymers*, 3rd ed.; Wiley; New York; 1980.

17. Plazek, D. J.; Zheng, X. D.; Ngai, K. L. Viscoelastic Properties of Amorphous Polymers. 1. Different Temperature Dependences of Segmental Relaxation and Terminal Dispersion. *Macromolecules*, **1992**, *25*, 4920-4924.

18. Colby, R. H.; Fetters, L. J.; Graessley, W. W. Melt Viscosity - Molecular Weight Relationship for Linear Polymers. *Macromolecules*, **1987**, *20,* 226-2237.

19. Gainaru, C.; Lips, O.; Troshagina, A.; Kahlau, R.; Brodin, A.; Fujara, F.; Rössler, E.A. On the Nature of the High-Frequency Relaxation in a Molecular Glass Former: A Joint Study of Glycerol by Field Cycling NMR, Dielectric Spectroscopy, and Light Scattering. *J. Chem. Phys*. **2008**, *128*, 174505.

20. Kariyo, S.; Gainaru, C.; Schick, H.; Brodin, A.; Rössler, E. A. From a Simple Liquid to a Polymer Melt: NMR Relaxometry Study of Polybutadiene. *Phys. Rev. Lett*. **2006**, *97*, 207803. Erratum: Kariyo, S.; Herrmann, A.; Gainaru, C.; Schick, H.; Brodin, A.; Rössler, E. A. *Phys. Rev. Lett*. **2008**, *100*, 109901.

21. Torrey, H. C. Nuclear Spin Relaxation by Translational Diffusion. *Phys. Rev*. **1953**, *92*, 962- 969.

22. Sholl, C. A. Nuclear Spin Relaxation by Translational Diffusion in Liquids and Solids: High- and Low-Frequency Limits. *J. Phys. C: Solid State Phys*. **1981**, *14*, 447-464.

23. Ayant, Y.; Beloritzky, E.; Alizon, J.; Gallice, J. Calcul des Densites Spectrales Resultant d´un Mouvement Aleatoire de Translation en Relaxation par Interaction Dipolaire Magnetique dans les Liquids. *J. Phys. (France)*, **1975**, *36*, 991-1004.

24. Ayant, Y.; Belorizky, E.; Fries, P.; Rosset, J. Effet des Interactions Dipolaires Magnetiques Intermoleculaires sur la Relaxation Nucleaire de Molecules Polyatomiques dans les Liquides. *J. Phys. (Paris)* **1977**, *38*, 325−337.

25. Fatkullin, N.; Gubaidullin, A.; Stapf, S. Features of Polymer Chain Dynamics as Revealed by Intermolecular Nuclear Magnetic Dipole-Dipole Interaction: Model Calculations and Field-Cycling NMR Relaxometry. *J. Chem Phys*, **2010**, *132*, 094903.

26. Kehr, M.; Fatkullin, N.; Kimmich, R. Molecular Diffusion on a Time Scale between Nano- and Milliseconds Probed by Field-Cycling NMR Relaxometry of Intermolecular Dipolar Interactions: Application to Polymer Melts. *J. Chem. Phys.*, **2007**, *126*, 094903.

27. Meier, R.; Kruk, D.; Rössler, E. A. Intermolecular Spin Relaxation and Translation Diffusion in Liquids and Polymer Melts: Insight from Field-Cycling ^{1}H NMR Relaxometry. *ChemPhysChem*, **2013**, *14,* 3071-3081.

28. Meier, R.; Kruk, D.; Gmeiner, J.; Rössler, E. A. Intermolecular Relaxation in Glycerol as Revealed by Field Cycling ^{1}H NMR Relaxometry Dilution Experiments. *J. Chem. Phys*. **2012**, *136*, 034508.

29. Kimmich, R.; Fatkullin, N. Self-diffusion studies by intra-and inter-molecular spin-lattice relaxometry using field-cycling: Liquids, plastic crystals, porous media, and polymer segments. *Progr. NMR Spectrosc*., **2017**, *101*, 18-50.

30. Fries, P.; Belorizky, E. Effect des fonctions de correlation de paire sur la relaxation nucleaire intermoleculaire par diffusion translationelle et rotationelle dans les liquides. *J. Phys. (France),* **1978**, *39*, 1263-1282.

31. Albrand, J.P.; M.C. Taieb, P.H. Fries, Beloritzky, E. Effects of eccentricity on nuclear magnetic relaxation by intermolecular dipole-dipole interactions: [13]C relaxation of neopentane. *J. Chem. Phys*. **1981**, *78*, 2141-2146.

32. Böttcher, C.J.F.; Bordewijk, P. *Theory of Electric Polarization*; Elsevier Science Ltd.; Amsterdam, The Netherlands; 1978.

33. Lunkenheimer, P.; Schneider, U.; Brand, R.; Loidl, A. Glassy Dynamics. *Contemp. Phys*. **2000**, *41*, 15−36.

34. Petzold, N.; Schmidtke, B.; Kahlau, R.; Bock, D.; Meier, R.; Micko, B.; Kruk, D.; Rössler, E.A. Evolution of the Dynamic Susceptibility in Molecular Glass Formers: Results from Light Scattering, Dielectric Spectroscopy, and NMR. *J. Chem. Phys*. **2013**, *138*, 12A510.

35. Kudlik, A.; Benkhof, S.; Blochowicz, T.; Tschirwitz, C.; Rössler, E.A. The dielectric response of simple organic glass formers. *J. Mol. Struct*. **1999**, *479*, 201-218.

36. Blochowicz, T.; Tschirwitz, C.; Benkhof, S.; Rössler, E.A. Susceptibility functions for slow relaxation processes in supercooled liquids and the search for universal relaxation patterns. *J. Chem. Phys*. **2003**, *118*, 7544-7555.

37. Hwang, L. P.; Freed, J. H. Dynamic effects of pair correlation functions on spin relaxation by translational diffusion in liquids. *J. Chem. Phys*. **1975**, *63*, 4017-4025.

38. Chang, I.; Sillescu, H. Heterogeneity at the Glass Transition: Translational and Rotational Self-Diffusion. *J. Phys. Chem. B,* **1997**, *101*, 8794-8801.

39. Meier, R.; Kruk, D.; Bourdick, A.; Schneider, E.; Rössler, E. A. Inter-and Intramolecular Relaxation in Molecular Liquids by Field Cycling ^{1}H NMR Relaxometry. *Appl. Magn. Reson.* **2013**, *44*, 153−168.

40. Gainaru, C.; Böhmer, R.; Kahlau, R.; Rössler, E. Energy Landscape in Molecular Glasses Probed by High-Resolution Dielectric Experiments. *Phys. Rev. B*, **2010**, *82,* 104205.

41. Gilroy, K. S.; and Phillips, W. A. An Asymmetric Double-Well Potential Model for Structural Relaxation Processes in Amorphous Materials *Philos. Mag. B* **1981**, *43*, 735-746.

42. Courtens, E. Scaling Dielectric Data on $Rb_{1-x}(NH_4)_xH_2PO_4$ Structural Glasses and Their Deuterated Isomorphs *Phys. Rev. B*, **1986**, *33*, 2975-2978.

43. Wiedersich, J.; Adichtchev, S.V.; Rössler, E. Spectral Shape of Relaxation in Silica Glass. *Phys. Rev. Lett.,* **2000**, *84*, 2718-2721.

44. Kahlau, R; Dörfler, T.; Rössler, E.A. Secondary Relaxations in a Series of Organic Phosphate Glasses Revealed by Dielectric Spectroscopy. *J. Chem. Phys.,* **2013**, *139*, 134504.

45. Noack, F.; Preissing G. Magnetische Relaxation in Glycerin. *Z. Naturforsch*. **1969**, *24a*, 143-153.

46. Preissing, G.; Noack, F.; Kosfeld, R.; Gross, B. Zur Deutung der Protonenrelaxation in Glycerin. *Z. Physik* **1971**, *246*, 84-90.

47. Kintzinger, J.P.; Zeidler, M.D. Nuclear Magnetic Relaxation Study of Glycerol. *Ber. Bunsenges. Phys. Ges*. **1973**, *77*, 98-103.

48. Brodin, A.; Rössler, E. A. Depolarized light scattering study of glycerol. *Eur. Phys. J. B*, **2005**, *44*, 3-14.

49. Brodin, A.; Gainaru, C.; Porokhonskyy, V.; Rössler, E.A. Evolution of dynamic susceptibility in molecular glass formers—a critical assessment. *J. Phys. Condens. Matter* **2007**, *19*, 205104.

50. Kruk, D.; Meier, R.; Rössler, E.A. Translational and Rotational Diffusion of Glycerol by Means of Field Cycling ^{1}H NMR Relaxometry. *J. Phys. Chem*. *B*, **2011**, *115*, 951-957.

51. Meier, R.; Kahlau, R.; Kruk, D.; Rössler, E.A.; Comparative studies of the dynamics in viscous liquids by means of dielectric spectroscopy and field cycling NMR. *J. Phys. Chem. A,* **2010**, *114,* 7847-7855.

52. Edward, T.J. Molecular Volumes and the Stokes-Einstein Equation. *J. Chem. Educ.* **1970**, *47*, 261-270.

53. Meier, R.; Schneider, E.; Rössler, E. A. Change of Translational-Rotational Coupling in Liquids Revealed by Field-Cycling ^{1}H NMR. *J. Chem. Phys*. **2015**, *142*, 034503.

54. Schnauss, W.; Fujara, F.; Sillescu, H. The Molecular Dynamics around the Glass Transition and in the Glassy State of Molecular Organic Systems: A 2H − Nuclear Magnetic Resonance Study. *J. Chem. Phys*. **1992**, *97*, 1378−1389.

55. Friedrich, A. ; Dölle, A. ; Zeidler, M. D. Reorientational Dynamics of Glycerol Derived from Temperature-Dependent Multi-Nuclear Magnetic Resonance Relaxation Data. *Magn. Reson. Chem.* **2003**, *41*, 813-818.

56. Noack, N. NMR Field-Cycling Spectroscopy: Principles and Applications. *Prog. NMR Spectrosc.* **1986,** *18*, 171-276.

57. Fujara, F.; Petry, W.; Diehl, R.M.; Schanuss, W.; Sillescu, H. Localized Motion in Supercooled Glycerol as Measured by ^{2}H-NMR Spin-Lattice Relaxation and Incoherent Neutron Scattering. *Europhys. Lett.* **1991***, 14*, 563-568.

58. Kimmich, R.; Anoardo, E. Field-Cycling NMR Relaxometry. *Progr. NMR Spectr.* **2004**, *44*, 257–320.

59. Dries, T.; Fujara; F.; Kiebel, M.; Rössler, E.A.; Sillescu, H. ^{2}H-NMR Study of the Glass Transition in Supercooled Ortho-Terphenyl. *J. Chem. Phys*. **1988**, *88*, 2139-2147.

60. Xu, M.; Eyring, E. M.; Petrucci, S. Dielectric Relaxation of Chloroform and Chloroform-Cyclohexane Mixtures at Gigahertz and Terahertz Frequencies. The Inertial Term. *J. Mol. Liq*. **1997**, *73*, 41-48.

61. Waggoner, R. A.; Blum, F. D.; MacElroy, J. M. D. Dependence of the Solvent Diffusion Coefficient on Concentration in Polymer Solutions. *Macromolecules*, **1993**, *26*, 6841-6848.

62. Schmidtke, B.; Petzold, N.; Kahlau, R.; Rössler, E. A. Reorientational Dynamics in Molecular Liquids as Revealed by Dynamic Light Scattering: From Boiling Point to Glass Transition Temperature. *J. Chem. Phys.*, **2013**, *139*, 084504.

63. Kaatze, U.; Pottel, R.; Schaefer, M. Dielectric Spectrum of Dimethyl Sulfoxide/Water Mixtures as a Function of Composition, *J. Phys. Chem.*, **1989**, *93,* 5623-5627.

64. Chen, B.; Sigmund, E. E.; Halperin, W. P. Stokes-Einstein Relation in Supercooled Aqueous Solutions of Glycerol, *Phys. Rev. Lett*. **2006**, *96*, 145502.

65. Holz, M.; Heil, S. R.; Sacco, A. Temperature-Dependent Self-Diffusion Coefficients of Water and Six Selected Molecular Liquids for Calibration in Accurate ^{1}H NMR PFG Measurements, *Phys. Chem. Chem. Phys.* **2000**, *2*, 4740-4742.

66. Angulo, G.; Brucka, M.; Gerecke, M.; Grampp, G.; Jeannerat, D.; Milkiewicz, J.; Mitrev, Y.; Radzewicz, C.; Rosspeintner, A.; Vauthey, E.; Wnuk, E. Characterization of Dimethylsulfoxide/Glycerol Mixtures: A Binary Solvent System for the Study of "Friction-Dependent" Chemical Reactivity, *Phys. Chem. Chem. Phys.* **2016**, *18*, 18460-18469.

67. Kintzinger, J. P.; Lehn, J. M. Nuclear Relaxation and Molecular Properties Part V. Molecular Dynamics of Liquid Pyridine from [2]D and [14]N Nuclear Quadrupolar Relaxation. *Mol. Phys.* **1971**, *22*, 273-287.

68. Lichtinger, A. Field-Cycling ^{1}H NMR und Dielektrische Spektroskopie an Monoalkoholen und binären Glasbildnern. Master Thesis, 2017, University Bayreuth.

69. Timmermans, J. Un Nouvel État Mésomorphe les Cristaux Organiques Plastiques. *J. Chem. Phys.* **1938**, *35*, 331-344.

70. Parsonage N. G.; Staveley, L. A. K. *Disorder in Crystals*; Oxford University, Oxford, 1978.

71. Sherwood, J. N. *The Plastically Crystalline State*; Wiley; New York, 1979.

72. Adachi, K.; Suga, H.; and Seki, S. Phase Changes in Crystalline and Glassy-Crystalline Cyclohexanol. *Bull. Chem. Soc. Jpn.* **1968**, *41*, 1073-1087.

73. Suga, H. Calorimetrici Investigation on Glassy Crystals. *Thermochim. Acta*, **1994**, *245*, 69-81.

74. Bee, M. *Quasielastic Neutron Scattering*; Adam Hilger; Bristol, 1988.

75. Stapf, S.; Kimmich, R. Translational Versus Rotational Molecular Dynamics in Plastic Crystals Studied by NMR Relaxometry and Diffusometry. *Mol. Phys.* **1997**, *92*, 1051-1060.

76. Benkhof, S.; Kudlik, A.; Blochowicz, T.; Rössler, E. Two Glass Transitions in Ethanol: A Comparative Dielectric Relaxation Study of the Supercooled Liquid and the Plastic Crystal. *J. Phys.: Condens. Matter*, **1998**, *10*, 8155-8171.

77. Jimenez-Ruiz, M.; Criado, A.; Bermejo, F. J.; Cuello, G. J.; Trouw, F. R.; Fernandez-Perea, R.; Löwen, H.; Cabrillo, C.; Fischer, H. E. Purely Dynamical Signature of the Orientational Glass Transition. *Phys. Rev. Lett.* **1999**, *83*, 2757-2760.

78. Brand, R.; Lunkenheimer, P.; Loidl, A. Relaxation Dynamics in Plastic Crystals. *J. Chem. Phys.* **2002**, *116*, 10386.

79. Micko, B.; Kruk, D.; Rössler, E. A. Primary and Secondary Relaxation Process in Plastically Crystalline Cyanocyclohexane Studied by ^{2}H Nuclear Magnetic Resonance. I. *J. Chem. Phys.* **2013**, *138*, 074503.

80. Kimmerle, F.; Majer, G.; Kaess, U.; Maeland, A.J.; Conradi, M.S.; McDowell, A.F. NMR Studies of Hydrogen Diffusion in $ZrBe_2H_{1.4}$. *J. Alloys and Compounds,* **1998**, *264*, 63-70.

81. Decressain, R.; Carpentier, L.; Cochin, E.; Amoureux, J.P. Modelling of Dynamical Processes in a Molecular Crystal by NMR J. *Eur. Phys. J. B,* **2007**, *58*, 223-230.

82. Foulon, M.; Amoureux, J. P.; Sauvajol, J. L.; Cavrot, J. P.; Muller, M. Different Aspects of an Interesting Glassy Crystal: 1-Cyanoadamantane. *J. Phys. C*, **1984**, *17*, 4213-4229.

83. Amoureux, J. P.; Decressain, M.; Sahour, M.; Cochon, E. Molecular Motions in Glassy Crystal Cyanoadamantane: A Proton Spin-Lattice Relaxation Study. *J. Phys. II France,* **1992**, *2*, 249-259.

84. Lusceac, S.A.; Roggatz, I.; Gmeiner, J.; Rössler, E.A. ^{2}H Nuclear Magnetic Resonance Study on the Molecular Motion in Cyanodamantane. II. Orientationally Ordered and Glassy Crystalline Phase. *J. Chem. Phys.* **2007**, *126*, 014701.

85. Chezeau, J. M.; Strange, J. H. Diffusion in Molecular Crystals. *Physics Reports*, **1979**, *53*, 1-92.

86. Lusceac, S.A.; Roggatz, I.; Medick, P.; Gmeiner, J.; Rössler, E.A. ^{2}H Nuclear Magnetic Resonance Study on the Molecular Motion in Cyanodamantane. I. Supercooled Plastically Crystalline Phase. *J. Chem. Phys.* **2004**, *121*, 4770-4780.

87. Amoureux, J. P.; Bee, M. Crystal Structure of 1-Cyanoadamantane, C10H15CN, in its Plastic Phase. *Acta Cryst. B*, **1979**, *35*, 2957-2962.

88. Amoureux, J.P.; Noyel, G.; Foulon, M.; Bee, M.; Jorat, L. Low Frequency Dielectric Properties of 1-Cyanoadamantane $C_{10}H_{15}CN$. *Mol. Phys.* **1984**, *52*, 161-171.

89. Pathmanathan, K.; Johari, G. P. Molecular Relaxations in a Rigid Molecular Glassy Crystal. *J. Phys. C,* **1985**, *18*, 6535-6545.

90. Tyagi, M.; Murthy, S. S. N. Study of the Nature of Glass Transitions in the Plastically Crystalline Phases of Cyclo-Octanol, Cycloheptanol, Cyanoadamantane and Cis-1,2-Dimethylcyclohexane. *J. Chem. Phys.* **2001**, *114*, 3640-3652.

91. Roggatz, I. *NMR-Untersuchungen zur Sondenbeweglichkeit in Ungeordneten Festkörpern*, Dissertation, University Bayreuth, 2000.

92. Singh, L. P.; Murthy, S. S. N. Study of Secondary Relaxation in Disordered Plastic Crystals of Isocyanocyclohexane, Cyanocyclohexane, and 1-Cyanoadamantane. *J. Chem. Phys.* **2008**, *129*, 094501.

93. Krivchikov, A. I.; Korolyuk, O. A.; Sharapova, I. V.; Tamarit. J. Ll.; Bermejo, F. J.; Pardo, L. C.; Rovira-Esteva, M.; Ruiz-Martin, M. D.; Jezowski, A.; Baran, J. Davydova, N. A.; Effects of Internal Molecular Degrees of Freedom on the Thermal Conductivity of Some Glasses and Disordered Crystals. *Phys. Rev. B*, **2012**, *85*, 014206.

94. Kishimoto, I.; Pnvidic, J. J.; Matsuo, T.; Suga, H. Phase Transition and Glass Transitions in Isocyanocyclohexane Studied by a Polaro-Calorimter. *Proc. Japan Acad. Ser. B*, **1991**, *67*, 66-71.

95. Gonthier-Vassal, A.; Szwarc, H. Glassy Crystals. Glass Transitions in Crystalline Fluoro- , Cyano-, and Isocyanocyclohexane. *Chem. Phys. Lett.* **1986**, *129*, 5-8.

96. Tschirwitz, C.; Benkhof, S.; Blochowicz, T.; Rössler, E. Dielectric Spectroscopy on the Plastically Crystalline Phase of Cyanocyclohexane. *J. Chem. Phys.* **2002**, *117*, 6281-6288.

97. Surovtsev, N. V.; Adichtchev, S. V.; Wiedersich, J.; Novikov, V. N.; Rössler, E. A. Fast Relaxation in the Structural Glass and Glassy Crystal of Ethanol and Cyano Cyclohexane: A Quasielastic Light Scattering Study. *J. Chem. Phys.* **2003**, *119*, 12399.

98. Bee, M.; Sauvajol, J. L.; Hédoux, A.; Amoureux, J. P. Molecular Reorientations of Triethylenediamine (TEDA) in its Plastic Solid Phase an Incoherent Quasielastic Neutron Scattering Study. *Mol. Phys.* **1985**, *55*, 637-652.

99. Nimmo, J. K.; Lucas, B. W. Solid-State Phase Transition in Triethylenediamine, $N(CH_2CH_2)N$. I. The Crystal Structure of Phase II at 298 K. *Acta Cryst. B,* **1976**, *32*, 348-353.

100. Smith, G. W. Proton Magnetic Resonance Studies of Solid Trethylenediamine – Molecular Structure and Motions. *J. Chem. Phys.* **1965**, *43*, 4325-4336.

101. Becher, M. TU Darmstadt, private communication.

102. Leites, L. A. Vibrational Spectroscopy of Carboranes and Parent Boranes and Its Capabilities in Carborane Chemistry. *Chem. Rev.* **1992**, *92*, 279-323.

103. Winterlich, M.; Zimmermann, H.; Böhmer, R. Phase Transition Kinetics and Reorientational Dynamics of the Plastic Crystal Meta-Carborane Studied by Deuteron NMR. *J. Non-Cryst. Sol.* **2002**, *307*, 442-448.

104. Winterlich, M.; Böhmer, R.; Diezemann, G.; Zimmermann, H. Rotational Motion in the Molecular Crystals Meta- and Ortho-Carborane Studied by Deuteron Nuclear Magnetic Resonance. *J. Chem. Phys.* **2005**, *123*, 094504.

105. Beckmann, P.; Wendel, A. Proton Spin-Lattice Relaxation in Meta-Carborane. *J. Chem. Phys.* **1980**, *73*, 3514-3515.

106. Evaluation performed by Körber, T. University Bayreuth.

Acknowledgement